Cover design

my mother
An Van de Vel


UNIVERSITEIT GENT

FACULTY OF **MEDICINE AND HEALTH SCIENCES**

Ghent University, Faculty of Medicine and Health Sciences

Lost in Transcription

Emergence of Epigenetic Drivers and MicroRNAs in T-cell Acute Lymphoblastic Leukemia

This thesis is submitted as fulfillment of the requirements for the degree of Doctor in Medical Sciences by ir. Joni Van der Meulen, 2014

Promotor
prof. dr. Frank Speleman

Co-promotor
prof. dr. Yves Benoit

Center for Medical Genetics
Ghent University Hospital, Medical Research Building
De Pintelaan 185, 9000 Gent, Belgium
+32-9-3326950
Joni.Vandermeulen@UGent.be

Thesis submitted to fulfill the requirements for the degree of Doctor in Medical Sciences

Promotor: prof. dr. Frank Speleman
Ghent University, Belgium

Co-promotor: prof. dr. Yves Benoit
Ghent University, Belgium

Members of the examination committee:

prof. dr. Omar I. Abdel-Wahab
Memorial Sloan-Kettering Cancer Center, NY, USA

prof. dr. Jan Cools
KULeuven, Belgium

dr. Tom Van Maerken
Ghent University, Belgium

prof. dr. Tessa Kerre
Ghent University, Belgium

dr. Steven Goossens
Ghent University, Belgium

dr. ir. Pieter Mestdagh
Ghent University, Belgium

prof. dr. Marc Bracke
Ghent University, Belgium

The research described in this thesis was conducted at the Center for Medical Genetics, Ghent University Hospital, Ghent, Belgium.

This work was supported by the Fund for Scientific Research (FWO) Flanders (PhD grant to Joni Van der Meulen and project grants); the Flemish Liga against Cancer (VLK) (Emmanuel van der Schueren scholarship to Joni Van der Meulen); the GOA-UGent; Belgian Foundation against Cancer, the Cancer Plan from the Federal Public Service of Health; the Children Cancer Fund Ghent; the Belgian Program of Interuniversity Poles of Attraction IUAP; the Belgian Foundation Against Cancer.

This thesis is dedicated to

my father
my mother and sister
my grandparents
my family and friends

Table of Contents

List of abbreviations

ALL	acute lymphoblastic leukemia
AML	acute myeloid leukemia
array CGH	array comparative genomic hybridization
ASO	antisense oligonucleotide
B-ALL	B-cell acute lymphoblastic leukemia
BFLS	Börjeson-Forssman-Lehmann syndrome
bHLH	basic helix-loop-helix
CBP	CREB binding protein
cDNA	complementary DNA
ChIP	chromatin immunoprecipitation
CIMP	CpG island methylator phenotype
CLL	chronic lymphoid leukemia
CML	chronic myeloid leukemia
CoA	coactivators
DNMT	DNA methyltransferase
DNMTi	DNA methyltransferase inhibitor
DSB	double-strand break
DZNep	3-deazaneplanocin A
ESC	embryonic stem cell
FDA	Food and Drug Administration
FISH	fluorescent in-situ hybridisation
gDNA	genomic DNA
GSI	gamma-secretase inhibitor
H	histone
H3K27ac	histone 3 lysine 27 acetylation
H3K27me3	histone 3 lysine 27 trimethylation
HAT	histone acetyltransferase
HDAC	histone deacetylase
HDACi	histone deacetylase inhibitor
HDM	histone demethylase
HMT	histone methyltransferase
HOX	homeobox
ICN	intracellular domain
K	lysine
lincRNA	long intergenic non-coding RNA
lncRNA	long non-coding RNA
LMO	LIM-only domain
LNA	locked nucleic acid
MBD	methyl-binding protein
MDS	myelodysplastic syndrome
miRISC	miRNA-associated multiprotein RNA-induced-silencing complex
miRNA	microRNA
nt	nucleotide
oncomiR	oncogenic miRNA
PHD	plant homeodomain
PRC	polycomb repressor complex
RNAPII	RNA polymerase II
SAM	S-adenosyl methionine
seq	sequencing

shRNA	short hairpin RNA
T-ALL	T-cell acute lymphoblastic leukemia
TCR	T-cell receptor
TSS	transcription start site
UTR	untranslated region

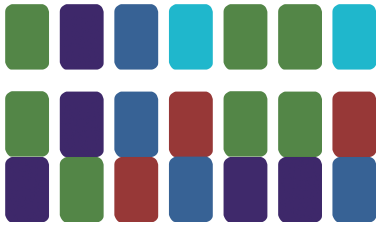

Chapter 1

Introduction

Introduction: PART I

1. The genomic landscape of T-cell acute lymphoblastic leukemia

Acute lymphoblastic leukemia (ALL) is an aggressive tumor entity of highly proliferative malignant lymphoid cells. This leukemia subtype occurs most frequently in children with incidence peaks between 2-5 years of age and is one of the most common childhood malignancies worldwide. Current overall cure rates in children are reaching more than 85%[1,2]. Age at diagnosis, leucocyte count, race, sex and immunophenotype are clinical prognostic parameters utilized to classify the patients into different risk groups[2]. Current treatment regimens encompass risk-adapted chemotherapy (including glucocorticoids, asparaginase, mercaptopurine, methotrexate and vincristine), hematopoietic stem-cell transplantation and supportive care. Currently, new treatment strategies are under evaluation as novel options for ALL therapy, including molecular therapies like tyrosine kinase inhibitors and immunotherapeutics like autologous or allogeneic T-cell therapies[1].

T-cell ALL (T-ALL) comprises 10-15% of pediatric and 25% of adult primary ALL patient cases[3] and is classified as a high-risk group in ALL[1]. Overall cure rates are reaching over 75% in children and ~50% in adult T-ALL cases[3]. Unfortunately, T-ALL patients often relapse quite early during treatment resulting in only a 7-23% 5-year survival rate of relapsed childhood T-ALL[1] and a 6.5% 5-year survival rate in relapsed adult T-ALL[4]. Of particular notice, T-ALL is characterized by a disturbed gender distribution towards man and boys (~3:1)[3]. Possible explanations for this unusual male/female imbalance are starting to emerge by X-linked genomic studies[5,6] (see **paper 1**; and Van der Meulen et al. submitted, see **paper 2**).

During normal T-cell development, the most early T-cell lineage committed precursor cells are the immature $CD34^+$ cells that have just entered the thymus and subsequently differentiate through various intermediate subsets into mature T-cells harboring a functional T-cell receptor (TCR) belonging to the TCRαβ or TCRγδ lineage (**Figure 1**)[7]. Primary T-ALL patient samples are characterized by clonal expansion of malignant T-cells arrested at a specific stage during T-cell differentiation[3].

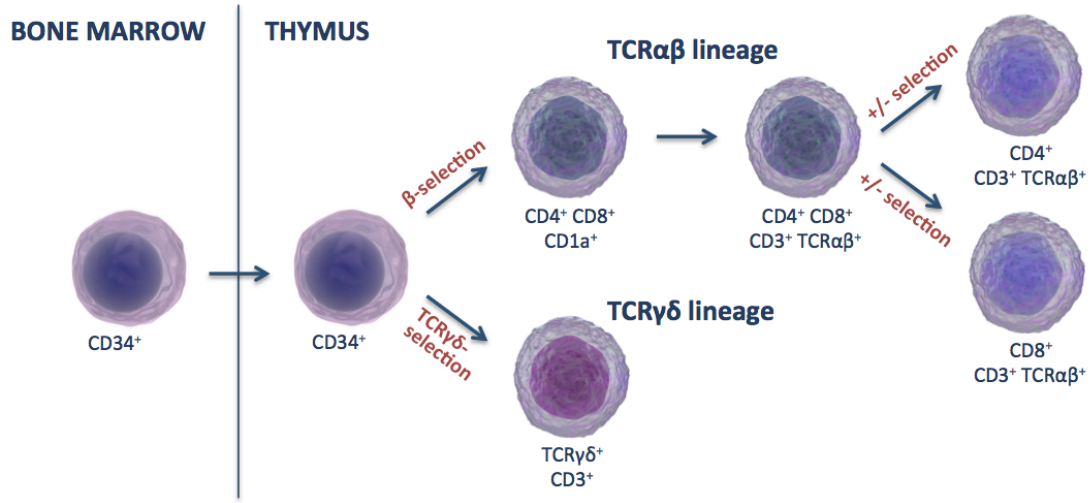

Figure 1. Schematic representation of the major T-cell differentiation stages during normal T-cell maturation in the thymus (adapted from Taghon et al. Curr Top Microbiol Immunol 2012[7], graphics from www.somersault1824.com)

1.1 Molecular-genetic T-ALL subgroups

Using karyotyping, fluorescence in-situ hybridization (FISH), array comparative genomic hybridization (array CGH) and microarray gene expression profiling, a set of well-defined genetic subgroups that are marked by an arrest at a specific stage of T-cell differentiation have been delineated in T-ALL (**Figure 2**)[3,8-10]. Genomic translocations are recurrent in leukemic samples resulting in the elevated expression of developmentally important transcription factor oncogenes. Hereby, T-cell oncogenes are placed under the control of strong T-cell specific enhancers of the *TCR*β and *TCRαδ* or strong regulatory sequences of T-cell specific genes. For example, the most common translocation t(10;14)(q24;q11) juxtaposes the homeobox (*HOX*) transcription factor *TLX1* to the T-cell specific enhancer of *TCRαδ*[11], whereas t(5;14)(q35;q32) translocates the *HOX* transcription factor *TLX3* to specific regulatory sequences of the T-cell regulator *BCL11B*[12]. Both translocations lead to strong transcriptional activation of the two *HOX* genes, *TLX1* and *TLX3*[8,11-15]. Interestingly, oncogenic activation of TLX1 in transgenic mouse gives rise to lymphoid tumors with long latency[16]. As TLX1 and TLX3 are closely related oncogenes in T-ALL sharing similar gene expression profiles[8-10] and interaction networks[17,18], a similar oncogenic role for TLX3 in T-ALL is presumed although no effective *in vivo* modeling of TLX3 has been reported yet.

Besides *TLX1* and *TLX3*, the following oncogenes have been implicated in chromosomal translocations in T-ALL and define different T-ALL subgroups: the basic helix-loop-helix (bHLH) transcription factors *TAL1*[19], *TAL2*[20], *LYL1*[21] en *BHLHB1*[22]; the LIM-only domain (*LMO*) transcription factors *LMO1*[23], *LMO2*[24] and *LMO3*[9]; the *HOX* genes *NKX2.1*[9], *NKX2.2*[9] and *HOXA*[10] and the transcription factor *MYB*[25]. Although the clinical relevance of genetic subtypes in T-ALL remains controversial, some studies proposed a good prognosis for the *TLX1*-[13] and *TAL1*-[26]rearranged T-ALL patient cases and a dismal prognosis for the *TLX3*-rearranged T-ALL patient cases[27,28].

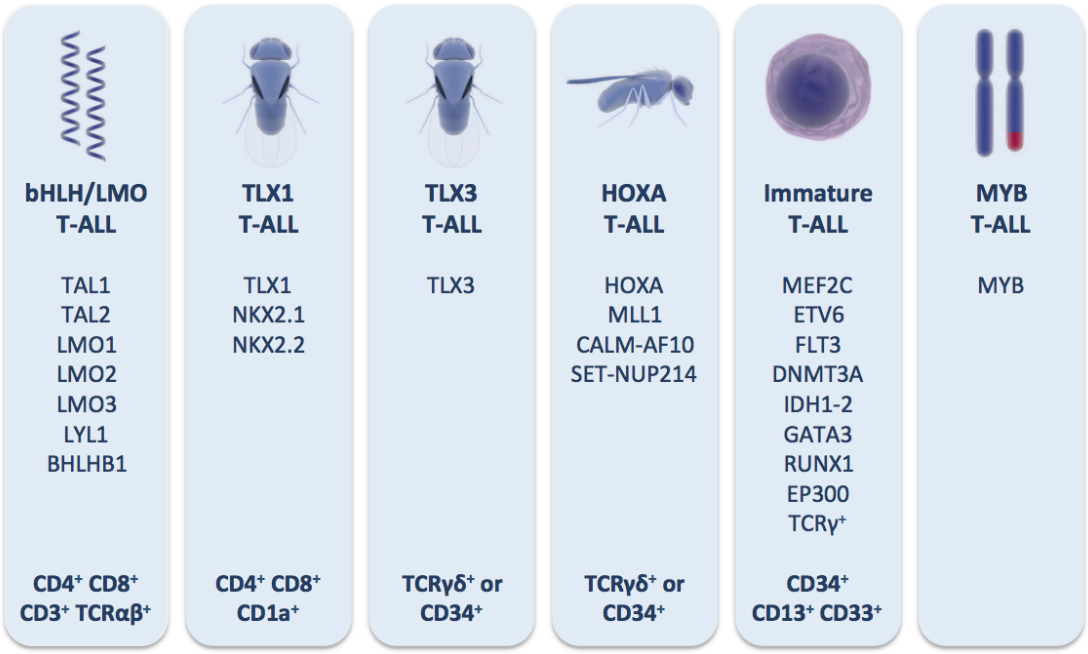

Figure 2. Genetic T-ALL subgroups marked by transcription factor oncogenes, genetic defects and specific T-cell differentiation arrest[3,9,29-32] (graphics from www.somersault1824.com)

Alternatively, genetic defects including chromosomal deletions, fusion genes and somatic mutations have been identified that further define the different T-ALL subgroups including

SIL-TAL1 deletions in the bHLH/LMO subgroup[19], the *CALM-AF10* fusion[33], the *SET-NUP214* fusion[34] and *MLL1* fusions[35] in the HOXA subgroup and mutations in *ETV6, FLT3, DNMT3A, IDH1, IDH2, GATA3, RUNX1* and *EP300* in the immature T-ALL subgroup[3,29-31,36] (**Figure 2**). Notably, the immature T-ALL subgroup is characterized by a gene expression signature associated with hematopoietic stem cells and myeloid progenitors and often shows expression of the myeloid antigens CD13 and CD33[8-10,29,37] and lack of biallelic TCRγ deletion (noted here as TCRγ^{+})[32]. Finally, a recent study demonstrated that immature T-ALLs often display elevated expression of the *MEF2C* transcription factor oncogene[9].

1.2 Defects across the T-ALL subgroups

The introduction of targeted and next-generation sequencing techniques further broadened the genetic landscape of T-ALL by the identification of many novel defects belonging to different molecular pathways[3,5,6,31] (see also **paper 1, 2**). These genetic lesions target genes with important roles in NOTCH1 signaling, cell cycle, hematopoiesis, signal transduction and ribosomal machinery (**Figure 3**). Importantly, like in any other tumor entity, recent sequencing efforts revealed the implication of several key regulators of epigenetic modifiers (**Figure 3**). These defects, together with the other mutations, define the genetic make-up of the malignant T-cells and are present in all T-ALL subgroups.

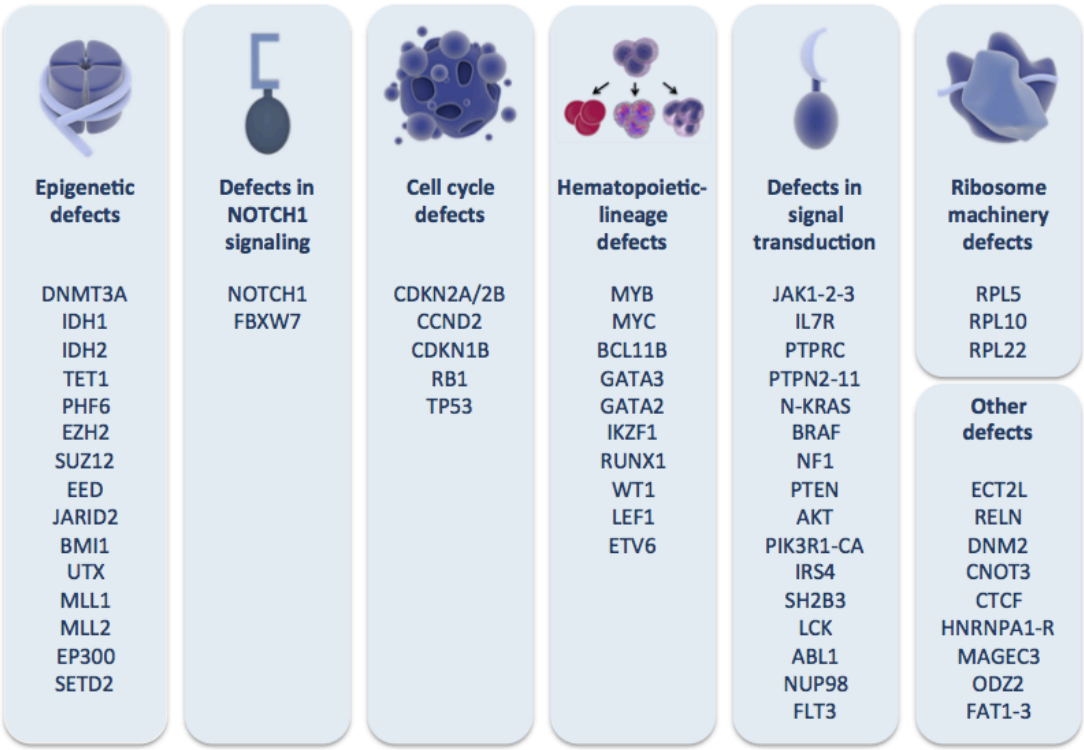

Figure 3. Defects in different molecular pathways contributing to T-ALL pathogenesis[3,6,30,31,36,38] (graphics from www.somersault1824.com)

In the following part, the NOTCH1 and MYB signaling pathways and their involvement in T-ALL will be described in detail, since both oncoproteins will also be discussed further in the thesis. The epigenetic defects will be discussed in-depth in the second part of the introduction (2. The epigenomic landscape of T-cell acute lymphoblastic leukemia and links with therapeutical options).

Defects in the NOTCH1 signaling pathway

The NOTCH1 signaling pathway is a strongly conserved pathway essential for normal T-cell development stimulated through interaction with different NOTCH1 ligands on the cell surface[38] (**Figure 4**). After NOTCH1 stimulation, the NOTCH1 heterodimer receptor is processed through 3 different proteolytic cleavages including the final cleavage by the gamma-secretase complex. The intracellular domain (ICN) of NOTCH1 subsequently translocates to the nucleus and associates with CSL, EP300, MAML and different coactivators (CoA) resulting in transcriptional activation of NOTCH1 target genes[38,39] (**Figure 4**). Important NOTCH1 direct and indirect targets in T-ALL are *MYC*[40,41], *HES1*[42], *CYLD*[43], *PTEN*[44], *IL7R*[45], *PTCRA*[46], *IGF1R*[47], *CCR7*[48], *CCND3*[49], *SKP2*[50] and the signaling pathways PI3K-AKT-mTOR[44,51] and NF-Kβ[43,52]. The E3 ubiquitin ligase FBXW7 subsequently targets NOTCH1 for proteasomal degradation as well as other important oncoproteins like MYC, cyclinE, JUN and MCL1[53,54].

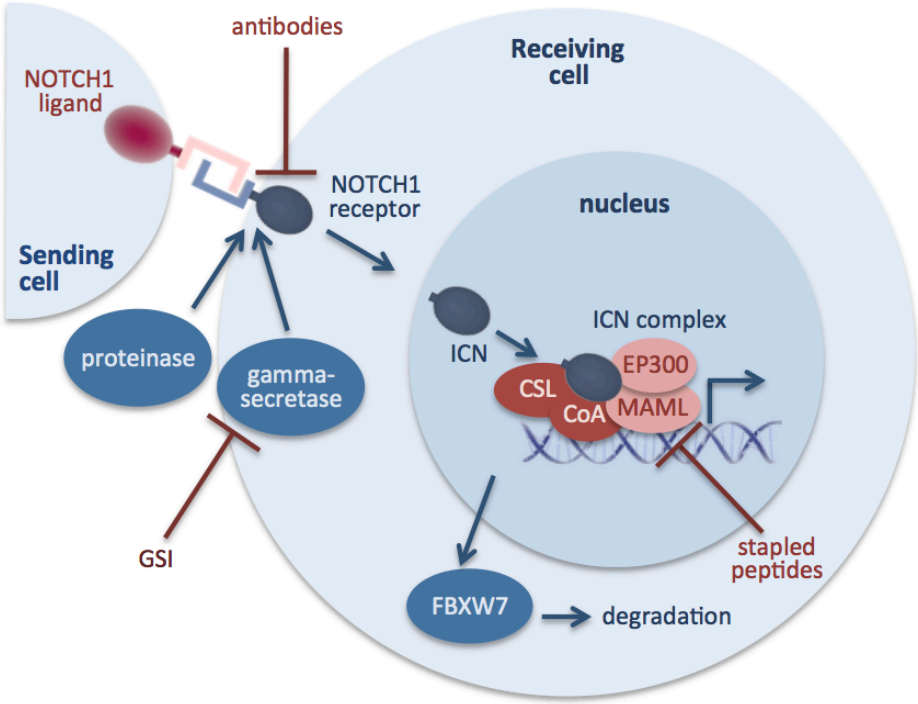

Figure 4. The NOTCH1 signaling pathway (adapted from Grabher et al. Nature Reviews Cancer 2006[39], graphics from www.somersault1824.com)

NOTCH1 is one of the major oncogenic drivers in T-ALL and is highly activated by specific *NOTCH1* mutations (>60% of T-ALL cases)[55], translocations of the strong T-cell specific enhancers of *TCR*β with *NOTCH1* (<1%)[56] or inactivating *FBXW7* mutations (~15%)[57,58]. Constitutive activation of NOTCH1 in a bone-marrow transplantation model provokes the quick formation of T-cell leukemias highlighting the oncogenic potential of NOTCH1 in T-ALL pathogenesis[59]. As the majority of T-ALL patient cases experience highly activated NOTCH1 signaling, therapeutic efforts have been exploited to target NOTCH1 in T-ALL including gamma-secretase inhibitors (GSIs)[38,40,55,60,61], NOTCH1-specific inhibitory antibodies[62] and stapled peptides targeting the NOTCH1 transcriptional complex[63] (**Figure 4**).

The first trials warned against the use of GSIs as single agent as GSI resistance may rapidly occur. Also, major side effects including severe gastrointestinal toxicity were observed in

early studies[60,64]. GSI resistance can result from *PTEN* or *FBXW7* mutations leading to a hyperactivated PI3K-AKT-mTOR signaling pathway[44,57,65]. Notably, combined treatment of GSI with the mTOR inhibitor rapamycin or a dual PI3K-mTOR inhibitor in a panel of T-ALL cell lines resulted in highly synergistic inhibition of T-ALL cell growth[51,66]. Most interestingly, these PI3K-AKT-mTOR pathway inhibitors seem to be the most effective in GSI-resistant cells harboring *PTEN* mutations[44,51].

In parallel, administration of GSI together with glucocorticoids reduced GSI-induced gut toxicity *in vivo* and most interestingly provoked effective cell death in glucocorticoid-resistant T-ALL[61,67]. In accordance with the successful combined treatment of GSIs with glucocorticoids, delivery of an AKT inhibitor together with glucocorticoids restored glucocorticoid-induced apoptosis in glucocorticoid-resistant T-ALL both *in vitro* and *in vivo*[68]. Furthermore, combination of the chemotherapeutic agent vincristine with a dual PI3K-mTOR inhibitor or dual PI3K-AKT inhibitor acted synergistically mediating effective cell death in T-ALLs with constitutive activation of PI3K-AKT-mTOR signaling[69,70]. All together, these studies underscore the importance of multi-drug treatment studies in T-ALL therapy.

As *MYC* is one of the key targets of NOTCH1 in T-ALL[40,41] and secondly also directly involved in T-ALL pathogenesis through chromosomal translocations[71], MYC represents an interesting therapeutic target in T-ALL. Effective MYC inhibition was recently demonstrated both *in vitro* and *in vivo* in many cancer types using small molecule inhibitors including JQ1, I-BET-762, I-BET-151 and PFI-1 against the BET family of chromatin acetyl group readers[72,73]. First clinical trials with the BET inhibitor I-BET-762 have just been initiated in NUT-midline carcinoma and other solid tumors[74]. These BET inhibitors specifically target genes with a super-enhancer controlling it's expression[75]. Also in T-cell leukemia samples, MYC is one of the key targets of these inhibitors[75]. Furthermore, treatment with JQ1 in human and murine T-ALL cell lines enabled a strong block in cell growth and reduction of MYC expression levels[76]. Moreover, JQ1 delivery also inhibited the growth of diagnostic, relapsed and induction-failure pediatric T-ALL patient samples *in vitro*, even in samples that failed to respond to GSI treatment[76]. These observations underscore the therapeutic potential of BET inhibitors in T-ALL, also in GSI-resistant T-ALL patient samples. In addition to MYC, another NOTCH1 target *IL7R* was shown to be sensitive to treatment with BET inhibitors in B-cell ALL (B-ALL) cell lines[77].

Defects in the MYB signaling pathway

The MYB protein is a leucine zipper transcription factor that mostly acts as a transcriptional activator in concert with co-activators CREB binding protein (CBP) and EP300, two histone acetyltransferases[78-80]. MYB expression levels are elevated during early hematopoietic stages and thereafter decrease during maturation[80]. MYB is crucial for hematopoiesis including thymopoiesis. *Myb* knockout mice die early *in utero* displaying severe anemia, likely due to a defect in the erythropoiesis in the fetal liver[81]. Furthermore, *Myb* loss demonstrated a role for MYB in adult hematopoietic stem cell renewal[82] and early T-cell development[83]. In addition, MYB also contributes to the β-selection phase in T-cell development and is critical for the survival of $CD4^+CD8^+$ T-cells and development of $CD4^+CD8^-$ mature thymocytes[84-86]. Furthermore, MYB transcriptionally controls more than 80 target genes[80] including genes of importance in T-cell development including *CD4*[87], *GATA3*[88], *RAG2*[89], *H2A.Z*[90], *BCL-2*[91] and *BCL-XL*[85].

A role for MYB in malignant T-cell development was first demonstrated by the appearance of high grade T-cell lymphomas when *v-Myb*, a truncated and rearranged form of *MYB*, was

ectopically expressed in T-cells in mice[92,93]. Also, mice developing T-cell lymphomas after retroviral infection commonly demonstrated retroviral insertion sites in the *Myb* locus[94,95]. In T-ALL pathogenesis, *MYB* was found to be highly expressed in a subset of T-ALL patients due to translocation of *MYB* to the T-cell specific enhancer of *TCR*β (t(6;7)(q23;q34) - 7%) or by somatic *MYB* duplications (10-15%)[25,96] (**Figure 5**). Notably, *MYB* translocated cases define a separate T-ALL subgroup marked by very young age (median age 2.2 years) and an elevated expression of genes linked to cell cycle, cell proliferation and mitosis[25]. In contrast, *MYB* duplications are identified in cases belonging to all different T-ALL subgroups[25]. The majority of *MYB* duplications are mediated by homologous recombination between Alu repeats resulting in tandem duplications of *MYB*[97]. Elevated MYB levels in T-ALL can also be caused directly by the oncogenic TAL1/GATA3/RUNX1 complex[98] or indirectly through the TAL1/miR-223/FBXW7 regulatory axis[99]. In leukemias harboring MLL1-fusions, *MYB* was shown to be an essential downstream target of MLL1-ENL and MLL1-AF9 contributing to leukemic transformation[100,101]. In addition, MYB also interacts with MENIN to form a complex with MLL1 itself and with MLL1-fusions[102].

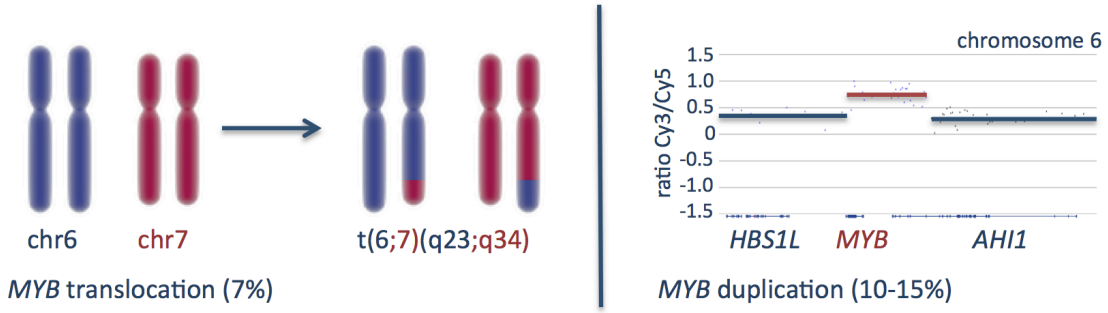

Figure 5. Schematic representation of a *MYB* translocation t(6;7)(q23;q34) detected by karyotype and FISH, and an array CGH plot of a focal *MYB* duplication on chromosome 6 (graphics from www.somersault1824.com)

Knockdown of MYB alone has only small effect on viability, proliferation and cell cycle; but combined knockdown of the T-ALL oncogenes *MYB* and *NOTCH1* in T-ALL cell lines showed a strong synergistic inhibitory effect on proliferation and viability. Furthermore, loss of MYB enabled irreversible T-cell differentiation of T-ALL cell lines[96] underscoring the importance of MYB directed therapies in T-ALL. Direct MYB targeting approaches include short hairpin (sh) RNA mediated decay[96,101] and antisense MYB oligodeoxynucleotides[103], the latter currently being tested in clinical trials[103]. Since MYB functions in concert with the co-activators EP300 and CBP, histone deacetylase inhibitors (HDACi) can be employed as indirect therapeutic approaches targeting MYB[104,105]. Treatment of the *MYB*-duplicated T-ALL cell line CCRF-CEM with HDACi trichostatin A was able to profoundly downregulate MYB expression, indicating that MYB is highly sensitive to histone hyper-acetylation in T-ALL[105]. Interestingly, recent studies identified a super-enhancer that regulates MYB expression[75], suggesting that MYB might also be sensitive to BET inhibitors. In contrast to *MYC* where his super-enhancer is found in many cancer types, the presence of the *MYB* super-enhancer seems to be more restricted to T-cell leukemia samples[75]. Moreover, the BET family inhibitors were shown to have an impact on the MYB pathway since many MYB target genes were affected after JQ1 treatment[101].

2. The epigenomic landscape of T-cell acute lymphoblastic leukemia and links with therapeutical options

DNA is built up from four nucleotides (adenine, cytosine, guanine and thymine). A stretch of 147 base pairs of DNA is wrapped around an octamer of 4 core histone (H) proteins (2 units of H2A, H2B, H3 and H4) shaping a nucleosome, a structure that enables efficient highly condensed DNA compaction in chromosomes during replication (**Figure 6**)[106]. The linker histone H1 is located between 2 nucleosomes enabling further compact packaging of the DNA[107]. The majority of our genome shows a closed compact conformation associated with transcriptional repression, whereas only a minority of our genome is actively transcribed and resides in an open transcriptional configuration[106]. Activation or repression of gene expression is enabled by intimately linked epigenetic modifications including DNA methylation, nucleosome remodeling, histone variants and histone modifications[108]. Epigenetic alterations encompass all heritable changes in gene expression that are not resulting from DNA changes[108]. Besides genetic defects, almost all human cancer types contain malignant epigenetic alterations that contribute to cancer formation[106]. Disturbance of correct epigenetic configuration is postulated to act as a first seminal event in carcinogenesis leading to early abnormal clonal expansion of stem/progenitor cells[106,109].

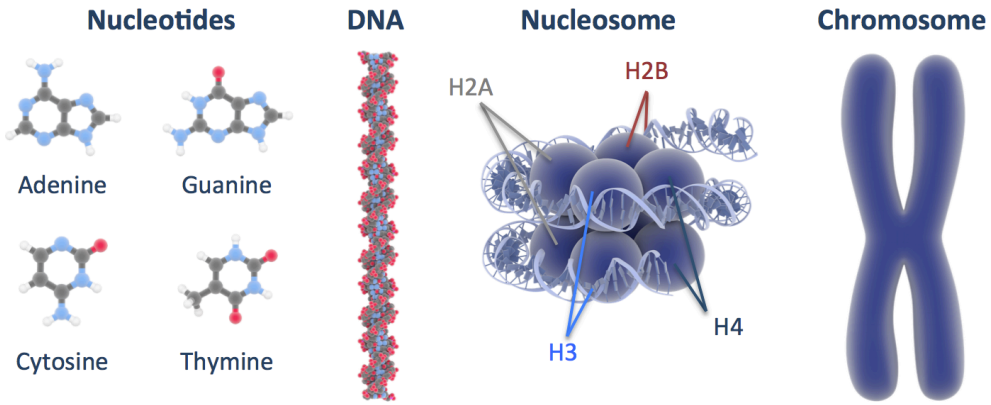

Figure 6. Graphical representation of DNA compaction into chromatin encompassing four nucleotides (adenine, cytosine, guanine and thymine) wrapped around histone proteins forming nucleosomes highly condensed packed in chromosomes during replication (graphics from www.somersault1824.com)

2.1 DNA methylation

DNA methylation encompasses the covalent addition of methyl groups to cytosines mainly in the CpG dinucleotide context[106]. CpG islands are more than 300bp in length, contain a CG content of over 50% and are present at more than half of the genes in vertebrates[110]. DNA methylation is executed by different DNA methyltransferases (DNMT) including DNMT1 for maintenance of DNA methylation and DNMT3A and DNMT3B for *de novo* methylation[106]. Moreover, DNMT3A and DNMT3B seem to cooperate with DNMT1 to maintain DNA methylation. Finally, DNMT3L is a catalytic inactive homologue of DNMT3A and DNMT3B, which is able to stimulate DNMT3A activity[110].

In general, DNA methylation of CpG islands at transcription start sites of the promoter regions results in gene silencing. In contrast, DNA methylation in gene bodies, largely devoid of CpG islands, might enhance transcriptional elongation and play a role in splicing[110] (**Figure**

7). During normal development, most CpG islands on autosomal genes remain unmethylated although the CpG island shores (2kb of sequence on either side of a CpG island) seem to become methylated[111]. Furthermore, large undermethylated regions over 3.5kb in length were recently identified in hematopoietic stem cells (HSCs), called methylation canyons. These hypomethylated regions are enriched for highly conserved, developmentally important genes; whereby active HSC canyons marked with H3K4 trimethylation often contain genes frequently deregulated in leukemia[112].

The cancer epigenome is marked by global hypomethylation and local hypermethylation at CpG islands of thousands of genes[73,108,109,113] (**Figure 7**). These hypermethylated genes can complement a single gene mutation or can collectively disrupt specific signaling pathways[109]. Global hypomethylation encompasses often megabase regions of multiple chromosomes, most frequently CpG-poor regions like repetitive and gene body sequences[73,109].

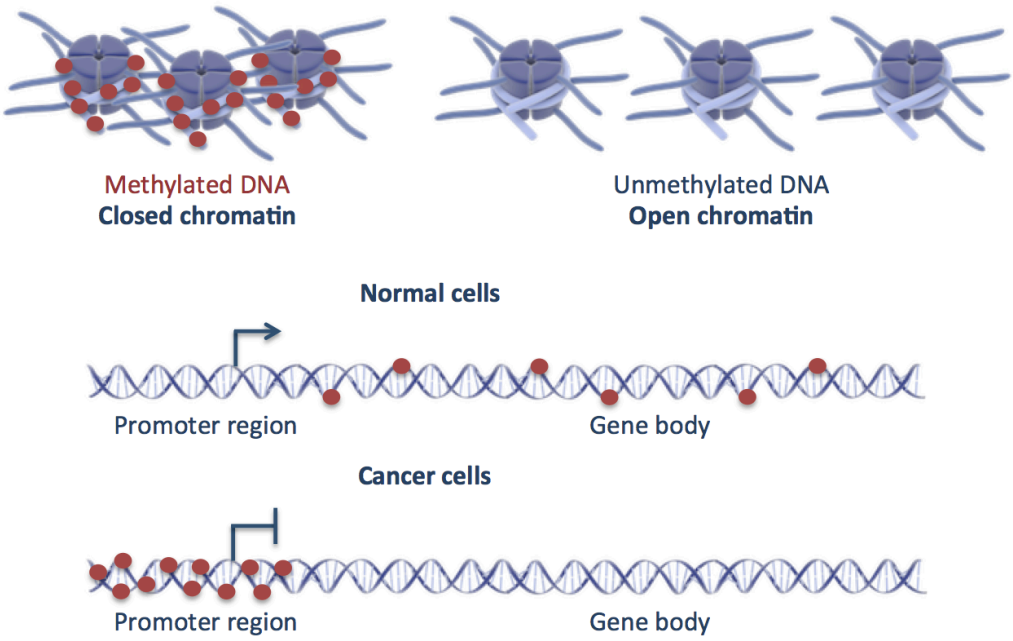

Figure 7. Graphical representation of DNA methylation. Methylated DNA contributes to a closed chromatin formation, whereas unmethylated DNA adds to an open chromatin state. In contrast to normal cells, cancer cells display in general local hypermethylation at CpG-rich promoter regions and global hypomethylation mainly at CpG-poor regions like gene bodies. (graphics from www.somersault1824.com)

In T-ALL, hypermethylation of tumor suppressor genes has been described at CpG islands in the promoter regions or first exons of *CDKN2B*[114], *SYK*[115], *C/EBPA*[116], *PAX5*[117], *ABCG2*[118] and *CDKN1A*[119]. A CpG island methylator phenotype (CIMP) was proposed in T-ALL and this hypermethylator profile (CIMP$^+$) was linked to poor prognosis[120,121]. Interestingly, the majority of genes prone to DNA hypermethylation in the CIMP$^+$ profile were lineage-commitment genes that are regulated by the Polycomb repressive complexes PRC1 and PRC2[73,109,120] and are thought to undergo an epigenetic switch from transient repression towards a tight silencing state[109].

Therapeutic opportunities targeting the DNA methylation machinery encompass DNMT inhibitors (DNMTi) that consist of cytosine analogs like 5-azacitidine (vidaza) and 5-aza-2'-deoxycytidine (decitabine), which have been approved by the US Food and Drug Administration (FDA) for treatment of myelodysplastic syndrome (MDS)[73,108]. These DNMTi

reverse DNMT mediated gene silencing which enables their anti-tumor activity[73]. Mechanistically, the cytosine analogs are integrated in the RNA and/or DNA during replication locking the DNMT through covalent binding[73]. Since $CIMP^+$ T-ALL cases are marked by a hypermethylation profile compared to $CIMP^-$ and normal T-cells[120,121], exploration of DNMTi treatment strategies in $CIMP^+$ T-ALLs would be of great therapeutic interest.

Very recently, *DNMT3A* mutations were identified in immature T-ALL[30,36,122]. In addition, mutations in *TET1*, a gene coding for an epigenetic regulator that converts 5-methylcytosine to 5-hydroxymethylcytosine using cofactors α-ketoglutarate and Fe(II)[123], were discovered in 6% of T-ALL cases[6]. Moreover, immature T-ALLs also show mutations targeting *IDH1* and *IDH2*[30]. Wild-type IDH proteins convert isocitrate and $NADP^+$ into α-ketoglutarate and NADPH. In contrast, mutant IDH proteins generate an overload of 2-hydroxyglutarate consuming α-ketoglutarate and NADPH, which in turn inhibits the TET proteins and JmjC-domain containing histone demethylases (HDM)[73,124]. Both *IDH* and *TET* mutations seem to provoke DNA hypermethylation in cancer pathogenesis[109]. Further exploration of the effects mediated by *DNMT3A*, *TET1, IDH1* and *IDH2* mutations are essential in the further unraveling of T-ALL pathogenesis. Notably, specific drugs targeting mutant IDH have shown effective growth arrest in glioma[125].

2.2 Nucleosome remodeling

Nucleosome remodeling is mediated by ATP-dependent multi-subunit chromatin remodeling complexes that execute unwrapping of the DNA from the histones, repositioning of nucleosomes, evicting histones of DNA, attracting transcription factors for DNA binding and switching of histone variants[73,126,127]. Five types of chromatin remodeling complexes have been identified including the SWI/SNF, the NuRD, the ISWI, the INO80 and the SWR1 families[73,127,128]. Of interest, specific subunits of these nucleosome remodelers enable a range of interactions depending on specific configurations of histones hereby granting different functions to these remodeling complexes. For example, the ATPases of SWI/SNF family consist of BRM and BRG1 and harbor a bromodomain for interaction with acetylated histone tails[129], whereas the CHD1-5 of the NuRD family contain chromodomains for interaction with methylated histone tails[130].

Importantly, ATPase remodelers can promote transcriptional activation by facilitating transcriptional elongation of RNA polymerase II (RNAPII) (primary role of SWI/SNF complexes) or induce transcriptional repression (primary role of NuRD complex)[127]. Of interest, the SWI/SNF protein BRM was shown to interact with the NOTCH1 signaling pathway promoting activation of NOTCH1 targets[131]. Besides their role in transcriptional regulation, nucleosome remodeling is also implicated in other cellular processes including DNA damage response, DNA replication and cellular identity determination[127]. For example, the INO80 and the NuRD family play a role in DNA damage repair upon the occurrence of DNA double-strand breaks (DSBs)[132-134]. In T-ALL, one *ETV6-INO80D* fusion has been detected in an immature T-ALL case[31], but, to date, no other recurrent genetic defects affecting ATPase remodeling complexes have been described.

2.3 Histone variants

Within a nucleosome, histones H2A, H2B and H3 can be exchanged with histone variants including H2A.X and H2A.Z[111,135]. These exchanges enable fast, replication-independent changes to the chromatin in contrast to deposition of the canonical histones[73,136]. Chaperones escort the histone variants to enable exchange of histones[136]. H2A harbors 6 histone variants of which H2A.X is present in 10-15% of nucleosomes. In particular, H2A.X is incorporated in nucleosomes guided by the FACT complex upon DNA damage, acting as a caretaker of our genome[126,136] (**Figure 8**). The FACT complex is essential for transcriptional elongation through nucleosomes by removing of core H2A/H2B dimers[137]. Then DSBs, leading to DNA damage, induce rapid phosphorylation of serine 139 of H2A.X forming γH2A.X in chromatin regions up to 1-2Mb around the DSBs[136]. The kinases ATM and ATR perform the specific phosphorylation of H2A.X and enable the assembly of DNA repair complexes like the INO80 remodeler[136,138]. The histone variant H2A.Z has a broad range of functions, is located mainly at transcription start sites but also in heterochromatin, and is guided by INO80 and SWR1 remodelers[136]. No mutations in histone variants or histone variant chaperones have been described in T-ALL so far, but loss of the T-ALL tumor suppressor PHF6 can exert an increase in global levels of γH2A.X indicating a putative role for PHF6 in DNA damage repair (see further) (**paper 1**)[5].

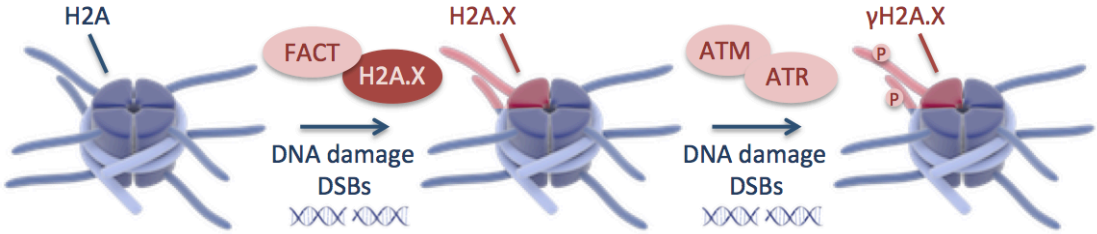

Figure 8. Exchange of the core histone H2A by the histone variant H2A.X guided by the chaperone FACT upon DNA damage caused by DSBs in the DNA. Subsequently, the kinases ATM and ATR catalyze the phosphorylation of H2A.X forming γH2A.X resulting in the attraction of the DNA repair machinery[136] (graphics from www.somersault1824.com)

2.4 Histone modifications & their mediators

Histone modifications on the globular domain and the histone tails include lysine (K) acetylation, lysine and arginine methylation, serine and threonine phosphorylation, lysine ubiquitynilation, lysine sumoylation, arginine deimination, proline isomerization and glutamic acid ADP-ribosylation[106,139]. These histone modifications are transferred by specific chromatin writers and modified or reverted by chromatin erasers. An additional set of chromatin regulators can read the histone modifications and subsequently mediate interactions between a protein or protein complex and the respective histone modification(s)[73].

Histone acetylation is linked to transcriptional active regions and is accomplished by neutralization of basic charges of lysines leading to unfolding of the DNA[138]. Acetylation of histones is applied by histone acetyltransferases (HAT) and removed by histone deacetylases (HDAC). Histone acetyltransferases can be divided into 3 families; the GNAT family, the MYST family and the CBP/EP300 family[138]. The HATs can acetylate multiple lysines of both core histone proteins and non-histone proteins including TP53, RB1 and E2F[138]. The HDAC

family consists of 18 HDACs that remove acetyl groups from histone tails and non-histone proteins like TP53, E2F and TFIIF[138].

In contrast, histone methylation can be associated with active or repressed gene expression depending on the lysine residue that is methylated and the degree of methylation (un, mono, di and trimethylated). For example, histone H3 lysine 27 trimethylation (H3K27me3) and H3K9me3 are linked to heterochromatin-associated gene silencing, whereas H3K4me3, H3K36me3 and H3K79me2 are linked to active transcription enriched in euchromatin[106,138]. H3K27me3 is the prototypical mark of the Polycomb repressors linked to a more transient repression of DNA called facultative heterochromatin, whereas H3K9me3 is mainly present in stable tightly packed DNA called constitutive heterochromatin[111]. In general, H3K4me3 is enriched at transcription start sites (TSS) in promoter regions of genes, whereas H3K36me3 and H3K79me2 are mainly detected in gene bodies[111]. Specific enhancers that contribute to gene expression are marked by histone 3 lysine 27 acetylation (H3K27ac) and H3K4me1-2 in active chromatin and contain H3K9me2-3 in a repressed transcriptional state[111]. Methyl groups on lysines are placed by histone methyltransferases (HMT) using the cofactor S-adenosyl methionine (SAM) and removed by histone demethylases (HDMs)[111].

In T-ALL, recurrent genetic defects have been identified in the putative histone reader *PHF6*[5] (see **paper 1**), the H3K27me3 HMT *PRC2* (targeting the members *EZH2, SUZ12, EED* and *JARID2*)[31,140,141], the H2A ubiquitinylase *PRC1* (targeting the member *BMI1*)[36], the H3K27me3 HDM *UTX*[6] (Van der Meulen et al. submitted) (see **paper 2**), the H3K4me3 HMTs *MLL1* and *MLL2*[36], the HAT *EP300*[31] and the H3K36me3 HMT *SETD2*[31].

The putative histone reader PHF6

The PHF6 protein belongs to a large family of proteins containing a plant homeodomain (PHD) finger, also found in nuclear proteins and chromatin-associated factors[142]. A Cys4-His-Cys3 motif characterizes the PHD finger and mediates the binding of two zinc ions[142]. Until now, about fifteen PHD finger-containing proteins have been identified that are capable of reading the H3K4me3 mark[142]. These PHD-containing proteins contain a specialized structural cage consisting of crucial hydrophobic or aromatic residues to enclose preferentially the H3K4me3 side chain[142]. Furthermore, the recognition of 3 other histone lysine modifications was demonstrated to be mediated by PHD-containing proteins, including unmodified H3K4[143], methylated H3K36[144] and methylated H3K9[145]. Moreover, PHD fingers can also bind acetylated lysines[146] and can interact with non-histone proteins like the third PHD finger of MLL1 that binds both H3K4me3 and the MLL1-associated co-repressor Cyp33 hereby switching between transcriptional activation and repression[147]. Regarding PHF6, no interactions between its two imperfect PHD fingers (Cys4-His-Cys-His) and specific histone H3 marks or non-histone proteins have been elucidated yet.

Next to two imperfect PHD fingers, four nuclear localization signals are present in the PHF6 protein targeting PHF6 to the nucleus and nucleolus[148]. In HEK293T cells, PHF6 protein levels are most profound in the nucleoplasm compared to the nucleolus measured by western blotting[133]. Mass spectrometry analysis in HEK293T cells enabled the identification of PHF6 interaction partners including CHD3, CHD4, RBBP4 and RBBP7 of the NuRD complex (**Figure 9**) next to histones, splicing factors, 40S and 60S ribosomal proteins, and other nucleolar proteins[133]. The NuRD-PHF6 complex was shown to be mainly present in the nucleoplasm, whereas PHF6 interacts with other proteins in the nucleolus probably mediating distinct functions[133]. Of interest, both RBBP4 and RBBP7 have been shown to interact with other

chromatin complexes including the PRC2 complex[149] (**Figure 9**). The histone-binding proteins RBBP4 and RBBP7 provide structural support and promote protein-protein interactions[134].

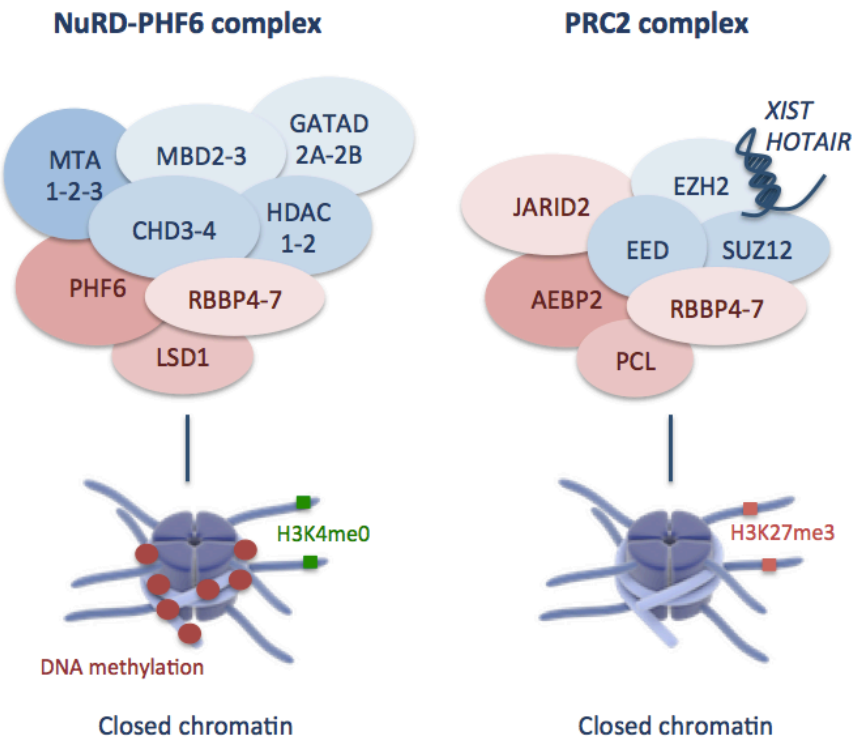

Figure 9. Graphical representation of the chromatin complexes NuRD-PHF6[133,134] and PRC2[150] with matched chromatin conformation (graphics from www.somersault1824.com)

Post-transcriptional regulation might further affect PHF6 function as it becomes phosphorylated during cell cycle progression[151] and after DNA damage by ATM and ATR[152]. In addition, loss of PHF6 significantly increases global levels of γH2A.X present in the chromatin, which has also been observed in the context of T-ALL cells[5,152]. The NuRD complex is also involved in DNA damage repair[133,134] and, likewise PHF6, target of the ATM and ATR DNA damage checkpoint kinases[152]. Therefore, besides a possible role of NuRD and PHF6 in transcriptional regulation, the NuRD-PHF6 complex might also be involved in active DNA repair[133].

The nucleolar localization of PHF6 has first been described by Lower et al. by co-localization studies with the nucleolar protein nucleolin[148]. The nucleolus is a subnuclear compartment primarily occupied by ribosomal biogenesis. Ribosomal genes (rDNA) are actively transcribed to generate mature rRNAs that subsequently assemble with ribosomal proteins to form the ribosome subunits[153]. In the nucleolus, PHF6 binds to rDNA promoter sequences resulting in repression of rDNA transcription. Loss of PHF6 establishes an arrest at the G2/M phase and inhibited cell proliferation, leading to DNA damage marked with increased level of γH2A.X at the rDNA promoter[154].

Recurrent inactivating mutations and deletions were identified in the X-linked *PHF6* gene in 16% of pediatric and 38% of adult T-ALL patient samples (see **paper 1**)[5]. Furthermore, hypermethylation of the *PHF6* promoter region occurs in 10% of T-ALL cases and has been proposed as an additional mechanism of *PHF6* inactivation[121]. The presence of *PHF6* mutations in T-ALL is significantly associated with *TLX1* and *TLX3* aberrations[5], *NOTCH1* mutations, *SET-NUP214* rearrangements and *JAK1* mutations[155]. Frequent somatic inactivating mutations affecting *PHF6* were also reported in acute myeloid leukemia

(AML)[156-158], chronic myeloid leukemia (CML) in blast crisis[159], bladder cancer[160] and hepatocellular carcinoma[157]. In a large AML study, somatic *PHF6* mutations were linked to a reduced overall survival[158]. Interestingly, *PHF6* mutations are more frequently found in male T-ALL and AML patients, two leukemia types that display a disturbed gender distribution with a higher prevalence in males (T-ALL: ~3/1; AML: ~1.3/1)[5,156]. The identified mutations in this X-linked gene might provide a possible explanation for the unbalanced male-to-female ratio present in these cancer types.

In developmental diseases, *PHF6* mutations were first reported in 2002 to be the causal event leading to the Börjeson-Forssman-Lehmann syndrome (BFLS)[148]. BFLS patients are characterized by large ears, small genitalia, epilepsy, obesity with gynaecomastia, shortened abnormal toes, tapered fingers and intellectual disability[161]. In general, BFLS affects predominantly males with milder or no symptoms in females[161] and *PHF6* defects have only been reported in 2 female BFLS patients[162]. Of interest, a BFLS patient was reported who developed T-ALL at age 7, suggesting that BFLS may represent a cancer predisposition syndrome[163]. A recent report identified *de novo PHF6* defects in 7 females that contain BFLS characteristics but are also marked with distinct features like linear skin hyperpigmentation, hypoplastic nails, dental anomalies, sparse hair and brachyclinodactyly hereby broadening this X-linked disorder[164]. Using whole-exome sequencing, two *de novo PHF6* mutations were also identified in patients with the Coffin-Siris syndrome, a syndrome caused mainly by mutations in genes coding for members of the SWI/SNF remodeling complex[165].

Furthermore, an important role for PHF6 in cortical neuronal migration was elucidated[166]. In the developing cerebral cortex, PHF6 interacts with the PAF1 transcription elongation complex promoting transcription of the neuronal gene NGC/CSPG5[166]. The disturbed PHF6-PAF1-NGC/CSPG5 pathway gave rise to heterotopias in the cerebral cortex in which neurons are hyperexcitable[166], which can contribute to the pathogenesis of the developmental disorders described above.

The Polycomb repressor complexes PRC1 & PRC2

The Polycomb repressor complexes encompass 2 multi-protein complexes, PRC1 and PRC2. PRC2 consist of the core members EZH1/2, SUZ12, EED and RBBP4/7, interacts with HDACs and DNMTs, and enables mainly di- and trimethylation of H3K27 provoking transcriptional repression[126,138,150] (**Figure 9**). PRC1 is built up with core components from 4 protein families including the RING1 family (RING1A/B), the CBX family (CBX2/4/6/7/8), the PCGF family (PCGF1/2/3/5/6 and BMI1) and the HPH family (HPH1/2/3)[107]. PRC1 recognizes H3K27me3 by a CBX member and mono-ubiquitinylates H2A by a RING family member. In this way, PRC1 maintains the silenced state by restraining RNAPII and preventing eviction of H2A-H2B dimers[107,150].

The PRC2 complex is mainly present at CpG-rich promoter regions, whereas the PRC1 complex binds to parts of the gene bodies as well[107]. The DNA-binding proteins AEBP2, JARID2 and the 3 PCL proteins PHF1, MTF2 and PHF19 were shown to co-localize with PRC2 and its H3K27me3 mark in CpG-rich promoters of PRC2 targets[143,204] (**Figure 9**). Furthermore, PRC2 acts in concert with the long intergenic non-coding RNAs (lincRNAs) *XIST* at the inactive X-chromosome and *HOTAIR* at the *HOXC* locus hereby possibly guiding PRC2 to these specific DNA sequences in the genome[111,150] (**Figure 9**). Besides CpG-rich promoters, the silencing mark H3K27me3 can also be found at intergenic regions, subtelomeric regions and long-terminal repeat retrotransposons[150]. Of interest, the Polycomb complexes are crucial during

normal embryonic development since deletion of *Ezh2, Suz12, Eed* or *Ring1B* leads to early embryonic lethality[150].

The Polycomb repressors are important for the maintenance of tissue-specific gene expression of several thousands of genes[111]. In particular, Polycomb proteins are essential for correct homeotic gene expression during animal development[150]. Furthermore, a dedicated role for Polycomb repressors is set in gene expression regulation in embryonic stem cells (ESCs). In ESCs, about a fifth of CpG-rich promoters are enriched for H3K27me3 but also contain H3K4me3 defining them as bivalent promoters that are transcriptionally silent[111,150]. Next to H3K27me3 and H3K4me3, bivalent promoters are also marked with the histone variant H2A.Z, paused RNAPII and lack of DNA methylation[107,150] (**Figure 10**). Interestingly, these poised bivalent promoters are mainly associated with developmentally important genes that can be rapidly switched on during differentiation[109,111]. In cancer, these gene promoters can become *de novo* methylated by interacting with DNMTs leading to constitutive silencing[109]. Of note, PRC1 localizes together with PRC2 to a smaller set of PRC2 targets including key developmental regulators[111], but PRC1 can also bind in the absence of PRC2[167].

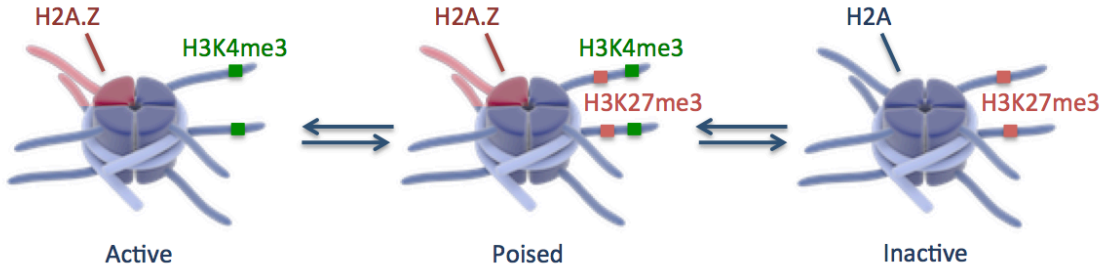

Figure 10. Active, poised and inactive promoters marked by presence or absence of H3K27me3, H3K4me3 and the histone variant H2A.Z in ESC respectively (graphics from www.somersault1824.com)

Intriguingly, PRC2 can act both as an oncogene or show tumor suppressor activity depending on its cellular context. Namely, heterozygous mutations at hotspot Tyr641 in *EZH2* were first identified in 2 lymphoma subtypes arising from germinal center B-cells including diffuse large B-cell lymphoma and follicular lymphoma. Co-occurrence of wild-type EZH2 with the Tyr641 mutant establishes an increase of H3K27me3 at Polycomb target genes[168,169]. The first inhibitor affecting H3K27me3 and EZH2 protein levels was the S-adenosylhomocysteine hydrolase inhibitor 3-deazaneplanocin A (DZNep) inducing reactivation of PRC2 target genes and apoptosis of cancer cell lines[170]. Next, specific EZH2 inhibitors like GSK-126 were discovered that provoke global H3K27me3 loss reactivating PRC2 target genes, which is observed most profoundly in lymphoma samples with activating *EZH2* mutations[171]. One EZH2 specific inhibitor, EPZ-6438, has already entered phase I/II clinical trials in solid tumors and B-cell lymphomas[74].
In contrast, inactivating deletions and mutations in *EZH2* and cofactors have been identified in malignant myeloid diseases[172,173] and T-ALL[31,140,141]. The tumor suppressor activity of PRC2 in the T-cell lineage was further confirmed using a conditional *Ezh2* knockout mouse model that spontaneously developed T-cell leukemia[140] and xenografts of human T-ALL cell lines[141]. Of note, NOTCH1 activation in T-ALL leads to a loss of H3K27me3 by eviction of the PRC2 complex of NOTCH1 target genes. Interestingly, NOTCH1 target genes are enriched for known PRC2 target genes[141].

The PRC1 member BMI1 was first linked to leukemogenesis through its interaction with the oncoprotein MYC in B-cell lymphomas[174], inhibiting *CDKN2A-B* expression and escaping cellular senescence[167,175]. Leukemias harboring MLL1 fusions cooperate with BMI1 to maintain leukemia initiating cells, whereas BMI1 drives progression to acute blast crisis in BCR-ABL1 rearranged CML cases[176]. Very recently, the first *BMI1* mutation was detected in immature T-ALL[36], but research is needed to further explore the prevalence of *BMI1* defects and their role in T-ALL pathogenesis.

The H3K27me3 demethylase UTX

Loss-of-function defects in the X-linked *UTX* gene are identified in a broad range of cancers[177] including T-ALL[6] (see **paper 2**) and can cause a specific hereditary disorder called the Kabuki syndrome[178]. The role of UTX in normal development and disease is discussed in detail in chapter 2 (review) of this doctoral thesis[179]. Briefly, the UTX family members UTX and JMJD3 were recently identified as histone H3K27me2/3 demethylases[180-183]. In contrast, no enzymatic activity was detected for the third family member UTY[180,184]. The catalytic activity of UTX is linked to *HOX*[181,182] and *RB*[185] network regulation in agreement with the co-operation of UTX with the MLL2-3 H3K4 methyltransferase complex[186,187] (**Figure 11**). In addition, an H3K27me2/3 demethylase independent function for the UTX family was uncovered in promoting general chromatin remodeling in concert with the BRG1-containing SWI/SNF remodeling complex[189]. Notably, UTX is essential for cellular reprogramming[190], embryonic development and tissue-specific differentiation, whereby UTY can surprisingly partly compensate a set of UTX functions[191-195].

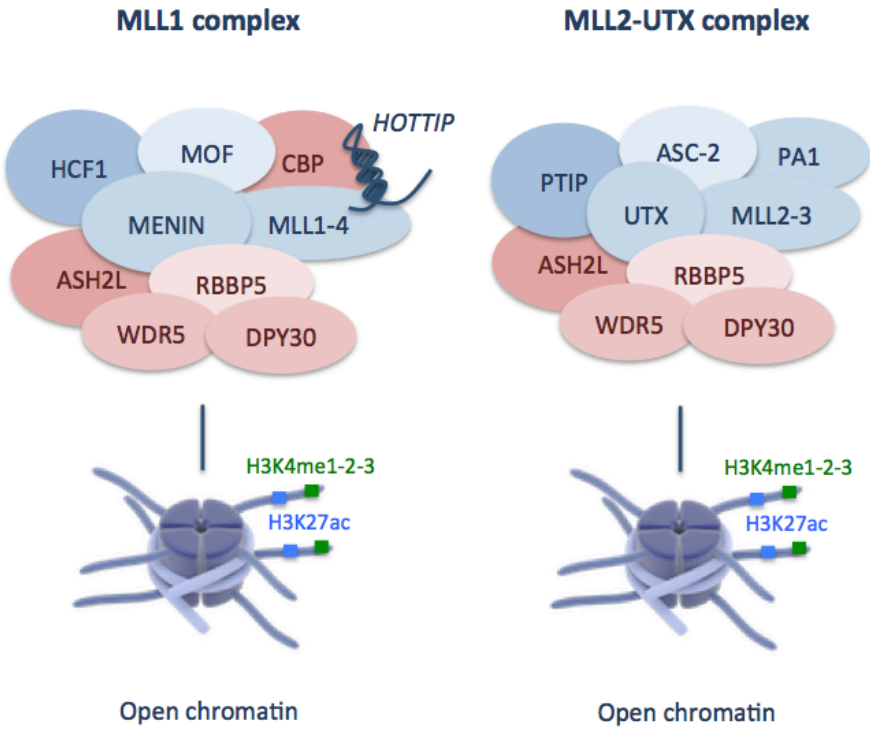

Figure 11. Graphical representation of the MLL1 complex[188] and the MLL2-UTX complex[186-188] with matched chromatin conformation (graphics from www.somersault1824.com)

The H3K4me3 histone methyltransferases MLL1 & MLL2

The MLL1 complex mediates active gene transcription and encompasses the core complex members WDR5, RBBP5 and ASH2L as well as the complex protein associate MENIN that can guide MLL1 to specific target genes[142,167] (**Figure 11**). The MLL1 protein has a SET domain to write the activation mark H3K4me3, a PHD finger domain to read H3K4me2/3 or Cyp33, a CXXC domain to recognize unmethylated CpG islands and a transactivation domain to interact with the HAT CBP[126,142,147,167,188]. The best-characterized MLL1 target genes are the *HOX* gene family members, involved in hematopoietic differentiation, animal body patterning and leukemogenesis[126]. The lincRNA *HOTTIP* can interact with WDR5 to guide WDR5-MLL1 complexes to *HOXA* loci inducing transcriptional activation[196]. Furthermore, MLL1 plays a role in cell cycle by directly regulating key targets involved in cell cycle like *cyclinA*, *cyclinB*, *cyclinE*, *CDKN2A* and *E2F*[197] and by controlled expression of MLL1 itself by SCF and APC/C[188] during different cell cycle transition phases[198]. In ESCs, MLL proteins contribute to stem cell gene activation through interaction of WDR5 with OCT4 to maintain high H3K4me3 levels at OCT4 target genes including self-renewal genes[199].

MLL1-rearranged leukemias display elevated *HOXA7*, *HOXA9, HOXA10* and *MEIS1* levels essential for leukemic transformation[74,109]. In T-ALL, *MLL1* fusions encompass most frequently *MLL1-AF4* and *MLL1-ENL* present in approximately 5% of cases[3]. MLL1-AF4 and MLL1-ENL leukemias have elevated H3K79 methylation levels through abnormal recruitment of the H3K79me3 HMT DOT1L[73,200,201]. Of interest, increased H3K79 methylation levels by enhanced DOT1L activity are also observed in CALM-AF10 fusion leukemias resulting in upregulation of *HOXA5*[202,203]. Notably, ENL is a subunit of the SWI/SNF remodeling complex whereby the MLL1-ENL fusion also cooperates with the SWI/SNF complex to activate *HOXA7* transcription[126,204].

Interestingly, DOT1L inhibitors have been generated that inhibit H3K79 methylation at MLL1-fusion target genes and specifically inhibit *MLL1*-rearranged leukemic cells both *in vitro* and *in vivo*[205]. Mechanistically, the DOT1L inhibitor competes with the SAM substrate that is essential for the HMT function of DOT1L. A phase I clinical trial has been initiated in acute leukemia patients[73]. Another player in normal MLL1 function and MLL1-rearranged leukemia is MENIN, which can be inhibited by the MI-2 inhibitor targeting the MLL1-MENIN interaction leading to effective apoptosis in MLL1-rearranged cells[206]. As MENIN is also important for normal MLL1 function, more research is needed to explore the possible side effects on normal hematopoiesis.

In addition, *MLL2* mutations were recently identified in 10% of adult immature T-ALL cases[36]. Of interest, an MLL2-3 complex was purified with main members WDR5, RBBP5, ASH2L, DPY30, PTIP, ASC-2, PA1 and the histone H3K27me2/3 eraser UTX[186,187] (**Figure 10**). So H3K4 methylation can possibly cooperate with removing of the H3K27me2/3 mark leading to gene activation. The oncogenic effect mediated by these *MLL2* mutations will need to be further explored in the pathogenesis of T-ALL.

The histone acetyltransferase EP300

EP300 belongs to the CBP/EP300 family of HATs and shares 63% of amino acids with CBP[207]. The 2 family members share common functional roles such as acting as a transcriptional cofactor for oncoproteins including MYB[78,79], but also serve specific non-overlapping roles in different cellular processes like the role of EP300 in the TGFβ signaling pathway[207,208].

Mechanistically, both EP300 and CBP can acetylate all core histone proteins resulting in active gene transcription[207] and acetylate non-histone proteins including MYB, TP53, E2F and RB1 contributing to enhanced transcriptional activation and protein-protein interactions[207].

In T-ALL, inactivating *EP300* mutations were identified in immature T-ALL cases[31]. Of interest, chimeras with loss of EP300 develop hematological malignancies including thymic lymphomas defining *EP300* as a tumor suppressor gene in leukemia[207]. HDAC inhibitors (HDACi) provoke a strong anti-tumor activity by reversing gene silencing[73]. Vorinostat (SAHA) and romidepsin are the first HDACi that are approved by the FDA for treatment of T-cell cutaneous lymphoma[108,109]. At present, clinical trials are initiated in a broad range of cancer types with the FDA approved as well as novel HDACi[73]. These HDACi might be also beneficial in treating T-ALL patient samples harboring inactivating *EP300* mutations.

The H3K36me3 histone methyltransferase SETD2

The SETD2 protein acts as a H3K36 methyltransferase enabling active gene transcription[209]. Unlike NSD1 and MMSET that are mono and dimethyltransferases of H3K36, SETD2 mainly trimethylates H3K36 and couples H3K36me3 to transcriptional elongation[209]. Furthermore, SETD2 has a role in splicing[210,211], interacts with hnRNPL[212] and TP53[213], and facilitates DNA mismatch repair during cell cycle[214]. Importantly, SETD2 plays a crucial role in embryonic development since homozygous knockout mice die at embryonic day E10.5-E11.5 marked with a loss of H3K36 trimethylation[215]. Mutations in *SETD2* were first reported in 3% of renal cell carcinoma samples[216] and were recently described in 8% of immature T-ALL cases[31].

2.5 Intimately linked epigenetic modifications

Aberrant DNA methylation is linked to altered histone modification patterns[73]. Silenced genes marked by hypermethylation of the CpG islands in their promoter regions are characterized by loss of H3-H4 acetylation, H2A.Z and H3K4 trimethylation; and gain of H3K9 di- and trimethylation[109,217]. DNA methylation is recognized by methyl-binding proteins (MBD) which are able to associate with complexes containing HDAC, HMT and chromatin remodeling activities[126]. In contrast, accessible H3K4me3-enriched regions at CpG-rich promoters are marked by hypomethylation, histone acetylation, RNAPII, occupancy of the histone H2A.Z variant and nucleosome-depleted regions upstream of their TSS[109,111]. Actively transcribed genes have elevated H3K36 methylation and are also marked by cytosine methylation and deacetylated lysines in their gene bodies, which might promote transcriptional elongation[109,218].

A direct interaction is also seen between different chromatin players, for example the H3K27me2/3 eraser UTX and H3K4me3 methyltransferase MLL2 reside in the same complex, erase the H3K27me3 mark and add the H3K4me3 mark, leading to transcriptional activation[142,186,187]. Furthermore, MLL1 has been co-purified with the HATs CBP and MYST hereby directly linking histone methylation and acetylation to gene activation[167].

Combination therapies between DNMTi and HDACi have shown synergistic activities probably due to the interrelationships between epigenetic silencing processes[108,109]. Clinical trials with this dual therapeutic epigenetic approach are ongoing in many cancer types[108,109]. Hence, a tight controlled interaction between histone modifiers, DNA methylation and ATP-dependent chromatin remodeling complexes is present and can be targeted simultaneously.

3. The microRNAome of T-cell acute lymphoblastic leukemia

3.1 MicroRNA biogenesis & function

Next to genetic and epigenetic regulation of gene expression, another layer of transcriptional regulation is executed by small non-coding RNAs called microRNAs (miRNAs) that repress (mainly in animals) or cleave (mainly in plants) their target genes resulting in negative transcriptional or translational regulation[219]. MiRNA genes are located intronic or exonic in coding regions or in intergenic regions in our genome[220]. The biogenesis of a miRNA starts with the transcription of the miRNA gene by mostly RNAPII (or sometimes RNAPIII) in the nucleus creating a long RNA precursor named pri-miRNA (**Figure 12**). Subsequently, the pri-miRNA is cleaved into a ~70 nucleotide (nt) long pre-miRNA by RNAse III enzyme Drosha with support of the double-stranded RNA-binding protein Pasha. Next, the pre-miRNA is transported by the nuclear transport receptor Exportin-5 to the cytoplasm and cleaved by the second RNAse III enzyme Dicer resulting in the formation of a ds ~22 nt long miRNA-miRNA* duplex. After unwinding of the miRNA-miRNA* duplex by helicases, the mature miRNA is incorporated in the miRNA-associated multiprotein RNA-induced-silencing complex (miRISC). The miRNA target genes are subsequently cleaved by ribonucleases present in the miRISC in case of perfect complementarity or translationally repressed through binding of the miRNA within the 3' untranslated region (UTR) of the mRNA in case of imperfect complementarity[219,220]. An unexpected role in translational activation of target genes by miRNAs was recently demonstrated, but more research is needed to further explore this surprising mechanism of action[221].

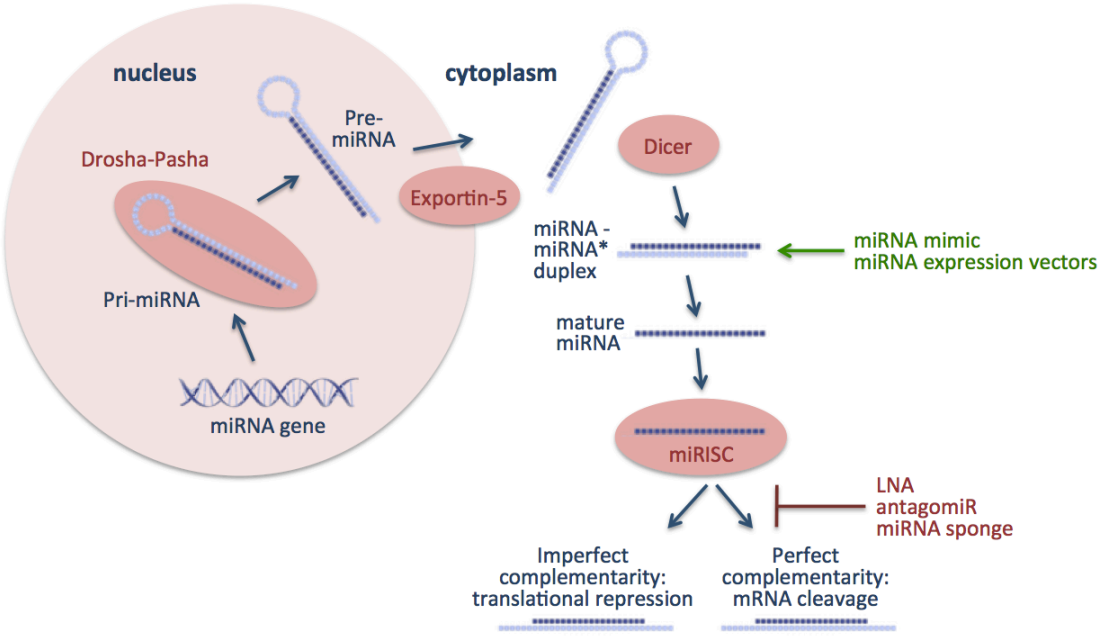

Figure 12. MicroRNA biogenesis pathway and miRNA therapeutic agents (adapted from Esquela-Kerscher & Slack Nature Reviews Cancer 2006[219], graphics from www.somersault1824.com)

To identify possible miRNA target genes, most bioinformatic algorithms base their search on the complementarity between the miRNA seed region (first 2-8 bases at 5'end) and the 3'UTR region of an mRNA. Each miRNA might target more than 200 mRNAs placing one third of mRNAs under the control of these non-coding RNA molecules[219]. MiRNAs play an

important role in many tissue-specific developmental processes like for example ESC differentiation by miR-134[222] and T-cell differentiation by miR-150[223] and miR-181a[224,225].

Abnormal miRNA expression can be caused by deletion, amplification, translocation, mutation or aberrant methylation provoking downregulation or overexpression of specific miRNAs contributing to disease and cancer[219]. In agreement, more than 50% of miRNAs are located in cancer-associated genomic regions that are prone to genomic alterations[226]. Of note, miRNA expression was found to be globally lower in cancer samples than in corresponding normal tissue[227]. Furthermore, miRNAs were shown to be able to classify human tumors according to their embryonic lineage whereby for example hematopoietic tumors cluster separately from the endothelial tumors[228]. Also, miRNA signatures or single miRNAs can harbor a diagnostic or prognostic value useful in the clinical management of cancer therapy[227]. For example, by use of a miRNA classifier the tissue of origin could be determined of metastatic tumors of unknown primary site, and is more efficient than an mRNA classifier[229]. So miRNAs can reflect the developmental history of the cancer types underscoring the role of miRNAs in tissue-specific developmental functions[219].

3.2 MicroRNAs in T-cell acute lymphoblastic leukemia

A classical mechanism of gene deregulation in T-ALL through TCR rearrangement driven formation of translocations was reported for the miR-17-92 cluster (juxtaposition to the *TCRA/D* promoter)[230]. Secondly, the miR-17-92 cluster resides in a region of recurrent gain on chromosome band 13q31.2-q31.3 in a subset of T-ALLs contributing to overexpression of the members miR-17, miR-20a and miR-19[231]. By use of the well-established NOTCH1 driven T-ALL inducing mouse model[59], ectopic expression of miR-19 and NOTCH1 resulted in a strong acceleration in T-ALL onset compared to NOTCH1 only murine T-ALLs[230]. Hence, miR-19 acts as a novel oncogenic miRNA (oncomiR) and can cooperate with NOTCH1 in T-ALL[230].

Subsequent to this observation, an unbiased shRNA screen was performed to identify protein-coding genes that would phenocopy miR-19 overexpression and thus could be further screened as bona fide miR-19 target genes[230]. Mechanistically, the shRNA encoding plasmids are integrated in the genome after efficient transduction of the leukemic cells. Next, the shRNAs are generated using the miRNA processing machinery mimicking pri-miRNAs[232]. The shRNA screen yielded a series of hits with the top candidates including Bim, Pten, Prkaa1 and Ppp2r5e[230]. Loss of Pten and Bim provided a strong acceleration of T-ALL onset in the NOTCH1 T-ALL mouse model in accordance with the introduction of miR-19[230]. In a collaborative effort with the Wendel lab (MSKCC, NY, USA), we further expanded this regulation to a network of interacting oncomiRs miR-20a, miR-92, miR-223, miR-26a, miR-27a and miR148a/152 with additional T-ALL tumor suppressor genes Phf6, Ikzf1, Nf1 and Fbxw7 (see **paper 3**)[233]. Finally, CYLD was discovered as yet another direct miR-19 target in T-ALL hereby negatively regulating the NF-κβ pathway[234].

Of interest, miR-223 overexpression also contributes to T-ALL, which is directly activated by the TAL1 oncoprotein subsequently leading to downregulation of the miR-223 target FBXW7[99,235]. In accordance, TAL1-positive T-ALL patient cases harbor a higher miR-223 expression than TAL1-negative cases[99]. Furthermore, miR-223 resembles *TAL1* expression during T-cell development with highest expression in very immature T-cell stages[99]. In addition, another group reported that T-ALL cases with a myeloid gene expression profile have an elevated miR-223 expression compared to other T-ALL cases[236].

Together with miR-223, the miRNAs miR-142 and miR-181 were among the first miRNAs found to be specifically expressed in hematopoietic cells[237]. MiR-142-3p is significantly higher expressed in T-ALL patient samples compared to healthy T-cell controls[238]. Furthermore, miR-142-3p targets the adenylyl cyclase 9 and the glucocorticoid receptor α contributing to the promotion of glucocorticoid resistance in T-ALL[238,239]. So inhibiting miR-142-3p activity might be of therapeutic interest in glucocorticoid resistant T-ALL patient samples. Next, miR-181a family members display elevated levels in T-ALL cells and these levels decline at remission[240]. Loss of the oncogenic miR-181a-1/b-1 delayed T-ALL onset in the NOTCH1 T-ALL mouse model and importantly, secondary transplants were not able to induce leukemia. MiR-181a-1/b-1 mediates this inhibitory effect on NOTCH1-driven T-ALL by dampening genes involved in NOTCH1 signaling, pre-TCR signaling and cytokine and apoptosis pathways[241].

Interestingly, two additional miRNAs miR-451 and miR-709 were identified that are able of blocking or slowing down NOTCH1-induced T-ALL growth when overexpressed in the NOTCH1 T-ALL mouse model[242], next to loss of miR-181a-1/b-1[241]. Both tumor suppressor miRNAs are direct transcriptional targets of the transcription factor E2A that itself is downregulated by NOTCH1[242]. MiR-451, but not miR-709, is conserved in humans and can negatively regulate MYC expression levels in human T-ALL cell lines and in murine T-ALL lymphoblasts[242]. Meanwhile miR-709 was shown to silence Myc, Akt and Rasgrf1 expression in malignant murine T-cells[242].

Finally, some T-ALL subgroup specific miRNAs have been identified. In the early immature T-ALL subgroup, miR-221 and miR-222 are upregulated and miR-19a and miR-363 are downregulated in comparison with non-immature T-ALLs[243]. In the HOXA T-ALL subgroup, the expression level of miR-196b is elevated together with *HOXA9* and *HOXA10*[244,245] in agreement with its location within the *HOXA* locus[244,245].

3.3 MicroRNA biomarkers & therapeutics

Circulating miRNAs present in the body fluid, including serum or plasma, can be used as non-invasive biomarkers in cancer[221]. These miRNAs are exported from the donor cells through passive leakage, packed in exosomes or microvesicles, or in conjunction with RNA-binding proteins or lipoproteins[221]. In cancer, the origin of the donor cells is not totally clarified yet. A study demonstrated that these circulating miRNAs are likely derived from tumor cells or tissues associated with neoplastic transformation[246], but others demonstrate that blood cells themselves can contribute to the pool of circulating miRNAs in plasma and serum[247]. Circulating miRNAs present in exosomes can be taken up by recipient cells, here surrounding immune cells of the tumor microenvironment[221,248,249]. In cancer therapy, expression profiles of circulating miRNAs can harbor a prognostic value or an indication for drug response[221].

The main advantage of miRNA therapeutics is the capacity of miRNAs to regulate simultaneously a set of coding genes from the same pathway and/or interacting pathways[221]. But caution is warranted in miRNA therapy as miRNAs direct transcriptional control in a tissue-specific manner, hereby miRNA delivery can be beneficial in one cell type but harmful in another cell type. Furthermore, delivery of precursor miRNAs using miRNA expression vectors should take into account that both strands of a miRNA (called 3p and 5p) can have a different function and different target genes in the same cell[221]. In the latter case, delivery of a mature miRNA using miRNA mimics can be employed to avoid unwanted phenotypic effects[221].

Two therapeutic strategies are used to restore tumor suppressor miRNAs back to normal expression levels, which encompass miRNA mimics and miRNA expression vectors (**Figure 12**). The miRNA mimic molecules are synthetic double-stranded miRNA oligonucleotides that are coupled with nanoparticles or packed into liposome or atelocollagen formulations[221]. The first liposome-based miRNA mimic MRX34 has gone into Phase I clinical trial, which can restore miR-34 levels in patients with advanced or metastatic liver cancer expectantly leading to a reduction of tumor growth[250]. Secondly, miRNA levels can be restored to normal tissue-specific levels by use of the miRNA expression vectors in which miRNAs are under the control of a specific promoter and can be delivered through viral particles[221].

To therapeutically target oncomiRs in cancer, several antisense oligonucleotides (ASO) approaches are used including antagomiRs, locked nucleic acids (LNA) antimiRs and tiny LNA antimiRs as well as the use of miRNA sponges[221] (**Figure 12**). The first ASO approach consist of synthetic RNAs that are conjugated with cholesterol for optimal cellular uptake and modified with 2'-O-methyl and phosphorothioate to improve binding affinity and inhibit nuclease action[251]. These antagomirs were first tested and proved efficacy *in vivo* against miR-122, an abundant liver-specific miRNA[251]. Unfortunately, the main disadvantage of these antagomiRs is the necessity of high dosages for effective miRNA targeting[221]. This shortcoming can be circumvented with the use of LNA-based ASOs, which are synthetic oligonucleotides in which some nucleotides are exchanged with bicyclic RNA analogues in a 'locked' conformation[221]. LNA antimiRs are 13-22 nucleotides long whereas tiny LNA antimiRs only consist of 8 nucleotides specific to the seed region of the miRNA hereby enabling silencing of multiple miRNAs from the same miRNA family[221]. A first LNA antimiR in Phase I and IIa clinical trials is the antiviral agent miravirsen targeting miR-122 in the treatment against hepatitis C virus[252]. Advantages of LNA based miRNA therapy are the lack of toxicities and the efficient cellular uptake without the requirement of specific delivery formulations[221]. Finally, miRNA sponges have shown efficacy to block an entire miRNA seed family. These synthetic RNA molecules contain several heptamer sequences that are complementary to the seed region of the miRNA seed family of interest, hereby preventing translational inhibition of the miRNA target genes. As high concentrations of miRNA sponges are again needed for efficient miRNA targeting, miRNA sponges are frequently incorporated in plasmids or viral vectors[221].

References

1. Bhojwani, D. & Pui, C.H. Relapsed childhood acute lymphoblastic leukaemia. *Lancet Oncol* **14**, e205-17 (2013).
2. Inaba, H., Greaves, M. & Mullighan, C.G. Acute lymphoblastic leukaemia. *Lancet* **381**, 1943-55 (2013).
3. Van Vlierberghe, P. & Ferrando, A. The molecular basis of T cell acute lymphoblastic leukemia. *J Clin Invest* **122**, 3398-406 (2012).
4. Marks, D.I. *et al.* T-cell acute lymphoblastic leukemia in adults: clinical features, immunophenotype, cytogenetics, and outcome from the large randomized prospective trial (UKALL XII/ECOG 2993). *Blood* **114**, 5136-45 (2009).
5. Van Vlierberghe, P. *et al.* PHF6 mutations in T-cell acute lymphoblastic leukemia. *Nat Genet* **42**, 338-42 (2010).
6. De Keersmaecker, K. *et al.* Exome sequencing identifies mutation in CNOT3 and ribosomal genes RPL5 and RPL10 in T-cell acute lymphoblastic leukemia. *Nat Genet* **45**, 186-90 (2013).
7. Taghon, T., Waegemans, E. & Van de Walle, I. Notch signaling during human T cell development. *Curr Top Microbiol Immunol* **360**, 75-97 (2012).
8. Ferrando, A.A. *et al.* Gene expression signatures define novel oncogenic pathways in T cell acute lymphoblastic leukemia. *Cancer Cell* **1**, 75-87 (2002).
9. Homminga, I. *et al.* Integrated transcript and genome analyses reveal NKX2-1 and MEF2C as potential oncogenes in T cell acute lymphoblastic leukemia. *Cancer Cell* **19**, 484-97 (2011).
10. Soulier, J. *et al.* HOXA genes are included in genetic and biologic networks defining human acute T-cell leukemia (T-ALL). *Blood* **106**, 274-86 (2005).
11. Hatano, M., Roberts, C.W., Minden, M., Crist, W.M. & Korsmeyer, S.J. Deregulation of a homeobox gene, HOX11, by the t(10;14) in T cell leukemia. *Science* **253**, 79-82 (1991).
12. Bernard, O.A. *et al.* A new recurrent and specific cryptic translocation, t(5;14)(q35;q32), is associated with expression of the Hox11L2 gene in T acute lymphoblastic leukemia. *Leukemia* **15**, 1495-504 (2001).
13. Ferrando, A.A. *et al.* Prognostic importance of TLX1 (HOX11) oncogene expression in adults with T-cell acute lymphoblastic leukaemia. *Lancet* **363**, 535-6 (2004).
14. Su, X.Y. *et al.* Various types of rearrangements target TLX3 locus in T-cell acute lymphoblastic leukemia. *Genes Chromosomes Cancer* **41**, 243-9 (2004).
15. Su, X.Y. *et al.* HOX11L2/TLX3 is transcriptionally activated through T-cell regulatory elements downstream of BCL11B as a result of the t(5;14)(q35;q32). *Blood* **108**, 4198-201 (2006).
16. De Keersmaecker, K. *et al.* The TLX1 oncogene drives aneuploidy in T cell transformation. *Nat Med* **16**, 1321-7 (2010).
17. Dadi, S. *et al.* TLX homeodomain oncogenes mediate T cell maturation arrest in T-ALL via interaction with ETS1 and suppression of TCRalpha gene expression. *Cancer Cell* **21**, 563-76 (2012).
18. Della Gatta, G. *et al.* Reverse engineering of TLX oncogenic transcriptional networks identifies RUNX1 as tumor suppressor in T-ALL. *Nat Med* **18**, 436-40 (2012).
19. Aplan, P.D. *et al.* Disruption of the human SCL locus by "illegitimate" V-(D)-J recombinase activity. *Science* **250**, 1426-9 (1990).
20. Xia, Y. *et al.* TAL2, a helix-loop-helix gene activated by the (7;9)(q34;q32) translocation in human T-cell leukemia. *Proc Natl Acad Sci U S A* **88**, 11416-20 (1991).

21. Mellentin, J.D., Smith, S.D. & Cleary, M.L. lyl-1, a novel gene altered by chromosomal translocation in T cell leukemia, codes for a protein with a helix-loop-helix DNA binding motif. *Cell* **58**, 77-83 (1989).
22. Wang, J. *et al.* The t(14;21)(q11.2;q22) chromosomal translocation associated with T-cell acute lymphoblastic leukemia activates the BHLHB1 gene. *Proc Natl Acad Sci U S A* **97**, 3497-502 (2000).
23. McGuire, E.A. *et al.* The t(11;14)(p15;q11) in a T-cell acute lymphoblastic leukemia cell line activates multiple transcripts, including Ttg-1, a gene encoding a potential zinc finger protein. *Mol Cell Biol* **9**, 2124-32 (1989).
24. Royer-Pokora, B., Loos, U. & Ludwig, W.D. TTG-2, a new gene encoding a cysteine-rich protein with the LIM motif, is overexpressed in acute T-cell leukaemia with the t(11;14)(p13;q11). *Oncogene* **6**, 1887-93 (1991).
25. Clappier, E. *et al.* The C-MYB locus is involved in chromosomal translocation and genomic duplications in human T-cell acute leukemia (T-ALL), the translocation defining a new T-ALL subtype in very young children. *Blood* **110**, 1251-61 (2007).
26. Bash, R.O. *et al.* Clinical features and outcome of T-cell acute lymphoblastic leukemia in childhood with respect to alterations at the TAL1 locus: a Pediatric Oncology Group study. *Blood* **81**, 2110-7 (1993).
27. van Grotel, M. *et al.* Prognostic significance of molecular-cytogenetic abnormalities in pediatric T-ALL is not explained by immunophenotypic differences. *Leukemia* **22**, 124-31 (2008).
28. Ballerini, P. *et al.* HOX11L2 expression defines a clinical subtype of pediatric T-ALL associated with poor prognosis. *Blood* **100**, 991-7 (2002).
29. Haydu, J.E. & Ferrando, A.A. Early T-cell precursor acute lymphoblastic leukaemia. *Curr Opin Hematol* **20**, 369-73 (2013).
30. Van Vlierberghe, P. *et al.* ETV6 mutations in early immature human T cell leukemias. *J Exp Med* **208**, 2571-9 (2011).
31. Zhang, J. *et al.* The genetic basis of early T-cell precursor acute lymphoblastic leukaemia. *Nature* **481**, 157-63 (2012).
32. Gutierrez, A. *et al.* Absence of biallelic TCRgamma deletion predicts early treatment failure in pediatric T-cell acute lymphoblastic leukemia. *J Clin Oncol* **28**, 3816-23 (2010).
33. Asnafi, V. *et al.* CALM-AF10 is a common fusion transcript in T-ALL and is specific to the TCRgammadelta lineage. *Blood* **102**, 1000-6 (2003).
34. Van Vlierberghe, P. *et al.* The recurrent SET-NUP214 fusion as a new HOXA activation mechanism in pediatric T-cell acute lymphoblastic leukemia. *Blood* **111**, 4668-80 (2008).
35. Rubnitz, J.E. *et al.* Childhood acute lymphoblastic leukemia with the MLL-ENL fusion and t(11;19)(q23;p13.3) translocation. *J Clin Oncol* **17**, 191-6 (1999).
36. Neumann, M. *et al.* Whole-exome sequencing in adult ETP-ALL reveals a high rate of DNMT3A mutations. *Blood* **121**, 4749-52 (2013).
37. Coustan-Smith, E. *et al.* Early T-cell precursor leukaemia: a subtype of very high-risk acute lymphoblastic leukaemia. *Lancet Oncol* **10**, 147-56 (2009).
38. Tosello, V. & Ferrando, A.A. The NOTCH signaling pathway: role in the pathogenesis of T-cell acute lymphoblastic leukemia and implication for therapy. *Ther Adv Hematol* **4**, 199-210 (2013).
39. Grabher, C., von Boehmer, H. & Look, A.T. Notch 1 activation in the molecular pathogenesis of T-cell acute lymphoblastic leukaemia. *Nat Rev Cancer* **6**, 347-59 (2006).

40. Palomero, T. *et al.* NOTCH1 directly regulates c-MYC and activates a feed-forward-loop transcriptional network promoting leukemic cell growth. *Proc Natl Acad Sci U S A* **103**, 18261-6 (2006).
41. Weng, A.P. *et al.* c-Myc is an important direct target of Notch1 in T-cell acute lymphoblastic leukemia/lymphoma. *Genes Dev* **20**, 2096-109 (2006).
42. Lu, F.M. & Lux, S.E. Constitutively active human Notch1 binds to the transcription factor CBF1 and stimulates transcription through a promoter containing a CBF1-responsive element. *Proc Natl Acad Sci U S A* **93**, 5663-7 (1996).
43. Espinosa, L. *et al.* The Notch/Hes1 pathway sustains NF-kappaB activation through CYLD repression in T cell leukemia. *Cancer Cell* **18**, 268-81 (2010).
44. Palomero, T. *et al.* Mutational loss of PTEN induces resistance to NOTCH1 inhibition in T-cell leukemia. *Nat Med* **13**, 1203-10 (2007).
45. Gonzalez-Garcia, S. *et al.* CSL-MAML-dependent Notch1 signaling controls T lineage-specific IL-7R{alpha} gene expression in early human thymopoiesis and leukemia. *J Exp Med* **206**, 779-91 (2009).
46. Reizis, B. & Leder, P. Direct induction of T lymphocyte-specific gene expression by the mammalian Notch signaling pathway. *Genes Dev* **16**, 295-300 (2002).
47. Medyouf, H. *et al.* High-level IGF1R expression is required for leukemia-initiating cell activity in T-ALL and is supported by Notch signaling. *J Exp Med* **208**, 1809-22 (2011).
48. Buonamici, S. *et al.* CCR7 signalling as an essential regulator of CNS infiltration in T-cell leukaemia. *Nature* **459**, 1000-4 (2009).
49. Sicinska, E. *et al.* Requirement for cyclin D3 in lymphocyte development and T cell leukemias. *Cancer Cell* **4**, 451-61 (2003).
50. Sarmento, L.M. *et al.* Notch1 modulates timing of G1-S progression by inducing SKP2 transcription and p27 Kip1 degradation. *J Exp Med* **202**, 157-68 (2005).
51. Chan, S.M., Weng, A.P., Tibshirani, R., Aster, J.C. & Utz, P.J. Notch signals positively regulate activity of the mTOR pathway in T-cell acute lymphoblastic leukemia. *Blood* **110**, 278-86 (2007).
52. Vilimas, T. *et al.* Targeting the NF-kappaB signaling pathway in Notch1-induced T-cell leukemia. *Nat Med* **13**, 70-7 (2007).
53. Inuzuka, H. *et al.* SCF(FBW7) regulates cellular apoptosis by targeting MCL1 for ubiquitylation and destruction. *Nature* **471**, 104-9 (2011).
54. Gupta-Rossi, N. *et al.* Functional interaction between SEL-10, an F-box protein, and the nuclear form of activated Notch1 receptor. *J Biol Chem* **276**, 34371-8 (2001).
55. Weng, A.P. *et al.* Activating mutations of NOTCH1 in human T cell acute lymphoblastic leukemia. *Science* **306**, 269-71 (2004).
56. Ellisen, L.W. *et al.* TAN-1, the human homolog of the Drosophila notch gene, is broken by chromosomal translocations in T lymphoblastic neoplasms. *Cell* **66**, 649-61 (1991).
57. O'Neil, J. *et al.* FBW7 mutations in leukemic cells mediate NOTCH pathway activation and resistance to gamma-secretase inhibitors. *J Exp Med* **204**, 1813-24 (2007).
58. Thompson, B.J. *et al.* The SCFFBW7 ubiquitin ligase complex as a tumor suppressor in T cell leukemia. *J Exp Med* **204**, 1825-35 (2007).
59. Pear, W.S. *et al.* Exclusive development of T cell neoplasms in mice transplanted with bone marrow expressing activated Notch alleles. *J Exp Med* **183**, 2283-91 (1996).
60. van Es, J.H. *et al.* Notch/gamma-secretase inhibition turns proliferative cells in intestinal crypts and adenomas into goblet cells. *Nature* **435**, 959-63 (2005).
61. Real, P.J. *et al.* Gamma-secretase inhibitors reverse glucocorticoid resistance in T cell acute lymphoblastic leukemia. *Nat Med* **15**, 50-8 (2009).

62. Wu, Y. *et al.* Therapeutic antibody targeting of individual Notch receptors. *Nature* **464**, 1052-7 (2010).
63. Moellering, R.E. *et al.* Direct inhibition of the NOTCH transcription factor complex. *Nature* **462**, 182-8 (2009).
64. Milano, J. *et al.* Modulation of notch processing by gamma-secretase inhibitors causes intestinal goblet cell metaplasia and induction of genes known to specify gut secretory lineage differentiation. *Toxicol Sci* **82**, 341-58 (2004).
65. Fu, L. *et al.* Perifosine inhibits mammalian target of rapamycin signaling through facilitating degradation of major components in the mTOR axis and induces autophagy. *Cancer Res* **69**, 8967-76 (2009).
66. Shepherd, C. *et al.* PI3K/mTOR inhibition upregulates NOTCH-MYC signalling leading to an impaired cytotoxic response. *Leukemia* **27**, 650-60 (2013).
67. Samon, J.B. *et al.* Preclinical analysis of the gamma-secretase inhibitor PF-03084014 in combination with glucocorticoids in T-cell acute lymphoblastic leukemia. *Mol Cancer Ther* **11**, 1565-75 (2012).
68. Piovan, E. *et al.* Direct Reversal of Glucocorticoid Resistance by AKT Inhibition in Acute Lymphoblastic Leukemia. *Cancer Cell* (2013).
69. Chiarini, F. *et al.* Dual inhibition of class IA phosphatidylinositol 3-kinase and mammalian target of rapamycin as a new therapeutic option for T-cell acute lymphoblastic leukemia. *Cancer Res* **69**, 3520-8 (2009).
70. Lonetti, A. *et al.* Activity of the pan-class I phosphoinositide 3-kinase inhibitor NVP-BKM120 in T-cell acute lymphoblastic leukemia. *Leukemia* (2013).
71. Erikson, J. *et al.* Deregulation of c-myc by translocation of the alpha-locus of the T-cell receptor in T-cell leukemias. *Science* **232**, 884-6 (1986).
72. Delmore, J.E. *et al.* BET bromodomain inhibition as a therapeutic strategy to target c-Myc. *Cell* **146**, 904-17 (2011).
73. Plass, C. *et al.* Mutations in regulators of the epigenome and their connections to global chromatin patterns in cancer. *Nat Rev Genet* **14**, 765-80 (2013).
74. Helin, K. & Dhanak, D. Chromatin proteins and modifications as drug targets. *Nature* **502**, 480-8 (2013).
75. Hnisz, D. *et al.* Super-enhancers in the control of cell identity and disease. *Cell* **155**, 934-47 (2013).
76. Roderick, J.E. *et al.* c-Myc inhibition prevents leukemia initiation in mice and impairs the growth of relapsed and induction failure pediatric T-ALL cells. *Blood* (2014).
77. Ott, C.J. *et al.* BET bromodomain inhibition targets both c-Myc and IL7R in high-risk acute lymphoblastic leukemia. *Blood* **120**, 2843-52 (2012).
78. Dai, P. *et al.* CBP as a transcriptional coactivator of c-Myb. *Genes Dev* **10**, 528-40 (1996).
79. Oelgeschlager, M., Janknecht, R., Krieg, J., Schreek, S. & Luscher, B. Interaction of the co-activator CBP with Myb proteins: effects on Myb-specific transactivation and on the cooperativity with NF-M. *EMBO J* **15**, 2771-80 (1996).
80. Ramsay, R.G. & Gonda, T.J. MYB function in normal and cancer cells. *Nat Rev Cancer* **8**, 523-34 (2008).
81. Mucenski, M.L. *et al.* A functional c-myb gene is required for normal murine fetal hepatic hematopoiesis. *Cell* **65**, 677-89 (1991).
82. Lieu, Y.K. & Reddy, E.P. Conditional c-myb knockout in adult hematopoietic stem cells leads to loss of self-renewal due to impaired proliferation and accelerated differentiation. *Proc Natl Acad Sci U S A* **106**, 21689-94 (2009).
83. Allen, R.D., 3rd, Bender, T.P. & Siu, G. c-Myb is essential for early T cell development. *Genes Dev* **13**, 1073-8 (1999).

84. Bender, T.P., Kremer, C.S., Kraus, M., Buch, T. & Rajewsky, K. Critical functions for c-Myb at three checkpoints during thymocyte development. *Nat Immunol* **5**, 721-9 (2004).
85. Yuan, J., Crittenden, R.B. & Bender, T.P. c-Myb promotes the survival of CD4+CD8+ double-positive thymocytes through upregulation of Bcl-xL. *J Immunol* **184**, 2793-804 (2010).
86. Pearson, R. & Weston, K. c-Myb regulates the proliferation of immature thymocytes following beta-selection. *EMBO J* **19**, 6112-20 (2000).
87. Siu, G., Wurster, A.L., Lipsick, J.S. & Hedrick, S.M. Expression of the CD4 gene requires a Myb transcription factor. *Mol Cell Biol* **12**, 1592-604 (1992).
88. Maurice, D., Hooper, J., Lang, G. & Weston, K. c-Myb regulates lineage choice in developing thymocytes via its target gene Gata3. *EMBO J* **26**, 3629-40 (2007).
89. Wang, Q.F., Lauring, J. & Schlissel, M.S. c-Myb binds to a sequence in the proximal region of the RAG-2 promoter and is essential for promoter activity in T-lineage cells. *Mol Cell Biol* **20**, 9203-11 (2000).
90. Hooper, J., Maurice, D., Argent-Katwala, M.J. & Weston, K. Myb proteins regulate expression of histone variant H2A.Z during thymocyte development. *Immunology* **123**, 282-9 (2008).
91. Taylor, D., Badiani, P. & Weston, K. A dominant interfering Myb mutant causes apoptosis in T cells. *Genes Dev* **10**, 2732-44 (1996).
92. Badiani, P.A., Kioussis, D., Swirsky, D.M., Lampert, I.A. & Weston, K. T-cell lymphomas in v-Myb transgenic mice. *Oncogene* **13**, 2205-12 (1996).
93. Davies, J., Badiani, P. & Weston, K. Cooperation of Myb and Myc proteins in T cell lymphomagenesis. *Oncogene* **18**, 3643-7 (1999).
94. Lund, A.H. *et al.* Genome-wide retroviral insertional tagging of genes involved in cancer in Cdkn2a-deficient mice. *Nat Genet* **32**, 160-5 (2002).
95. Kim, R. *et al.* Genome-based identification of cancer genes by proviral tagging in mouse retrovirus-induced T-cell lymphomas. *J Virol* **77**, 2056-62 (2003).
96. Lahortiga, I. *et al.* Duplication of the MYB oncogene in T cell acute lymphoblastic leukemia. *Nat Genet* **39**, 593-5 (2007).
97. O'Neil, J. *et al.* Alu elements mediate MYB gene tandem duplication in human T-ALL. *J Exp Med* **204**, 3059-66 (2007).
98. Sanda, T. *et al.* Core transcriptional regulatory circuit controlled by the TAL1 complex in human T cell acute lymphoblastic leukemia. *Cancer Cell* **22**, 209-21 (2012).
99. Mansour, M.R. *et al.* The TAL1 complex targets the FBXW7 tumor suppressor by activating miR-223 in human T cell acute lymphoblastic leukemia. *J Exp Med* **210**, 1545-57 (2013).
100. Hess, J.L. *et al.* c-Myb is an essential downstream target for homeobox-mediated transformation of hematopoietic cells. *Blood* **108**, 297-304 (2006).
101. Zuber, J. *et al.* An integrated approach to dissecting oncogene addiction implicates a Myb-coordinated self-renewal program as essential for leukemia maintenance. *Genes Dev* **25**, 1628-40 (2011).
102. Jin, S. *et al.* c-Myb binds MLL through menin in human leukemia cells and is an important driver of MLL-associated leukemogenesis. *J Clin Invest* **120**, 593-606 (2010).
103. Gewirtz, A.M. Myb targeted therapeutics for the treatment of human malignancies. *Oncogene* **18**, 3056-62 (1999).
104. Amaru Calzada, A. *et al.* The HDAC inhibitor Givinostat modulates the hematopoietic transcription factors NFE2 and C-MYB in JAK2(V617F) myeloproliferative neoplasm cells. *Exp Hematol* **40**, 634-45 e10 (2012).

105. Chambers, A.E. *et al.* Histone acetylation-mediated regulation of genes in leukaemic cells. *Eur J Cancer* **39**, 1165-75 (2003).
106. Ting, A.H., McGarvey, K.M. & Baylin, S.B. The cancer epigenome--components and functional correlates. *Genes Dev* **20**, 3215-31 (2006).
107. Di Croce, L. & Helin, K. Transcriptional regulation by Polycomb group proteins. *Nat Struct Mol Biol* **20**, 1147-55 (2013).
108. Jones, P.A. & Baylin, S.B. The epigenomics of cancer. *Cell* **128**, 683-92 (2007).
109. Baylin, S.B. & Jones, P.A. A decade of exploring the cancer epigenome - biological and translational implications. *Nat Rev Cancer* **11**, 726-34 (2011).
110. Jones, P.A. Functions of DNA methylation: islands, start sites, gene bodies and beyond. *Nat Rev Genet* **13**, 484-92 (2012).
111. Zhou, V.W., Goren, A. & Bernstein, B.E. Charting histone modifications and the functional organization of mammalian genomes. *Nat Rev Genet* **12**, 7-18 (2011).
112. Jeong, M. *et al.* Large conserved domains of low DNA methylation maintained by Dnmt3a. *Nat Genet* **46**, 17-23 (2014).
113. Riggs, A.D. & Jones, P.A. 5-methylcytosine, gene regulation, and cancer. *Adv Cancer Res* **40**, 1-30 (1983).
114. Batova, A. *et al.* Frequent and selective methylation of p15 and deletion of both p15 and p16 in T-cell acute lymphoblastic leukemia. *Cancer Res* **57**, 832-6 (1997).
115. Goodman, P.A., Burkhardt, N., Juran, B., Tibbles, H.E. & Uckun, F.M. Hypermethylation of the spleen tyrosine kinase promoter in T-lineage acute lymphoblastic leukemia. *Oncogene* **22**, 2504-14 (2003).
116. Terriou, L. *et al.* C/EBPA methylation is common in T-ALL but not in M0 AML. *Blood* **113**, 1864-6; author reply 1866 (2009).
117. Hutter, G. *et al.* Epigenetic regulation of PAX5 expression in acute T-cell lymphoblastic leukemia. *Leuk Res* **35**, 614-9 (2011).
118. Bram, E.E., Stark, M., Raz, S. & Assaraf, Y.G. Chemotherapeutic drug-induced ABCG2 promoter demethylation as a novel mechanism of acquired multidrug resistance. *Neoplasia* **11**, 1359-70 (2009).
119. Davies, C. *et al.* p53-independent epigenetic repression of the p21(WAF1) gene in T-cell acute lymphoblastic leukemia. *J Biol Chem* **286**, 37639-50 (2011).
120. Borssen, M. *et al.* Promoter DNA methylation pattern identifies prognostic subgroups in childhood T-cell acute lymphoblastic leukemia. *PLoS One* **8**, e65373 (2013).
121. Kraszewska, M.D. *et al.* DNA methylation pattern is altered in childhood T-cell acute lymphoblastic leukemia patients as compared with normal thymic subsets: insights into CpG island methylator phenotype in T-ALL. *Leukemia* **26**, 367-71 (2012).
122. Grossmann, V. *et al.* The molecular profile of adult T-cell acute lymphoblastic leukemia: mutations in RUNX1 and DNMT3A are associated with poor prognosis in T-ALL. *Genes Chromosomes Cancer* **52**, 410-22 (2013).
123. Tahiliani, M. *et al.* Conversion of 5-methylcytosine to 5-hydroxymethylcytosine in mammalian DNA by MLL partner TET1. *Science* **324**, 930-5 (2009).
124. Sasaki, M. *et al.* IDH1(R132H) mutation increases murine haematopoietic progenitors and alters epigenetics. *Nature* **488**, 656-9 (2012).
125. Rohle, D. *et al.* An inhibitor of mutant IDH1 delays growth and promotes differentiation of glioma cells. *Science* **340**, 626-30 (2013).
126. Hake, S.B., Xiao, A. & Allis, C.D. Linking the epigenetic 'language' of covalent histone modifications to cancer. *Br J Cancer* **90**, 761-9 (2004).
127. Wang, G.G., Allis, C.D. & Chi, P. Chromatin remodeling and cancer, Part II: ATP-dependent chromatin remodeling. *Trends Mol Med* **13**, 373-80 (2007).

128. Saha, A., Wittmeyer, J. & Cairns, B.R. Chromatin remodelling: the industrial revolution of DNA around histones. *Nat Rev Mol Cell Biol* **7**, 437-47 (2006).
129. Hassan, A.H. *et al.* Function and selectivity of bromodomains in anchoring chromatin-modifying complexes to promoter nucleosomes. *Cell* **111**, 369-79 (2002).
130. Flanagan, J.F. *et al.* Double chromodomains cooperate to recognize the methylated histone H3 tail. *Nature* **438**, 1181-5 (2005).
131. Kadam, S. & Emerson, B.M. Transcriptional specificity of human SWI/SNF BRG1 and BRM chromatin remodeling complexes. *Mol Cell* **11**, 377-89 (2003).
132. van Attikum, H., Fritsch, O., Hohn, B. & Gasser, S.M. Recruitment of the INO80 complex by H2A phosphorylation links ATP-dependent chromatin remodeling with DNA double-strand break repair. *Cell* **119**, 777-88 (2004).
133. Todd, M.A. & Picketts, D.J. PHF6 interacts with the nucleosome remodeling and deacetylation (NuRD) complex. *J Proteome Res* **11**, 4326-37 (2012).
134. Lai, A.Y. & Wade, P.A. Cancer biology and NuRD: a multifaceted chromatin remodelling complex. *Nat Rev Cancer* **11**, 588-96 (2011).
135. Talbert, P.B. & Henikoff, S. Histone variants--ancient wrap artists of the epigenome. *Nat Rev Mol Cell Biol* **11**, 264-75 (2010).
136. Skene, P.J. & Henikoff, S. Histone variants in pluripotency and disease. *Development* **140**, 2513-24 (2013).
137. Belotserkovskaya, R., Saunders, A., Lis, J.T. & Reinberg, D. Transcription through chromatin: understanding a complex FACT. *Biochim Biophys Acta* **1677**, 87-99 (2004).
138. Wang, G.G., Allis, C.D. & Chi, P. Chromatin remodeling and cancer, Part I: Covalent histone modifications. *Trends Mol Med* **13**, 363-72 (2007).
139. Kouzarides, T. Chromatin modifications and their function. *Cell* **128**, 693-705 (2007).
140. Simon, C. *et al.* A key role for EZH2 and associated genes in mouse and human adult T-cell acute leukemia. *Genes & Development* **26**, 651-656 (2012).
141. Ntziachristos, P. *et al.* Genetic inactivation of the polycomb repressive complex 2 in T cell acute lymphoblastic leukemia. *Nat Med* **18**, 298-301 (2012).
142. Chi, P., Allis, C.D. & Wang, G.G. Covalent histone modifications--miswritten, misinterpreted and mis-erased in human cancers. *Nat Rev Cancer* **10**, 457-69 (2010).
143. Lan, F. *et al.* Recognition of unmethylated histone H3 lysine 4 links BHC80 to LSD1-mediated gene repression. *Nature* **448**, 718-22 (2007).
144. Li, B. *et al.* Combined action of PHD and chromo domains directs the Rpd3S HDAC to transcribed chromatin. *Science* **316**, 1050-4 (2007).
145. Karagianni, P., Amazit, L., Qin, J. & Wong, J. ICBP90, a novel methyl K9 H3 binding protein linking protein ubiquitination with heterochromatin formation. *Mol Cell Biol* **28**, 705-17 (2008).
146. Zeng, L. *et al.* Mechanism and regulation of acetylated histone binding by the tandem PHD finger of DPF3b. *Nature* **466**, 258-62 (2010).
147. Wang, Z. *et al.* Pro isomerization in MLL1 PHD3-bromo cassette connects H3K4me readout to CyP33 and HDAC-mediated repression. *Cell* **141**, 1183-94 (2010).
148. Lower, K.M. *et al.* Mutations in PHF6 are associated with Borjeson-Forssman-Lehmann syndrome. *Nat Genet* **32**, 661-5 (2002).
149. Kuzmichev, A., Nishioka, K., Erdjument-Bromage, H., Tempst, P. & Reinberg, D. Histone methyltransferase activity associated with a human multiprotein complex containing the Enhancer of Zeste protein. *Genes Dev* **16**, 2893-905 (2002).
150. Margueron, R. & Reinberg, D. The Polycomb complex PRC2 and its mark in life. *Nature* **469**, 343-9 (2011).
151. Dephoure, N. *et al.* A quantitative atlas of mitotic phosphorylation. *Proc Natl Acad Sci U S A* **105**, 10762-7 (2008).

152. Matsuoka, S. *et al.* ATM and ATR substrate analysis reveals extensive protein networks responsive to DNA damage. *Science* **316**, 1160-6 (2007).
153. Boisvert, F.M., van Koningsbruggen, S., Navascues, J. & Lamond, A.I. The multifunctional nucleolus. *Nat Rev Mol Cell Biol* **8**, 574-85 (2007).
154. Wang, J. *et al.* PHF6 regulates cell cycle progression by suppressing ribosomal RNA synthesis. *J Biol Chem* **288**, 3174-83 (2013).
155. Wang, Q. *et al.* Mutations of PHF6 are associated with mutations of NOTCH1, JAK1 and rearrangement of SET-NUP214 in T-cell acute lymphoblastic leukemia. *Haematologica* **96**, 1808-14 (2011).
156. Van Vlierberghe, P. *et al.* PHF6 mutations in adult acute myeloid leukemia. *Leukemia* **25**, 130-4 (2011).
157. Yoo, N.J., Kim, Y.R. & Lee, S.H. Somatic mutation of PHF6 gene in T-cell acute lymphoblatic leukemia, acute myelogenous leukemia and hepatocellular carcinoma. *Acta Oncol* **51**, 107-11 (2012).
158. Patel, J.P. *et al.* Prognostic relevance of integrated genetic profiling in acute myeloid leukemia. *N Engl J Med* **366**, 1079-89 (2012).
159. Li, X. *et al.* Somatic mutations of PHF6 in patients with chronic myeloid leukemia in blast crisis. *Leuk Lymphoma* **54**, 671-2 (2013).
160. Kandoth, C. *et al.* Mutational landscape and significance across 12 major cancer types. *Nature* **502**, 333-9 (2013).
161. Gecz, J., Turner, G., Nelson, J. & Partington, M. The Borjeson-Forssman-Lehman syndrome (BFLS, MIM #301900). *Eur J Hum Genet* **14**, 1233-7 (2006).
162. Berland, S., Alme, K., Brendehaug, A., Houge, G. & Hovland, R. PHF6 Deletions May Cause Borjeson-Forssman-Lehmann Syndrome in Females. *Mol Syndromol* **1**, 294-300 (2011).
163. Chao, M.M. *et al.* T-cell acute lymphoblastic leukemia in association with Borjeson-Forssman-Lehmann syndrome due to a mutation in PHF6. *Pediatr Blood Cancer* **55**, 722-4 (2010).
164. Zweier, C. *et al.* A new face of Borjeson-Forssman-Lehmann syndrome? De novo mutations in PHF6 in seven females with a distinct phenotype. *J Med Genet* **50**, 838-47 (2013).
165. Wieczorek, D. *et al.* A comprehensive molecular study on Coffin-Siris and Nicolaides-Baraitser syndromes identifies a broad molecular and clinical spectrum converging on altered chromatin remodeling. *Hum Mol Genet* **22**, 5121-35 (2013).
166. Zhang, C. *et al.* The X-linked intellectual disability protein PHF6 associates with the PAF1 complex and regulates neuronal migration in the mammalian brain. *Neuron* **78**, 986-93 (2013).
167. Mills, A.A. Throwing the cancer switch: reciprocal roles of polycomb and trithorax proteins. *Nat Rev Cancer* **10**, 669-82 (2010).
168. Morin, R.D. *et al.* Somatic mutations altering EZH2 (Tyr641) in follicular and diffuse large B-cell lymphomas of germinal-center origin. *Nat Genet* **42**, 181-5 (2010).
169. Sneeringer, C.J. *et al.* Coordinated activities of wild-type plus mutant EZH2 drive tumor-associated hypertrimethylation of lysine 27 on histone H3 (H3K27) in human B-cell lymphomas. *Proc Natl Acad Sci U S A* **107**, 20980-5 (2010).
170. Tan, J. *et al.* Pharmacologic disruption of Polycomb-repressive complex 2-mediated gene repression selectively induces apoptosis in cancer cells. *Genes Dev* **21**, 1050-63 (2007).
171. McCabe, M.T. *et al.* EZH2 inhibition as a therapeutic strategy for lymphoma with EZH2-activating mutations. *Nature* **492**, 108-12 (2012).
172. Ernst, T. *et al.* Inactivating mutations of the histone methyltransferase gene EZH2 in myeloid disorders. *Nat Genet* **42**, 722-6 (2010).

173. Nikoloski, G. *et al.* Somatic mutations of the histone methyltransferase gene EZH2 in myelodysplastic syndromes. *Nat Genet* **42**, 665-7 (2010).
174. van Lohuizen, M. *et al.* Identification of cooperating oncogenes in E mu-myc transgenic mice by provirus tagging. *Cell* **65**, 737-52 (1991).
175. Jacobs, J.J. *et al.* Bmi-1 collaborates with c-Myc in tumorigenesis by inhibiting c-Myc-induced apoptosis via INK4a/ARF. *Genes Dev* **13**, 2678-90 (1999).
176. Radulovic, V., de Haan, G. & Klauke, K. Polycomb-group proteins in hematopoietic stem cell regulation and hematopoietic neoplasms. *Leukemia* **27**, 523-33 (2013).
177. van Haaften, G. *et al.* Somatic mutations of the histone H3K27 demethylase gene UTX in human cancer. *Nat Genet* **41**, 521-3 (2009).
178. Lederer, D. *et al.* Deletion of KDM6A, a histone demethylase interacting with MLL2, in three patients with Kabuki syndrome. *Am J Hum Genet* **90**, 119-24 (2012).
179. Van der Meulen, J., Speleman, F. & Van Vlierberghe, P. The H3K27me3 demethylase UTX in normal development and disease. *Epigenetics* **9**(2014).
180. Lan, F. *et al.* A histone H3 lysine 27 demethylase regulates animal posterior development. *Nature* **449**, 689-94 (2007).
181. Agger, K. *et al.* UTX and JMJD3 are histone H3K27 demethylases involved in HOX gene regulation and development. *Nature* **449**, 731-4 (2007).
182. Lee, M.G. *et al.* Demethylation of H3K27 regulates polycomb recruitment and H2A ubiquitination. *Science* **318**, 447-50 (2007).
183. De Santa, F. *et al.* The histone H3 lysine-27 demethylase Jmjd3 links inflammation to inhibition of polycomb-mediated gene silencing. *Cell* **130**, 1083-94 (2007).
184. Hong, S. *et al.* Identification of JmjC domain-containing UTX and JMJD3 as histone H3 lysine 27 demethylases. *Proc Natl Acad Sci U S A* **104**, 18439-44 (2007).
185. Wang, J.K. *et al.* The histone demethylase UTX enables RB-dependent cell fate control. *Genes Dev* **24**, 327-32 (2010).
186. Issaeva, I. *et al.* Knockdown of ALR (MLL2) reveals ALR target genes and leads to alterations in cell adhesion and growth. *Mol Cell Biol* **27**, 1889-903 (2007).
187. Cho, Y.W. *et al.* PTIP associates with MLL3- and MLL4-containing histone H3 lysine 4 methyltransferase complex. *J Biol Chem* **282**, 20395-406 (2007).
188. Schuettengruber, B., Martinez, A.M., Iovino, N. & Cavalli, G. Trithorax group proteins: switching genes on and keeping them active. *Nat Rev Mol Cell Biol* **12**, 799-814 (2011).
189. Miller, S.A., Mohn, S.E. & Weinmann, A.S. Jmjd3 and UTX play a demethylase-independent role in chromatin remodeling to regulate T-box family member-dependent gene expression. *Mol Cell* **40**, 594-605 (2010).
190. Mansour, A.A. *et al.* The H3K27 demethylase Utx regulates somatic and germ cell epigenetic reprogramming. *Nature* **488**, 409-13 (2012).
191. Lee, S., Lee, J.W. & Lee, S.K. UTX, a histone H3-lysine 27 demethylase, acts as a critical switch to activate the cardiac developmental program. *Dev Cell* **22**, 25-37 (2012).
192. Welstead, G.G. *et al.* X-linked H3K27me3 demethylase Utx is required for embryonic development in a sex-specific manner. *Proc Natl Acad Sci U S A* **109**, 13004-9 (2012).
193. Wang, C. *et al.* UTX regulates mesoderm differentiation of embryonic stem cells independent of H3K27 demethylase activity. *Proc Natl Acad Sci U S A* **109**, 15324-9 (2012).
194. Shpargel, K.B., Sengoku, T., Yokoyama, S. & Magnuson, T. UTX and UTY demonstrate histone demethylase-independent function in mouse embryonic development. *PLoS Genet* **8**, e1002964 (2012).
195. Thieme, S. *et al.* The histone demethylase UTX regulates stem cell migration and hematopoiesis. *Blood* **121**, 2462-73 (2013).

196. Wang, K.C. *et al.* A long noncoding RNA maintains active chromatin to coordinate homeotic gene expression. *Nature* **472**, 120-4 (2011).
197. Tyagi, S., Chabes, A.L., Wysocka, J. & Herr, W. E2F activation of S phase promoters via association with HCF-1 and the MLL family of histone H3K4 methyltransferases. *Mol Cell* **27**, 107-19 (2007).
198. Liu, H., Cheng, E.H. & Hsieh, J.J. Bimodal degradation of MLL by SCFSkp2 and APCCdc20 assures cell cycle execution: a critical regulatory circuit lost in leukemogenic MLL fusions. *Genes Dev* **21**, 2385-98 (2007).
199. Ang, Y.S. *et al.* Wdr5 mediates self-renewal and reprogramming via the embryonic stem cell core transcriptional network. *Cell* **145**, 183-97 (2011).
200. Krivtsov, A.V. *et al.* H3K79 methylation profiles define murine and human MLL-AF4 leukemias. *Cancer Cell* **14**, 355-68 (2008).
201. Mueller, D. *et al.* A role for the MLL fusion partner ENL in transcriptional elongation and chromatin modification. *Blood* **110**, 4445-54 (2007).
202. Lin, Y.H. *et al.* Global reduction of the epigenetic H3K79 methylation mark and increased chromosomal instability in CALM-AF10-positive leukemias. *Blood* **114**, 651-8 (2009).
203. Okada, Y. *et al.* Leukaemic transformation by CALM-AF10 involves upregulation of Hoxa5 by hDOT1L. *Nat Cell Biol* **8**, 1017-24 (2006).
204. Nie, Z. *et al.* Novel SWI/SNF chromatin-remodeling complexes contain a mixed-lineage leukemia chromosomal translocation partner. *Mol Cell Biol* **23**, 2942-52 (2003).
205. Daigle, S.R. *et al.* Selective killing of mixed lineage leukemia cells by a potent small-molecule DOT1L inhibitor. *Cancer Cell* **20**, 53-65 (2011).
206. Grembecka, J. *et al.* Menin-MLL inhibitors reverse oncogenic activity of MLL fusion proteins in leukemia. *Nat Chem Biol* **8**, 277-84 (2012).
207. Iyer, N.G., Ozdag, H. & Caldas, C. p300/CBP and cancer. *Oncogene* **23**, 4225-31 (2004).
208. Suganuma, T., Kawabata, M., Ohshima, T. & Ikeda, M.A. Growth suppression of human carcinoma cells by reintroduction of the p300 coactivator. *Proc Natl Acad Sci U S A* **99**, 13073-8 (2002).
209. Wagner, E.J. & Carpenter, P.B. Understanding the language of Lys36 methylation at histone H3. *Nat Rev Mol Cell Biol* **13**, 115-26 (2012).
210. de Almeida, S.F. *et al.* Splicing enhances recruitment of methyltransferase HYPB/Setd2 and methylation of histone H3 Lys36. *Nat Struct Mol Biol* **18**, 977-83 (2011).
211. Yoh, S.M., Lucas, J.S. & Jones, K.A. The Iws1:Spt6:CTD complex controls cotranscriptional mRNA biosynthesis and HYPB/Setd2-mediated histone H3K36 methylation. *Genes Dev* **22**, 3422-34 (2008).
212. Yuan, W. *et al.* Heterogeneous nuclear ribonucleoprotein L Is a subunit of human KMT3a/Set2 complex required for H3 Lys-36 trimethylation activity in vivo. *J Biol Chem* **284**, 15701-7 (2009).
213. Xie, P. *et al.* Histone methyltransferase protein SETD2 interacts with p53 and selectively regulates its downstream genes. *Cell Signal* **20**, 1671-8 (2008).
214. Li, F. *et al.* The histone mark H3K36me3 regulates human DNA mismatch repair through its interaction with MutSalpha. *Cell* **153**, 590-600 (2013).
215. Hu, M. *et al.* Histone H3 lysine 36 methyltransferase Hypb/Setd2 is required for embryonic vascular remodeling. *Proc Natl Acad Sci U S A* **107**, 2956-61 (2010).
216. Dalgliesh, G.L. *et al.* Systematic sequencing of renal carcinoma reveals inactivation of histone modifying genes. *Nature* **463**, 360-3 (2010).
217. Esteller, M. Epigenetics in cancer. *N Engl J Med* **358**, 1148-59 (2008).

218. Mellor, J. It takes a PHD to read the histone code. *Cell* **126**, 22-4 (2006).
219. Esquela-Kerscher, A. & Slack, F.J. Oncomirs - microRNAs with a role in cancer. *Nat Rev Cancer* **6**, 259-69 (2006).
220. Bartel, D.P. MicroRNAs: genomics, biogenesis, mechanism, and function. *Cell* **116**, 281-97 (2004).
221. Ling, H., Fabbri, M. & Calin, G.A. MicroRNAs and other non-coding RNAs as targets for anticancer drug development. *Nat Rev Drug Discov* **12**, 847-65 (2013).
222. Tay, Y., Zhang, J., Thomson, A.M., Lim, B. & Rigoutsos, I. MicroRNAs to Nanog, Oct4 and Sox2 coding regions modulate embryonic stem cell differentiation. *Nature* **455**, 1124-8 (2008).
223. Ghisi, M. *et al.* Modulation of microRNA expression in human T-cell development: targeting of NOTCH3 by miR-150. *Blood* **117**, 7053-62 (2011).
224. Neilson, J.R., Zheng, G.X., Burge, C.B. & Sharp, P.A. Dynamic regulation of miRNA expression in ordered stages of cellular development. *Genes Dev* **21**, 578-89 (2007).
225. Li, Q.J. *et al.* miR-181a is an intrinsic modulator of T cell sensitivity and selection. *Cell* **129**, 147-61 (2007).
226. Calin, G.A. *et al.* Human microRNA genes are frequently located at fragile sites and genomic regions involved in cancers. *Proc Natl Acad Sci U S A* **101**, 2999-3004 (2004).
227. Calin, G.A. & Croce, C.M. MicroRNA signatures in human cancers. *Nat Rev Cancer* **6**, 857-66 (2006).
228. Lu, J. *et al.* MicroRNA expression profiles classify human cancers. *Nature* **435**, 834-8 (2005).
229. Rosenfeld, N. *et al.* MicroRNAs accurately identify cancer tissue origin. *Nat Biotechnol* **26**, 462-9 (2008).
230. Mavrakis, K.J. *et al.* Genome-wide RNA-mediated interference screen identifies miR-19 targets in Notch-induced T-cell acute lymphoblastic leukaemia. *Nat Cell Biol* **12**, 372-9 (2010).
231. Yu, L. *et al.* Microarray detection of multiple recurring submicroscopic chromosomal aberrations in pediatric T-cell acute lymphoblastic leukemia. *Leukemia* **25**, 1042-6 (2011).
232. Paddison, P.J., Caudy, A.A., Bernstein, E., Hannon, G.J. & Conklin, D.S. Short hairpin RNAs (shRNAs) induce sequence-specific silencing in mammalian cells. *Genes Dev* **16**, 948-58 (2002).
233. Mavrakis, K.J. *et al.* A cooperative microRNA-tumor suppressor gene network in acute T-cell lymphoblastic leukemia (T-ALL). *Nat Genet* **43**, 673-8 (2011).
234. Ye, H. *et al.* MicroRNA and transcription factor co-regulatory network analysis reveals miR-19 inhibits CYLD in T-cell acute lymphoblastic leukemia. *Nucleic Acids Res* **40**, 5201-14 (2012).
235. Correia, N.C. *et al.* Novel TAL1 targets beyond protein-coding genes: identification of TAL1-regulated microRNAs in T-cell acute lymphoblastic leukemia. *Leukemia* **27**, 1603-6 (2013).
236. Chiaretti, S. *et al.* Gene expression profiling identifies a subset of adult T-cell acute lymphoblastic leukemia with myeloid-like gene features and over-expression of miR-223. *Haematologica* **95**, 1114-21 (2010).
237. Chen, C.Z., Li, L., Lodish, H.F. & Bartel, D.P. MicroRNAs modulate hematopoietic lineage differentiation. *Science* **303**, 83-6 (2004).
238. Lv, M. *et al.* An oncogenic role of miR-142-3p in human T-cell acute lymphoblastic leukemia (T-ALL) by targeting glucocorticoid receptor-alpha and cAMP/PKA pathways. *Leukemia* **26**, 769-77 (2012).

239. Huang, B. *et al.* miR-142-3p restricts cAMP production in CD4+CD25- T cells and CD4+CD25+ TREG cells by targeting AC9 mRNA. *EMBO Rep* **10**, 180-5 (2009).
240. Landgraf, P. *et al.* A mammalian microRNA expression atlas based on small RNA library sequencing. *Cell* **129**, 1401-14 (2007).
241. Fragoso, R. *et al.* Modulating the strength and threshold of NOTCH oncogenic signals by mir-181a-1/b-1. *PLoS Genet* **8**, e1002855 (2012).
242. Li, X., Sanda, T., Look, A.T., Novina, C.D. & von Boehmer, H. Repression of tumor suppressor miR-451 is essential for NOTCH1-induced oncogenesis in T-ALL. *J Exp Med* **208**, 663-75 (2011).
243. Coskun, E. *et al.* MicroRNA profiling reveals aberrant microRNA expression in adult ETP-ALL and functional studies implicate a role for miR-222 in acute leukemia. *Leuk Res* **37**, 647-56 (2013).
244. Schotte, D. *et al.* Expression of miR-196b is not exclusively MLL-driven but is especially linked to activation of HOXA genes in pediatric acute lymphoblastic leukemia. *Haematologica* **95**, 1675-82 (2010).
245. Schotte, D. *et al.* Identification of new microRNA genes and aberrant microRNA profiles in childhood acute lymphoblastic leukemia. *Leukemia* **23**, 313-22 (2009).
246. Chen, X. *et al.* Characterization of microRNAs in serum: a novel class of biomarkers for diagnosis of cancer and other diseases. *Cell Res* **18**, 997-1006 (2008).
247. Pritchard, C.C. *et al.* Blood cell origin of circulating microRNAs: a cautionary note for cancer biomarker studies. *Cancer Prev Res (Phila)* **5**, 492-7 (2012).
248. Fabbri, M. *et al.* MicroRNAs bind to Toll-like receptors to induce prometastatic inflammatory response. *Proc Natl Acad Sci U S A* **109**, E2110-6 (2012).
249. Valadi, H. *et al.* Exosome-mediated transfer of mRNAs and microRNAs is a novel mechanism of genetic exchange between cells. *Nat Cell Biol* **9**, 654-9 (2007).
250. Bader, A.G. miR-34 - a microRNA replacement therapy is headed to the clinic. *Front Genet* **3**, 120 (2012).
251. Krutzfeldt, J. *et al.* Silencing of microRNAs in vivo with 'antagomirs'. *Nature* **438**, 685-9 (2005).
252. Janssen, H.L. *et al.* Treatment of HCV infection by targeting microRNA. *N Engl J Med* **368**, 1685-94 (2013).

Introduction. PART II

1. Review: The H3K27me3 demethylase UTX in normal development and disease

Van der Meulen J, Speleman F, Van Vlierberghe P. Epigenetics. 2014 Feb 21;9(5).

REVIEW

Epigenetics 9:5, 1–11; May 2014; © 2014 Landes Bioscience

The H3K27me3 demethylase UTX in normal development and disease

Joni Van der Meulen, Frank Speleman, and Pieter Van Vlierberghe*

Center for Medical Genetics; Ghent University; Ghent, Belgium

Keywords: UTX, H3K27, MLL2, HOX, RB, SWI/SNF, reprogramming, embryogenesis, Kabuki, cancer

Abbreviations: CBP, CREB-binding protein; ChIP, chromatin immunoprecipitation; CMML, chronic myelomonocytic leukemia; E, embryonic day; ESC, embryonic stem cell; H3K27me2/3, histone 3 lysine 27 di- and tri-methylation; HOX, homeobox; IPA, Ingenuity Pathway Analysis; iPSC, induced pluripotent stem cell; JmjC, Jumonji C; JMJD3, Jumonji D3; KO, knockout; lincRNA, long intergenic non-coding RNA; LSD1, Lysine-Specific Demethylase 1; MEF, mouse embryonic fibroblast; PRC2, Polycomb Repressor Complex 2; TCGA, The Cancer Genome Atlas; TPR, tetratricopeptide repeat; Trr, Trithorax related; TSS, transcriptional start site; UTX, ubiquitously transcribed tetratricopeptide repeat on chromosome X; UTY, ubiquitously transcribed tetratricopeptide repeat on chromosome Y

In 2007, the *Ubiquitously Transcribed Tetratricopeptide Repeat on chromosome X* (UTX) was identified as a histone demethylase that specifically targets di- and tri-methyl groups on lysine 27 of histone H3 (H3K27me2/3). Since then, UTX has been proven essential during normal development, as it is critically required for correct reprogramming, embryonic development and tissue-specific differentiation. UTX is a member of the MLL2 H3K4 methyltransferase complex and its catalytic activity has been linked to regulation of *HOX* and *RB* transcriptional networks. In addition, an H3K27me2/3 demethylase independent function for UTX was uncovered in promoting general chromatin remodeling in concert with the BRG1-containing SWI/SNF remodeling complex. Constitutional inactivation of *UTX* causes a specific hereditary disorder called the Kabuki syndrome, whereas somatic loss of *UTX* has been reported in a variety of human cancers. Here, we compile the breakthrough discoveries made from the first disclosure of UTX as a histone demethylase till the identification of disease-related *UTX* mutations and specific UTX inhibitors.

Introduction

A decade ago, the identification of the first histone demethylase *Lysine (K)-Specific Demethylase 1* (LSD1) served as a landmark discovery that triggered research on dynamic regulation of histone methylation.[1] In the following years, numerous additional histone demethylases, that execute the removal of methyl groups on specific lysine residues of the histone tails and of non-histone substrates, were characterized in more detail (reviewed in ref. 2). In 2007, several groups identified *Ubiquitously Transcribed Tetratricopeptide Repeat on chromosome X* (UTX) and *Jumonji D3* (JMJD3) as novel histone demethylases that catalyze the removal of di- and trimethyl groups on histone H3 lysine 27, thereby promoting target gene activation.[3-6] Notably, *Ubiquitously Transcribed Tetratricopeptide Repeat on chromosome Y* (UTY) is a closely related homolog of UTX on the Y-chromosome but, up until now, no enzymatic H3K27me2/3 demethylase activity has been reported for UTY.[3,7]

The X-linked H3K27me2/3 eraser UTX is a member of the MLL2 histone H3K4 methyltransferase complex[8,9] and contributes to animal body patterning by regulation of homeobox (*HOX)* genes.[4,5] In contrast, a histone demethylation-independent role for UTX and JMJD3 has been demonstrated in normal and malignant T-cells through interaction with the BRG1-containing SWI/SNF remodeling complex.[10] *UTX* knockout (KO) studies have unraveled important roles for UTX in many developmental processes, including cardiac development and hematopoiesis, but also suggested that UTX and UTY might have redundant functions during embryonic development.[11-17]

Upon the establishment of UTX as a histone eraser in the context of normal development, a number of studies started to report genetic defects targeting *UTX* as the underlying cause of specific diseases. In 2009, a role for the histone H3K27me2/3 demethylase UTX as tumor suppressor was initially postulated in several human tumors including multiple myeloma, esophageal and renal cancer.[18] In 2012, specific loss-of-function defects in *UTX* were identified in patients with a specific hereditary disorder named the Kabuki syndrome.[19] In this review, we summarize the current knowledge on UTX in normal development and highlight recent findings on its implication in cancer and hereditary disease.

*Correspondence to: Pieter Van Vlierberghe;
Email: pieter.vanvlierberghe@ugent.be
Submitted: 01/24/2014; Revised: 02/12/2014; Accepted: 02/19/2014;
Published Online: 02/21/2014; http://dx.doi.org/10.4161/epi.28298

UTX Drives Context Dependent Transcriptional Regulation Mainly Through its H3K27 Demethylase Activity

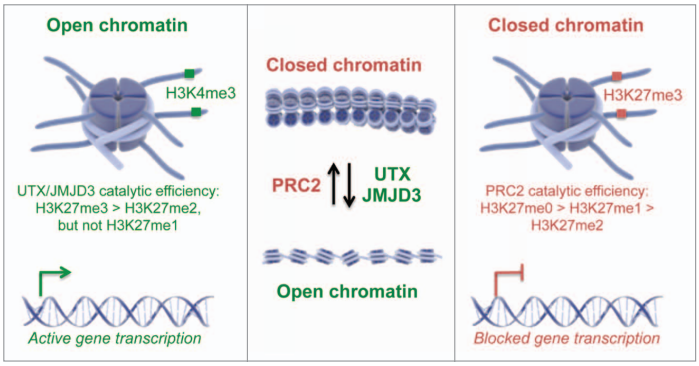

Figure 1. The UTX family mediates H3K27me2/3 demethylation. Graphical illustration of open and closed chromatin states that are mediated by the histone demethylases UTX and JMJD3 and the histone methyltransferase PRC2 hereby erasing or writing methyl groups on H3K27 enabling activation or blockage of gene transcription, respectively (graphics from www.somersault1824.com).

H3K27me2/3 demethylation

Methylation of H3K27 is a critical mediator of transcriptional gene repression and contributes to important biological processes including X-inactivation, genomic imprinting, stem cell maintenance, animal body patterning, circadian rhythms and cancer.[5,20] Regulation of cellular H3K27me3 levels is mainly mediated by the H3K27 methyltransferase *Polycomb Repressor Complex 2* (PRC2) and the H3K27me2/3 demethylases UTX and JMJD3 (**Fig. 1**).[3-6,21-24] Two main classes of histone demethylases have been discovered until now including the flavin-dependent amine oxidases, such as LSD1,[1] and the iron and α-ketoglutarate-dependent dioxygenases with a Jumonji C (JmjC) catalytic domain, such as UTX and JMJD3.[3-7]

The H3K27me2/3 demethylases UTX and JMJD3 preferentially demethylate H3K27me3 followed by H3K27me2 in vitro and in vivo. This demethylase activity is dependent on the catalytic JmjC domain, which contains conserved residues for binding with the co-factors iron and α-ketoglutarate.[3-7] Moreover, a newly identified zinc-binding domain within these H3K27me2/3 erasers provides specificity toward the histone lysine H3K27 and excludes interaction with the near-cognate histone lysine H3K9.[25,26] Notably, the family member UTY lacks H3K27me2/3 erasing activity in vitro and in vivo despite a conserved JmjC domain and 88% sequence homology with the UTX protein.[3,7,14] Finally, UTX and UTY proteins contain tetratricopeptide repeats (TPRs) at their N-terminal regions that are important for protein-protein interactions. These TPRs are lacking in the JMJD3 protein,[3-7] which might suggest lack of redundant functions between the H3K27me2/3 demethylases UTX and JMJD3.

UTX, UTY and JMJD3 are evolutionary conserved from *Caenorhabditis elegans* (*C. elegans*) to human.[3-7] The mouse genome contains the three H3K27me2/3 demethylase family members *Utx*, *Uty* and *Jmjd3*, whereas the genome of *Drosophila melanogaster* harbors only one ortholog of the mammalian H3K27me2/3 demethylases called *dUTX*.[27] The *C. elegans* genome possesses 4 orthologs whereby *UTX-1* resembles the mammalian *UTX* and the three other orthologs are more related to *JMJD3*.[28]

UTX is a member of the MLL2 H3K4 methyltransferase complex

In 2007, an MLL2 (also called ALR and formerly called MLL4) complex was identified in different mammalian cell types containing 12 protein members including MLL2, PTIP, UTX, ASC-2, ASH2L, RBBP5, WDR5, DPY30, matrin3, MGC4606, α- and β-tubulin.[8] Furthermore, the 3 complex members MLL2, PTIP and UTX were shown to co-localize at promoter regions and first exons of MLL2 target genes marked with the transcriptional activation mark H3K4me3.[8] Another group confirmed the identification of a similar H3K4 methyltransferase complex in which MLL2, MLL3, PTIP, UTX, ASC-2, ASH2L, RBBP5, WDR5, DPY30 and PA1 were also linked to H3K4 methylation activity (**Fig. 2**).[9] Interestingly, the composition of the MLL2 complex was confirmed in the *Drosophila* ortholog Trithorax related (Trr) complex[29] and the *C. elegans* ortholog SET-16 complex.[28] Hence, this conserved MLL2 complex acts like a classical H3K4 methyltransferase complex,[8] which suggests a dynamic interplay between H3K27me2/3 demethylation and H3K4 methylation during transcriptional gene activation.

In flies, *dUTX* mutant tissues are marked by an increase in global H3K27me3 levels and surprisingly also a reduction in global H3K4me1 levels.[20,30] The effect on H3K4me1, a mark enriched at enhancer regions and at gene bodies of actively transcribed genes, seems to be independent of the demethylation capacity of dUTX.[20,30] Similarly, loss of the Trr H3K4 methyltransferase complex results in a global profound reduction of H3K4me1 levels in many tissues.[30,31] Notably, Trr and dUTX are enriched genome-wide near transcriptional start sites (TSSs) (enriched for H3K4me3 and RNAP II) but also on active enhancers (enriched for H3K4me1) indicating a promoter-proximal role as well as a promoter-distal role for the Trr-dUtx complex in transcriptional regulation.[30] Importantly, loss of Trr provoked the most profound reduction in H3K4me1 levels at the enhancer regions compared with dUTX loss[30] indicating that the Trr complex itself is the main driver of H3K4 monomethylation with support of dUTX.

UTX interacts with the SWI/SNF remodeling complex and the histone acetyltransferase CBP

Besides regulation of histone modifications like H3K27me3, ATPase-dependent remodeling complexes including the SWI/SNF family contribute to regulation of chromatin accessibility hereby enabling transcriptional activation and repression.[32] The SWI/SNF family is mainly linked to transcriptional activation whereby the ATPase complex members BRG1 and BRM interact

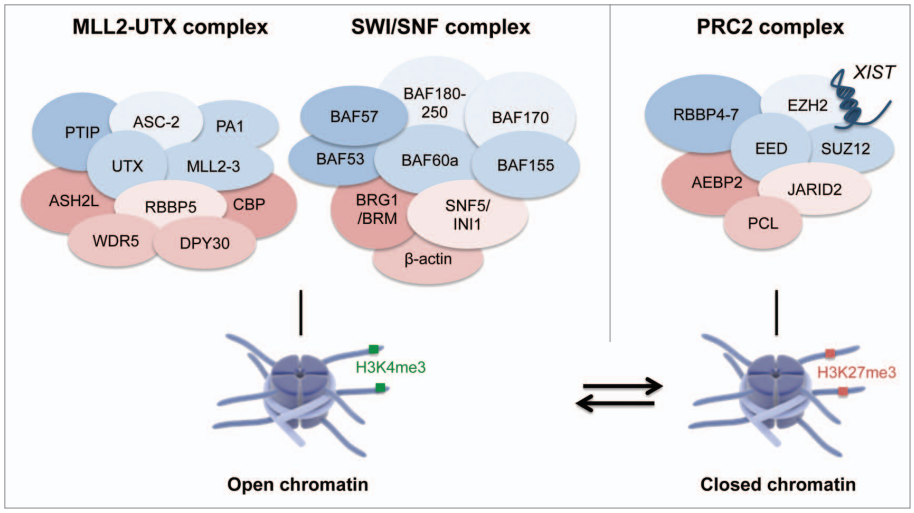

Figure 2. The chromatin complexes MLL2-UTX, SWI/SNF and PRC2 contribute to open and closed chromatin conformations. Schematic representation of the H3K4 methyltransferase complex MLL2-UTX, the SWI/SNF ATPase remodeling complex and the H3K27 methyltransferase complex PRC2 composed out of different protein-coding and non-protein-coding members. The histone eraser UTX is part of the MLL2 complex leading to a dynamic interplay between H3K4 methylation and H3K27me2/3 demethylation. Furthermore, UTX can cooperate with the BRG1-containing SWI/SNF complex where it plays a role in general chromatin remodeling independent of its H3K27 demethylase function. The MLL2-UTX and SWI/SNF complexes both contribute to an open chromatin formation. The PRC2 complex enables efficient methylation of H3K27 thereby promoting gene silencing and chromatin compaction (graphics from www.somersault1824.com).

with acetylated histone tails through their bromodomain (**Fig. 2**).[33,34] An interaction between the Brg1-containing SWI/SNF remodeling complex and the histone H3K27me2/3 erasers Utx and Jmjd3 was demonstrated promoting general chromatin remodeling that was independent of their H3K27me2/3 demethylase potential. Furthermore, UTX and JMJD3 were shown to be functionally required for transcriptional activation of lineage-defining T-box transcription factors (including T-bet, Eomes and Tbx5),[10] which represent essential transcriptional regulators in early cell-fate decisions, differentiation and organogenesis.[35]

An interaction between the histone acetyltransferase Creb-binding protein (CBP) and the SWI/SNF remodeling complex is observed in mammals[10,36] and *Drosophila*.[37] In flies, CBP and the PRC2 complex act antagonistically in the regulation of active and repressed chromatin states at Polycomb target genes by acetylation and methylation of H3K27, respectively (**Fig. 2**).[37] H3K27 acetylation is mainly detected at enhancers, promoters and gene bodies of actively transcribed genes.[30] To enable efficient H3K27 acetylation, CBP was shown to associate with dUTX and the ATPase Brm of the SWI/SNF complex.[37] The ATPase Brm in flies resembles the 2 mammalian orthologs BRM and BRG1 of the SWI/SNF complexes.[32,37] Genome-wide binding studies showed that the chromatin components dUTX, Brm and CBP co-occurred at Polycomb target genes enriched for H3K27ac, suggesting a collaborative effort antagonizing Polycomb mediated gene silencing.[37] Of note, loss of dUTX or Trr results in a reduction of global H3K27ac levels in various tissues,[30,37] so dUTX might be capable of promoting H3K27 acetylation and H3K4 monomethylation in concert with Trr, Brm and CBP.

UTX regulates dynamic *HOX* expression

The *HOX* genes are highly conserved transcriptional regulators essential during development of the anterior-posterior axis (head-tail).[38] The *HOX* family in humans consists of 39 *HOX* genes that encode 4 clusters of HOX proteins, i.e., HOXA to HOXD.[39] Aberrant expression of *HOX* genes leads to developmental defects and disease.[39] Polycomb and Trithorax proteins are implicated in the complex regulation of spatio-temporal expression of *HOX* genes thereby regulating animal body patterning and cell differentiation.[40] Evidence for direct involvement of UTX in regulation of *HOX* gene activity was demonstrated through UTX knockdown experiments in HEK293T cells in which loss of UTX induced transcriptional repression of *HOXA* and *HOXC* clusters.[5] Furthermore, UTX loss also resulted in an increase of H3K27me2/3 levels at the promoter regions of *HOXA13* and *HOXC4*, whereas no changes in MLL2 and PRC2 occupancy were observed.[5]

Chromatin immunoprecipitation (ChIP) of UTX followed by *HOX*-specific ultra-dense tiling microarrays (ChIP-chip) showed a strong UTX binding to narrow windows within 500 base pairs downstream of the TSSs of many *HOX* genes in human fibroblasts, but not in mouse embryonic stem cells (ESCs) where *HOX* genes are silenced. Importantly, H3K27 trimethylation was concomitantly diminished at UTX binding sites.[3] Hence, *HOX* expression is tightly regulated by opposing activities of the

H3K27me3 writer PRC2 and the H3K27me2/3 eraser UTX in order to enable context dependent transcriptional regulation.

UTX regulates a retinoblastoma gene network

Genome-wide ChIP-chip analysis of UTX, H3K4me2 and H3K27me3 in human fibroblasts identified UTX binding at 1945 promoters mostly upstream of TSS.[41] Out of these, the majority of UTX targets were enriched for H3K4me2 (62%) and showed transcriptional activity. This observation is consistent with UTX being a member of the H3K4 methyltransferase MLL2 complex.[8,9,41] Using Ingenuity Pathway analysis (IPA), a RB gene network including *RB1, HBP1* and *RBBP4, 5, 6* and *9* was discovered as the most significant network of UTX-bound genes enriched for H3K4me2.[41] Loss of UTX in human fibroblasts and mouse embryonic fibroblasts (MEFs) confirmed increased levels of H3K27me3 at promoters of genes from the identified RB-network thereby contributing to deregulated RB-dependent cell cycle arrest leading to ectopic cell proliferation.[41,42]

UTX Escapes X-Inactivation

The female genome harbors 2 X-chromosomes of which one X-chromosome is silenced to compensate the difference in gene dosage with males.[43] X-inactivation is mediated by the long intergenic non-coding RNA (lincRNA) *XIST*, which coats the inactive X-chromosome. Next, the PRC2 complex is guided by *XIST* to the inactive X-chromosome hereby enabling H3K27 methylation leading to the formation of facultative heterochromatin and gene silencing (**Fig. 2**).[44]

Utx is one of the few genes that can escape X-inactivation in female mice and human.[45] In agreement, Utx shows higher expression in female tissue of brain, liver, neurons and sexual organs.[46,47] In line with this observation, a female-specific function was reported for Utx in the regulation of the X-linked homeobox genes *Rhox6* and *Rhox9*.[46] It was shown that Utx is expressed at higher levels in undifferentiated female ESCs as compared with male ESCs, which resulted in a stronger Utx binding in the promoter regions of *Rhox6* and *Rhox9* in females. Subsequently, Utx mediates a more profound H3K27me3 removal and transcriptional activation of these homeobox genes in female cells.[46]

The Role of UTX in Cellular Reprogramming

Pluripotency is the unique characteristic of ESCs and the early developmental stage embryo to induce the generation of the three germ layers endoderm, ectoderm and mesoderm finally constituting all tissues of the adult organism.[48] Through in vitro reprogramming of somatic cells via induction of the four transcription factors OCT4, SOX2, KLF4 and MYC; pluripotency can be re-established hereby generating induced pluripotent stem cells (iPSC).[48,49] During reprogramming, genome-wide changes in the transcriptome and the chromatin structure are induced to achieve the switch to the pluripotent state.[48]

The histone H3K27me3 demethylase Utx has a critical role in efficient induction or re-establishment of pluripotency during the generation of iPSCs in vitro, but is dispensable for maintenance of pluripotency.[50] The requirement for UTX to ensure correct reprogramming depends on its H3K27me3 demethylase activity.[50] During iPSC induction, Utx target genes that are enriched with H3K4me3 in *Utx* wild-type MEFs aberrantly accumulate H3K27me3 in *Utx* mutant MEFs. These loci, including the stem-cell maintenance genes *Sall1*, *Sall4,* and *Utf1* as well as validated *Klf4* and *Oct4* target genes, fail to reactivate during reprogramming due to loss of Utx.[50] Hence, Utx seems to play a crucial role during reprogramming through its H3K27me2/3 demethylation activity in correct re-activation of essential pluripotency genes.

A Critical Role for UTX in Embryonic Stem Cells and Embryonic Development

Embryonic stem cells

H3K27 methylation is important in the maintenance of self-renewing ESCs by repressing tissue-specific developmental genes.[51-53] During ESC differentiation, the re-activation of developmental genes is associated with loss of H3K27me3.[51] Loss of Utx does not influence ESC self-renewal and proliferation, but seems to provoke an effect on the differentiation capacity of ESCs.[11,12,50,54] This differentiation defect is reflected by loss of induction of a set of developmental genes including some ectoderm markers (*Otx2, Msi1, Sox1,* and *Pax6*),[54] endoderm markers (*Gata4*, *Gata6, Foxa2, Sox17, Gsc,* and *Ncad*)[12,55] and mesoderm markers (*Vegfr2, Wnt3,* and *Brachyury*),[12,13,54,55] presumably due to loss of Utx binding to the promoter regions of these genes.[54]

Contradicting studies report on whether the effect of UTX loss on ESC differentiation depends on its H3K27me3 demethylase activity.[12,13,54,55] Namely, male *UTX* KO ESCs that express a catalytic inactive or wild-type Utx protein both could rescue the induction of expression of the mesoderm genes *Wnt3* and *Brachyury* supporting an H3K27me3-demethylase-independent role of Utx during ESC differentiation.[54] Furthermore, Utx binds directly to the promoters of the ectoderm genes *Msi1* and *Sox1* and the mesoderm gene *Brachyury* marked with an increase in H3K4me3 levels but without a change in H3K27me3 levels.[54] In contrast, a decrease in H3K27me3 levels and an increase in H3K4me3 levels was seen at the promoter of the Utx target *Hoxb1* during differentiation of Utx wild-type ESCs confirming that Utx still plays an H3K27me3 demethylase-dependent role in transcriptional regulation of homeotic and developmental genes.[54] Therefore, UTX regulates transcriptional activation of UTX target genes during ESC differentiation in different ways dependent or independent of its H3K27me2/3 demethylation activity.

Embryonic development in mice

Several groups have shown that complete loss of Utx in $Utx^{\Delta/\Delta}$ female mice leads to embryonic lethality between embryonic day (E) 10.5 and E12.5, whereas $Utx^{\Delta/+}$ heterozygous female mice are

viable and fertile.[11-15] Surprisingly, $Utx^{\Delta/Y}$ male mice are marked by a diverse outcome ranging from embryonic lethality to tumor formation in adults.[11-15] The viable adult $Utx^{\Delta/Y}$ male mice are smaller in size compared with their littermates[12,14] and remain fertile indicating that Utx is not required for male fertility.[12] Interestingly, $Utx^{\Delta/Uty\Delta}$ male mice, in which both *Utx* and *Uty* are eliminated, phenocopy the $Utx^{\Delta/\Delta}$ female mice,[14] suggesting that the Y-linked *Uty* gene can partially rescue the effect of complete loss of Utx.[11] In addition, Utx and Uty can both interact with Rbbp5 (member of the Mll2 complex) regulating H3K4 methylation rather than H3K27me2/3 demethylation at Utx and Uty target genes.[14]

Embryonic development in *Drosophila melanogaster*

Homozygous *dUTX Drosophila* mutants are lethal, with only 5% of the animals that survive the pupal stage although not reaching adulthood.[20] More specifically, $dUTX^{\Delta}$ homozygotes that lack both maternal and zygotic dUTX protein ($dUTX^{\Delta mat-zyg-}$) die as larvae, whereas $dUTX^{\Delta}$ homozygotes that lack only zygotic dUTX protein ($dUTX^{\Delta mat+zyg-}$) can develop further but die quickly after the pupal stage.[56] dUTX was shown to be necessary for the controlled expression of 2 specific homeotic genes *Ubx* and *Abd-B* in very early fly development.[56] Furthermore, sex combs malformation, rough eyes, wrinkled wings and wing vein defects are observed in the *dUTX* mutants which resembles some characteristics of Trithorax mutants and is in concordance with the effect of these proteins on *Hox* gene regulation.[20,56]

Embryonic development in *Caenorhabditis elegans*

In agreement with *Drosophila*, *UTX-1* mutant worms lacking both maternal and zygotic UTX-1 protein ($UTX\text{-}1^{m-z-}$) die as late stage embryos or malformed L1 larvae. Mutants with loss of only the zygotic UTX-1 ($UTX\text{-}1^{m+z-}$) protein are viable and reach adulthood, but a reduction in fertility is observed due to defects in gonad migration and oocyte organization. The $UTX\text{-}1^{m-z-}$ mutants show an increase in global H3K27me2/3 levels at the embryonic stage, but introduction of a catalytic inactive mutant of UTX-1 in $UTX\text{-}1^{m+z-}$ mutant animals rescued the fertility indicating that the UTX-1 demethylase activity is not necessary for this developmental process. Interestingly, loss of UTX-1 complex members SET-16 (MLL2–3), PIS-1 (PTIP), WDR-5.1 (WDR5) and F21H12.1 (RBBP5) also resulted in posterior and gonadal defects further confirming that these genes are acting in the same genetic complex.[28]

A Critical Role for UTX in Tissue-Specific and Developmental Processes

UTX contributes to a variety of tissue-specific and developmental processes including cardiac development,[11-15] hematopoiesis,[13,15,57,58] myogenesis,[16,17,27,59] osteogenic differentiation,[60] wound healing,[61] and aging.[62,63] Cardiac development and hematopoiesis will be discussed in further detail.

Cardiac development

The histone eraser Utx seems to play an important role in cardiac development. $Utx^{\Delta/Y}$ ESCs that in vitro differentiate into mature cardiac cells show absence of effective heart-like rhythmic contractions due to a failure of inducing cardiac-specific gene expression.[11] Furthermore, $Utx^{\Delta/\Delta}$ female mice and $Utx^{\Delta/Uty\Delta}$ male mice exhibited strong cardiac developmental and neural tube closure defects (cranioschisis) at day E9-E10.5.[11-15] This cardiac malformation is presumably caused by 2 mechanisms. First, loss of Utx disables the induction of transcriptional activation of cardiac-specific genes mediated by H3K27me2/3 demethylation, whereby the core cardiac transcription factors Nkx2-5, Tbx5, Gata4 and Srf specifically guide Utx to the promoter regions of cardiac-specific genes (**Fig. 3**).[11] Second, loss of Utx disturbs the interaction between the Brg1-containing SWI/SNF chromatin remodeling complex and the core cardiac transcription factor Tbx5, an effect that is thought to be independent from the H3K27me2/3 demethylase activity of UTX (**Fig. 3**).[10,11] This dual role of UTX is further supported by an independent study showing that UTX and UTY can physically interact with BRG1, NKX2-5, SRF and TBX5 hereby inducing expression of cardiac-specific genes.[14] Hence UTX enables transcriptional activation of cardiac-specific genes through H3K27me3 demethylase dependent and independent mechanisms during cardiac development.

Hematopoiesis

Utx expression levels peak in hematopoietic stem and progenitor cells and drop during hematopoietic differentiation.[58] In $Utx^{\Delta/\Delta}$ female mice embryos (E10.5), a lack of red bloods cells (anemia) was observed indicating a critical role for Utx in hematopoiesis.[13] Furthermore, female adult mice in which *Utx* was homozygously eliminated at 11–14 wk of age showed an enlarged spleen, reduced hemoglobin levels, anemia, thrombocytopenia and mild leukocytopenia compared with normal controls. In addition, hematopoietic transcription factors *Tal1*, *Gata1* and *Lyl1* were downregulated in the bone marrow of Utx KO female mice.[15] Furthermore, Utx was identified as an essential regulator of stem cell migration since loss of Utx blocked the migration potential of hematopoietic progenitor cells in vitro and of primordial germ cells in vivo.[15]

Constitutional UTX Defects Cause the Kabuki Syndrome

Constitutional loss-of-function defects in *UTX* cause the so-called Kabuki syndrome. This rare congenital anomaly syndrome, also called the Kabuki make-up syndrome, was first described by Niikawa and Kuroki in 1981.[64,65] The Kabuki syndrome is characterized by moderate-to-severe mental retardation, visceral and skeletal abnormalities, postnatal growth impairment (short stature) and facial abnormalities including large protruding ears.[64-66] The Kabuki syndrome has a prevalence of about 1 in 32 000 live births.[65] Using whole-exome sequencing, nonsense and frameshift mutations in the *MLL2* gene were first identified as a cause of the Kabuki syndrome[67] in 74% of these patients.[68] Two years later, 3 focal deletions targeting the histone demethylase *UTX* were identified in 1 male and 2 female Kabuki patients.[69] Subsequently, 2 nonsense mutations and a small

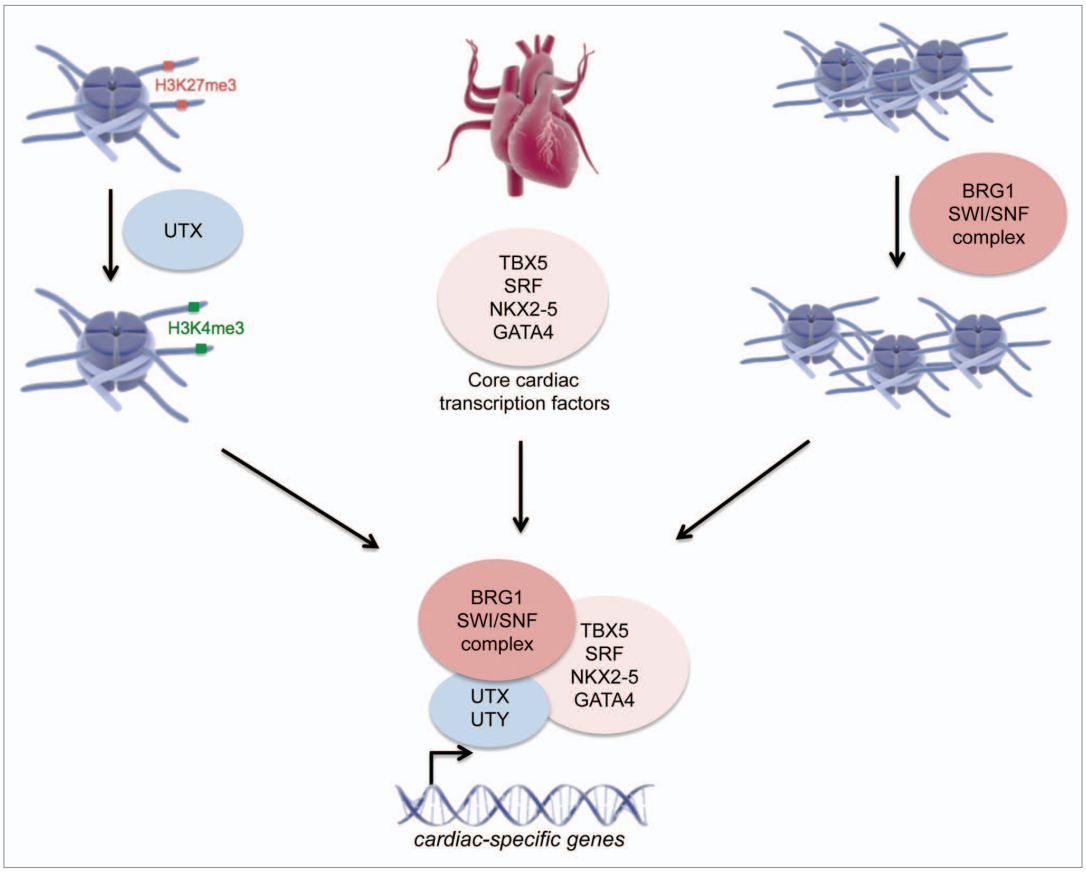

Figure 3. The involvement of UTX in genetic regulation of cardiac development. During cardiac development UTX, guided by the core cardiac transcription factors NKX2–5, TBX5, GATA4 and SRF, promotes specific gene activation of cardiac-specific genes through demethylation of H3K27me2/3 at their promoter regions. In addition, UTX and UTY can interact with the BRG1-containing SWI/SNF chromatin remodeling complex enabling general chromatin remodeling at these cardiac-specific gene loci (graphics from www.somersault1824.com).

indel mutation were discovered in 1 female and 2 male Kabuki patients.[19]

As discussed in the next part, both the *MLL2* and the *UTX* gene have been reported as important histone modifier genes involved in cancer pathogenesis. Until now, 6 Kabuki patients have been described that developed different types of cancer including pre-B-ALL,[70] hepatoblastoma,[71] neuroblastoma,[71,72] Burkitt lymphoma,[73] and fibromyxoid sarcoma[74] marking the Kabuki syndrome as a cancer predisposition syndrome.

UTX as a Bona Fide Tumor Suppressor Gene in Cancer Biology

Over the last years, deregulated histone methylation became a major theme in cancer biology research including the balance of H3K27 methylation. In 2009, somatic loss-of-function mutations and deletions targeting the *UTX* gene were identified in multiple cancer types including multiple myeloma, esophageal and renal cancer.[18] This notion was further supported by subsequent identification of recurrent inactivating *UTX* mutations and deletions in several leukemia as well as solid tumor types (**Fig. 4**; **Fig. S1**; **Tables S1 and 2**), mainly through exome- or genome-wide sequencing strategies.[75-84] Furthermore, a recent study of The Cancer Genome Atlas (TCGA) in which whole-exome sequencing was performed on 3281 tumors derived from 12 tumor types identified 127 significantly mutated genes including the tumor suppressor gene *UTX*.[85]

Bladder cancer has one of the highest frequencies of *UTX* mutations (**Fig. 4**) typically consisting of truncating mutations in the region coding for the functional JmjC domain of UTX. Interestingly, more than 50% of bladder cancer patients harbor genetic aberrations in a bigger set of chromatin remodeling genes including *UTX, CREBBP, EP300, ARID1A, CHD6,*

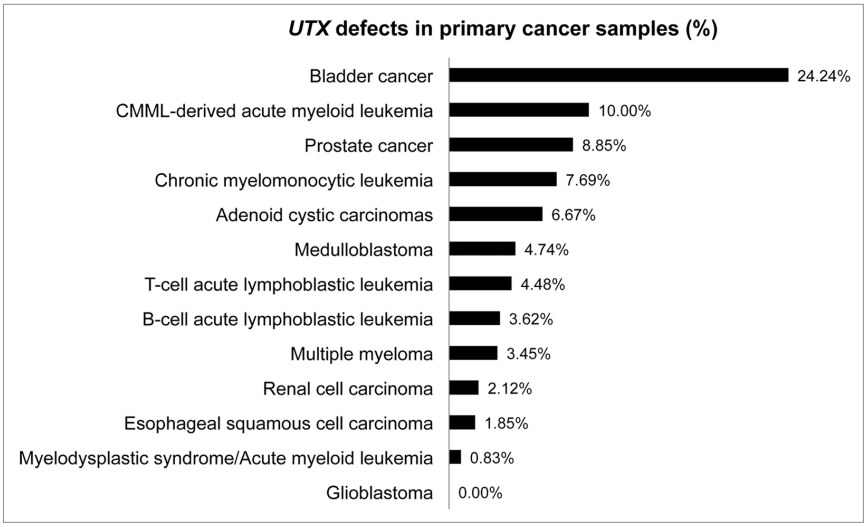

Figure 4. *UTX* defects in primary cancer samples. Schematic representation of the presence of *UTX* defects (%) in primary cancer samples of a broad range of leukemic and solid cancer types investigated in multiple genomic studies.

MLL1, MLL3, and *NCOR1*.[77] Furthermore, multiple myeloma cases harboring mutations in *UTX* or in the Trithorax complex members *MLL1, MLL2,* and *MLL3* were linked with high expression of *HOXA9*[76] confirming the role of UTX in *HOX* gene regulation.[3]

Interestingly, a study in chronic myelomonocytic leukemia (CMML) identified loss-of-function mutations in both *UTX* and *EZH2* despite their opposing roles on H3K27me3 regulation. Notably, these mutations occurred in a mutually exclusive manner in CMML patient samples.[86] *UTX* and *EZH2* defects in CMML were associated with *ASXL1*[87] and *TET2*[88] loss-of-function mutations, two genes also implicated in epigenetic regulation of gene expression.[86] These studies indicate that the chromatin regulatory machinery is a recurrent mutational target in a broad range of cancer types highlighting the importance of correct regulation of chromatin remodeling in the homeostasis of normal tissues.[32]

Whole-exome and whole-genome next-generation sequencing studies in medulloblastoma identified mutations in different chromatin regulators including *UTX*, *MLL2*, *MLL3*, *SMARCA4 (BRG1), ZMYM3,* and *CREBBP*.[78-80] In general, four prognostically relevant subgroups (SHH-subgroup, WNT-subgroup, subgroup 3 and subgroup 4) are defined in this malignant childhood brain tumor.[80] Of particular interest, medulloblastoma is marked by a disturbed gender distribution toward males in subgroups 3 and 4[89] and mutations targeting the X-linked *UTX* gene were exclusively identified in these 2 subgroups.[79,80,90] In line with the fact that *UTX* escapes X-inactivation,[45] female medulloblastoma patients harboring *UTX* defects showed bi-allelic *UTX* inactivation (splice-site *UTX* mutation and deletion[80] or missense mutation and loss of chromosome X[79]), suggesting that complete loss of UTX is required for malignant transformation. In addition, more than 50% of *UTX* mutant male medulloblastoma patients had a deletion of the Y-chromosome (including the UTX family member *UTY*) compared with less than 10% of *UTX* wild-type males.[80] Furthermore, gain or overexpression of the H3K27 methyltransferase *EZH2* as well as inactivating mutations in H3K4me3 regulators *CHD7* and *ZMYM3* were also present in subgroups 3 and 4 of medulloblastoma. All together, these data indicate that deregulation of H3K27 and H3K4 methylation is a core oncogenic component of medulloblastoma. Importantly, mutations targeting the X-linked gene *UTX* might partially explain the higher male prevalence in medulloblastoma subgroups 3 and 4.[80]

So far, the functional consequences of cancer related *UTX* mutations have been poorly characterized. Western blot analyses show lack of UTX protein expression in *UTX* mutant cancer cell lines.[18] Furthermore, re-expression of UTX in *UTX* mutant cancer cell lines was associated with lower H3K27me3 levels at the promoters of Polycomb target genes and concomitant inhibition of cell proliferation.[18] In adenoid cystic carcinomas, the impact of the identified *UTX* missense mutations was evaluated by introduction of these *UTX* mutants in HEK293T cells, which led to an increase in cell growth and a decrease in H3K27me3 levels.[84] Finally, a *Sleeping Beauty* based insertional mutagenesis screen using a *Kras* driven pancreatic mouse model identified 543 candidate cancer driver genes with 10% of the genes involved in chromatin regulation including the *Utx* gene. This un-biased screening approach provides an independent in vivo confirmation of the potential role of *Utx* as a bona fide tumor suppressor gene in cancer biology.[91]

Targeting UTX by Small Molecule Inhibitors

The most selective compound against JMJD3 and UTX, GSK-J1, was discovered based on the structural insights of the human and mouse JMJD3 protein with an IC_{50} of 60nM for inhibiting JMJD3. Furthermore, GSK-J1 is active against both H3K27me3 erasers UTX and JMJD3 but inactive against a panel of demethylases of the JmjC family. Notably, the cell-penetrating derivative GSK-J4 was able to inhibit the JMJD3-induced loss of total nuclear H3K27me3 levels and to enable specific inhibition of H3K27 demethylation at promoter regions of JMJD3 and UTX target genes.[92]

Several general inhibitors of JmjC demethylases have been identified including the α-ketoglutaric acid mimics N-oxalylglycine,[93,94] methylstat[95] and 2,4-dicarboxypyridine; the iron-chelating agent deferoxamine[95]; the pyridine hydrazone JIB-04[96] and catechols.[97] Unfortunately, these inhibitors are selective against some or all JmjC enzymes but are unable to target one specific JmjC member.

Conclusions

In this review, we have summarized and discussed the identification of the histone H3K27me2/3 erasers UTX and JMJD3, and the role of UTX in normal development and disease. UTX cooperates with a set of chromatin players, including the histone methyltransferase complex MLL2, the histone acetyltransferase CBP and the BRG1-containing SWI/SNF remodeling complex,[8-10,37] to trigger active gene transcription by H3K27me2/3 demethylation or H3K4 methylation.[3-6,8-10,30,37] Up until now, the main direct target genes of UTX encompass a broad set of *HOX* genes important in animal body patterning[3,5] and a *RB* gene network implicated in cell fate control.[41] Furthermore, UTX loss can lead to the development of the Kabuki syndrome[69] and can contribute to cancer pathogenesis.[18]

The third UTX family member UTY has no clear enzymatic demethylase activity despite the presence of a conserved JmjC domain and high amino acid conservation.[3,7,14] Surprisingly, UTY can partly compensate UTX functions including the cooperation with the MLL2 and BRG1-containing SWI/SNF complexes.[14] Also, UTY can partially rescue embryonic lethality in *UTX* KO male mice.[11-15] Furthermore, *UTX* mutations are frequently found together with deletions encompassing the *UTY* gene locus in male cancer patients.[18,80] Hence, a set of overlapping functions between UTX and UTY in transcriptional regulation seems present despite the lack of H3K27me2/3 demethylase activity for UTY.

All together, the complexity of biological functions assigned to UTX is just starting to emerge and will trigger additional research in a broad range of developmental processes. Multiple studies have highlighted UTX as an important player in cancer biology, but its role as a bona fide tumor suppressor still needs further confirmation using genetically engineered in vivo models. Ultimately, these biological insights will clarify to what extend loss of UTX provides therapeutic opportunities for human disease.

Disclosure of Potential Conflicts of Interest

No potential conflicts of interest were disclosed.

Acknowledgments

This work is supported by the Fund for Scientific Research (FWO) Flanders (postdoctoral grant to P.V.V., PhD grant to J.V.d.M., Odysseus grant to P.V.V, project grants G.0198.08, G.0564.13N, G.0550.13N, G.0869.10N to F.S. and G.A001.13N to P.V.V.); the Flemish Liga against Cancer (VLK) (PhD grant to J.V.d.M.); the GOA-UGent (grant no. 12051203 to F.S.); the Cancer Plan from the Federal Public Service of Health (F.S.); the Children Cancer Fund Ghent (F.S.); the Belgian Program of Interuniversity Poles of Attraction IUAP (F.S.) and the Belgian Foundation Against Cancer (365O9110 to F.S.).

Supplemental Materials

Supplemental materials may be found here:
www.landesbioscience.com/journals/epigenetics/article/28298

References

1. Shi Y, Lan F, Matson C, Mulligan P, Whetstine JR, Cole PA, Casero RA, Shi Y. Histone demethylation mediated by the nuclear amine oxidase homolog LSD1. Cell 2004; 119:941-53; PMID:15620353; http://dx.doi.org/10.1016/j.cell.2004.12.012
2. Kooistra SM, Helin K. Molecular mechanisms and potential functions of histone demethylases. Nat Rev Mol Cell Biol 2012; 13:297-311; PMID:22473470
3. Lan F, Bayliss PE, Rinn JL, Whetstine JR, Wang JK, Chen S, Iwase S, Alpatov R, Issaeva I, Canaani E, et al. A histone H3 lysine 27 demethylase regulates animal posterior development. Nature 2007; 449:689-94; PMID:17851529; http://dx.doi.org/10.1038/nature06192
4. Agger K, Cloos PA, Christensen J, Pasini D, Rose S, Rappsilber J, Issaeva I, Canaani E, Salcini AE, Helin K. UTX and JMJD3 are histone H3K27 demethylases involved in HOX gene regulation and development. Nature 2007; 449:731-4; PMID:17713478; http://dx.doi.org/10.1038/nature06145
5. Lee MG, Villa R, Trojer P, Norman J, Yan KP, Reinberg D, Di Croce L, Shiekhattar R. Demethylation of H3K27 regulates polycomb recruitment and H2A ubiquitination. Science 2007; 318:447-50; PMID:17761849; http://dx.doi.org/10.1126/science.1149042
6. De Santa F, Totaro MG, Prosperini E, Notarbartolo S, Testa G, Natoli G. The histone H3 lysine-27 demethylase Jmjd3 links inflammation to inhibition of polycomb-mediated gene silencing. Cell 2007; 130:1083-94; PMID:17825402; http://dx.doi.org/10.1016/j.cell.2007.08.019
7. Hong S, Cho YW, Yu LR, Yu H, Veenstra TD, Ge K. Identification of JmjC domain-containing UTX and JMJD3 as histone H3 lysine 27 demethylases. Proc Natl Acad Sci U S A 2007; 104:18439-44; PMID:18003914; http://dx.doi.org/10.1073/pnas.0707292104
8. Issaeva I, Zonis Y, Rozovskaia T, Orlovsky K, Croce CM, Nakamura T, Mazo A, Eisenbach L, Canaani E. Knockdown of ALR (MLL2) reveals ALR target genes and leads to alterations in cell adhesion and growth. Mol Cell Biol 2007; 27:1889-903; PMID:17178841; http://dx.doi.org/10.1128/MCB.01506-06
9. Cho YW, Hong T, Hong S, Guo H, Yu H, Kim D, Guszczynski T, Dressler GR, Copeland TD, Kalkum M, et al. PTIP associates with MLL3- and MLL4-containing histone H3 lysine 4 methyltransferase complex. J Biol Chem 2007; 282:20395-406; PMID:17500065; http://dx.doi.org/10.1074/jbc.M701574200
10. Miller SA, Mohn SE, Weinmann AS. Jmjd3 and UTX play a demethylase-independent role in chromatin remodeling to regulate T-box family member-dependent gene expression. Mol Cell 2010; 40:594-605; PMID:21095589; http://dx.doi.org/10.1016/j.molcel.2010.10.028
11. Lee S, Lee JW, Lee SK. UTX, a histone H3-lysine 27 demethylase, acts as a critical switch to activate the cardiac developmental program. Dev Cell 2012; 22:25-37; PMID:22192413; http://dx.doi.org/10.1016/j.devcel.2011.11.009
12. Welstead GG, Creyghton MP, Bilodeau S, Cheng AW, Markoulaki S, Young RA, Jaenisch R. X-linked H3K27me3 demethylase Utx is required for embryonic development in a sex-specific manner. Proc Natl Acad Sci U S A 2012; 109:13004-9; PMID:22826230; http://dx.doi.org/10.1073/pnas.1210787109

13. Wang C, Lee JE, Cho YW, Xiao Y, Jin Q, Liu C, Ge K. UTX regulates mesoderm differentiation of embryonic stem cells independent of H3K27 demethylase activity. Proc Natl Acad Sci U S A 2012; 109:15324-9; PMID:22949634; http://dx.doi.org/10.1073/pnas.1204166109
14. Shpargel KB, Sengoku T, Yokoyama S, Magnuson T. UTX and UTY demonstrate histone demethylase-independent function in mouse embryonic development. PLoS Genet 2012; 8:e1002964; PMID:23028370; http://dx.doi.org/10.1371/journal.pgen.1002964
15. Thieme S, Gyárfás T, Richter C, Özhan G, Fu J, Alexopoulou D, Muders MH, Michalk I, Jakob C, Dahl A, et al. The histone demethylase UTX regulates stem cell migration and hematopoiesis. Blood 2013; 121:2462-73; PMID:23365460; http://dx.doi.org/10.1182/blood-2012-08-452003
16. Seenundun S, Rampalli S, Liu QC, Aziz A, Palii C, Hong S, Blais A, Brand M, Ge K, Dilworth FJ. UTX mediates demethylation of H3K27me3 at muscle-specific genes during myogenesis. EMBO J 2010; 29:1401-11; PMID:20300060; http://dx.doi.org/10.1038/emboj.2010.37
17. Wang AH, Zare H, Mousavi K, Wang C, Moravec CE, Sirotkin HI, Ge K, Gutierrez-Cruz G, Sartorelli V. The histone chaperone Spt6 coordinates histone H3K27 demethylation and myogenesis. EMBO J 2013; 32:1075-86; PMID:23503590; http://dx.doi.org/10.1038/emboj.2013.54
18. van Haaften G, Dalgliesh GL, Davies H, Chen L, Bignell G, Greenman C, Edkins S, Hardy C, O'Meara S, Teague J, et al. Somatic mutations of the histone H3K27 demethylase gene UTX in human cancer. Nat Genet 2009; 41:521-3; PMID:19330029; http://dx.doi.org/10.1038/ng.349
19. Miyake N, Mizuno S, Okamoto N, Ohashi H, Shiina M, Ogata K, Tsurusaki Y, Nakashima M, Saitsu H, Niikawa N, et al. KDM6A point mutations cause Kabuki syndrome. Hum Mutat 2013; 34:108-10; PMID:23076834; http://dx.doi.org/10.1002/humu.22229
20. Herz HM, Madden LD, Chen Z, Bolduc C, Buff E, Gupta R, Davuluri R, Shilatifard A, Hariharan IK, Bergmann A. The H3K27me3 demethylase dUTX is a suppressor of Notch- and Rb-dependent tumors in Drosophila. Mol Cell Biol 2010; 30:2485-97; PMID:20212086; http://dx.doi.org/10.1128/MCB.01633-09
21. Cao R, Wang L, Wang H, Xia L, Erdjument-Bromage H, Tempst P, Jones RS, Zhang Y. Role of histone H3 lysine 27 methylation in Polycomb-group silencing. Science 2002; 298:1039-43; PMID:12351676; http://dx.doi.org/10.1126/science.1076997
22. Czermin B, Melfi R, McCabe D, Seitz V, Imhof A, Pirrotta V. Drosophila enhancer of Zeste/ESC complexes have a histone H3 methyltransferase activity that marks chromosomal Polycomb sites. Cell 2002; 111:185-96; PMID:12408863; http://dx.doi.org/10.1016/S0092-8674(02)00975-3
23. Kuzmichev A, Nishioka K, Erdjument-Bromage H, Tempst P, Reinberg D. Histone methyltransferase activity associated with a human multiprotein complex containing the Enhancer of Zeste protein. Genes Dev 2002; 16:2893-905; PMID:12435631; http://dx.doi.org/10.1101/gad.1035902
24. Müller J, Hart CM, Francis NJ, Vargas ML, Sengupta A, Wild B, Miller EL, O'Connor MB, Kingston RE, Simon JA. Histone methyltransferase activity of a Drosophila Polycomb group repressor complex. Cell 2002; 111:197-208; PMID:12408864; http://dx.doi.org/10.1016/S0092-8674(02)00976-5
25. Kim E, Song JJ. Diverse ways to be specific: a novel Zn-binding domain confers substrate specificity to UTX/KDM6A histone H3 Lys 27 demethylase. Genes Dev 2011; 25:2223-6; PMID:22056667; http://dx.doi.org/10.1101/gad.179473.111
26. Sengoku T, Yokoyama S. Structural basis for histone H3 Lys 27 demethylation by UTX/KDM6A. Genes Dev 2011; 25:2266-77; PMID:22002947; http://dx.doi.org/10.1101/gad.172296.111
27. Smith ER, Lee MG, Winter B, Droz NM, Eissenberg JC, Shiekhattar R, Shilatifard A. Drosophila UTX is a histone H3 Lys27 demethylase that colocalizes with the elongating form of RNA polymerase II. Mol Cell Biol 2008; 28:1041-6; PMID:18039863; http://dx.doi.org/10.1128/MCB.01504-07
28. Vandamme J, Lettier G, Sidoli S, Di Schiavi E, Nørregaard Jensen O, Salcini AE. The C. elegans H3K27 demethylase UTX-1 is essential for normal development, independent of its enzymatic activity. PLoS Genet 2012; 8:e1002647; PMID:22570628; http://dx.doi.org/10.1371/journal.pgen.1002647
29. Mohan M, Herz HM, Smith ER, Zhang Y, Jackson J, Washburn MP, Florens L, Eissenberg JC, Shilatifard A. The COMPASS family of H3K4 methylases in Drosophila. Mol Cell Biol 2011; 31:4310-8; PMID:21875999; http://dx.doi.org/10.1128/MCB.06092-11
30. Herz HM, Mohan M, Garruss AS, Liang K, Takahashi YH, Mickey K, Voets O, Verrijzer CP, Shilatifard A. Enhancer-associated H3K4 monomethylation by Trithorax-related, the Drosophila homolog of mammalian Mll3/Mll4. Genes Dev 2012; 26:2604-20; PMID:23166019; http://dx.doi.org/10.1101/gad.201327.112
31. Kanda H, Nguyen A, Chen L, Okano H, Hariharan IK. The Drosophila ortholog of MLL3 and MLL4, trithorax related, functions as a negative regulator of tissue growth. Mol Cell Biol 2013; 33:1702-10; PMID:23459941; http://dx.doi.org/10.1128/MCB.01585-12
32. Plass C, Pfister SM, Lindroth AM, Bogatyrova O, Claus R, Lichter P. Mutations in regulators of the epigenome and their connections to global chromatin patterns in cancer. Nat Rev Genet 2013; 14:765-80; PMID:24105274; http://dx.doi.org/10.1038/nrg3554
33. Hassan AH, Prochasson P, Neely KE, Galasinski SC, Chandy M, Carrozza MJ, Workman JL. Function and selectivity of bromodomains in anchoring chromatin-modifying complexes to promoter nucleosomes. Cell 2002; 111:369-79; PMID:12419247; http://dx.doi.org/10.1016/S0092-8674(02)01005-X
34. Wang GG, Allis CD, Chi P. Chromatin remodeling and cancer, Part II: ATP-dependent chromatin remodeling. Trends Mol Med 2007; 13:373-80; PMID:17822959; http://dx.doi.org/10.1016/j.molmed.2007.07.004
35. Wilson V, Conlon FL. The T-box family. Genome Biol 2002; 3:REVIEWS3008; PMID:12093383; http://dx.doi.org/10.1186/gb-2002-3-6-reviews3008
36. Naidu SR, Love IM, Imbalzano AN, Grossman SR, Androphy EJ. The SWI/SNF chromatin remodeling subunit BRG1 is a critical regulator of p53 necessary for proliferation of malignant cells. Oncogene 2009; 28:2492-501; PMID:19448667; http://dx.doi.org/10.1038/onc.2009.121
37. Tie F, Banerjee R, Conrad PA, Scacheri PC, Harte PJ. Histone demethylase UTX and chromatin remodeler BRM bind directly to CBP and modulate acetylation of histone H3 lysine 27. Mol Cell Biol 2012; 32:2323-34; PMID:22493065; http://dx.doi.org/10.1128/MCB.06392-11
38. Mallo M, Alonso CR. The regulation of Hox gene expression during animal development. Development 2013; 140:3951-63; PMID:24046316; http://dx.doi.org/10.1242/dev.068346
39. Shah N, Sukumar S. The Hox genes and their roles in oncogenesis. Nat Rev Cancer 2010; 10:361-71; PMID:20357775; http://dx.doi.org/10.1038/nrc2826
40. Bracken AP, Dietrich N, Pasini D, Hansen KH, Helin K. Genome-wide mapping of Polycomb target genes unravels their roles in cell fate transitions. Genes Dev 2006; 20:1123-36; PMID:16618801; http://dx.doi.org/10.1101/gad.381706
41. Wang JK, Tsai MC, Poulin G, Adler AS, Chen S, Liu H, Shi Y, Chang HY. The histone demethylase UTX enables RB-dependent cell fate control. Genes Dev 2010; 24:327-32; PMID:20123895; http://dx.doi.org/10.1101/gad.1882610
42. Terashima M, Ishimura A, Yoshida M, Suzuki Y, Sugano S, Suzuki T. The tumor suppressor Rb and its related Rbl2 genes are regulated by Utx histone demethylase. Biochem Biophys Res Commun 2010; 399:238-44; PMID:20650264; http://dx.doi.org/10.1016/j.bbrc.2010.07.061
43. Wutz A. Gene silencing in X-chromosome inactivation: advances in understanding facultative heterochromatin formation. Nat Rev Genet 2011; 12:542-53; PMID:21765457; http://dx.doi.org/10.1038/nrg3035
44. Margueron R, Reinberg D. The Polycomb complex PRC2 and its mark in life. Nature 2011; 469:343-9; PMID:21248841; http://dx.doi.org/10.1038/nature09784
45. Greenfield A, Carrel L, Pennisi D, Philippe C, Quaderi N, Siggers P, Steiner K, Tam PP, Monaco AP, Willard HF, et al. The UTX gene escapes X inactivation in mice and humans. Hum Mol Genet 1998; 7:737-42; PMID:9499428; http://dx.doi.org/10.1093/hmg/7.4.737
46. Berletch JB, Deng X, Nguyen DK, Disteche CM. Female bias in Rhox6 and 9 regulation by the histone demethylase KDM6A. PLoS Genet 2013; 9:e1003489; PMID:23658530; http://dx.doi.org/10.1371/journal.pgen.1003489
47. Xu J, Deng X, Watkins R, Disteche CM. Sex-specific differences in expression of histone demethylases Utx and Uty in mouse brain and neurons. J Neurosci 2008; 28:4521-7; PMID:18434530; http://dx.doi.org/10.1523/JNEUROSCI.5382-07.2008
48. Rada-Iglesias A, Wysocka J. Epigenomics of human embryonic stem cells and induced pluripotent stem cells: insights into pluripotency and implications for disease. Genome Med 2011; 3:36; PMID:21658297; http://dx.doi.org/10.1186/gm252
49. Takahashi K, Yamanaka S. Induction of pluripotent stem cells from mouse embryonic and adult fibroblast cultures by defined factors. Cell 2006; 126:663-76; PMID:16904174; http://dx.doi.org/10.1016/j.cell.2006.07.024
50. Mansour AA, Gafni O, Weinberger L, Zviran A, Ayyash M, Rais Y, Krupalnik V, Zerbib M, Amann-Zalcenstein D, Maza I, et al. The H3K27 demethylase Utx regulates somatic and germ cell epigenetic reprogramming. Nature 2012; 488:409-13; PMID:22801502; http://dx.doi.org/10.1038/nature11272
51. Boyer LA, Plath K, Zeitlinger J, Brambrink T, Medeiros LA, Lee TI, Levine SS, Wernig M, Tajonar A, Ray MK, et al. Polycomb complexes repress developmental regulators in murine embryonic stem cells. Nature 2006; 441:349-53; PMID:16625203; http://dx.doi.org/10.1038/nature04733
52. Bernstein BE, Mikkelsen TS, Xie X, Kamal M, Huebert DJ, Cuff J, Fry B, Meissner A, Wernig M, Plath K, et al. A bivalent chromatin structure marks key developmental genes in embryonic stem cells. Cell 2006; 125:315-26; PMID:16630819; http://dx.doi.org/10.1016/j.cell.2006.02.041
53. Lee TI, Jenner RG, Boyer LA, Guenther MG, Levine SS, Kumar RM, Chevalier B, Johnstone SE, Cole MF, Isono K, et al. Control of developmental regulators by Polycomb in human embryonic stem cells. Cell 2006; 125:301-13; PMID:16630818; http://dx.doi.org/10.1016/j.cell.2006.02.043

54. Morales Torres C, Laugesen A, Helin K. Utx is required for proper induction of ectoderm and mesoderm during differentiation of embryonic stem cells. PLoS One 2013; 8:e60020; PMID:23573229; http://dx.doi.org/10.1371/journal.pone.0060020
55. Jiang W, Wang J, Zhang Y. Histone H3K27me3 demethylases KDM6A and KDM6B modulate definitive endoderm differentiation from human ESCs by regulating WNT signaling pathway. Cell Res 2013; 23:122-30; PMID:22907667; http://dx.doi.org/10.1038/cr.2012.119
56. Copur Ö, Müller J. The histone H3-K27 demethylase Utx regulates HOX gene expression in Drosophila in a temporally restricted manner. Development 2013; 140:3478-85; PMID:23900545; http://dx.doi.org/10.1242/dev.097204
57. Chaturvedi CP, Hosey AM, Palii C, Perez-Iratxeta C, Nakatani Y, Ranish JA, Dilworth FJ, Brand M. Dual role for the methyltransferase G9a in the maintenance of beta-globin gene transcription in adult erythroid cells. Proc Natl Acad Sci U S A 2009; 106:18303-8; PMID:19822740; http://dx.doi.org/10.1073/pnas.0906769106
58. Liu J, Mercher T, Scholl C, Brumme K, Gilliland DG, Zhu N. A functional role for the histone demethylase UTX in normal and malignant hematopoietic cells. Exp Hematol 2012; 40:487-98, e3; PMID:22306297; http://dx.doi.org/10.1016/j.exphem.2012.01.017
59. Caretti G, Di Padova M, Micales B, Lyons GE, Sartorelli V. The Polycomb Ezh2 methyltransferase regulates muscle gene expression and skeletal muscle differentiation. Genes Dev 2004; 18:2627-38; PMID:15520282; http://dx.doi.org/10.1101/gad.1241904
60. Hemming S, Cakouros D, Isenmann S, Cooper L, Menicanin D, Zannettino A, Gronthos S. EZH2 and KDM6A act as an epigenetic switch to regulate mesenchymal stem cell lineage specification. Stem Cells 2014; 32:802-15; PMID:24123378; http://dx.doi.org/10.1002/stem.1573
61. Shaw T, Martin P. Epigenetic reprogramming during wound healing: loss of polycomb-mediated silencing may enable upregulation of repair genes. EMBO Rep 2009; 10:881-6; PMID:19575012; http://dx.doi.org/10.1038/embor.2009.102
62. Maures TJ, Greer EL, Hauswirth AG, Brunet A. The H3K27 demethylase UTX-1 regulates C. elegans lifespan in a germline-independent, insulin-dependent manner. Aging Cell 2011; 10:980-90; PMID:21834846; http://dx.doi.org/10.1111/j.1474-9726.2011.00738.x
63. Jin C, Li J, Green CD, Yu X, Tang X, Han D, Xian B, Wang D, Huang X, Cao X, et al. Histone demethylase UTX-1 regulates C. elegans life span by targeting the insulin/IGF-1 signaling pathway. Cell Metab 2011; 14:161-72; PMID:21803287; http://dx.doi.org/10.1016/j.cmet.2011.07.001
64. Niikawa N, Matsuura N, Fukushima Y, Ohsawa T, Kajii T. Kabuki make-up syndrome: a syndrome of mental retardation, unusual facies, large and protruding ears, and postnatal growth deficiency. J Pediatr 1981; 99:565-9; PMID:7277096; http://dx.doi.org/10.1016/S0022-3476(81)80255-7
65. Niikawa N, Kuroki Y, Kajii T, Matsuura N, Ishikiriyama S, Tonoki H, Ishikawa N, Yamada Y, Fujita M, Umemoto H, et al. Kabuki make-up (Niikawa-Kuroki) syndrome: a study of 62 patients. Am J Med Genet 1988; 31:565-89; PMID:3067577; http://dx.doi.org/10.1002/ajmg.1320310312
66. Miyake N, Koshimizu E, Okamoto N, Mizuno S, Ogata T, Nagai T, Kosho T, Ohashi H, Kato M, Sasaki G, et al. MLL2 and KDM6A mutations in patients with Kabuki syndrome. Am J Med Genet A 2013; 161:2234-43; PMID:23913813; http://dx.doi.org/10.1002/ajmg.a.36072
67. Ng SB, Bigham AW, Buckingham KJ, Hannibal MC, McMillin MJ, Gildersleeve HI, Beck AE, Tabor HK, Cooper GM, Mefford HC, et al. Exome sequencing identifies MLL2 mutations as a cause of Kabuki syndrome. Nat Genet 2010; 42:790-3; PMID:20711175; http://dx.doi.org/10.1038/ng.646
68. Hannibal MC, Buckingham KJ, Ng SB, Ming JE, Beck AE, McMillin MJ, Gildersleeve HI, Bigham AW, Tabor HK, Mefford HC, et al. Spectrum of MLL2 (ALR) mutations in 110 cases of Kabuki syndrome. Am J Med Genet A 2011; 155A:1511-6; PMID:21671394; http://dx.doi.org/10.1002/ajmg.a.34074
69. Lederer D, Grisart B, Digilio MC, Benoit V, Crespin M, Ghariani SC, Maystadt I, Dallapiccola B, Verellen-Dumoulin C. Deletion of KDM6A, a histone demethylase interacting with MLL2, in three patients with Kabuki syndrome. Am J Hum Genet 2012; 90:119-24; PMID:22197486; http://dx.doi.org/10.1016/j.ajhg.2011.11.021
70. Scherer S, Theile U, Beyer V, Ferrari R, Kreck C, Rister M. Patient with Kabuki syndrome and acute leukemia. Am J Med Genet A 2003; 122A:76-9; PMID:12949977; http://dx.doi.org/10.1002/ajmg.a.20261
71. Tumino M, Licciardello M, Sorge G, Cutrupi MC, Di Benedetto F, Amoroso L, Catania R, Pennisi M, D'Amico S, Di Cataldo A. Kabuki syndrome and cancer in two patients. Am J Med Genet A 2010; 152A:1536-9; PMID:20503331
72. Merks JH, Caron HN, Hennekam RC. High incidence of malformation syndromes in a series of 1,073 children with cancer. Am J Med Genet A 2005; 134A:132-43; PMID:15712196; http://dx.doi.org/10.1002/ajmg.a.30603
73. Ijichi O, Kawakami K, Matsuda Y, Ikarimoto N, Miyata K, Takamatsu H, Tokunaga M. A case of Kabuki make-up syndrome with EBV+Burkitt's lymphoma. Acta Paediatr Jpn 1996; 38:66-8; PMID:8992864; http://dx.doi.org/10.1111/j.1442-200X.1996.tb03439.x
74. Shahdadpuri R, O'Meara A, O'Sullivan M, Reardon W. Low-grade fibromyxoid sarcoma: yet another malignancy associated with Kabuki syndrome. Clin Dysmorphol 2008; 17:199-202; PMID:18541969; http://dx.doi.org/10.1097/MCD.0b013e3282f5f4e3
75. De Keersmaecker K, Atak ZK, Li N, Vicente C, Patchett S, Girardi T, Gianfelici V, Geerdens E, Clappier E, Porcu M, et al. Exome sequencing identifies mutation in CNOT3 and ribosomal genes RPL5 and RPL10 in T-cell acute lymphoblastic leukemia. Nat Genet 2013; 45:186-90; PMID:23263491; http://dx.doi.org/10.1038/ng.2508
76. Chapman MA, Lawrence MS, Keats JJ, Cibulskis K, Sougnez C, Schinzel AC, Harview CL, Brunet JP, Ahmann GJ, Adli M, et al. Initial genome sequencing and analysis of multiple myeloma. Nature 2011; 471:467-72; PMID:21430775; http://dx.doi.org/10.1038/nature09837
77. Gui Y, Guo G, Huang Y, Hu X, Tang A, Gao S, Wu R, Chen C, Li X, Zhou L, et al. Frequent mutations of chromatin remodeling genes in transitional cell carcinoma of the bladder. Nat Genet 2011; 43:875-8; PMID:21822268; http://dx.doi.org/10.1038/ng.907
78. Jones DT, Jäger N, Kool M, Zichner T, Hutter B, Sultan M, Cho YJ, Pugh TJ, Hovestadt V, Stütz AM, et al. Dissecting the genomic complexity underlying medulloblastoma. Nature 2012; 488:100-5; PMID:22832583; http://dx.doi.org/10.1038/nature11284
79. Pugh TJ, Weeraratne SD, Archer TC, Pomeranz Krummel DA, Auclair D, Bochicchio J, Carneiro MO, Carter SL, Cibulskis K, Erlich RL, et al. Medulloblastoma exome sequencing uncovers subtype-specific somatic mutations. Nature 2012; 488:106-10; PMID:22820256; http://dx.doi.org/10.1038/nature11329
80. Robinson G, Parker M, Kranenburg TA, Lu C, Chen X, Ding L, Phoenix TN, Hedlund E, Wei L, Zhu X, et al. Novel mutations target distinct subgroups of medulloblastoma. Nature 2012; 488:43-8; PMID:22722829; http://dx.doi.org/10.1038/nature11213
81. Dalgliesh GL, Furge K, Greenman C, Chen L, Bignell G, Butler A, Davies H, Edkins S, Hardy C, Latimer C, et al. Systematic sequencing of renal carcinoma reveals inactivation of histone modifying genes. Nature 2010; 463:360-3; PMID:20054297; http://dx.doi.org/10.1038/nature08672
82. Grasso CS, Wu YM, Robinson DR, Cao X, Dhanasekaran SM, Khan AP, Quist MJ, Jing X, Lonigro RJ, Brenner JC, et al. The mutational landscape of lethal castration-resistant prostate cancer. Nature 2012; 487:239-43; PMID:22722839; http://dx.doi.org/10.1038/nature11125
83. Lindberg J, Mills IG, Klevebring D, Liu W, Neiman M, Xu J, Wikström P, Wiklund P, Wiklund F, Egevad L, et al. The mitochondrial and autosomal mutation landscapes of prostate cancer. Eur Urol 2013; 63:702-8; PMID:23265383; http://dx.doi.org/10.1016/j.eururo.2012.11.053
84. Ho AS, Kannan K, Roy DM, Morris LG, Ganly I, Katabi N, Ramaswami D, Walsh LA, Eng S, Huse JT, et al. The mutational landscape of adenoid cystic carcinoma. Nat Genet 2013; 45:791-8; PMID:23685749; http://dx.doi.org/10.1038/ng.2643
85. Kandoth C, McLellan MD, Vandin F, Ye K, Niu B, Lu C, Xie M, Zhang Q, McMichael JF, Wyczalkowski MA, et al. Mutational landscape and significance across 12 major cancer types. Nature 2013; 502:333-9; PMID:24132290; http://dx.doi.org/10.1038/nature12634
86. Jankowska AM, Makishima H, Tiu RV, Szpurka H, Huang Y, Traina F, Visconte V, Sugimoto Y, Prince C, O'Keefe C, et al. Mutational spectrum analysis of chronic myelomonocytic leukemia includes genes associated with epigenetic regulation: UTX, EZH2, and DNMT3A. Blood 2011; 118:3932-41; PMID:21828135; http://dx.doi.org/10.1182/blood-2010-10-311019
87. Fisher CL, Berger J, Randazzo F, Brock HW. A human homolog of Additional sex combs, ADDITIONAL SEX COMBS-LIKE 1, maps to chromosome 20q11. Gene 2003; 306:115-26; PMID:12657473; http://dx.doi.org/10.1016/S0378-1119(03)00430-X
88. Ito S, D'Alessio AC, Taranova OV, Hong K, Sowers LC, Zhang Y. Role of Tet proteins in 5mC to 5hmC conversion, ES-cell self-renewal and inner cell mass specification. Nature 2010; 466:1129-33; PMID:20639862; http://dx.doi.org/10.1038/nature09303
89. Taylor MD, Northcott PA, Korshunov A, Remke M, Cho YJ, Clifford SC, Eberhart CG, Parsons DW, Rutkowski S, Gajjar A, et al. Molecular subgroups of medulloblastoma: the current consensus. Acta Neuropathol 2012; 123:465-72; PMID:22134537; http://dx.doi.org/10.1007/s00401-011-0922-z
90. Dubuc AM, Remke M, Korshunov A, Northcott PA, Zhan SH, Mendez-Lago M, Kool M, Jones DT, Unterberger A, Morrissy AS, et al. Aberrant patterns of H3K4 and H3K27 histone lysine methylation occur across subgroups in medulloblastoma. Acta Neuropathol 2013; 125:373-84; PMID:23184418; http://dx.doi.org/10.1007/s00401-012-1070-9
91. Mann KM, Ward JM, Yew CC, Kovochich A, Dawson DW, Black MA, Brett BT, Sheetz TE, Dupuy AJ, Chang DK, et al.; Australian Pancreatic Cancer Genome Initiative. Sleeping Beauty mutagenesis reveals cooperating mutations and pathways in pancreatic adenocarcinoma. Proc Natl Acad Sci U S A 2012; 109:5934-41; PMID:22421440; http://dx.doi.org/10.1073/pnas.1202490109

92. Kruidenier L, Chung CW, Cheng Z, Liddle J, Che K, Joberty G, Bantscheff M, Bountra C, Bridges A, Diallo H, et al. A selective jumonji H3K27 demethylase inhibitor modulates the proinflammatory macrophage response. Nature 2012; 488:404-8; PMID:22842901; http://dx.doi.org/10.1038/nature11262
93. Kristensen JB, Nielsen AL, Jørgensen L, Kristensen LH, Helgstrand C, Juknaite L, Kristensen JL, Kastrup JS, Clausen RP, Olsen L, et al. Enzyme kinetic studies of histone demethylases KDM4C and KDM6A: towards understanding selectivity of inhibitors targeting oncogenic histone demethylases. FEBS Lett 2011; 585:1951-6; PMID:21575637; http://dx.doi.org/10.1016/j.febslet.2011.05.023
94. Hamada S, Kim TD, Suzuki T, Itoh Y, Tsumoto H, Nakagawa H, Janknecht R, Miyata N. Synthesis and activity of N-oxalylglycine and its derivatives as Jumonji C-domain-containing histone lysine demethylase inhibitors. Bioorg Med Chem Lett 2009; 19:2852-5; PMID:19359167; http://dx.doi.org/10.1016/j.bmcl.2009.03.098
95. Luo X, Liu Y, Kubicek S, Myllyharju J, Tumber A, Ng S, Che KH, Podoll J, Heightman TD, Oppermann U, et al. A selective inhibitor and probe of the cellular functions of Jumonji C domain-containing histone demethylases. J Am Chem Soc 2011; 133:9451-6; PMID:21585201; http://dx.doi.org/10.1021/ja201597b
96. Wang L, Chang J, Varghese D, Dellinger M, Kumar S, Best AM, Ruiz J, Bruick R, Peña-Llopis S, Xu J, et al. A small molecule modulates Jumonji histone demethylase activity and selectively inhibits cancer growth. Nat Commun 2013; 4:2035; PMID:23792809
97. Nielsen AL, Kristensen LH, Stephansen KB, Kristensen JB, Helgstrand C, Lees M, Cloos P, Helin K, Gajhede M, Olsen L. Identification of catechols as histone-lysine demethylase inhibitors. FEBS Lett 2012; 586:1190-4; PMID:22575654; http://dx.doi.org/10.1016/j.febslet.2012.03.001

Supplemental Figure Legends

Supplemental Figure 1. *UTX* defects in cancer cell lines
Schematic representation of the presence of *UTX* defects (%) in cancer cell lines derived from a broad range of leukemic and solid cancer types

Supplemental Figure 1

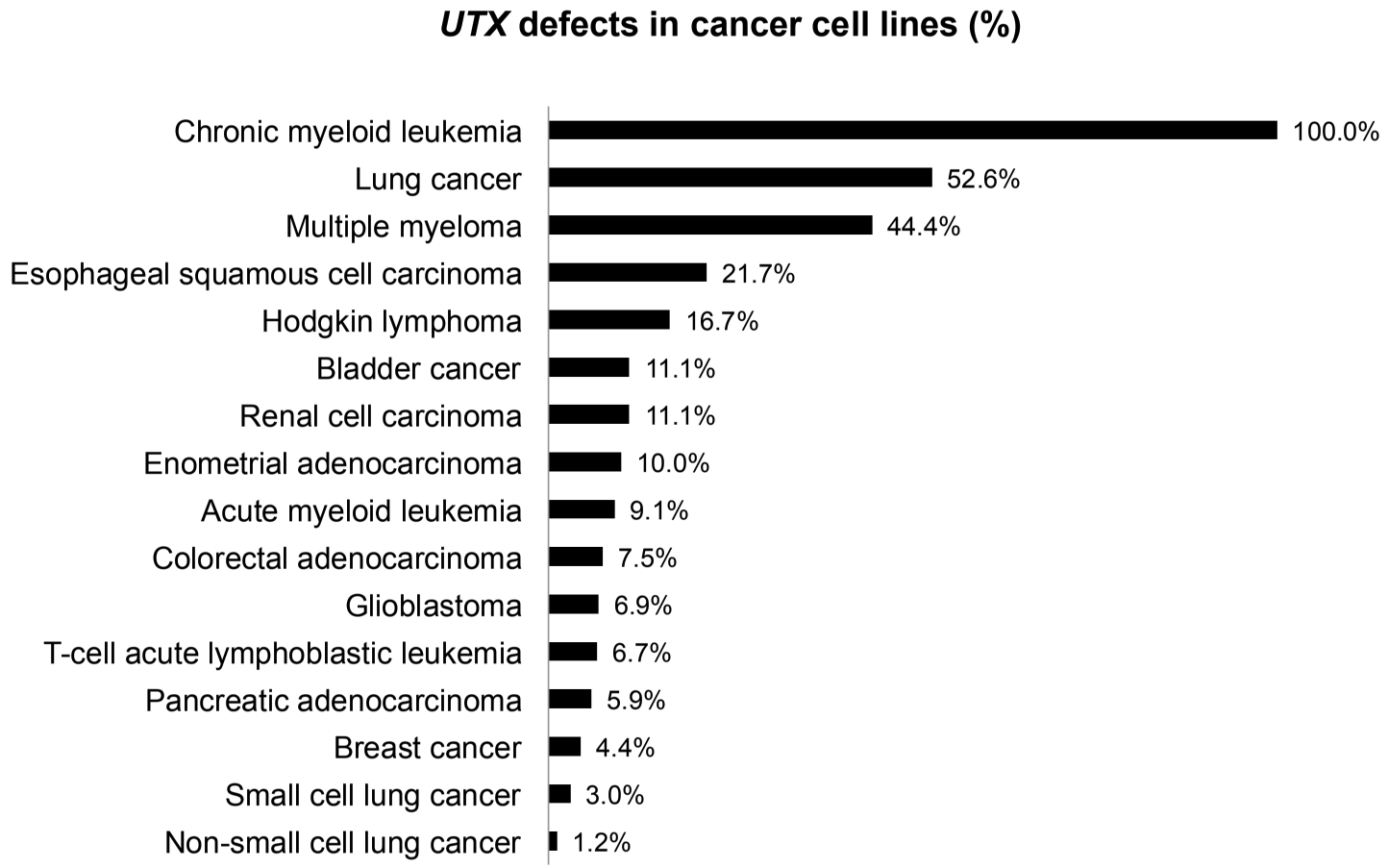

Supplemental Table 1. *UTX* defects in primary cancer samples

Cancer type	Defects (%)	Paper
Multiple myeloma	2/49 (4.1%)	van Haaften et al. Nature Genetics 2009
Esophageal squamous cell carcinoma	1/54 (1.85%)	
Renal cell carcinoma	4/401 (1%)	
Glioblastoma	0/96 (0%)	
T-cell acute lymphoblastic leukemia	3/67 (4.48%)	De Keersmaecker et al. Nature Genetics 2013
B-cell acute lymphoblastic leukemia	5/138 (3.62%)	Mar et al. Leukemia 2012
Acute myeloid leukemia	0/50 (0%)	
Myelodysplastic syndrome / Acute myeloid leukemia	1/40 (2.5%)	Gelsi-Boyer et al. BJH 2009
Acute myeloid leukemia	1/150 (0.67%)	Wartman et al. JCI 2011
Chronic myelomonocytic leukemia	4/52 (7.69%)	Jankowska et al. Blood 2011
CMML-derived acute myeloid leukemia	2/20 (10%)	
Multiple myeloma	1/38 (2.63%)	Chapman et al. Nature 2011
Bladder cancer	22/97 (22.68%)	Gui et al. Nature Genetics 2011
Bladder cancer	10/35 (29%)	Ross et al. Modern Pathology 2013
Medulloblastoma	5/125 (4%)	Jones et al. Nature 2012
Medulloblastoma	3/92 (3.26%)	Pugh et al. Nature 2012
Medulloblastoma	8/93 (8.6%)	Robinson et al. Nature 2012
Medulloblastoma	7/175 (4%)	Dubuc et al. Acta Neuropathol 2013
Renal Cell Carcinoma	12/412 (2.91%)	Dalgliesh et al. Nature 2010
Renal Cell Carcinoma	4/132 (3.3%)	Gossage et al. Genes, chromosomes & cancer 2013
Adenoid cystic carcinoma	4/60 (6.67%)	Ho et al. Nature Genetics 2013
Prostate cancer	6/50 (12%)	Grasso et al. Nature 2012
Prostate cancer	4/63 (6.35%)	Lindberg et al. European Urology 2013

Supplemental Table 2. *UTX* defects in cancer cell lines

Cancer type	Defects (%)	Paper
Multiple myeloma	4/9 (44.4%)	van Haaften et al. Nature Genetics 2009
Esophageal squamous cell carcinoma	5/23 (21.7%)	
Renal cell carcinoma	2/18 (11.1%)	
Glioblastoma	2/29 (6.9%)	
Acute myeloid leukemia	2/22 (9.1%)	
Bladder cancer	2/18 (11.1%)	
Breast cancer	2/45 (4.4%)	
Chronic myeloid leukemia	3/3 (100%)	
Colorectal adenocarcinoma	3/40 (7.5%)	
Endometrial adenocarcinoma	1/10 (10%)	
Hodgkin lymphoma	1/6 (16.7%)	
Non-small cell lung cancer	1/85 (1.2%)	
Pancreatic adenocarcinoma	1/17 (5.9%)	
Small cell lung cancer	2/66 (3.0%)	
T-cell acute lymphoblastic leukemia	1/15 (6.7%)	
Lung cancer	10/19 (52.6%)	Liu et al. Genome Research 2012

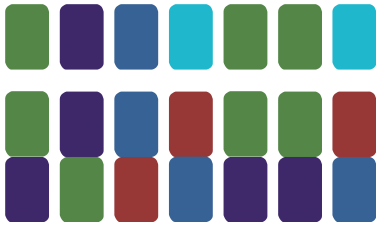

Chapter 2

Research Objectives

Research Objectives

T-ALL is an aggressive hematological cancer with cure rates ranging from 50-75% depending on the age. Regrettably, in a significant number of adult and pediatric T-ALL patients relapse occurs early during therapy whereby only a fifteenth till a quarter survives the next 5 years, respectively. The exploration of the genetic make-up of T-ALL by karyotyping, FISH, arrayCGH, sequencing and gene expression profiling has lead to the classification of T-ALL patient cases in a set of well-defined T-ALL subgroups of which some are linked to good or dismal prognosis. Moreover, the advances in identifying and characterizing the multiple genetic events occurring in T-ALL is paving the way towards individualized treatment regimes, also coined precision medicine, as novel drugs targeting cancer cells with particular genetic alterations are rapidly emerging and being tested.

AIM 1. Identification of X-linked epigenetic drivers in T-ALL and their role in sensitivity to epigenetic therapy

T-ALL is one of the few cancers characterized by a gender bias, with a threefold higher T-ALL occurrence in males. A possible reason for this skewed gender distribution towards males in T-ALL could be the presence of tumor suppressor genes on the X-chromosome. To test this hypothesis, we investigated the possible presence of recurrent genetic defects on the X-chromosome in primary T-ALL patient samples (**paper 1**). By sequencing of the entire X-chromosome exome followed by targeted sequencing of the identified candidates, we detected recurrent loss-of-function mutations in the putative chromatin reader PHF6 in a large proportion of pediatric and adult T-ALL patient samples, marking PHF6 as one of the major novel tumor suppressor genes in T-ALL (**paper 1, Nature Genetics, 2010**).

In view of the rapidly emerging importance of epigenetic regulators in cancer, we further sought for additional candidate tumor suppressor genes. One of the possible candidates, the *Ubiquitously Transcribed tetratricopeptide repeat on chromosome X* or UTX, was also located on the X-chromosome and was already found to be mutated in other cancer entities. We therefore hypothesized that a second X-linked tumor suppressor gene could be implicated in T-ALL. Subsequent mutation analysis indeed revealed inactivating mutations in this histone H3K27me2/3 demethylase (**paper 2, submitted**) with further *in vivo* experiments supporting an important role for UTX in T-ALL pathogenesis (**paper 2**). In a next step, we took advantage of the rapid development of novel epigenetic drugs and explored their effects on malignant T-cell lymphoblasts harboring different epigenetic defects. The results of this translational component are also presented in **paper 2**.

AIM 2. Search for deregulated microRNA networks in T-ALL

Next to defects in protein-coding genes that contribute to T-ALL formation, we wanted to explore the possible involvement of miRNAs in T-ALL. MiRNAs are small non-coding RNA molecules that negatively regulate mRNA target gene expression. Therefore deregulation of miRNAs might execute another mechanism of malignant activation of T-ALL oncogenes or tumor suppressor genes. First, we wanted to identify oncogenic miRNAs (oncomiRs) in T-cell leukemia formation. To this end, we profiled the miRNAome of a set of T-ALL patient samples and normal thymocytes at different stages of differentiation and evaluated the oncogenicity of the top candidate oncomiRs in a NOTCH1 T-ALL mouse model. This work, for the first time, uncovered an extensive miRNA-tumor suppressor gene network in T-ALL (**paper 3, Nature Genetics, 2011**).

Following the discovery of these oncomiRs, we also explored a possible role for tumor suppressive miRNAs in T-ALL development. First, we took advantage of an in house optimized 3'UTR library screen allowing the unbiased identification of miRNAs targeting selected T-ALL oncogenes. Following this approach, we identified miR-193b-3p as a novel tumor suppressor miRNA targeting the *MYB* proto-oncogene, the latter playing a crucial role in normal T-cell maturation and T-ALL oncogenesis. Further *in vitro* and *in vivo* functional studies confirmed the presumed tumor suppressor role of miR-193b-3p. The results of the latter work are presented in **paper 4** (**in preparation**).

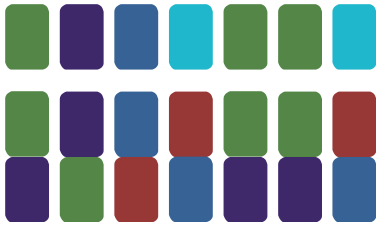

Chapter 3

Results

Results

1. Epigenetic drivers in T-cell acute lymphoblastic leukemia

PAPER 1
PHF6 mutations in T-cell acute lymphoblastic leukemia

PAPER 2
The H3K27me3 demethylase *UTX* is a gender-specific tumor suppressor in T-cell acute lymphoblastic leukemia

PAPER 1

PHF6 mutations in T-cell acute lymphoblastic leukemia

Van Vlierberghe P*, Palomero T*, Khiabanian H, Van der Meulen J, Castillo M, Van Roy N, De Moerloose B, Philippé J, González-García S, Toribio ML, Taghon T, Zuurbier L, Cauwelier B, Harrison CJ, Schwab C, Pisecker M, Strehl S, Langerak AW, Gecz J, Sonneveld E, Pieters R, Paietta E, Rowe JM, Wiernik PH, Benoit Y, Soulier J, Poppe B, Yao X, Cordon-Cardo C, Meijerink J, Rabadan R, Speleman F* & Ferrando AA*. Nat Genet. 2010 Apr;42(4):338-42.

nature genetics

PHF6 mutations in T-cell acute lymphoblastic leukemia

Pieter Van Vlierberghe[1–3,21], Teresa Palomero[1,4,21], Hossein Khiabanian[5], Joni Van der Meulen[2], Mireia Castillo[4], Nadine Van Roy[2], Barbara De Moerloose[6], Jan Philippé[7], Sara González-García[8], María L Toribio[8], Tom Taghon[7], Linda Zuurbier[3], Barbara Cauwelier[9], Christine J Harrison[10], Claire Schwab[10], Markus Pisecker[11], Sabine Strehl[11], Anton W Langerak[12], Jozef Gecz[13,14], Edwin Sonneveld[15], Rob Pieters[3,15], Elisabeth Paietta[16], Jacob M Rowe[17], Peter H Wiernik[16], Yves Benoit[6], Jean Soulier[18], Bruce Poppe[2], Xiaopan Yao[19], Carlos Cordon-Cardo[4], Jules Meijerink[3], Raul Rabadan[5], Frank Speleman[2,22] & Adolfo Ferrando[1,4,20,22]

Tumor suppressor genes on the X chromosome may skew the gender distribution of specific types of cancer[1,2]. T-cell acute lymphoblastic leukemia (T-ALL) is an aggressive hematological malignancy with an increased incidence in males[3]. In this study, we report the identification of inactivating mutations and deletions in the X-linked plant homeodomain finger 6 (*PHF6*) gene in 16% of pediatric and 38% of adult primary T-ALL samples. Notably, *PHF6* mutations are almost exclusively found in T-ALL samples from male subjects. Mutational loss of *PHF6* is importantly associated with leukemias driven by aberrant expression of the homeobox transcription factor oncogenes *TLX1* and *TLX3*. Overall, these results identify *PHF6* as a new X-linked tumor suppressor in T-ALL and point to a strong genetic interaction between *PHF6* loss and aberrant expression of TLX transcription factors in the pathogenesis of this disease.

T-ALL is an aggressive malignancy in which multiple genetic defects collaborate in the transformation of T-cell progenitors[4,5]. Notably, T-ALL has a threefold higher incidence in males[3], whereas other immature hematological tumors such as precursor B-lineage ALL are equally frequent in males and females[3].

To identify a possible X-linked tumor suppressor in T-ALL, we performed an X-chromosome-targeted mutational analysis in tumor DNA samples from 12 males with T-ALL. For each sample, we performed in-solution DNA capture of 7,674 regions encompassing 3,045,708 nucleotides corresponding to 5,215 X-chromosome exons using the Agilent Sure Select oligonucleotide capture system[6]. DNA samples enriched for X-chromosome exons were then analyzed by next-generation sequencing using the SOLiD 3 platform from Applied Biosystems. This analysis identified 66 candidate previously uncharacterized nonsynonymous single-nucleotide variants and 7 positions with high confidence calls for containing complex variants such as insertions or deletions (**Fig. 1a**). Dideoxynucleotide DNA sequencing of PCR products encompassing affected exons confirmed the presence of 92% (61/66) of these single-nucleotide variants and 57% (4/7) of the more complex variants, including 2 insertions and 2 deletions (**Supplementary Tables 1** and **2**). Sequence analysis of paired DNA samples obtained at the time of clinical remission showed that most of these variants corresponded to previously unreported germline polymorphisms. However, and most notably, we also identified three somatically acquired changes corresponding to two nonsynonymous single-nucleotide substitutions (A902G T300A and A990G H330R) and a frameshift-creating insertion of five nucleotides (124_125insAGGCA, H43fs) in the *PHF6* gene (**Fig. 1a**).

In a complementary approach we analyzed X-chromosome array comparative genome hybridization (array-CGH) data from 246 primary T-ALL samples (179 male and 67 female) in a multicenter setting. These analyses revealed the presence of recurrent deletions in chromosomal band Xq26 in 8 out of 246 (~3%) T-ALL samples (**Table 1**). For three del(X)(q26)-positive T-ALL samples, we performed array-CGH analysis against the corresponding remission material, which showed that these Xq26 deletions were somatically acquired leukemia-associated genetic events (**Table 1**). Reanalysis of all eight del(X)(q26)-positive T-ALL samples on a custom

[1]Institute for Cancer Genetics, Columbia University Medical Center, New York, New York, USA. [2]Center for Medical Genetics, Ghent University Hospital, Ghent, Belgium. [3]Department of Pediatric Oncology/Hematology, Erasmus MC, Rotterdam, The Netherlands. [4]Department of Pathology, Columbia University Medical Center, New York, New York, USA. [5]Center for Computational Biology and Bioinformatics, Columbia University, New York, New York, USA. [6]Department of Pediatric Hemato-Oncology, Ghent University Hospital, Ghent, Belgium. [7]Department of Clinical Chemistry, Immunology and Microbiology, Ghent University Hospital, Ghent, Belgium. [8]Centro de Biología Molecular "Severo Ochoa", Consejo Superior de Investigaciones Científicas (CSIC), Universidad Autónoma de Madrid (UAM), Madrid, Spain. [9]Department of Hematology, Hospital St-Jan, Bruges, Belgium. [10]Leukaemia Research Cytogenetics Group, Northern Institute for Cancer Research, Newcastle University, Newcastle, UK. [11]Children's Cancer Research Institute, St. Anna Kinderkrebsforschung, Vienna, Austria. [12]Department of Immunology, Erasmus MC, Rotterdam, The Netherlands. [13]Department of Genetics and Molecular Pathology, University of Adelaide, Adelaide, Australia. [14]Department of Pediatrics, University of Adelaide, Adelaide, Australia. [15]On behalf of the Dutch Childhood Oncology Group (DCOG), The Hague, The Netherlands. [16]Montefiore Medical Center North, Bronx, New York, USA. [17]Rambam Medical Center and Technion, Israel Institute of Technology, Haifa, Israel. [18]Hematology Laboratory APHP, INSERM U944, Hôpital Saint Louis, Paris, France. [19]Department of Biostatistics and Computational Biology, Dana-Farber Cancer Institute, Boston, Massachusetts, USA. [20]Department of Pediatrics, Columbia University Medical Center, New York, New York, USA. [21]These authors contributed equally to this work. [22]These authors jointly directed this work. Correspondence should be addressed to A.F. (af2196@columbia.edu).

Received 11 November 2009; accepted 3 February 2010; published online 14 March 2010; doi:10.1038/ng.542

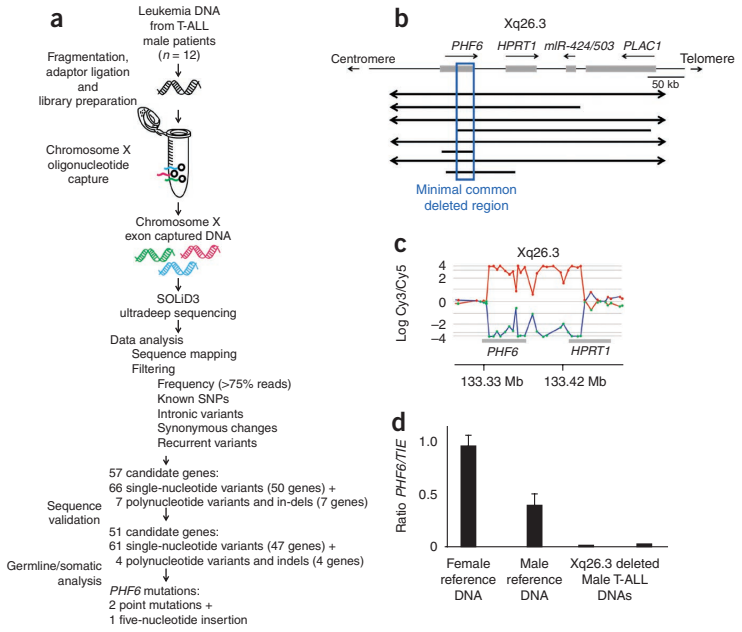

Figure 1 Next-generation sequencing and microarray-based comparative genomic hybridization (array-CGH) analysis of the X chromosome identifies *PHF6* mutations in human T-cell acute lymphoblastic leukemia (T-ALL). (**a**) Overview of mutation screening approach of the human X-chromosome exome in a panel of tumor DNA samples from 12 males with T-ALL using oligonucleotide sequence capture and next-generation sequencing with SOLiD 3. After filtering and confirmation of high-throughput sequencing data, analysis of corresponding remission DNA samples led to the identification of three somatically acquired changes in *PHF6*. (**b**) Schematic overview of the recurrent genomic deletions involving chromosomal band Xq26.3 in eight human T-ALL samples. Specific genes located in Xq26.3 are shown. (**c**) Detailed view of a representative oligonucleotide array-CGH plot of leukemia DNA/control DNA ratios (blue trace) versus the dye-swap experiment (red trace) in an individual harboring an Xq26.3 deletion. (**d**) DNA quantitative PCR analysis of *PHF6* copy number dose in female and male reference genomic DNAs and two primary samples from males with T-ALL harboring Xq26.3 deletions.

high-resolution X-chromosome oligonucleotide array (**Fig. 1b**,**c**) narrowed down the common minimally deleted region to an area of 80 kb containing the *PHF6* gene. Consistently, quantitative PCR analysis confirmed loss of the *PHF6* locus in the del(X)(q26)-positive cases (**Fig. 1d**). The convergent findings of our X-chromosome exon mutation analysis and analysis of copy number alterations by array-CGH thus identified *PHF6* as a new tumor suppressor gene mutated and deleted in T-ALL.

PHF6 encodes a plant homeodomain (PHD) factor containing four nuclear localization signals and two imperfect PHD zinc-finger domains[7] with a proposed role in controlling gene expression[7]. Notably, inactivating mutations in *PHF6* cause Börjeson-Forssman-Lehmann syndrome (MIM301900), a relatively uncommon type of X-linked familial syndromic mental retardation that has not been associated with increased incidence of T-ALL[7–9]. Quantitative RT-PCR analysis demonstrated ubiquitous expression of *PHF6* transcripts in human tissues, with highest levels of expression in thymus, ovary and thyroid, and moderate levels of expression in spleen, testes and adipose tissue (**Supplementary Fig. 1**). Consistent with these results, PHF6 was readily detected by immunohistochemistry in mouse thymus (**Supplementary Fig. 1**). Finally, quantitative RT-PCR analysis of human thymocyte populations at different stages of development showed variable levels of *PHF6* expression, with marked upregulation of *PHF6* transcripts in CD4/CD8 double-positive cells (**Supplementary Fig. 1**).

Mutational analysis of *PHF6* in an extended panel of pediatric and adult T-ALL primary samples identified truncating or missense mutations in *PHF6* in 38% (16/42) of adult and ~16% (14/89) of pediatric T-ALL samples (**Fig. 2a** and **Table 1**). In all available cases (7/30), analysis of matched buccal and/or bone marrow remission genomic DNA confirmed the somatic origin of *PHF6* mutations (4/21 frameshift mutations and 3/9 missense mutations) (**Fig. 2b** and **Table 1**). Finally, no mutations in *PHF6* were identified in DNA samples from B-lineage ALL ($n = 62$), suggesting that mutational loss of *PHF6* in lymphoid tumors could be restricted to T-ALL.

Nonsense and frameshift mutations accounted for 70% (21/30) of all *PHF6* mutations identified in our series and were evenly distributed throughout the gene. Missense mutations accounted for the remaining 30% (9/30) of *PHF6* lesions and recurrently involved codon C215 and the second zinc-finger domain of the protein (**Fig. 2a**). DNA sequence analysis of *PHF6* in a panel of 15 well-characterized T-ALL cell lines (**Supplementary Table 3**) showed the presence of truncating mutations in *PHF6* in the DND41, HPB-ALL and T-ALL1 cell lines. Protein blot analysis and immunohistochemical staining demonstrated robust expression and nuclear localization of PHF6 in *PHF6* wild-type tumors and complete loss of PHF6 protein in T-ALL cell lines harboring mutations in *PHF6* (**Fig. 2c**,**d**).

PHD finger-containing proteins have been implicated in numerous cellular functions, including transcriptional regulation and in some instances as specialized reader modules that recognize the methylation status of histone lysine residues[10]. In addition, PHF6 has been reported to be phosphorylated during mitosis[11] and by the ATM and ATR kinases upon DNA damage[12], which suggests a dynamic regulation of PHF6 during cell cycle and DNA repair. Consistent with this notion, short hairpin RNA (shRNA) knockdown of PHF6 resulted in increased levels of phosphorylated H2AX (γ-H2AX), a post-translational modification associated with the presence of DNA double-strand breaks[13] (**Fig. 2e**).

Sex determination in humans is controlled by differential representation of the X and Y chromosomes, with the presence of an XY pair in males and two copies of the X chromosome in females. The presence of numerous genes in the nonautosomal region of the X chromosome could result in a genetic imbalance between male and female cells, which is compensated for by random chromosomal inactivation of one copy of the X chromosome in female cells[14]. However, allelic-expression analysis has shown that some genes can escape X-chromosome inactivation in certain tissues[1,2,15]. To test the possibility that *PHF6* could escape X-chromosome inactivation in T-ALL cells, we performed allelic-expression analysis of a silent SNP (rs17317724) located in the 3′ UTR of *PHF6* in lymphoblasts from three informative samples from females with T-ALL. In each of these samples, *PHF6* was monoallelically expressed, suggesting that biallelic

Table 1 Characteristics of 38 primary T-ALL samples showing *PHF6* inactivation

ID	Sex	Age	WBC (x 10^9 l^{-1})	Immuno-phenotype	Genetic subtype	*NOTCH1*	Type of alteration	Deletion size or predicted *PHF6* protein lesion	Germline or somatic
1	M	Ped	77	Cortical	*TLX3*	Mut	Deletion	0.55 Mb	NA
2	M	Ped	46	Pre-T	*TLX3*	WT	Deletion	0.23 Mb	NA
3	M	Ped	31	Pre-T	*TLX3*	NA	Deletion	1.50 Mb	NA
4	M	Ped	2	Pre-T	Unknown	NA	Deletion	0.27 Mb	NA
5	M	Ped	NA	Cortical	*HOXA*	NA	Deletion	1.90 Mb	Somatic
6	M	Ped	NA	Cortical	Unknown	NA	Deletion	0.20 Mb	Somatic
7	M	Ped	NA	Cortical	*TLX1*	NA	Deletion	0.08 Mb	Somatic
8	M	Adult	NA	Pre-T	Unknown	NA	Deletion	0.11 Mb	NA
9	M	Ped	185	Cortical	*TLX3*	WT	Nonsense	G122X	NA
10	M	Ped	417	Pre-T	*TLX3*	Mut	Nonsense	R116X	NA
11	F	Ped	280	Pre-T	*TLX1*	Mut	Frameshift	F172fs	NA
12	M	Ped	405	Pre-T	*TLX3*	Mut	Frameshift	Y303fs	NA
13	M	Ped	159	Pre-T	*TLX1*	Mut	Nonsense	K235X	NA
14	M	Ped	500	Pre-T	*TLX3*	Mut	Frameshift	A41fs	NA
15	M	Ped	347	Cortical	*HOXA*	Mut	Nonsense	K274X	NA
16	M	Ped	129	Cortical	Unknown	Mut	Frameshift	D333fs	NA
17	M	Ped	174	Cortical	*TLX3*	Mut	Nonsense	R225X	NA
18	M	Ped	27	Cortical	*TLX1*	WT	Nonsense	R116X	NA
19	M	Ped	310	Cortical	*TAL1*	Mut	Missense	C283R	NA
20	M	Ped	189	Cortical	*TAL1*	Mut	Frameshift	C28fs	NA
21	M	Adult	170	Cortical	*TLX3*	WT	Frameshift	H44fs	NA
22	M	Adult	21	Cortical	*TLX1*	Mut	Frameshift	H43fs	Somatic
23	M	Adult	NA	Pre-T	*TLX3*	Mut	Frameshift	T98fs	Somatic
24	M	Adult	14	Pre-T	*TLX3*	WT	Frameshift	Y105fs	NA
25	M	Adult	28	Mature	*TLX3*	WT	Frameshift	S158fs	NA
26	M	Adult	NA	Cortical	*TLX3*	Mut	Missense	C215Y	NA
27	M	Adult	NA	Pre-T	Unknown	Mut	Missense	C215F	NA
28	M	Adult	31	Cortical	Unknown	Mut	Missense	C215Y	NA
29	M	Adult	NA	Mature	*TLX3*	Mut	Missense	T300A	Somatic
30	M	Adult	21	Cortical	*TLX1*	WT	Missense	A311P	NA
31	M	Adult	30	Mature	Unknown	WT	Missense	C280Y	NA
32	M	Adult	23	Cortical	Unknown	WT	Missense	H329R	Somatic
33	M	Ped	NA	NA	*TAL1*	NA	Nonsense	R257X	Somatic
34	M	Ped	NA	NA	*TLX1*	NA	Frameshift	S191fs	Somatic
35	M	Adult	NA	NA	*TLX1*	NA	Missense	C215F	Somatic
36	M	Adult	NA	NA	*TLX1*	NA	Nonsense	Y303X	NA
37	M	Adult	NA	NA	Unknown	NA	Nonsense	R274X	NA
38	M	Adult	NA	NA	Unknown	NA	Frameshift	H135fs	NA

Mb, megabases; Mut, mutated; NA, not available; Ped, pediatric; WT, wild-type; X, stop codon.

expression of *PHF6* is not commonly found in T-ALL (**Fig. 3a**). Most notably, we found that *PHF6* mutations are almost exclusively found in samples from males with T-ALL. *PHF6* mutations were present in 32% (29/92) of males and in only ~2.5% (1/39) of females ($P < 0.001$; **Fig. 3b** and **Supplementary Table 4**). Moreover, all eight *PHF6* deletions identified by array-CGH analysis were found in samples from males with T-ALL, and each of the three cell lines with mutations in *PHF6* were derived from males with T-ALL.

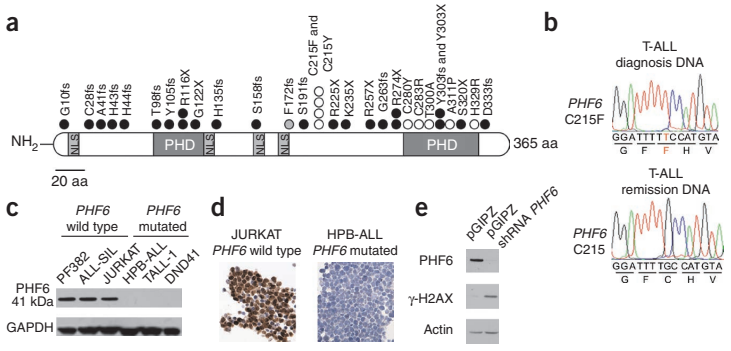

Figure 2 *PHF6* mutations and expression in T-cell acute lymphoblastic leukemia (T-ALL) lymphoblasts. (**a**) Structure of the PHF6 protein, including four nuclear localization signals (NLSs) and two imperfect plant homeodomain (PHD) zinc-finger domains. Overview of all *PHF6* mutations identified in primary T-ALL samples and T-ALL cell lines. Filled circles represent nonsense and frameshift mutations, whereas missense mutations are depicted as open circles. The circle filled in gray indicates the mutation identified in a sample from a female with T-ALL. aa, amino acids. (**b**) Representative DNA sequencing chromatograms of paired diagnosis and remission genomic T-ALL DNA samples showing a somatic mutation in exon 7 of *PHF6*. (**c**) Protein blot analysis of T-ALL cell lines revealed complete loss of PHF6 protein expression in the *PHF6*-mutated T-ALL cell lines. (**d**) PHF6 immunostaining in the Jurkat and HPB-ALL, wild-type and mutant T-ALL cell lines, respectively. (**e**) Protein blot analysis of PHF6 and γ-H2AX expression in HEK293T cells upon PHF6 short hairpin RNA knockdown. Actin concentrations are shown as a loading control.

Immunohistochemical analysis of PHF6 expression in wild-type primary T-ALL samples showed positive PHF6 immunostaining ($n = 5$; three males and two females), whereas cases with *PHF6*-truncating mutations ($n = 4$) (**Fig. 3c**) or a point mutation in C215 (C215F) were negative for PHF6 protein expression (**Fig. 3c**). In contrast, primary T-ALL cells harboring a *PHF6* point mutation in the PHD2 domain (T300A) were positive for PHF6 protein expression (**Fig. 3c**). Overall, these results suggest that truncating mutations and point mutations in C215 impair PHF6 expression, whereas amino acid substitutions in the PHD2 domain of PHF6 may selectively impair the tumor suppressor function of this protein.

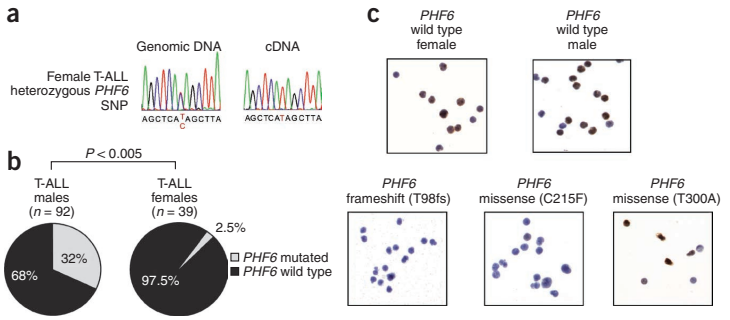

Figure 3 *PHF6* expression in T-cell acute lymphoblastic leukemia (T-ALL) lymphoblasts. (**a**) Sequence analysis of paired genomic DNA and complementary DNA samples shows monoallelic expression of *PHF6* SNP rs17317724 in lymphoblasts from a wild-type *PHF6* female with T-ALL. (**b**) Differential distribution of *PHF6* mutations in samples from males and females with T-ALL. (**c**) Immunohistochemical analysis of PHF6 expression in wild-type and mutant T-ALL lymphoblasts.

Leukemic transformation of immature thymocytes is the result of a multistep process involving numerous genetic abnormalities, which can be associated with different clinical features, including age and prognosis. Notably, *PHF6* mutations were significantly more prevalent in adult T-ALL patients (16/42; 38%) than in pediatric patients (14/89; 16%) ($P = 0.005$; **Fig. 4a**). Detailed genetic information was available for T-ALL cases treated in Dutch Childhood Oncology Group (DCOG) clinical trials ($n = 65$) (**Supplementary Table 5**). In this cohort, *PHF6* mutations were significantly associated with the aberrant expression of *TLX1* and *TLX3* ($P < 0.005$; **Fig. 4b** and **Supplementary Table 5**), two related oncogenes activated by chromosomal translocations in T-ALL[16–18]. No significant associations were observed between *PHF6* mutations and *NOTCH1*, *FBXW7* or *PTEN* mutations in either pediatric ($n = 65$) or adult ($n = 34$) T-ALL cohorts (**Supplementary Tables 5** and **6**). Overall survival in *PHF6* wild-type children with T-ALL treated on DCOG protocols[19] was 65% (33/51) vs. 71% (10/14) for *PHF6*-mutated cases (log-rank $P = 0.71$) (**Fig. 4c**). Overall survival in *PHF6* wild-type adults with T-ALL treated in the Eastern Cooperative Oncology Group ECOG-2993 clinical trial was 36% (7/12) vs. 58% (8/22) for *PHF6*-mutated samples (log-rank $P = 0.24$) (**Fig. 4d**).

Overall, these results identify *PHF6* as a new X-linked tumor suppressor gene and imply a specific interaction between the oncogenic programs activated by aberrant expression of TLX transcription factors and mutational loss of *PHF6* in the pathogenesis of T-ALL.

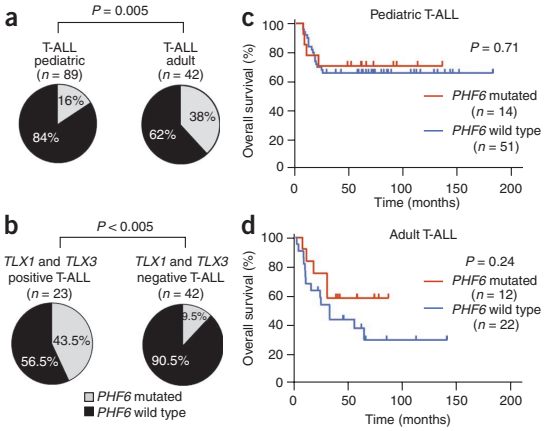

Figure 4 Clinical and biological characteristics associated with *PHF6* mutations in T-cell acute lymphoblastic leukemia (T-ALL). (**a**) Frequencies of *PHF6* mutations in pediatric and adult T-ALL samples. (**b**) Differential distribution of *PHF6* mutations in *TLX1/TLX3*-positive and *TLX1/TLX3*-negative T-ALL samples. (**c**) Kaplan-Meier curve of overall survival in pediatric T-ALL cases from Dutch Childhood Oncology Group trials ALL7, ALL8 and ALL9 with and without *PHF6* mutations. (**d**) Kaplan-Meier survival curve in adult T-ALL cases with and without mutations in *PHF6* treated in Eastern Cooperative Oncology Group clinical trial ECOG2993.

METHODS

Methods and any associated references are available in the online version of the paper at http://www.nature.com/naturegenetics/.

Note: Supplementary information is available on the Nature Genetics website.

ACKNOWLEDGMENTS

This study was supported by the Fund for Scientific Research (FWO) Flanders (postdoctoral grants to P.V.V. and T.T., PhD grant to J.V.d.M., senior clinical investigator award to B.P. and project grants G.0198.08 and G.0869.10N to F.S.); the GOA-UGent (grant no. 12051203); the IWT-Vlaanderen (SBO grant no. 060848); the Children Cancer Fund Ghent (F.S.); Leukemia Research UK (C.J.H.); the Stichting Kinderen Kankervrij (KiKa; grant no. KiKa 2007-012 to L.Z.); the Belgian Program of Interuniversity Poles of Attraction; the Belgian Foundation against Cancer; the Austrian Ministry of Science and Research (GEN-AU Child, GZ 200.136/1-VI/1/2005 to S.S.), the US National Library of Medicine (1R01LM010140-01 to R.R. and H.K.); the ECOG and DCOG tumor banks; grants from Spain's Plan Nacional (BFU 2007-60990 and PlanE2009-0110 to M.L.T.), Comunidad de Madrid (S-SAL0304-2006 to M.L.T.), Fundación MM (M.L.T.), Instituto de Salud Carlos III (RECAVA RD06/0014/1012 to M.L.T.), an Institutional Grant from the Fundación Ramón Areces (M.L.T.), the Alex's Lemonade Stand Foundation Young Investigator Award (T.P.); a US Northeast Biodefense Center ARRA award (U54-AI057158 to R.R.); the US National Institutes of Health (R01CA120196 and R01CA129382 to A.F.); the Rally across America Foundation (A.F); the Swim across America Foundation (A.F.); the Golfers against Cancer Foundation (A.F.); and a Leukemia and Lymphoma Society Scholar Award (A.F.). We thank the Pediatric Cardiosurgery Units from Centro Especial Ramón y Cajal and Ciudad Sanitaria La Paz (Madrid, Spain) for thymus samples.

AUTHOR CONTRIBUTIONS

P.V.V. performed array-CGH and mutation analysis of *PHF6* and wrote the manuscript. T.P. performed exon capture and next-generation sequencing of T-ALL samples and wrote the manuscript. H.K. analyzed next-generation sequencing data. J.V.d.M. performed additional array-CGH analysis and *PHF6* mutation screening in T-ALL and BCP-ALL samples. T.T., N.V.R. and A.W.L. performed experiments. M.C. and C.C.-C. performed and analyzed histological and immunohistochemical staining. J.P. collaborated on *PHF6* mutation screening

in BCP-ALL samples. C.J.H. and C.S. collaborated on additional screening for genomic *PHF6* deletions in T-ALL. Y.B., B.D.M. and B.C. collaborated on the *PHF6* mutation screening. R.P., M.P., S.S. and J.S. collaborated on the multicenter array-CGH study. S.G.-G. and M.L.T. performed the isolation of T-cell progenitor cells for expression analysis of *PHF6*. X.Y. performed survival analysis of ECOG T-ALL patients. J.G. provided critical reagents and discussion. E.S. provided samples and correlative clinical data from DCOG. E.P., J.M.R. and P.H.W. provided samples and correlative clinical data from ECOG. J.M. and L.Z. collaborated on the multicenter array-CGH study and *PHF6* mutation analysis, provided molecular data on the characterization of T-ALL and performed survival analysis of *PHF6* mutations in the DCOG series. R.R. designed and directed the analysis of next-generation sequencing results. F.S. and B.P. designed the studies and directed research. A.F. designed the studies, directed research and wrote the manuscript.

COMPETING FINANCIAL INTERESTS

The authors declare no competing financial interests.

Published online at http://www.nature.com/naturegenetics/.
Reprints and permissions information is available online at http://npg.nature.com/reprintsandpermissions/.

1. Carrel, L., Cottle, A.A., Goglin, K.C. & Willard, H.F. A first-generation X-inactivation profile of the human X chromosome. *Proc. Natl. Acad. Sci. USA* **96**, 14440–14444 (1999).
2. Carrel, L. & Willard, H.F. X-inactivation profile reveals extensive variability in X-linked gene expression in females. *Nature* **434**, 400–404 (2005).
3. Goldberg, J.M. *et al.* Childhood T-cell acute lymphoblastic leukemia: the Dana-Farber Cancer Institute acute lymphoblastic leukemia consortium experience. *J. Clin. Oncol.* **21**, 3616–3622 (2003).
4. Aifantis, I., Raetz, E. & Buonamici, S. Molecular pathogenesis of T-cell leukaemia and lymphoma. *Nat. Rev. Immunol.* **8**, 380–390 (2008).
5. Pui, C.H., Robison, L.L. & Look, A.T. Acute lymphoblastic leukaemia. *Lancet* **371**, 1030–1043 (2008).
6. Gnirke, A. *et al.* Solution hybrid selection with ultra-long oligonucleotides for massively parallel targeted sequencing. *Nat. Biotechnol.* **27**, 182–189 (2009).
7. Lower, K.M. *et al.* Mutations in *PHF6* are associated with Borjeson-Forssman-Lehmann syndrome. *Nat. Genet.* **32**, 661–665 (2002).
8. Borjeson, M., Forssman, H. & Lehmann, O. An X-linked, recessively inherited syndrome characterized by grave mental deficiency, epilepsy, and endocrine disorder. *Acta Med. Scand.* **171**, 13–21 (1962).
9. Turner, G. *et al.* The clinical picture of the Borjeson-Forssman-Lehmann syndrome in males and heterozygous females with *PHF6* mutations. *Clin. Genet.* **65**, 226–232 (2004).
10. Baker, L.A., Allis, C.D. & Wang, G.G. PHD fingers in human diseases: disorders arising from misinterpreting epigenetic marks. *Mutat. Res.* **647**, 3–12 (2008).
11. Dephoure, N. *et al.* A quantitative atlas of mitotic phosphorylation. *Proc. Natl. Acad. Sci. USA* **105**, 10762–10767 (2008).
12. Matsuoka, S. *et al.* ATM and ATR substrate analysis reveals extensive protein networks responsive to DNA damage. *Science* **316**, 1160–1166 (2007).
13. Lowndes, N.F. & Toh, G.W. DNA repair: the importance of phosphorylating histone H2AX. *Curr. Biol.* **15**, R99–R102 (2005).
14. Payer, B. & Lee, J.T. X chromosome dosage compensation: how mammals keep the balance. *Annu. Rev. Genet.* **42**, 733–772 (2008).
15. Carrel, L. & Willard, H.F. Heterogeneous gene expression from the inactive X chromosome: an X-linked gene that escapes X inactivation in some human cell lines but is inactivated in others. *Proc. Natl. Acad. Sci. USA* **96**, 7364–7369 (1999).
16. Ferrando, A.A. *et al.* Gene expression signatures define novel oncogenic pathways in T cell acute lymphoblastic leukemia. *Cancer Cell* **1**, 75–87 (2002).
17. Soulier, J. *et al.* HOXA genes are included in genetic and biologic networks defining human acute T-cell leukemia (T-ALL). *Blood* **106**, 274–286 (2005).
18. Van Vlierberghe, P. *et al.* The recurrent SET-NUP214 fusion as a new HOXA activation mechanism in pediatric T-cell acute lymphoblastic leukemia. *Blood* **111**, 4668–4680 (2008).
19. van Grotel, M. *et al.* The outcome of molecular-cytogenetic subgroups in pediatric T-cell acute lymphoblastic leukemia: a retrospective study of patients treated according to DCOG or COALL protocols. *Haematologica* **91**, 1212–1221 (2006).

ONLINE METHODS

Clinical samples and cell lines. Leukemic DNA and cryopreserved lymphoblast samples were provided by collaborating institutions in the United States (ECOG), The Netherlands (DCOG), France (Hôpital Saint-Louis, Paris), Austria (Children's Cancer Research Institute, St. Anna Kinderkrebsforschung, Vienna) and Belgium (Department of Pediatric Hemato-Oncology, Ghent University Hospital, Ghent; Department of Hematology, Hospital St.-Jan, Bruges). All samples were collected in clinical trials with informed consent and under the supervision of local institutional review board committees. The subjects' parents or their legal guardians provided informed consent to use leftover material for research purposes according to the Declaration of Helsinki. T-cell phenotype was confirmed by flow cytometry. Survival analysis was performed in pediatric T-ALL samples from DCOG trials ALL7, ALL8 and ALL9 (ref. 19) and from adults with T-ALL treated in the ECOG2993 clinical trial[20].

Jurkat and PF382 cells were obtained from the American Type Culture Collection. The ALL-SIL, HPB-ALL and T-ALL-1 cell lines were from the DSMZ repository (the German national resource center for biological material). The DND41 cell line was a gift from A.T. Look (Dana-Farber Cancer Institute). T-ALL cell lines were cultured in RPMI 1640 medium supplemented with 10% fetal bovine serum, 100 U/ml penicillin G and 100 µg/ml streptomycin at 37 °C in a humidified atmosphere under 5% CO_2.

X chromosome exome capture and next-generation sequencing. Libraries of synthetic biotinylated RNA oligonucleotides (baits) targeting the X-chromosome exons were obtained from Agilent Technologies. The targeted region includes 5,217 exons for a total of 3 megabases and is designed to capture 85% of the exons on the human X chromosome. Fragment libraries using 2–4 µg of genomic DNA as starting material were prepared following the SOLiD standard library preparation protocol with some modifications, including the use of shortened adaptors and a precapture amplification for six cycles. A total of 500 ng of captured library were hybridized with the baits for 42 h, washed and eluted using the protocol provided by Agilent. The resulting captured DNA was amplified using Herculase II Fusion DNA polymerase (Agilent) for 18 cycles. Enrichment in the targeted regions was calculated by real-time PCR quantification of single exons within four X-chromosome loci (*ARSF*, *OTC*, *NAP1L3* and *SOX3*), which showed an average enrichment of 400- to 1,200-fold for the different loci across the 12 different samples. After library quantification by real-time PCR, the amplified captured libraries were subjected to emulsion PCR and sequenced following standard SOLiD 3 protocols by depositing 10–15 million beads per sample using an eight-region mask.

Data analysis SOLiD3 ultradeep sequencing. A reference genome of the captured regions was created based on the March 2006 human reference sequence (hg18). To map the sequence data into this reference genome, we used the SHRiMP algorithm with its default parameters[21]. SOLiD platform employs a two-base encoding system, where a single variation in the color space solely indicates a sequencing error and two consecutive variations in the color space point to a base change in the nucleotide-space. In our analysis we included only the reads with a maximum number of two color-space mismatches that are also uniquely mapped to the reference genome. An average 90.1% of the reference genome is covered in the 12 samples, where the mean depth is 42 per base. Less restrictive filtering increases the false-positive rate of candidate genomic variants without improving the coverage to any great extent. We found 66 candidates of exonic nonsynonymous single-nucleotide variation by requiring each variation to be reported in a minimum 75% of at least three reads mapping to its position. These candidates exclude the previously reported SNPs in the human genome. Using ParMap, an algorithm specifically developed to identify small deletions and insertions (along with their nucleotide sequence) through statistical analysis of partially mapped reads[22], we identified seven candidates of such complex variations. Validation of the next-generation sequencing results was done by Sanger sequencing of PCR amplified exons. Overall, 89% of all previously uncharacterized candidate variants were confirmed.

Microarray-based comparative genomic hybridization. Analysis of X-chromosome array-CGH data was performed in a multicenter setting. Depending on the institution of origin, array-CGH analysis was performed using an oligonucleotide array-CGH platform[18,23] (Agilent) or a tiling path BAC array-CGH platform[24]. To determine the exact size of the recurrent Xq26 deletions, we reanalyzed all eight del(X)(q26)-positive T-ALL cases using a custom high-resolution X-chromosome oligonucleotide array with an average resolution of 3 kb according to the manufacturer's instructions (Agilent). Slides were scanned in a 2565AA DNA microarray scanner (Agilent). Microarray images were analyzed using Feature Extraction software (Agilent), and the data were subsequently imported into array-CGH Analytics software (Agilent).

Real-time quantification of DNA copy number. Chromosome Xq26.3 deletions were confirmed with real-time quantitative DNA PCR using the Fast SYBR Green Master Mix (Applied Biosystems) and the LightCycler 480 Real-Time PCR System (Roche Diagnostics) as described[25] using *TIE2* as control gene. Data were analyzed using the comparative ΔΔCT method (Applied Biosystems). The primers used for the quantitative PCR analysis of the *PHF6* locus are shown in **Supplementary Table 7**.

***PHF6* mutation analysis.** *PHF6* mutations were analyzed by PCR amplification of *PHF6* exons 2–10 followed by direct bidirectional DNA sequencing. The primers used for *PHF6* mutation detection are summarized in **Supplementary Table 7**.

Protein blot and immunohistochemistry. Protein blot analysis was performed using a rabbit polyclonal antibody specific to PHF6 (1:10,000; Novus Biologicals) recognizing a C-terminal (amino acids 315–365) epitope in PHF6; a mouse monoclonal antibody (1:1,000) recognizing an N-terminal (amino acids 120–140) PHF6 epitope[26]; an antibody specific to γ-H2AX (1:1,000; Cell Signaling Technologies) and a mouse monoclonal antibody specific to GAPD (1:1000; Santa Cruz Biotechnology) using standard procedures.

Immunohistochemistry analysis was performed as described following the standard avidin-biotin immunoperoxidase staining procedure using an N-terminal antibody to PHF6. Briefly, PHF6 immunostaining of formalin-fixed paraffin-embedded tissue sections was performed after heat-induced epitope retrieval in a microwave in citrate buffer, pH 6.0. Subsequently, sections were incubated in 10% normal goat serum for 30 min, followed by primary antibody incubation (amino acids 1–94 of rabbit polyclonal antibody to PHF6; Sigma Prestige Antibodies, dilution 1:100) overnight at 4 °C. Next, slides were incubated with biotinylated immunoglobulins specific to rabbit at a 1:1000 dilution (Vector Laboratories) for 30 min, followed by avidin-biotin peroxidase complexes at a 1:25 dilution (Vector Laboratories) for 30 min. Diaminobenzidine was used as the chromogen and hematoxylin as a nuclear counterstain.

Quantitative real-time PCR. Thymocyte populations were isolated from human thymi as described before[27]. Total RNA was extracted using the Trizol method (Invitrogen) following the manufacturer's instructions. Total RNA from 20 different normal human tissues was obtained from the FirstChoice Human Total RNA Survey Panel (Applied Biosystems). Complementary DNA (cDNA) was generated with the ThermoScript RT-PCR system (Invitrogen) and analyzed by quantitative real-time PCR using the SYBR Green RT-PCR Core Reagents kit (Applied Biosystems) and the 7300 Real-Time PCR System (Applied Biosystems). *PHF6* expression levels were calculated using *GAPDH* as a reference gene. Primers used for *PHF6* expression analysis are shown in **Supplementary Table 7**.

SNP genotyping. Genotyping of SNP rs17317724 located in the 3′ UTR region of *PHF6* was performed using a TaqMan SNP Genotyping Assay (Assay ID C__34812972_10, Applied Biosystems) according to manufacturer's instructions in DNA samples from females with wild-type *PHF6* T-ALL. Genotyping was confirmed by direct DNA sequencing of PCR products encompassing the 3′ UTR of *PHF6*. Allelic expression analysis was performed in cDNA samples from heterozygous females with T-ALL so as to evaluate monoallelic and biallelic *PHF6* expression. Before cDNA synthesis, RNA samples were treated with DNase I using the DNA-free DNase Treatment kit (Applied Biosystems) to remove any traces of genomic DNA. The *PHF6* 3′ UTR-specific primers used for amplification of SNP rs17317724 are also summarized in **Supplementary Table 7**.

***PHF6* shRNA knockdown.** We produced lentiviral particles driving the expression of a shRNA directed against *PHF6* (target sequence CAGAATTTGGAGACTTTGA) using the pGIPZ Lentiviral shRNAmir vector system (V2LHS_138602, Open Biosystems) as described[28]. We infected HEK293T cells with viral supernatants generated with pGIPZ PHF6 or an empty pGIPZ control using spinoculation in the presence of polybrene. PHF6 knockdown was evaluated by protein blot analysis at 72 h as described above.

Statistical analysis. Fisher's exact test was used to compare the frequency of *PHF6* mutations between clinical and genetic groups of T-ALL. Bar graphs represent mean values ± s.e.m. Therapeutic outcome was analyzed in leukemia patients treated in DCOG trials ALL7, ALL8 and ALL9 and in ECOG trial 2993 according to overall survival. Kaplan-Meier curves were used to assess survival, and differences between groups were compared by the log-rank test.

20. Marks, D.I. *et al.* T-cell acute lymphoblastic leukemia in adults: clinical features, immunophenotype, cytogenetics, and outcome from the large randomized prospective trial (UKALL XII/ECOG 2993). *Blood* **114**, 5136–5145 (2009).
21. Rumble, S.M. *et al.* SHRiMP: accurate mapping of short color-space reads. *PLOS Comput. Biol.* **5**, e1000386 (2009).
22. Khiabanian, H., Van Vlierberghe, P., Palomero, T., Ferrando, A.A. & Rabadan, R. ParMap, an algorithm for the identification of complex genomic variations in nextgen sequencing data. *Nature Precedings* published online, <http://hdl.handle.net/10101/npre.2010.4145.1> (12 January 2010).
23. Clappier, E. *et al.* The C-MYB locus is involved in chromosomal translocation and genomic duplications in human T-cell acute leukemia (T-ALL), the translocation defining a new T-ALL subtype in very young children. *Blood* **110**, 1251–1261 (2007).
24. Erdogan, F. *et al.* Impact of low copy repeats on the generation of balanced and unbalanced chromosomal aberrations in mental retardation. *Cytogenet. Genome Res.* **115**, 247–253 (2006).
25. Lahortiga, I. *et al.* Duplication of the *MYB* oncogene in T cell acute lymphoblastic leukemia. *Nat. Genet.* **39**, 593–595 (2007).
26. Voss, A.K. *et al.* Protein and gene expression analysis of *Phf6*, the gene mutated in the Borjeson-Forssman-Lehmann syndrome of intellectual disability and obesity. *Gene Expr. Patterns* **7**, 858–871 (2007).
27. González-García, S. *et al.* CSL-MAML-dependent Notch1 signaling controls T lineage-specific IL-7Rα gene expression in early human thymopoiesis and leukemia. *J. Exp. Med.* **206**, 779–791 (2009).
28. Moffat, J. *et al.* A lentiviral RNAi library for human and mouse genes applied to an arrayed viral high-content screen. *Cell* **124**, 1283–1298 (2006).

PHF6 mutations in T-cell acute lymphoblastic leukemia

Pieter Van Vlierberghe, Teresa Palomero, Hossein Khiabanian, Joni Van der Meulen, Mireia Castillo, Nadine Van Roy, Barbara De Moerloose, Jan Philippé, Sara González-García, María L Toribio, Tom Taghon, Linda Zuurbier, Barbara Cauwelier, Christine J Harrison, Claire Schwab, Markus Pisecker, Sabine Strehl, Anton W Langerak, Jozef Gecz, Edwin Sonneveld, Rob Pieters, Elisabeth Paietta, Jacob M Rowe, Peter H. Wiernik, Yves Benoit, Jean Soulier, Bruce Poppe, Xiaopan Yao, Carlos Cordon-Cardo, Jules Meijerink, Raul Rabadan, Frank Speleman and Adolfo Ferrando

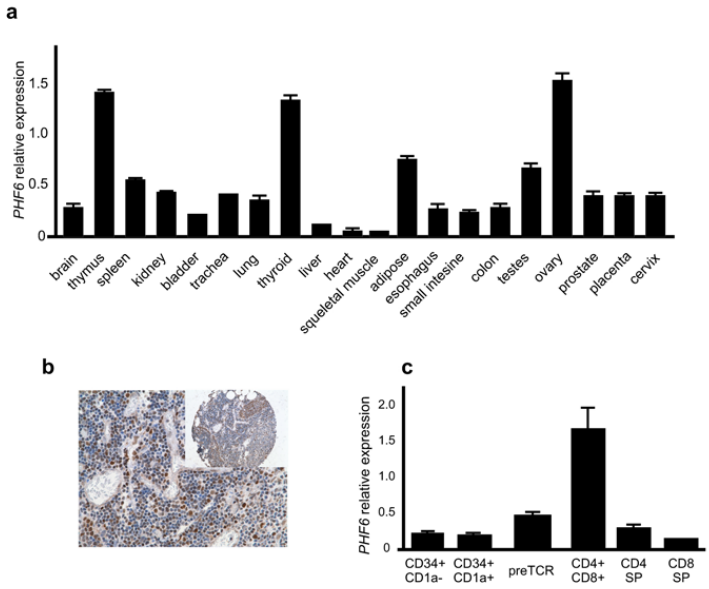

Figure S1. *PHF6* expression in normal tissues and lymphoid progenitors.

(**a**) Quantitative RT-PCR analysis of *PHF6* transcripts in human tissues. (**b**) PHF6 immunostaining in mouse thymus. (**c**) Quantitative RT-PCR analysis of *PHF6* expression normalized to *GAPDH* in lymphoid populations isolated from human thymus. Error bars indicate s.d.

Nature Genetics: doi:10.1038/ng.542

Table S1. Novel non-synonymous single nucleotide variants identified in T-ALL samples

Sample	Gene	Position*	Variant Hits	Hits	% variant	Mutation	Ref. Seq.	Validation		
								Diagnosis	Remission	Germline SNP /somatic mutation
1	FAM47A	34059251	3	4	0.75	T	C	Confirmed	Confirmed	SNP
1	PAGE1	49341043	27	27	1	T	C	Confirmed	Confirmed	SNP
1	PHF6	133378928	30	31	0.97	G	A	Confirmed	Not present	***Somatic***
1	VCX	7771747	5	6	0.83	C	T	Confirmed	Confirmed	SNP
2	ARSF	3009043	15	16	0.94	T	C	Confirmed	Confirmed	SNP
2	BEND2	18131667	50	62	0.81	C	A	Confirmed	Confirmed	SNP
2	BEND2	18131901	42	50	0.84	A	C	Confirmed	Confirmed	SNP
2	BEX2	102451354	6	6	1	C	T	Confirmed	Confirmed	SNP
2	ERCC6L	71344776	21	21	1	C	T	Confirmed	Confirmed	SNP
2	FAM123B	63329016	48	48	1	G	C	Confirmed	Confirmed	SNP
2	FRMD7	131047629	17	17	1	C	A	Confirmed	Confirmed	SNP
2	GUCY2F	108578040	28	29	0.97	G	T	Confirmed	Confirmed	SNP
2	ITIH5L	54800677	47	48	0.98	G	A	Confirmed	Confirmed	SNP
2	ITIH5L	54831790	6	6	1	C	G	Confirmed	Confirmed	SNP
2	MXRA5	3250445	73	85	0.86	A	G	Confirmed	Confirmed	SNP
2	RENBP	152860231	11	14	0.79	T	G	Confirmed	Confirmed	SNP
2	SATL1	84249820	10	13	0.77	C	T	Confirmed	Confirmed	SNP
2	TKTL1	153177429	31	31	1	T	C	Confirmed	Confirmed	SNP
2	ZCCHC13	73440929	9	9	1	A	G	Confirmed	Confirmed	SNP
3	AMOT	111908546	14	14	1	G	C	Confirmed	Confirmed	SNP
3	PJA1	68297890	19	19	1	C	G	Confirmed	Confirmed	SNP
3	RENBP	152860231	6	6	1	T	G	Confirmed	Confirmed	SNP
3	GPR112	135258600	28	28	1	A	C	Confirmed	Confirmed	SNP
4	ARSD	2837930	9	9	1	T	C	Confirmed	Confirmed	SNP
4	ATP6AP1	153317004	13	14	0.93	C	A	Confirmed	Confirmed	SNP
4	DDX53	22929591	21	21	1	T	G	Confirmed	Confirmed	SNP
4	GPR50	150100218	4	4	1	T	C	Confirmed	Confirmed	SNP
4	EFNB1	67976537	14	14	1	T	C	Confirmed	Confirmed	SNP
4	FAM123B	63329016	42	42	1	G	C	Confirmed	Confirmed	SNP
4	GPR112	135324123	26	27	0.96	A	G	Confirmed	Confirmed	SNP
4	MAGEB10	27749463	9	10	0.9	A	C	Confirmed	Confirmed	SNP
4	MXRA5	3249674	30	31	0.97	A	G	Confirmed	Confirmed	SNP

Nature Genetics: doi:10.1038/ng.542

4	NHS	17654740	47	47	1	A	G	Confirmed	Confirmed	SNP
4	RS1	18575263	24	24	1	C	T	Confirmed	Confirmed	SNP
4	SSX6	47863860	37	38	0.97	A	G	Confirmed	Confirmed	SNP
4	XPNPEP2	128709366	29	31	0.94	T	C	Confirmed	Confirmed	SNP
5	DOCK11	117561529	6	6	1	G	C	Confirmed	Confirmed	SNP
6	ABCD1	152661670	3	4	0.75	C	T	Confirmed	Confirmed	SNP
6	ATP6AP1	153310652	4	4	1	G	A	Confirmed	Confirmed	SNP
6	BEX1	102204608	27	27	1	T	C	Confirmed	Confirmed	SNP
6	CCDC120	48809978	5	6	0.83	T	G	Confirmed	Confirmed	SNP
6	GJB1	70360986	7	7	1	G	T	Confirmed	Confirmed	SNP
6	MAGEB10	27749463	3	3	1	A	C	Confirmed	Confirmed	SNP
6	PCDH19	99437939	25	25	1	T	C	Confirmed	Confirmed	SNP
6	RENBP	152860140	6	8	0.75	C	G	Confirmed	Confirmed	SNP
6	RGAG1	109583439	12	12	1	C	A	Confirmed	Confirmed	SNP
6	TKTL1	153177429	15	15	1	T	C	Confirmed	Confirmed	SNP
6	YY2	21785569	32	32	1	G	A	Confirmed	Confirmed	SNP
7	ARSF	3012475	34	35	0.97	G	A	Confirmed	Confirmed	SNP
7	FRMPD4	12644571	26	26	1	T	G	Confirmed	Confirmed	SNP
7	WNK3	54337883	16	18	0.89	A	C	Confirmed	Confirmed	SNP
7	XPNPEP2	128722831	7	7	1	T	C	Confirmed	Confirmed	SNP
8	ACSL4	108795370	36	36	1	C	T	Confirmed	Confirmed	SNP
8	APEX2	55049841	10	10	1	T	C	Confirmed	Confirmed	SNP
8	KLHL13	116927943	23	24	0.96	A	G	Confirmed	Confirmed	SNP
8	PHF6	133386914	6	6	1	G	A	Confirmed	Not present	***Somatic***
9	GPR112	135315560	10	10	1	T	G	Confirmed	Confirmed	SNP
9	IQSEC2	53294754	7	7	1	T	C	Confirmed	Confirmed	SNP
10	PLAC1	133528065	4	4	1	A	G	Confirmed	Confirmed	SNP
10	SLC9A7	46395735	26	34	0.76	A	T	Not confirmed	Not confirmed	Not confirmed
10	TEX11	69859222	11	11	1	T	G	Confirmed	Confirmed	SNP
11	BCAP31	152621624	54	70	0.77	C	G	Not confirmed	Not confirmed	Not confirmed
11	CENPI	100251615	3	3	1	C	T	Not confirmed	Not confirmed	Not confirmed
11	VCX	7771747	3	3	1	C	T	Not confirmed	Not confirmed	Not confirmed
12	CYLC1	83028235	22	22	1	G	A	Confirmed	Confirmed	SNP
12	FAM47A	34059265	3	3	1	T	C	Not confirmed	Not confirmed	Not confirmed

*genomic localisation is based upon the USCS genome browser (Assembly March 2006)

Nature Genetics: doi:10.1038/ng.542

Table S2. Novel complex variants identified in T-ALL samples

Sample	Gene	Chromosome X_position*	Number of Raw Reads	Sequences	Seq. Percent	% variant	Validation		
							Diagnosis	Remission	Germline variant/somatic mutation
4	USP26	131989551	23	TGTGCTAGA	0.91	21	ins(CAA)	ins(CAA)	Germline variant
5	PHF6	133339436	17	AGGCACACCA	0.94	16	ins (AGGCA)	Not confirmed	**Somatic mutation**
2	PASD1	150544606	6	AAA	1	6	Not confirmed	Not confirmed	Not confirmed
5	FLNA	153243644	6	TAGACTAG	1	6	Not confirmed	Not confirmed	Not confirmed
3	DACH2	85290321	5	AGAGAGGAA	1	5	Not confirmed	Not confirmed	Not confirmed
3	GPR112	135302111	5	ATT	1	5	del (ATG)	del (ATG)	Germline variant
9	MED12	70258307	5	CCCCTGCCG	1	5	del(AGCACA)	del(AGCACA)	Germline variant

*Genomic position based upon USCS genome browser (Assembly March 2006)

Nature Genetics: doi:10.1038/ng.542

Table S3. *PHF6* mutations in T-ALL cell lines

T-ALL cell line	Gender	Translocation-associated T-ALL oncogene	*PHF6* mutation	
DND41	M	*TLX3*	Frameshift	p.G10fs
HPB-ALL	M	*TLX3*	Nonsense	p.S320X
T-ALL1	M	Unknown	Frameshift	p.G263fs
JURKAT	M	*TAL1*	Wildtype	
LOUCY	F	*SET-NUP214*	Wildtype	
MOLT16	F	*MYC*	Wildtype	
PEER	F	*NKX2.5*	Wildtype	
PF382	F	Unknown	Wildtype	
SKW3	M	Unknown	Wildtype	
RPMI8402	F	*LMO1*	Wildtype	
P12-ICHIKAWA	M	Unknown	Wildtype	
CUTLL1	M	*NOTCH1*	Wildtype	
KOPTK1	M	*TAL1*	Wildtype	
HSB2	M	*LCK*	Wildtype	
ALL-SIL	M	*TLX1*	Wildtype	

Nature Genetics: doi:10.1038/ng.542

Table S4. Gender distribution of *PHF6* mutations in T-ALL

	PHF6 mutation	*PHF6* wild-type	Total	P-Value[a]
Male	29	63	92	***0.0001***
Female	1	38	39	
Total	30	101	131	

[a]Fisher's exact test

Nature Genetics: doi:10.1038/ng.542

Table S5. Molecular characterization of pediatric T-ALL cases treated in DCOG studies ALL7, ALL8 and ALL9 (n=65).

	All patients	*PHF6* mutation	*PHF6* wild-type	P-value[a]
Number	65	14 (21.5%)	51 (78.5%)	
Genetic subgroup				
TLX1	6 (9%)	3 (50%)	3 (50%)	0.108
TLX3	17 (26%)	7 (41%)	10 (59%)	***0.037***
TLX1/TLX3	23 (35%)	10 (43%)	13 (57%)	***0.0032***
HOXA	5 (8%)	1 (20%)	4 (80%)	0.708
TAL1/2 or *LMO1/2*	26 (40%)	2 (8%)	24 (92%)	***0.033***
Mutations				
NOTCH1	40 (61%)	11 (27%)	29 (73%)	0.216
FBXW7	11 (17%)	2 (18%)	9 (82%)	1.00
PTEN	8 (12%)	0 (0%)	8 (100%)	0.185

[a] Fisher's exact test

Nature Genetics: doi:10.1038/ng.542

Table S6. Molecular characterization of adult T-ALL cases from ECOG study 2993 (n=34).

	All patients	*PHF6* mutation	*PHF6* wild-type	P-value[a]
Number	34	13 (38%)	21 (62%)	
NOTCH1	20 (62%)	8 (40%)	12 (60%)	1.00
FBXW7	6 (18%)	2 (33%)	4 (67%)	1.00
PTEN	4 (12%)	0	4 (100%)	0.14

[a] Fisher's exact test

Nature Genetics: doi:10.1038/ng.542

Table S7. List of primer sequences

	Forward primer	Reverse primer
Genomic DNA quantitative PCR		
PHF6	CTCGGCGAACAAGTGCAA	GGGGCAGGATCAGAGGAGA
HPRT1	TACCACCGTGTGTTAGAAAA	ATTCCAGGACAGAACAAAAC
miR-424/503	AGGAGCGACTTGACATCA	ACACCCCAGCTGAGTTAT
miR-450/542	TTTTTGCGATGTGTTCCTA	CCCTCCATCTTTTCATCTG
TIE	CGAGATCCAGCTGACATGGAA	CTCCACAACGTACTTGGATATTGG
PHF6 mutation analysis		
PHF6 Exon 2	TTTCTTGGGGCTTAGAGTG	AAATGGCATAGCATTAGTGA
PHF6 Exon 3	GCTATGCCATTTTTACTAGAAA	GCTGGCTCAGAGAAAAAAAA
PHF6 Exon 4	CCCCAGAAGAATTTTATTCC	AAACGTGGCTAAATGATGTA
PHF6 Exon 5	AAAGGGTGTTTTTGATAAGA	AAACGTGGCTAAATGATGTA
PHF6 Exon 6	GGGTGGCTTTATTGAACAT	GCTATCGGTATTTCAAGCTTA
PHF6 Exon 7	TTGGATTCTTACTTTTGTTGC	GGGGAAATTTTTTGGTTACTA
PHF6 Exon 8	TTTTCCTGCATTTTTCTTCT	GCAAATGCCTTGAAATGTAT
PHF6 Exon 9	GAGGGCTTATCAAAGTATGG	AGGAAAATGCCAATTGTAGT
PHF6 Exon 10	AGCCTCATCCACTAATGTTG	GAGTTGGGCAGTAAAAAGTT
PHF6 mono/bi-allelic expression analysis		
PHF6 Exon 11 (3'UTR)	AGGCTGAGTTTGACATGTT	CAAGCCCTACAAGAAGAAA
PHF6 quantitative RT-PCR analysis		
PHF6	AAAAGGGCCTACAAGACAG	ACAATGGCACAAAGAACAC

Nature Genetics: doi:10.1038/ng.542

PAPER 2

The H3K27me3 demethylase *UTX* is a gender-specific tumor suppressor in T-cell acute lymphoblastic leukemia

Van der Meulen J, Sanghvi V, Mavrakis K, Durinck K, Fang F, Matthijssens F, Rondou P, Vandenberghe P, Delabesse E, Lammens T, De Moerloose B, Menten B, Van Roy N, Verhasselt B, Poppe B, Benoit Y, Taghon T, Melnick A, Speleman F, Wendel HG* & Van Vlierberghe P*. Submitted to Cancer Discovery (April 2014).

The H3K27me3 demethylase *UTX* is a gender-specific tumor suppressor in T-cell acute lymphoblastic leukemia

Joni Van der Meulen[1], Viraj Sanghvi[2], Konstantinos Mavrakis[2], Kaat Durinck[1], Fang Fang[3], Filip Matthijssens[1], Pieter Rondou[1], Peter Vandenberghe[4], Eric Delabesse[5], Tim Lammens[6], Barbara De Moerloose[6], Björn Menten[1], Nadine Van Roy[1], Bruno Verhasselt[7], Bruce Poppe[1], Yves Benoit[6], Tom Taghon[7], Ari Melnick[3], Frank Speleman[1], Hans-Guido Wendel[2]* and Pieter Van Vlierberghe[1]*

[1]Center for Medical Genetics, Ghent University, Ghent, Belgium; [2]Cancer Biology & Genetics, Memorial Sloan-Kettering Cancer Center, NY, USA; [3]Department of Medicine, Weill Cornell Medical College, NY, USA; [4]Centre for Human Genetics, University Hospital Leuven, Leuven, Belgium; [5]INSERM U563, Toulouse, France; [6]Department of Pediatric Hematology-Oncology and Stem Cell Transplantation, Ghent University Hospital, Ghent, Belgium; [7]Department of Clinical Chemistry, Microbiology and Immunology, Ghent University, Ghent, Belgium.
**Shared last authors*

Running Title
UTX as a tumor suppressor in T-ALL

Keywords
Leukemia, T-ALL, epigenetics, UTX, PRC2

Financial Support
This work is supported by the Fund for Scientific Research (FWO) Flanders (postdoctoral grants to P.V.V., P.R. and T.T., PhD grant to J.V.d.M., B.P. and P.V. are Senior Clinical Investigators of FWO-Flanders, Odysseus grant to P.V.V and T.T. and project grants G.0198.08, G.0564.13N, G.0550.13N and G.0869.10N to F.S., G.A001.13N to P.V.V. and G0B2913N and 3G002711 to T.T.); the Flemish Liga against Cancer (VLK) (PhD grant to J.V.d.M. and postdoctoral grant to F.M.); the Agency for Innovation by Science and Technology (IWT) (PhD grant to K.D.); the GOA-UGent (grant no. 12051203 to F.S.); Belgian Foundation against Cancer, the Cancer Plan from the Federal Public Service of Health (F.S.); the Children Cancer Fund Ghent (F.S.); the Belgian Program of Interuniversity Poles of Attraction IUAP; the Belgian Foundation Against Cancer (project grant 2010-187 to T.L., 365O9110 to F.S.); the NCI R01-CA142798-01 (H-G.W.) and U01CA105492-08 (H-G.W.); the Leukemia Research Foundation (H-G.W.); the Experimental Therapeutics Center at MSKCC (H-G.W.), the American Cancer Society (H-G.W.) and the Geoffrey Beene Cancer Center (H-G.W.). A.M. is supported by LLS SCOR 7006-13 and LLS TRP 6141-14, and the Burroughs Wellcome Foundation.

Corresponding author
Pieter Van Vlierberghe, PhD
Center for Medical Genetics Ghent (CMGG)
Ghent University Hospital
Medical Research Building (MRB), 2nd floor, room 120.032
De Pintelaan 185
9000 Ghent, Belgium
Tel: +32-9-3326950
Fax: +32-9-3324970
pieter.vanvlierberghe@ugent.be

Disclosure of Potential Conflicts of Interest
No potential conflicts of interest.

Word count: 3500 words excluding Title page, Abstract, Methods, References & Supplementary

Figures and tables: 4 figures, 5 supplementary figures & 8 supplementary tables

ABSTRACT

T-cell acute lymphoblastic leukemia (T-ALL) is an aggressive form of human leukemia that is mainly diagnosed in children and shows a skewed gender distribution towards males. Here, we report somatic loss-of-function mutations in the X-linked histone H3K27me3 demethylase *UTX* in human T-ALL. Interestingly, *UTX* mutations were exclusively present in male T-ALL patients and allelic expression analysis revealed that *UTX* escapes X inactivation in female T-ALL lymphoblasts. The Polycomb repressive complex 2 (PRC2) regulates gene repression through methylation of H3K27 and therefore counteracts UTX activity. Notably, we demonstrate *in vivo* that - despite encoding opposing activities - the H3K27me3 demethylase Utx and the PRC2 H3K27me3 methyltransferase complex both function as *bona fide* tumor suppressors in T-ALL. Moreover, T-ALL driven by *UTX* inactivation exhibits collateral sensitivity to pharmacological H3K27me3 inhibition. All together, our results show how a gender-specific and therapeutically relevant defect in balancing H3K27 methylation contributes to T-cell leukemogenesis.

STATEMENT OF SIGNIFICANCE

The H3K27me3 demethylase *UTX* is recurrently mutated in primary T-ALL patient samples, most exclusively in males. Loss of UTX contributes to T-ALL formation and confers sensitivity to H3K27me3 inhibition.

INTRODUCTION

T-cell acute lymphoblastic leukemia (T-ALL) is an aggressive hematological malignancy that occurs in children and adolescents and is diagnosed more frequently in males than females. Current treatment schedules consist of intensified chemotherapy and are often associated with considerable side effects (1, 2). T-ALL arises from a multistep oncogenic process in which different genetic alterations drive malignant transformation of immature T-cell progenitors. Several key oncogenic drivers mark particular molecular-genetic subgroups as demonstrated by genome-wide transcriptome studies on large cohorts of primary T-ALL samples (3-5). Activation of NOTCH signaling has been recognized as an oncogenic hallmark of T-ALL driven by activating *NOTCH1* mutations (6) and loss-of-function mutations targeting the E3-ubiquitin ligase *FBXW7* (7, 8). Furthermore, a plethora of additional mechanisms of T-cell transformation have been elucidated involving an increasing number of T-ALL oncogenes and tumor suppressors (9).

Recent sequencing studies have identified the core components EZH2, EED and SUZ12 of the PRC2 complex, which mediates gene silencing through tri-methylation of H3K27 (10), as tumor suppressors in the pathogenesis of T-ALL (9, 11, 12). Moreover, conditional ablation of *Ezh2* in mouse hematopoietic stem cells was shown to be sufficient for murine T-ALL development (12). The histone demethylase *Ubiquitously Transcribed X Chromosome Tetratricopeptide Repeat Protein* (UTX) counters the enzymatic activity of PRC2 by removing di- and trimethyl groups from H3K27 (13, 14). In 2009, somatic loss-of-function mutations targeting the *UTX* gene were identified in a variety of human tumors including multiple myeloma, esophageal and renal cancer (15). In that study, re-expression of UTX in *UTX* mutant cancer cell lines was associated with lower H3K27me3 levels at the promoters of Polycomb target genes and concomitant inhibition of cell proliferation. Recently, a general role for UTX as tumor suppressor in human cancer was further supported by the identification of recurrent inactivating *UTX* mutations in several leukemia and solid tumor cancer types (15-17).

In this report, we report the identification of somatic loss-of-function mutations targeting the histone demethylase *UTX* in human T-ALL and provide *in vitro* and *in vivo* evidence for its tumor suppressor function. Notably, our study unravels that, despite their putative opposite effects on H3K27me3 levels, both the PRC2 complex as well as the histone demethylase UTX can serve as *bona fide* tumor suppressors in the molecular pathogenesis of T-ALL. Finally, we show that *UTX* mutant leukemias are more sensitive to treatment with an H3K27me3 inhibitor providing new opportunities for epigenetically targeted therapy in T-ALL.

RESULTS

Mutations recurrently target the H3K27me3 demethylase *UTX* in male T-ALL patients

To identify a potential role for the H3K27me3 demethylase UTX in the molecular pathogenesis of T-ALL, we performed sequencing and copy number analysis in a series of 35 primary leukemia samples (10 female versus 25 male), including 25 pediatric and 10 adult T-ALL cases. We identified loss-of-function mutations in *UTX* in 5 out of 35 (14.3%) primary T-ALL patient samples (Fig. 1A, Supplementary Table S1) including 3 frameshift and 2 in-frame insertion/deletion mutations. *UTX* mutations were localized in a hotspot region within the catalytic Jumonji C (JmjC) domain of the protein (Fig. 1B) and sequencing of available remission material confirmed the somatic origin of these mutations (Fig. 1A). The somatic *UTX* mutations in our patient population were exclusively identified in samples from male origin.

Equal dosage of chromosome X genes between male and female cells is regulated by random inactivation of one copy of the X chromosome in female cells. However, previous studies have shown that some genes, including *UTX* (18), can escape chromosome X inactivation in certain tissues. Notably, we analyzed two silent SNPs, rs181547731 situated in the 3' UTR and rs20539 situated in exon 20 of *UTX*, in lymphoblasts from 3 female T-ALL patients and confirmed bi-allelic expression of *UTX* in female T-ALL lymphoblasts (Fig. 1C).

In T-ALL, a wide variety of oncogenic lesions cooperate to induce T-cell transformation. To identify genetic lesions that co-occur with loss of *UTX* in T-ALL, we classified our cohort into the known molecular genetic subgroups based upon the aberrant expression of transcription factor oncogenes (3-5) (Fig. 1D). Furthermore, we screened our patient population for alterations targeting T-ALL specific oncogenes and tumor suppressors (Fig. 1D, Supplementary Fig. S1). This analysis showed that *UTX* mutations co-occur with aberrant expression of the *TLX3* oncogene, activating *NOTCH1* mutations, and mutations or deletions targeting the putative chromatin remodeling factors *PHF6* or *SUZ12* (Fig. 1D).

Oncogenic advantage for Utx knockdown in murine T-ALL

To functionally validate the role of Utx as a putative tumor suppressor in the context of malignant T-cell transformation, we used the interleukin (IL2/IL7) dependent murine T-ALL cell line MOHITO (19). We transduced MOHITO cells with Utx and Suz12 shRNAs (Supplementary Fig. S2A-B) and an empty vector control and examined GFP enrichment after successive rounds of interleukin depletion as an indicator of tumor promoting activity (Supplementary Fig. S2C). Notably, murine tumor cells infected with functional Utx shRNA#1, Utx shRNA#3 and Suz12 shRNA#3 showed significant GFP enrichment over MOHITO cells infected with the non-functional Utx shRNA#2 or an empty vector control (Supplementary Fig. S2D-E).

Next, we used a bone marrow transplant mouse model of *NOTCH1*-induced T-ALL (20) (Fig. 2A) to study the *in vivo* role of Utx in the pathogenesis of T-ALL. Leukemic onset in mouse recipients receiving fetal liver cells with enforced NOTCH1 expression occurred around 55 days (n=14, mean latency = 54 days) (Fig. 2B). Co-introduction of Utx shRNA#1 caused a strong acceleration in leukemic onset (n=7, $p<0.0001$, mean latency = 29 days), whereas introduction of Utx shRNA#3 provided a milder effect on T-ALL latency (n=4, $p=0.02$, mean latency = 43.5 days; Fig. 2B). Similarly, infection of fetal liver cells with Suz12 shRNA#3 resulted in an augmentation of T-ALL onset (n=9, $p=0.0002$, mean latency = 41 days, Fig. 2B)

confirming the previously established *in vivo* tumor suppressor role of the PRC2 complex in T-ALL (9, 11, 12).

In all murine tumors, histological analysis revealed aggressive leukemia phenotypes marked by absence of apoptosis, high proliferation and infiltration of lymphoblasts in different organs (Supplementary Fig. S3A). In addition, evaluation of Utx and Suz12 knockdown confirmed the validity of the shRNAs *in vivo* (Fig. 2C and Supplementary Fig. S3B). Notably, immunohistochemistry revealed a marked decrease in H3K27me3 levels in lymphoblasts from Suz12 driven tumors as compared to NOTCH1 driven control tumors, in line with the role of the PRC2 complex in H3K27 methylation (Fig. 2D). In contrast, H3K27me3 levels between Utx driven and control murine T-cell tumors were largely comparable (Fig. 2D). Hence, our *in vivo* data surprisingly shows that loss of the H3K27 demethylase Utx promotes T-ALL development in the same manner as loss of the H3K27 methyltransferase complex member Suz12.

Finally, immunophenotypic characterization of mouse leukemias indicated an earlier T-cell maturation arrest for tumors driven by loss of Utx or Suz12 as compared to NOTCH1 control tumors (Fig. 2E, Supplementary Table S2-5). The NOTCH1 only controls were typically $Cd4^{+}Cd8^{+}$ double positive, whereas tumor cells driven by loss of Suz12 expressed Cd8 with mixed levels of Cd4. In contrast, immunophenotypic marker expression in Utx driven tumors was more heterogeneous including cell populations that lacked both Cd8 and Cd4 surface expression (Fig. 2E, Supplementary Table S2-5).

Transcriptional programs driven by loss of Utx in murine T-ALL models

To gain more insight in the oncogenic mechanisms mediated by loss of the H3K27me3 demethylase Utx, we performed gene expression profiling of NOTCH control tumors and mouse leukemias driven by loss of *Utx*. Supervised gene expression analysis (FC>1.5, $p<0.05$; Fig. 3A) showed that *Utx* deficient mouse tumors are associated with a specific gene expression signature that is characterized by down regulation of the T-ALL tumor suppressor genes *Ect2l* (11) and *Nf1* (21) and activation of the T-ALL oncogene *Tal1* (22) (Fig. 3A). Furthermore, Gene Set Enrichment Analysis (GSEA) (23) in these mouse tumors driven by loss of *Utx* showed enrichment of gene sets linked to early T-cell lymphocytes (24) ($p<0.01$; Fig. 3B; Supplementary Fig. S4A) and *LYL1* neighbouring genes in T-ALL (3) ($p=0.02$; Supplementary Fig. S4B), in line with the early immunophenotypic arrest observed in these murine leukemias (Fig. 2E).

Next, we performed H3K27me3 chromatin immunoprecipitation (ChIP) sequencing analysis on murine tumor material, to evaluate if genes down regulated in Utx driven mouse leukemias show differential H3K27me3 levels at their respective promoters. Notably, this analysis revealed accumulation of H3K27me3 at promoter regions of some of these transcripts, including genes with putative tumor suppressor activity like *Pcgf2* (25), *Lzts2* (26), *Dock4* (27), *Pura* (28), *Col2a1* (29), *Slc26a4* (30) (Fig. 3C, Supplementary Fig. S5).

To further explore the relationship between the genetic program mediated by *Utx* in the *in vivo* transplant model and the *in vitro* MOHITO model, we performed GSEA (23) of gene expression signatures associated with *Utx* knockdown in MOHITO cells. Interestingly, this analysis revealed a significant enrichment of genes down regulated upon loss of Utx in the mouse leukemias in Utx deficient MOHITO cells ($p=0.007$; 82 of 252 probes in core enrichment, Fig. 3D). Notably, the *Ect2l* (11) tumor suppressor was amongst the top-ranking genes in the leading edge of the GSEA plot (Fig. 3D). Therefore, consistent down regulation

in both *in vitro* and *in vivo* Utx knockdown model systems suggests that *Ect2l* (11) might act as an important target downstream of UTX in the biology of T-ALL.

Loss of Utx provides a selective pressure towards DZNep treatment

As loss of UTX will affect the genome-wide distribution of H3K27me3, we hypothesized that decreased UTX levels would render leukemia cells more vulnerable to treatment with 3-Deazaneplanocin A (DZNep), an epigenetic compound that specifically targets H3K27me3 (31). Treatment of three T-ALL cell lines with DZNep demonstrated enhanced sensitivity of the *UTX* mutant cell line PF-382 as compared to the PEER cell line and the *EZH2* mutant cell line TALL-1 (Fig. 4A-D). Moreover, TALL-1 cells were strongly resistant to DZNep treatment even at 100 µM presumably because of very low H3K27me3 levels (Fig. 4C-D). As expected, DZNep treatment of PF-382 and PEER resulted in decreased levels of H3K27me3 (31) as determined by western blot (Fig. 4E). In parallel, we confirmed that MOHITO cells showed enhanced sensitivity towards DZNep treatment upon Utx knockdown as compared to control cells (Fig. 4F). Notably, although control and Utx knockdown MOHITO cells show comparable baseline levels of H3K27me3, DZNep treatment induced a stronger decrease in H3K27me3 expression in the Utx knockdown samples as compared to the empty vector controls (Fig. 4G). Hence, UTX deficient T-ALL shows collateral sensitivity to H3K27me3 inhibition.

DISCUSSION

A role for *UTX* as tumor suppressor was initially postulated in several human tumors including multiple myeloma, esophageal and renal cancer (15). Notably, *UTX* deletions and mutations have also been identified in patients with the Kabuki syndrome, a rare congenital anomaly syndrome (32). Interestingly, a 2-year old Kabuki patient developed pre-B-ALL suggesting an increased susceptibility to cancer for patients carrying abnormalities in *UTX* (33). In this study, we identified gender-restricted somatic loss-of-function mutations targeting the histone demethylase *UTX* in male T-ALL patients and demonstrate its tumor suppressor function. In contrast to other X-linked tumor suppressor genes in T-ALL (*PHF6* (34) and *RPL10* (35)), *UTX* escapes chromosome X-inactivation in female T-ALL blasts, suggesting that females are protected against single copy loss of one *UTX* allele. Therefore, *UTX* is the first X-linked tumor suppressor gene that might partially explain the skewed gender distribution in T-ALL towards males on a genetic level.

The PRC2 complex mediates H3K27 methylation and therefore counteracts UTX activity. Tri-methylation of lysine 27 on histone 3 is a chromatin state that is usually associated with transcriptional gene repression. Depending on the tissue-type and cellular context, the PRC2 complex can function as an oncogene (for example in B-cell lymphoma (36)) or tumor suppressor gene (for example in T-ALL (9, 11, 12)). In addition, *Ezh2* loss was sufficient to induce murine T-ALL development further supporting a tumor suppressive activity for EZH2 in the context of T-ALL (12). In agreement with these findings, we identified mutations and deletions targeting *SUZ12* and *EED* in our T-ALL patient cohort. Notably, in our patient series, mutations or deletions in *EZH2* were absent.

Given that both opposite H3K27me3 modulators *PRC2* and *UTX* are targeted by loss-of-function alterations in primary T-ALL, we explored their tumor suppressor activity using *in vitro* and *in vivo* perturbation model systems. First, *Utx* or *Suz12* knockdown both provided murine leukemia cells with an oncogenic advantage after interleukin depletion using the IL2-IL7 dependent MOHITO culture system (19). Second, loss of *Suz12* or *Utx* resulted in significant acceleration of leukemia onset in a NOTCH1-induced T-ALL mouse model (20). For the first time, these functional *in vitro* and *in vivo* data firmly establish *Utx* as a bona fide tumor suppressor involved in murine T-cell transformation.

The PRC2 complex and UTX have opposing roles on cellular H3K27me3 levels but both act as *bona fide* tumor suppressors in T-ALL. Therefore, these epigenetic regulators most probably exert different biological roles in T-cell transformation and do not simply represent enzymatically opposing elements. In addition, differences in tumor immunophenotype between mouse leukemias driven by loss of Utx or Suz12 suggest that the tumor suppressor activity of these H3K27me3 regulators could depend on the maturation arrest or cell of origin during murine T-cell transformation.

Transcriptional profiling of the *in vivo* transplant model revealed that loss of *Utx* drives a unique gene expression signature in NOTCH1 driven mouse leukemias. Notably, an important part of this gene expression profile most likely reflects the immunophenotypic differences observed between control and Utx deficient tumors. However, ChIP seq analysis confirmed that some of the transcriptional differences are associated with accumulation of H3K27me3 at the promoter regions and therefore most probably reflect direct consequences of loss of Utx during malignant T-cell transformation.

Epigenetic drugs are currently developed and evaluated in different cancer subtypes. Since we identified UTX as a bona fide tumor suppressor gene in the pathogenesis of T-ALL, we hypothesized that loss of UTX would render leukemia cells more vulnerable to treatment with particular chromatin modifying drugs. As loss of UTX is associated with enhanced H3K27me3 levels, we explored the effect of DZNep, an epigenetic compound that specifically targets the H3K27me3 mark. Previous studies reported a strong apoptotic effect after DZNep administration in cancer cells whereas normal cells were not affected (31). Importantly, in our study, we showed in both murine and human *in vitro* T-ALL model systems that loss of UTX/Utx renders the leukemic population more sensitive to DZNep treatment. Importantly, such proof of principle data should be further validated in a preclinical setting in which H3K27me3 modifying agents are formally tested in well-characterized genetic animal models of T-ALL.

In conclusion, our results provide new insights into the pathogenesis and gender distribution in T-ALL. Furthermore, we identified *UTX* as an X-linked tumor suppressor gene and showed that Utx and Suz12 both act as *bona fide* tumor suppressors in T-ALL. All together, our study reveals how maintaining and pharmacologically restoring the precise balance of H3K27 methylation can restrain T-cell leukemia.

METHODS

Collection of T-ALL patient samples

A cohort of 35 bone marrow samples from primary T-ALL patients was collected from different medical institutes (UZ Ghent, Ghent, Belgium; UZ Leuven, Leuven, Belgium; Hôpital Purpan, Toulouse, France). This study was approved by the Medical Ethical Commission of Ghent University Hospital (Ghent, Belgium, B67020084745). DNA isolation was performed using the QIAamp DNA Mini kit (Qiagen).

Murine and human T-ALL cell lines

The MOHITO T-ALL mouse cell line was cultured in RPMI-1640 supplemented with 20% FCS, glutamine (2 mM), penicillin (100 U/ml)-streptomycin (100 µg/ml), IL-7 (10 ng/mL) and IL-2 (5 ng/ml) (Peprotech)(19).
Human T-ALL cell lines PEER, TALL-1 and PF-382 were obtained from the DSMZ repository. The cell lines were cultured in RPMI-1640 medium supplemented with 10% or 20% FCS, glutamine (2 mM), penicillin (100 U/ml) and streptomycin (100 µg/ml) under controlled conditions (37°C, 5% CO_2).

Sequencing analysis

We sequenced all coding exons of *PTEN*, *PHF6* and *UTX,* and mutation hotspot regions for *NOTCH1* and *FBXW7* in 35 T-ALL patient samples by Sanger sequencing. Primer sequences are noted in Table S6. The PCRx enhancer system (Invitrogen) was used for *NOTCH1* PCR reactions. *FBXW7, PTEN, PHF6* and *UTX* amplification was performed using the KAPATaq HotStart kit (KapaBiosystems). For all reactions, the following PCR protocol was used: 95°C for 10 min, (96°C for 15 sec, 57°C for 1 min, then 72°C for 1 min) for 40 cycles, then 72°C for 10 min. PCR products were purified and analyzed using the Applied Biosystems 3730XL DNA Analyzer.
MISEQ next-generation sequencing of *EZH2, SUZ12* and *EED* in the 35 human T-ALL patient samples, Sanger sequencing of *Utx, Ezh2, Suz12* and *Eed* in the MOHITO cell line, and Sanger sequencing of *UTX, EZH2, SUZ12* and *EED* on human T-ALL cell lines was performed at the Geoffrey Beene Translational Oncology Core Facility at MSKCC.

Array Comparative Genomic Hybridization (array CGH)

T-ALL patient samples were profiled for copy number analysis on SurePrint G3 Human 4x180K CGH Microarrays (Agilent Technologies). In brief, patient and control genomic DNAs were labeled using random prime labeling with Cy3 and Cy5 dyes (Perkin Elmer), respectively. Next, hybridization was performed according to the manufacturer's instructions (Agilent Technologies) followed by data-analysis using the in-house developed analysis tool arrayCGHbase (37).

SNP genotyping

Genotyping and allelic expression analysis of SNPs rs181547731 and rs20539 located in the 3' UTR and exon 20 of *UTX* respectively was performed in both genomic DNA (gDNA) and cDNA samples of 3 female T-ALL patients. The standard PCR and sequencing protocols were used as described above. Primer sequences are listed in Table S6.

Real-Time quantitative Polymerase Chain Reaction (qPCR)

RNA isolation of human T-ALL patient samples, normal T-cell populations, MOHITO samples and mouse leukemia samples were performed using the miRNeasy mini kit with DNA digestion on-column (Qiagen). Next, RNA concentration was measured on the NanoDrop 1000 Spectrophotometer followed by RNA quality assessment using the Experion Automated Electrophoresis System according to the manufacturer's instructions (Bio-rad). After quality assessment, complementary DNA (cDNA) synthesis was performed using the iScript cDNA Synthesis Kit (Bio-rad) followed by qPCR analysis. The qPCR reaction was performed using the LightCycler 480 (Roche) and qPCR data was analysed by the ΔΔCt method using the in-house developed qPCR analysis program qBasePlus (Biogazelle). Primers used to measure the expression of the genes of interest and reference genes are provided in Table S7.

Interleukin depletion assay

Short hairpin RNAs (shRNAs) were designed using the online program Designer of Small Interfering RNA (DSIR) followed by cloning into the retroviral MLS vector backbone, which also encodes for GFP co-expression. Next, the interleukin (IL-2/IL-7) dependent MOHITO cell line was transduced with shRNAs against Suz12 and Utx, and GFP percentage was evaluated using the GUAVA Flow Cytometer (Millipore). Subsequently, MOHITO cells were depleted of IL-2 and IL-7 until less than 10% of viable cells were detected followed by rescue through supplementing IL-2 and IL-7 back in the media. After each round of interleukin depletion, the GFP percentage was measured. The sequences of the shRNAs are listed in Table S8.

T-ALL mouse model

Fetal liver cells were isolated at embryonic day 13-14 followed by retroviral transduction of shRNAs or empty control labeled with GFP (MLS backbone) and *NOTCH1* labeled with mCherry (MIG backbone) (20). Next, the transduced fetal liver cells were tail vein injected after lethal irradiation of mouse recipients. Subsequently, mouse recipients were monitored for leukemia onset by analysis of lymphoblast counts in blood smears and by physical appearance. By the time of leukemia formation, various tissues including spleen, lungs, liver, kidney and lymph nodes were fixed for histological evaluation. Furthermore, the lymphoblasts from spleen and thymus were mashed to single-cell suspensions and frozen in 10% DMSO. Survival data was analyzed using the Kaplan-Meier method and statistical significance was calculated using the log-rank (Mantel-Cox) test.

Immunophenotypic analysis

Surface marker analysis of murine tumor cells was performed using a BD LSR II flow cytometer with monoclonal antibodies CD3-APC (BD Biosciences), CD8a-PECY7 (eBioscience) and CD4-biotin (Pharmingen). Data were analyzed with FACSDiva 6.1.2 software (BD Biosciences) and compensations were set using OneComp eBeads (eBioscience).

Histology

Histological analysis including Hematoxylin & Eosin (H&E) staining, Ki67 staining, H3K27me3 staining and Terminal deoxynucleotidyl transferase dUTP nick end labeling (TUNEL) assay of the different mouse leukemias was performed at the Laboratory of Comparative Pathology of MSKCC.

Western Blotting

Cells were lysed using a lysis buffer containing 2% SDS, 62.5 mM Tris pH 6.8, 10% glycerol, 5% β-mercaptoethanol, supplemented with EDTA free protease inhibitor cocktail (Roche). Denaturated samples were loaded on 10% or 7.5% gels (1h15min, 250V) (Bio-rad) for electrophoresis, followed by immunoblotting on PVDF membranes using a wet blotting system (1h, 250V) (Bio-rad). Membranes were incubated with primary and secondary antibody dilutions in 5% milk/TBST solutions, developed using SuperSignal West Dura Chemiluminescent Substrate (Pierce) and visualised on ChemiDoc-It imaging system 500 (UVP). Following antibodies were used: Utx (155 kDa, A302-374A, Bethyl Laboratories), Suz12 (83 kDa, 3737, Cell Signaling), H3K27me3 (17 kDa, 9733, Cell Signaling), Ezh2 (95-100 kDA, 612666, BD Biosciences), tubulin (50 kDa, T5168, Sigma).

Gene expression arrays

From the mouse leukemia and MOHITO samples, RNA was isolated using the miRNeasy mini kit with DNA digestion on-column (Qiagen). RNA concentration was measured on the NanoDrop 1000 Spectrophotometer followed by RNA quality assessment by use of the Experion Automated Electrophoresis System according to the manufacturer's instructions (Bio-rad). Next, RNA samples were profiled for gene expression analysis on SurePrint G3 Mouse 8x60K Microarrays according to the manufacturer's instructions (Agilent Technologies). Normalisation of gene expression data was done by quantile normalisation using R. Background correction was done based on the dark corner probe group of the Agilent slides. Differential gene expression analysis was performed using fold change analysis and p-value calculation based on unpaired t-test. Biased gene set enrichment analysis (GSEA) was performed using a gene set consisting of differential probes between the Utx sh#1 and control murine leukemias, and evaluated against gene expression data of the Utx deficient MOHITO samples. Unbiased GSEA was executed against annotated gene sets of the Molecular Signatures Database (MSigDB).

ChIP-sequencing

Lymphoblasts from murine leukemias were cross-linked in 1% formaldehyde for 10 min on rotating platform in 37°C oven. Next, 2.5M of glycine (0.122M final concentration) was added for 5 min at 37°C to quench the cross-linking reaction. The cells were subsequently pelleted at 4°C for 5 min at 1750 rpm followed by three washing steps in cold PBS. The final pellet was stored at -80°C. Following H3K27me3 ChIP-procedure was performed as previously described (Beguelin et al. Cancer Cell 2013) (38). H3K27me3 ChIP-seq libraries were prepared using the Illumina ChIP-Seq sample kits based on the manufacturer. Libraries were validated using the Agilent Technologies 2100 Bioanalyzer and 8-10pM was sequenced on HiSeq2000 sequencer. The raw data were aligned to mm9 genome using ELAND. Reads were normalizing for total ChIP-seq reads and quantified in 1 kb bins genome-wide. The enriched regions were identified as consecutive bins with read counts greater than 1 standard deviation of the genome-wide mean.

Cell viability assay

Murine and human T-ALL cell lines were treated with 3-Deazaneplanocin A hydrochloride (DZNep, Sigma) using a dilution series ranging from 50 nM to 100 µM. After 24 hours, cell viability was measured using the luminescence detection kit CellTiter Glo Cell Viability Assay (Promega).

ACKNOWLEDGEMENTS

We would like to thank the members of the Wendel lab and the members of the Speleman lab for experimental support and fruitful suggestions/ discussions during this research project; and Aline Eggermont for excellent technical assistance. The Geoffrey Beene Translational Oncology Core Facility at MSKCC for the sequencing support and the Flow Cytometry Facility at MSKCC for cell sorting assistance. The Memorial Sloan Kettering (MSK) animal facility and Research Animal Resource Center (RARC) for assistance with mouse experiments and the Laboratory of Comparative Pathology for histological analysis.

AUTHOR'S CONTRIBUTIONS

J.V.d.M. performed analysis of genomic data in T-ALL patient samples and performed *in vitro* and *in vivo* experiments. K.M., V.S., K.D., F.M., P.R. and B.V. assisted with *in vitro* and *in vivo* experiments. F.F and A.M. performed and supervised ChIP-sequencing experiments and data analysis. B.M. supervised array CGH and gene expression analysis. P.V., E.D., T.L., B.D.M., B.P., N.V.R. and Y.B. collected primary T-ALL patient samples. T.T. supervised immunophenotypic analysis of mouse leukemias. P.V.V., H-G.W., F.S. and J.V.d.M. designed the experiments and wrote the manuscript.

REFERENCES

1. Goldberg JM, Silverman LB, Levy DE, Dalton VK, Gelber RD, Lehmann L, et al. Childhood T-cell acute lymphoblastic leukemia: the Dana-Farber Cancer Institute acute lymphoblastic leukemia consortium experience. Journal of clinical oncology : official journal of the American Society of Clinical Oncology. 2003;21:3616-22.
2. Van Vlierberghe P, Ferrando A. The molecular basis of T cell acute lymphoblastic leukemia. The Journal of clinical investigation. 2012;122:3398-406.
3. Ferrando AA, Neuberg DS, Staunton J, Loh ML, Huard C, Raimondi SC, et al. Gene expression signatures define novel oncogenic pathways in T cell acute lymphoblastic leukemia. Cancer cell. 2002;1:75-87.
4. Homminga I, Pieters R, Langerak AW, de Rooi JJ, Stubbs A, Verstegen M, et al. Integrated transcript and genome analyses reveal NKX2-1 and MEF2C as potential oncogenes in T cell acute lymphoblastic leukemia. Cancer cell. 2011;19:484-97.
5. Soulier J, Clappier E, Cayuela JM, Regnault A, Garcia-Peydro M, Dombret H, et al. HOXA genes are included in genetic and biologic networks defining human acute T-cell leukemia (T-ALL). Blood. 2005;106:274-86.
6. Weng AP, Ferrando AA, Lee W, Morris JPt, Silverman LB, Sanchez-Irizarry C, et al. Activating mutations of NOTCH1 in human T cell acute lymphoblastic leukemia. Science. 2004;306:269-71.
7. O'Neil J, Grim J, Strack P, Rao S, Tibbitts D, Winter C, et al. FBW7 mutations in leukemic cells mediate NOTCH pathway activation and resistance to gamma-secretase inhibitors. The Journal of experimental medicine. 2007;204:1813-24.
8. Thompson BJ, Buonamici S, Sulis ML, Palomero T, Vilimas T, Basso G, et al. The SCFFBW7 ubiquitin ligase complex as a tumor suppressor in T cell leukemia. The Journal of experimental medicine. 2007;204:1825-35.
9. Ntziachristos P, Tsirigos A, Van Vlierberghe P, Nedjic J, Trimarchi T, Flaherty MS, et al. Genetic inactivation of the polycomb repressive complex 2 in T cell acute lymphoblastic leukemia. Nature medicine. 2012;18:298-301.
10. Cao R, Wang L, Wang H, Xia L, Erdjument-Bromage H, Tempst P, et al. Role of histone H3 lysine 27 methylation in Polycomb-group silencing. Science. 2002;298:1039-43.
11. Zhang J, Ding L, Holmfeldt L, Wu G, Heatley SL, Payne-Turner D, et al. The genetic basis of early T-cell precursor acute lymphoblastic leukaemia. Nature. 2012;481:157-63.
12. Simon C, Chagraoui J, Krosl J, Gendron P, Wilhelm B, Lemieux S, et al. A key role for EZH2 and associated genes in mouse and human adult T-cell acute leukemia. Genes & development. 2012;26:651-6.
13. Agger K, Cloos PA, Christensen J, Pasini D, Rose S, Rappsilber J, et al. UTX and JMJD3 are histone H3K27 demethylases involved in HOX gene regulation and development. Nature. 2007;449:731-4.
14. Lan F, Bayliss PE, Rinn JL, Whetstine JR, Wang JK, Chen S, et al. A histone H3 lysine 27 demethylase regulates animal posterior development. Nature. 2007;449:689-94.
15. van Haaften G, Dalgliesh GL, Davies H, Chen L, Bignell G, Greenman C, et al. Somatic mutations of the histone H3K27 demethylase gene UTX in human cancer. Nature genetics. 2009;41:521-3.
16. Robinson G, Parker M, Kranenburg TA, Lu C, Chen X, Ding L, et al. Novel mutations target distinct subgroups of medulloblastoma. Nature. 2012;488:43-8.
17. Gui Y, Guo G, Huang Y, Hu X, Tang A, Gao S, et al. Frequent mutations of chromatin remodeling genes in transitional cell carcinoma of the bladder. Nature genetics. 2011;43:875-8.
18. Greenfield A, Carrel L, Pennisi D, Philippe C, Quaderi N, Siggers P, et al. The UTX gene escapes X inactivation in mice and humans. Human molecular genetics. 1998;7:737-42.

19. Kleppe M, Mentens N, Tousseyn T, Wlodarska I, Cools J. MOHITO, a novel mouse cytokine-dependent T-cell line, enables studies of oncogenic signaling in the T-cell context. Haematologica. 2011;96:779-83.
20. Pear WS, Aster JC, Scott ML, Hasserjian RP, Soffer B, Sklar J, et al. Exclusive development of T cell neoplasms in mice transplanted with bone marrow expressing activated Notch alleles. The Journal of experimental medicine. 1996;183:2283-91.
21. Balgobind BV, Van Vlierberghe P, van den Ouweland AM, Beverloo HB, Terlouw-Kromosoeto JN, van Wering ER, et al. Leukemia-associated NF1 inactivation in patients with pediatric T-ALL and AML lacking evidence for neurofibromatosis. Blood. 2008;111:4322-8.
22. Chen Q, Yang CY, Tsan JT, Xia Y, Ragab AH, Peiper SC, et al. Coding sequences of the tal-1 gene are disrupted by chromosome translocation in human T cell leukemia. The Journal of experimental medicine. 1990;172:1403-8.
23. Subramanian A, Tamayo P, Mootha VK, Mukherjee S, Ebert BL, Gillette MA, et al. Gene set enrichment analysis: a knowledge-based approach for interpreting genome-wide expression profiles. Proceedings of the National Academy of Sciences of the United States of America. 2005;102:15545-50.
24. Lee MS, Hanspers K, Barker CS, Korn AP, McCune JM. Gene expression profiles during human CD4+ T cell differentiation. International immunology. 2004;16:1109-24.
25. Kanno M, Hasegawa M, Ishida A, Isono K, Taniguchi M. mel-18, a Polycomb group-related mammalian gene, encodes a transcriptional negative regulator with tumor suppressive activity. The EMBO journal. 1995;14:5672-8.
26. Johnson DT, Luong R, Lee SH, Peng Y, Shaltouki A, Lee JT, et al. Deletion of leucine zipper tumor suppressor 2 (Lzts2) increases susceptibility to tumor development. The Journal of biological chemistry. 2013;288:3727-38.
27. Yajnik V, Paulding C, Sordella R, McClatchey AI, Saito M, Wahrer DC, et al. DOCK4, a GTPase activator, is disrupted during tumorigenesis. Cell. 2003;112:673-84.
28. Lezon-Geyda K, Najfeld V, Johnson EM. Deletions of PURA, at 5q31, and PURB, at 7p13, in myelodysplastic syndrome and progression to acute myelogenous leukemia. Leukemia. 2001;15:954-62.
29. Tarpey PS, Behjati S, Cooke SL, Van Loo P, Wedge DC, Pillay N, et al. Frequent mutation of the major cartilage collagen gene COL2A1 in chondrosarcoma. Nature genetics. 2013;45:923-6.
30. Kroeger H, Jelinek J, Estecio MR, He R, Kondo K, Chung W, et al. Aberrant CpG island methylation in acute myeloid leukemia is accentuated at relapse. Blood. 2008;112:1366-73.
31. Tan J, Yang X, Zhuang L, Jiang X, Chen W, Lee PL, et al. Pharmacologic disruption of Polycomb-repressive complex 2-mediated gene repression selectively induces apoptosis in cancer cells. Genes & development. 2007;21:1050-63.
32. Miyake N, Mizuno S, Okamoto N, Ohashi H, Shiina M, Ogata K, et al. KDM6A point mutations cause Kabuki syndrome. Human mutation. 2013;34:108-10.
33. Scherer S, Theile U, Beyer V, Ferrari R, Kreck C, Rister M. Patient with Kabuki syndrome and acute leukemia. American journal of medical genetics Part A. 2003;122A:76-9.
34. Van Vlierberghe P, Palomero T, Khiabanian H, Van der Meulen J, Castillo M, Van Roy N, et al. PHF6 mutations in T-cell acute lymphoblastic leukemia. Nature genetics. 2010;42:338-42.
35. De Keersmaecker K, Atak ZK, Li N, Vicente C, Patchett S, Girardi T, et al. Exome sequencing identifies mutation in CNOT3 and ribosomal genes RPL5 and RPL10 in T-cell acute lymphoblastic leukemia. Nature genetics. 2013;45:186-90.
36. Morin RD, Johnson NA, Severson TM, Mungall AJ, An J, Goya R, et al. Somatic mutations altering EZH2 (Tyr641) in follicular and diffuse large B-cell lymphomas of germinal-center origin. Nature genetics. 2010;42:181-5.

37. Menten B, Pattyn F, De Preter K, Robbrecht P, Michels E, Buysse K, et al. arrayCGHbase: an analysis platform for comparative genomic hybridization microarrays. BMC bioinformatics. 2005;6:124.
38. Beguelin W, Popovic R, Teater M, Jiang Y, Bunting KL, Rosen M, et al. EZH2 is required for germinal center formation and somatic EZH2 mutations promote lymphoid transformation. Cancer cell. 2013;23:677-92.

FIGURE LEGENDS

Figure 1. *UTX* mutations in human T-ALL

A, DNA sequencing chromatogram showing a *UTX* mutation in the gDNA of a male primary T-ALL patient sample. The mutation is absent in remission material of the same patient. **B**, graphical representation of the localization of genetic lesions in the UTX protein structure (TPR = tetratricopeptide repeat, JmjC = Jumonji C). In-frame deletion/insertion mutations are depicted in orange circles, frameshift mutations in blue circles. **C**, genotyping and allelic expression analysis of SNP rs181547731 in gDNA and cDNA derived from female T-ALL lymphoblasts. **D**, graphical representation of the different mutations (depicted by dark orange rectangles) and deletions (depicted by light orange rectangles) present in a set of T-ALL oncogenes and tumor suppressor genes in 35 primary T-ALL patient samples. The different T-ALL subgroups include TAL-LMO, TLX3, TLX1, HOXA and patients for which the subgroup is unknown. The age subgroups include children (age ≤ 15 years, depicted in dark red rectangles) and adults (age > 15 years, depicted in light red rectangles). Male and female T-ALL patient samples are presented in dark blue and light blue rectangles, respectively.

Figure 2. Loss of Utx accelerates leukemia development in a NOTCH1-induced T-ALL mouse model

A, graphical illustration of NOTCH1-induced T-ALL mouse model. Fetal liver cells are partially transduced with vectors encoding NOTCH1 (ICN) (co-expressing mCherry) and the shRNA or empty vector control (co-expressing GFP) followed by tail vein injection in lethally irradiated mouse recipients and monitoring of leukemia onset. **B**, Kaplan-Meier curves and log-rank (mantel-cox) analysis show accelerated leukemia onset in Utx sh#1 (n=7, $p<0.0001$, blue), Utx sh#3 (n=4, $p=0.02$, green) and Suz12 sh#3 (n=9, $p=0.0002$, red) mice as compared to empty vector (n=14, black) mouse recipients. **C**, western blot analysis of Utx and Suz12 in a representative Utx sh#1 and Suz12 sh#3 mouse leukemia sample, respectively. Utx and Suz12 protein levels are quantified by Image J, normalized to tubulin levels, and compared to expression levels in control mice. **D**, H3K27me3 staining of the lymphoblasts on lymph node tissue of a representative Utx sh#1, Suz12 sh#3 and empty vector control mouse leukemia sample (20x magnification). **E**, immunophenotypical FACS analysis of Cd4 and Cd8 T-cell markers in the Utx, Suz12 and empty vector control mouse leukemias. A representative example of each subtype is depicted.

Figure 3. Gene networks regulated by Utx in T-ALL

A, differentially expressed genes (FC>1.5; $p<0.01$) between Utx knockdown and control murine leukemias are represented in a heat map. A selection of genes is shown in rows and each column represents one individual mouse leukemia sample. The scale bar shows color-coded differential expression from the mean in standard deviation units with red indicating higher levels and blue lower levels of expression. **B**, unbiased GSEA of gene expression signatures associated with murine leukemias driven by loss of *Utx* or NOTCH1 only vector controls. Gene sets involving early T-lymphocytes ($p<0.01$) are significantly enriched in Utx driven leukemias. **C**, H3K27me3 ChIP-seq profiles at 2 specific gene loci (*Lzts2* and *Pcgf2*) in murine leukemias driven by loss of *Utx* or NOTCH1 only vector controls. **D**, GSEA of transcripts significantly down regulated upon Utx knockdown in murine leukemias (FC>1.5, $p<0.05$, 252 probes) in gene expression signatures obtained from MOHITO samples driven by loss of *Utx.* Heatmap displays the TOP25 leading edge of this gene set in Utx driven MOHITO samples.

Figure 4. Human cell lines are more sensitive for H3K27me3 inhibition

A, genomic DNA sequencing chromatograms representing 2 missense mutations in the *EZH2* gene detected in the T-ALL cell line TALL-1. **B**, DNA sequencing chromatogram representing a nonsense mutation in the *UTX* gene detected in the human T-ALL cell line PF-382. **C**, western blot analysis of EZH2, H3K27me3 and tubulin in the human T-ALL cell lines PF-382, TALL-1 and PEER. Ezh2 protein and H3K27me3 levels are quantified by Image J, normalized to tubulin levels. **D**, luminescence-based viability assay after 24 hours (24h) of DZNep administration in 3 different T-ALL cell lines (TALL-1: black, PEER: red, PF-382: green) using a range of DZNep concentrations from 0 to 100µM. The experiment was done using 6 replicates, and repeated two times independently. The viability score for each concentration was significantly different between the 3 T-ALL cell lines (*Kruskal-Wallis test, $p<0.0001$). **E**, western blot analysis of H3K27me3 and tubulin 24h after DZNep administration (1000nM & 500nM) in 2 different T-ALL cell lines (PEER: red, PF-382: green). H3K27me3 levels are quantified by Image J, normalized to tubulin levels. DZNep treated samples are compared to expression levels in untreated samples. **F**, luminescence-based viability assay after 24h of DZNep administration in Utx knockdown and control MOHITO samples (vector: black, Utx sh#1: green). The experiment was done in fourfold (unpaired t-test: *$p<0.0001$). **G**, western blot analysis of H3K27me3 and tubulin 24h after DZNep administration (1000nM & 500nM) in Utx knockdown and control MOHITO samples (vector: black, Utx sh#1: green). H3K27me3 levels are quantified by Image J, normalized to tubulin levels. DZNep treated samples are compared to expression levels in untreated samples.

SUPPLEMENTARY FIGURE LEGENDS

Figure S1. *SUZ12* mutation and deletion in primary T-ALL patient samples
A, DNA sequencing chromatogram representing a *SUZ12* mutation in a male primary T-ALL patient. **B**, array CGH plot of leukemia DNA/control DNA ratios in a male primary T-ALL patient sample that harbors a deletion encompassing the *SUZ12* gene (deletion indicated with red line).

Figure S2. Knockdown of Utx augments the oncogenic activity in the murine T-ALL cell line MOHITO
A-B, western blot analysis of GFP sorted MOHITO knockdown samples containing 3 different hairpins against Utx (A) and Suz12 (B) compared to empty vector control. Blots were incubated with antibodies against Utx, Suz12 and tubulin. Expression levels were normalized to tubulin levels and compared to the vector control. **C**, graphical illustration of the interleukin depletion assay in the IL2-IL7 dependent MOHITO cell line. MOHITO cells are partially transduced with vectors encoding shRNA against Utx or Suz12 and co-expressing GFP, after which the GFP percentage is measured by FACS analysis before and after successive rounds of interleukin depletion. **D**, GFP percentage measured at Day 0, and after 1^{st} and 2^{nd} depletion rounds in Utx sh#1, Utx sh#2 and Utx sh#3 knockdown samples and controls. The depletion assay was repeated twice. The GFP enrichment was statistically significant after the 1^{st} depletion for Utx sh#1* and Utx sh#3** and after the 2^{nd} depletion for Utx sh#1*** compared to empty vector control respectively (unpaired t-test: *p=0.005, **p=0.049, ***p=0.008). **E**, GFP percentage measured at Day 0, and upon the 1^{st}, 2^{nd} and 3^{th} depletion round in Suz12 sh#3 knockdown samples and controls. The depletion assay was repeated twice. The GFP enrichment was statistically significant after the 2^{nd} and 3^{th} depletion for Suz12 sh#3 compared to empty vector control respectively (unpaired t-test: *p=0.0438, **p=0.029).

Figure S3. Aggressive leukemia phenotype in NOTCH1-induced T-ALL mouse model
A, representative images of H&E, TUNEL and Ki67 stainings of T-ALL lymphoblasts in spleen, kidney, lung and liver of an Utx sh#1 mouse leukemia (20x magnification). The pathologic appearance of Utx sh#1 driven leukemias, Suz12 sh#3 driven leukemias and empty vector controls is identical (not shown). **B**, gene expression analysis of Utx and Suz12 in a representative Utx sh#1 and Suz12 sh#3 mouse leukemia sample, respectively. The expression levels are compared to levels in control mice. Vector: black, shRNA: green.

Figure S4. Gene sets enriched in Utx knockdown driven murine leukemias
A-B, unbiased GSEA of gene expression signatures associated with murine leukemias driven by loss of *Utx* or NOTCH1 only vector controls. Gene sets involving early T-lymphocytes ($p<0.01$) and *LYL1* neighbouring genes ($p=0.02$) in T-AL are significantly enriched in Utx driven leukemias.

Figure S5. ChIP-seq profiles of H3K27me3 in Utx knockdown and vector control murine leukemias
H3K27me3 ChIP-seq profiles at 4 specific gene loci (*Dock4, Pura, Col2a1* and *Slc26a4*) in murine leukemias driven by loss of *Utx* or NOTCH1 only vector controls.

Figure 1

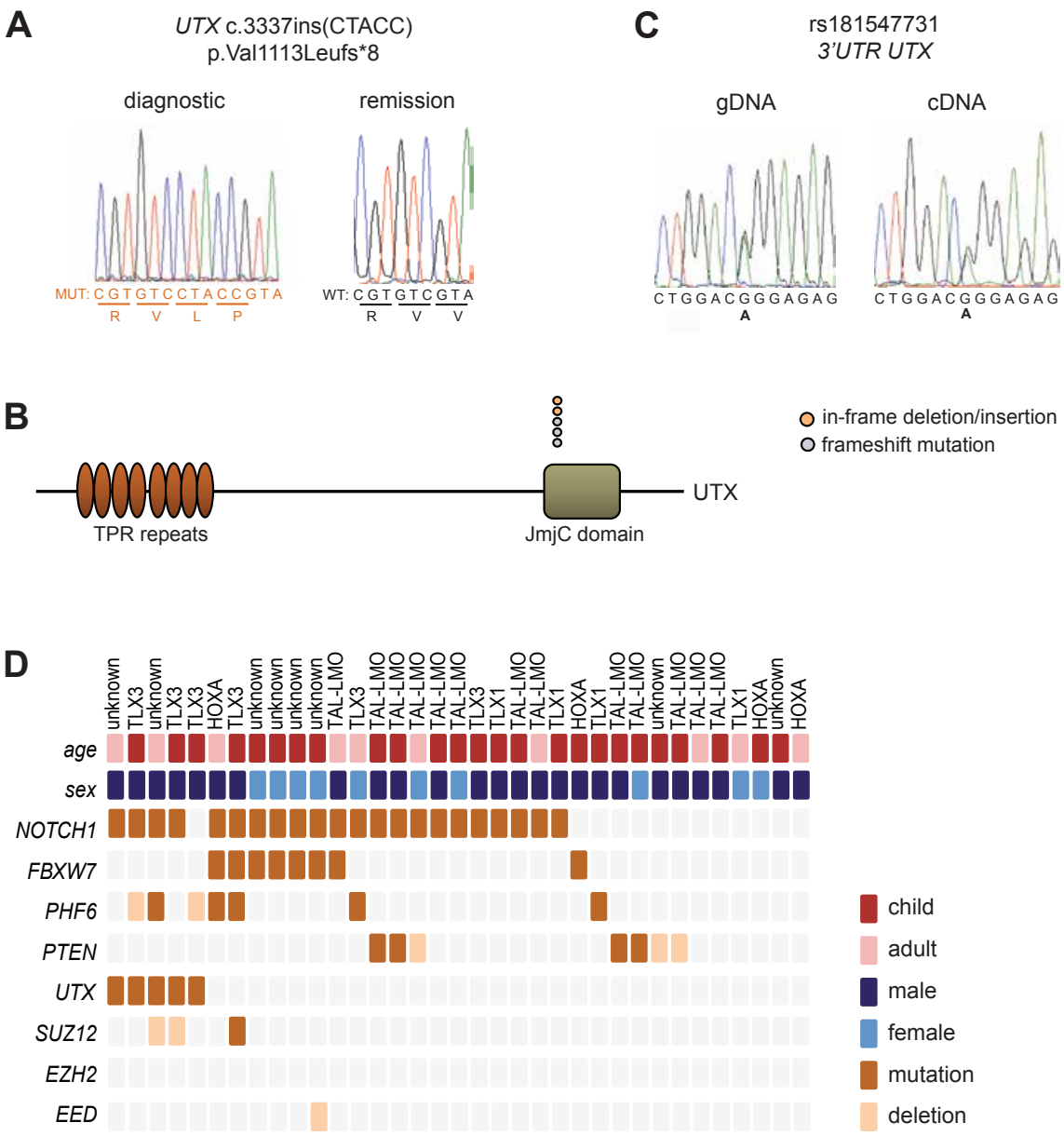
A
UTX c.3337ins(CTACC)
p.Val1113Leufs*8
diagnostic
remission
MUT: C G T G T C C T A C C G T A
R V L P
WT: C G T G T C G T A
R V V
C
rs181547731
3'UTR UTX
gDNA
cDNA
C T G G A C G G G A G A G
A
C T G G A C G G G A G A G
A
B
in-frame deletion/insertion
frameshift mutation
UTX
TPR repeats
JmjC domain
D
unknown
TLX3
unknown
TLX3
TLX3
HOXA
TLX3
unknown
unknown
unknown
unknown
TAL-LMO
TLX3
TAL-LMO
TAL-LMO
TAL-LMO
TAL-LMO
TLX3
TLX1
TAL-LMO
TAL-LMO
TLX1
HOXA
TLX1
TAL-LMO
TAL-LMO
unknown
TAL-LMO
TAL-LMO
TLX1
HOXA
unknown
HOXA
age
sex
NOTCH1
FBXW7
PHF6
PTEN
UTX
SUZ12
EZH2
EED
child
adult
male
female
mutation
deletion

Figure 2

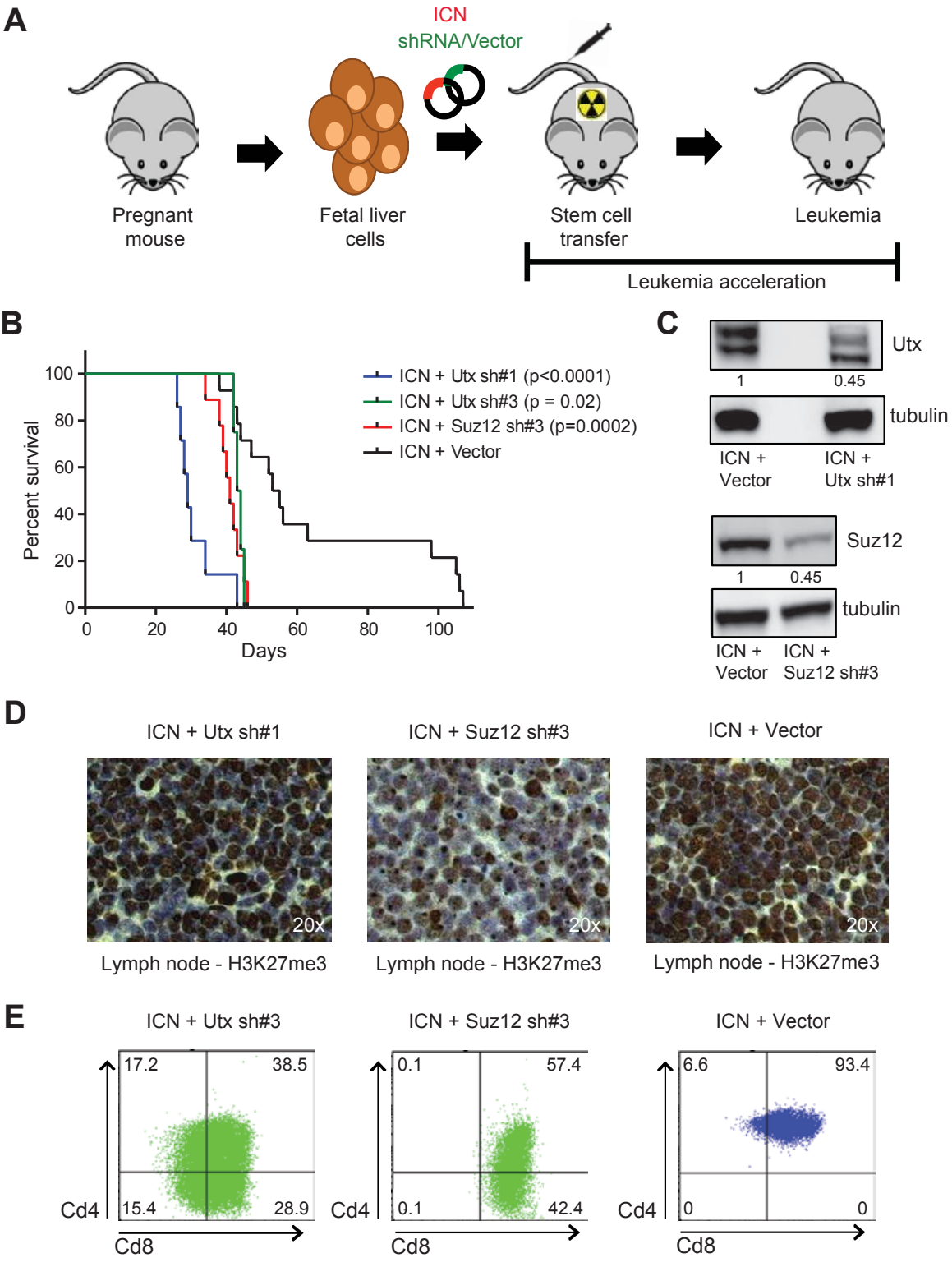
A
ICN
shRNA/Vector
Pregnant mouse
Fetal liver cells
Stem cell transfer
Leukemia
Leukemia acceleration
B
Percent survival
Days
ICN + Utx sh#1 (p<0.0001)
ICN + Utx sh#3 (p = 0.02)
ICN + Suz12 sh#3 (p=0.0002)
ICN + Vector
C
Utx
tubulin
ICN + Vector
ICN + Utx sh#1
Suz12
tubulin
ICN + Vector
ICN + Suz12 sh#3
D
ICN + Utx sh#1
ICN + Suz12 sh#3
ICN + Vector
20x
Lymph node - H3K27me3
E
ICN + Utx sh#3
ICN + Suz12 sh#3
ICN + Vector
Cd4
Cd8
17.2
38.5
15.4
28.9
0.1
57.4
0.1
42.4
6.6
93.4
0
0

Figure 3

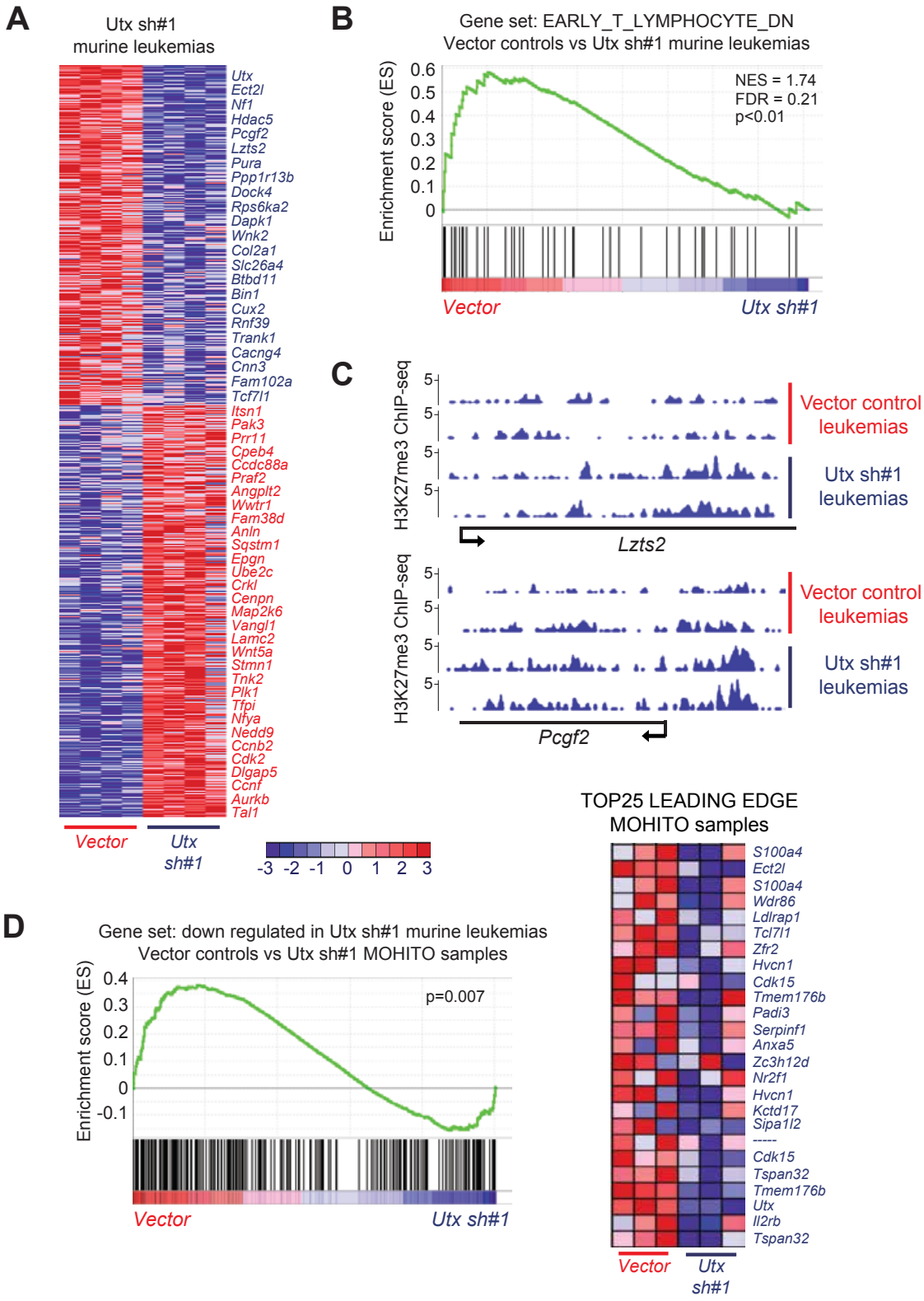
A
Utx sh#1
murine leukemias
Utx
Ect2l
Nf1
Hdac5
Pcgf2
Lzts2
Pura
Ppp1r13b
Dock4
Rps6ka2
Dapk1
Wnk2
Col2a1
Slc26a4
Btbd11
Bin1
Cux2
Rnf39
Trank1
Cacng4
Cnn3
Fam102a
Tcf7l1
Itsn1
Pak3
Prr11
Cpeb4
Ccdc88a
Praf2
Angplt2
Wwtr1
Fam38d
Anln
Sqstm1
Epgn
Ube2c
Crkl
Cenpn
Map2k6
Vangl1
Lamc2
Wnt5a
Stmn1
Tnk2
Plk1
Tfpi
Nfya
Nedd9
Ccnb2
Cdk2
Dlgap5
Ccnf
Aurkb
Tal1
Vector
Utx sh#1
-3 -2 -1 0 1 2 3
B
Gene set: EARLY_T_LYMPHOCYTE_DN
Vector controls vs Utx sh#1 murine leukemias
Enrichment score (ES)
0.6
0.5
0.4
0.3
0.2
0.1
0
NES = 1.74
FDR = 0.21
p<0.01
Vector
Utx sh#1
C
H3K27me3 ChIP-seq
Vector control leukemias
Utx sh#1 leukemias
Lzts2
H3K27me3 ChIP-seq
Vector control leukemias
Utx sh#1 leukemias
Pcgf2
D
Gene set: down regulated in Utx sh#1 murine leukemias
Vector controls vs Utx sh#1 MOHITO samples
Enrichment score (ES)
0.4
0.3
0.2
0.1
0
-0.1
p=0.007
Vector
Utx sh#1
TOP25 LEADING EDGE
MOHITO samples
S100a4
Ect2l
S100a4
Wdr86
Ldlrap1
Tcl7l1
Zfr2
Hvcn1
Cdk15
Tmem176b
Padi3
Serpinf1
Anxa5
Zc3h12d
Nr2f1
Hvcn1
Kctd17
Sipa1l2

Cdk15
Tspan32
Tmem176b
Utx
Il2rb
Tspan32
Vector
Utx sh#1

Figure 4

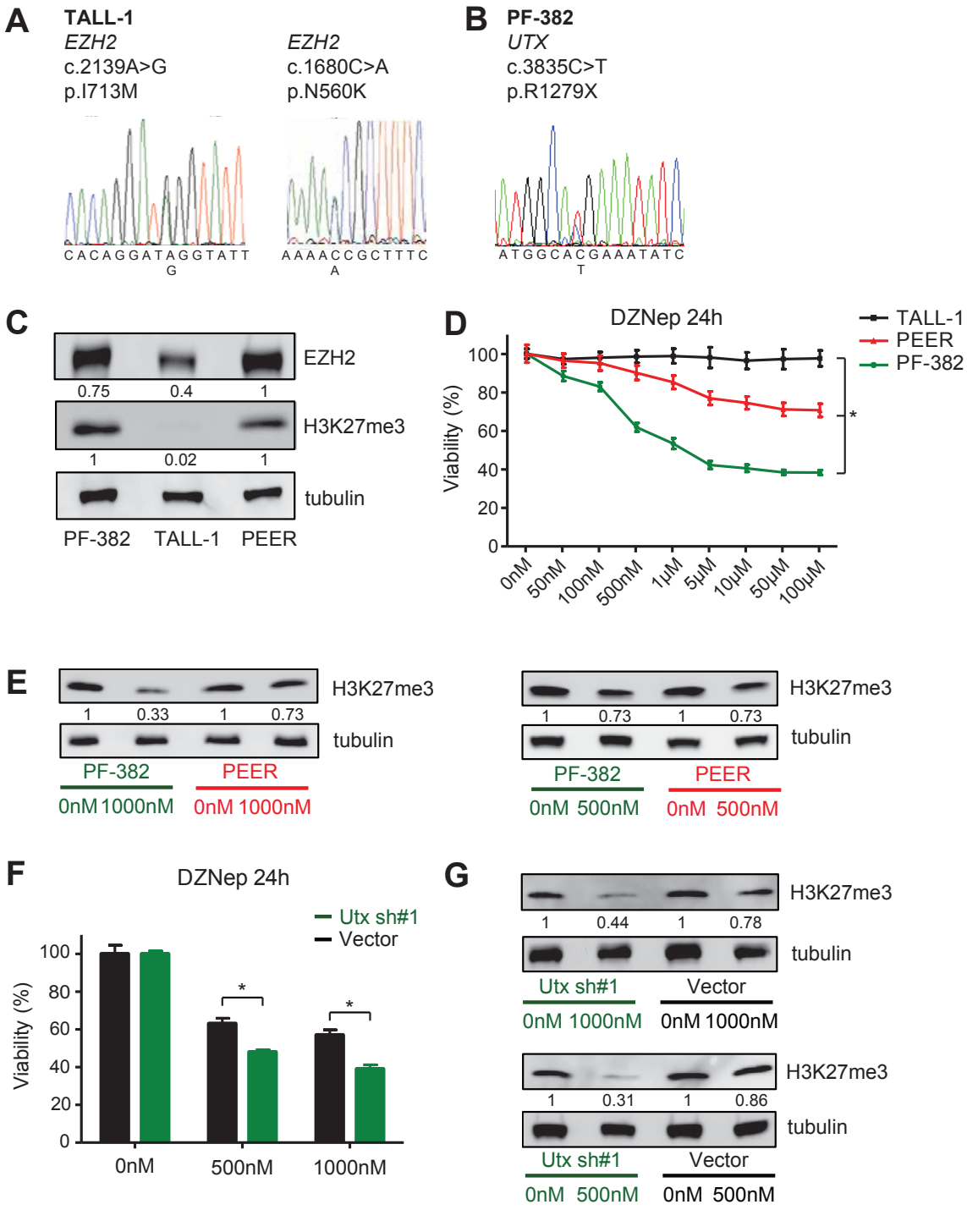
A
TALL-1
EZH2
c.2139A>G
p.I713M
EZH2
c.1680C>A
p.N560K
CACAGGATAGGTATT
G
AAAACCGCTTTC
A
B
PF-382
UTX
c.3835C>T
p.R1279X
ATGGCACGAAATATC
T
C
EZH2
0.75 0.4 1
H3K27me3
1 0.02 1
tubulin
PF-382 TALL-1 PEER
D
DZNep 24h
TALL-1
PEER
PF-382
Viability (%)
100
80
60
40
20
0
*
0nM 50nM 100nM 500nM 1μM 5μM 10μM 50μM 100μM
E
H3K27me3
1 0.33 1 0.73
tubulin
PF-382 PEER
0nM 1000nM 0nM 1000nM
H3K27me3
1 0.73 1 0.73
tubulin
PF-382 PEER
0nM 500nM 0nM 500nM
F
DZNep 24h
Utx sh#1
Vector
Viability (%)
100
80
60
40
20
0
*
*
0nM 500nM 1000nM
G
H3K27me3
1 0.44 1 0.78
tubulin
Utx sh#1 Vector
0nM 1000nM 0nM 1000nM
H3K27me3
1 0.31 1 0.86
tubulin
Utx sh#1 Vector
0nM 500nM 0nM 500nM

Figure S1

A

SUZ12
c.1214C>G
p.S404*

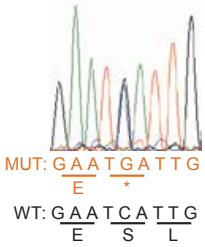

B

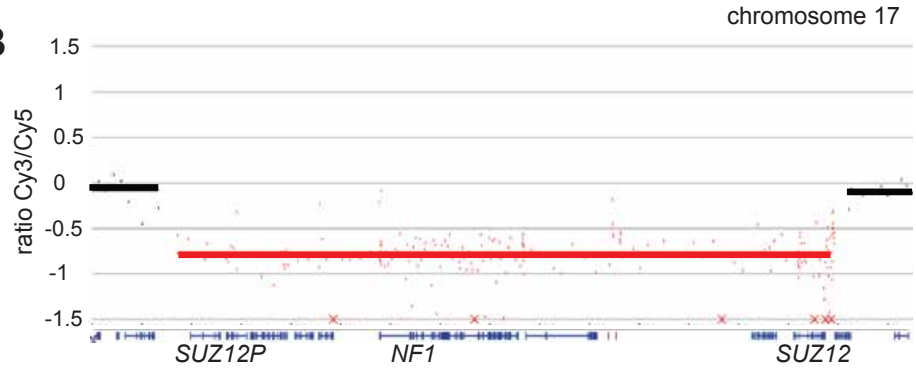

Figure S2

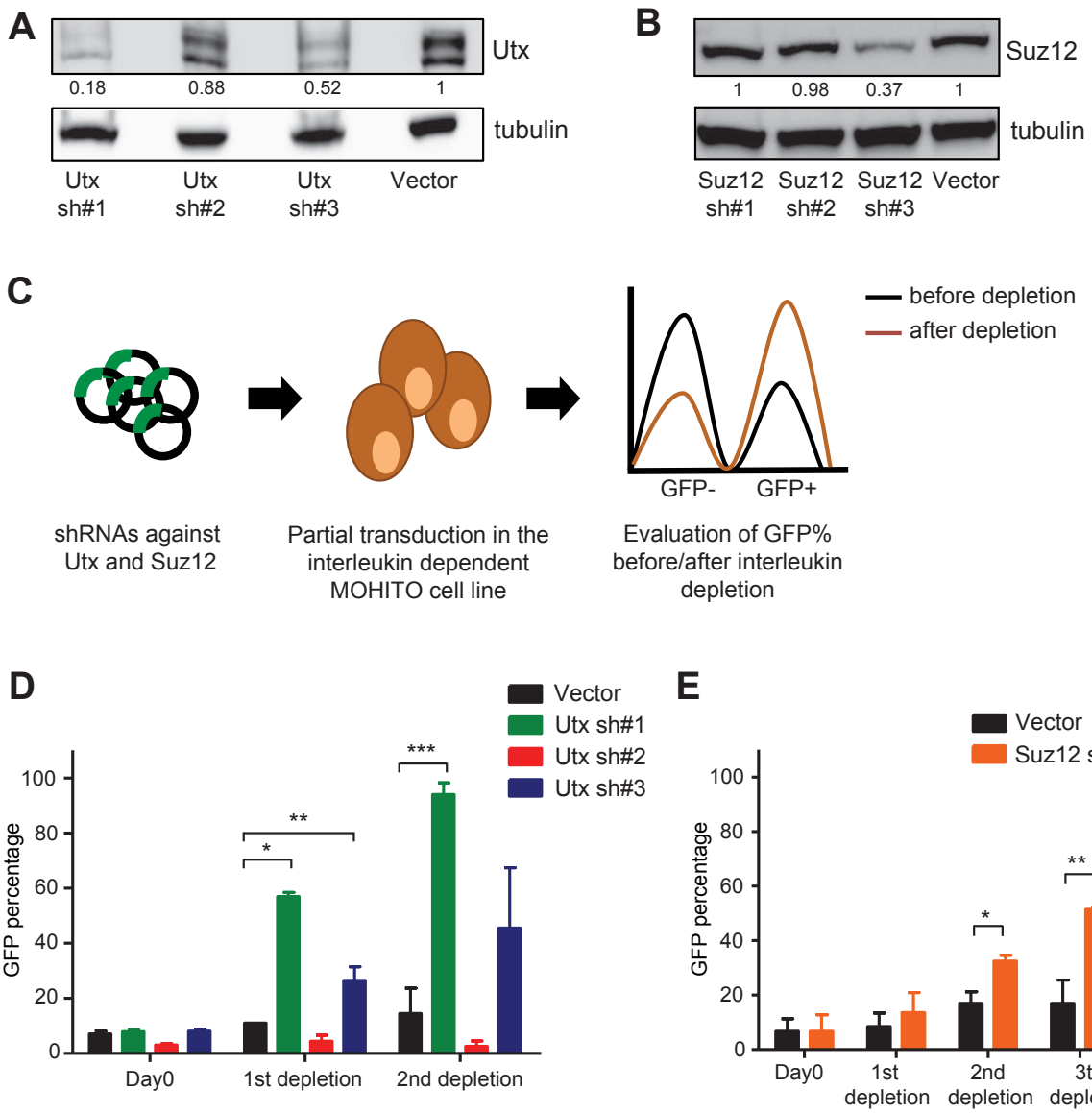
A
Utx
0.18
0.88
0.52
1
tubulin
Utx sh#1
Utx sh#2
Utx sh#3
Vector
B
Suz12
1
0.98
0.37
1
tubulin
Suz12 sh#1
Suz12 sh#2
Suz12 sh#3
Vector
C
before depletion
after depletion
GFP-
GFP+
shRNAs against Utx and Suz12
Partial transduction in the interleukin dependent MOHITO cell line
Evaluation of GFP% before/after interleukin depletion
D
Vector
Utx sh#1
Utx sh#2
Utx sh#3
GFP percentage
100
80
60
40
20
0
*
**
***
Day0
1st depletion
2nd depletion
E
Vector
Suz12 sh#3
GFP percentage
100
80
60
40
20
0
*
**
Day0
1st depletion
2nd depletion
3th depletion

Figure S3

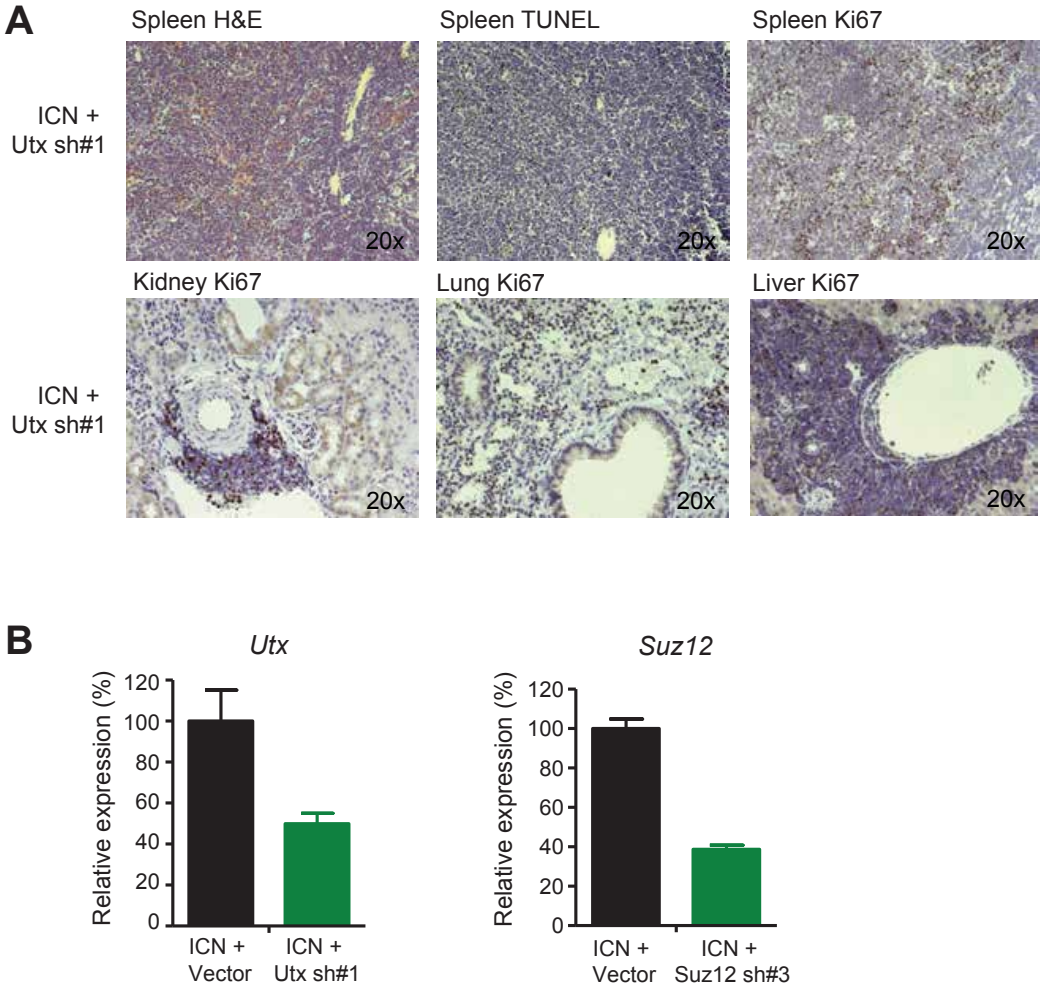
A
Spleen H&E
Spleen TUNEL
Spleen Ki67
ICN +
Utx sh#1
20x
20x
20x
Kidney Ki67
Lung Ki67
Liver Ki67
ICN +
Utx sh#1
20x
20x
20x
B
Utx
Relative expression (%)
120
100
80
60
40
20
0
ICN +
Vector
ICN +
Utx sh#1
Suz12
Relative expression (%)
120
100
80
60
40
20
0
ICN +
Vector
ICN +
Suz12 sh#3

Figure S4

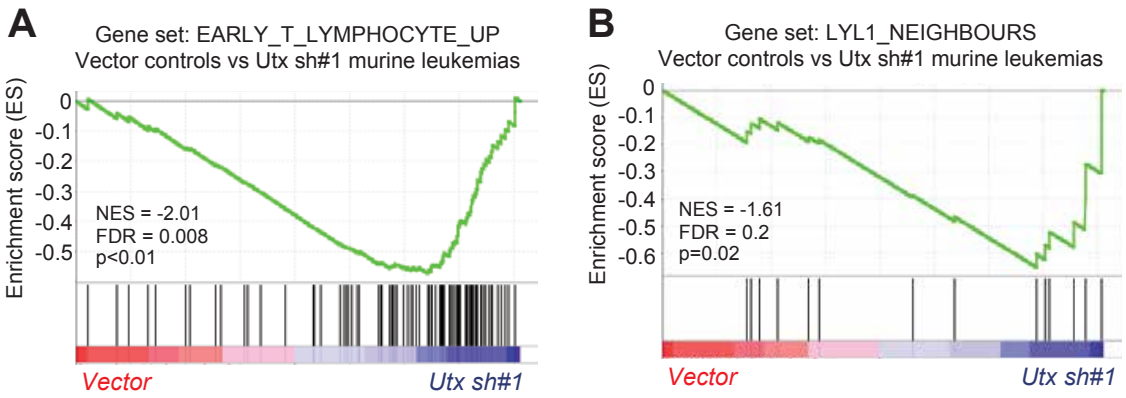
A
Gene set: EARLY_T_LYMPHOCYTE_UP
Vector controls vs Utx sh#1 murine leukemias
Enrichment score (ES)
0
-0.1
-0.2
-0.3
-0.4
-0.5
NES = -2.01
FDR = 0.008
p<0.01
Vector
Utx sh#1
B
Gene set: LYL1_NEIGHBOURS
Vector controls vs Utx sh#1 murine leukemias
Enrichment score (ES)
0
-0.1
-0.2
-0.3
-0.4
-0.5
-0.6
NES = -1.61
FDR = 0.2
p=0.02
Vector
Utx sh#1

Figure S5

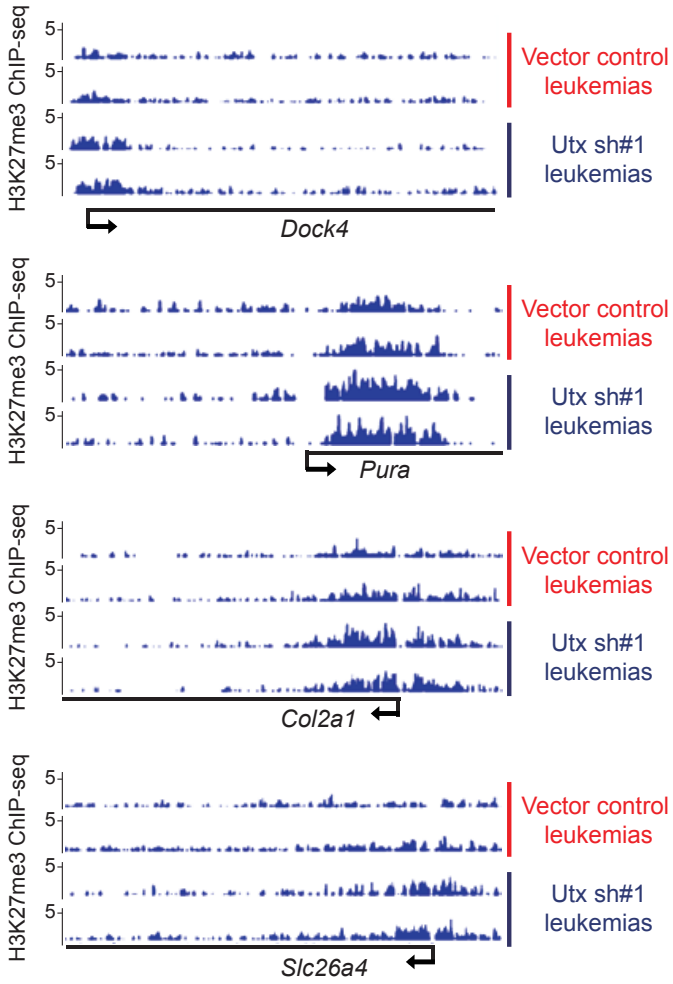
H3K27me3 ChIP-seq
5
5
5
5
Vector control leukemias
Utx sh#1 leukemias
Dock4
H3K27me3 ChIP-seq
5
5
5
5
Vector control leukemias
Utx sh#1 leukemias
Pura
H3K27me3 ChIP-seq
5
5
5
5
Vector control leukemias
Utx sh#1 leukemias
Col2a1
H3K27me3 ChIP-seq
5
5
5
5
Vector control leukemias
Utx sh#1 leukemias
Slc26a4

SUPPLEMENTARY TABLES

Table S1. *UTX* mutations in primary T-ALL patient samples

***UTX* mutation (DNA)**	**UTX mutation (protein)**	**Remission**
c.3337G>TCC	p.Val1113SerfsX7	Yes, mutation absent
c.3337ins(CTACC)	p.Val1113LeufsX8	Yes, mutation absent
c.3338ins(TGTGGGCCCG)	p.Val1113Val, Ser1114TrpfsX40	NA
c.[3331delC;3331_3332insTGGG]	p.[Arg1111Trp; Arg1111_Val1112insGly]	NA
c.[3337_3342delGTATCA; 3337_3343insTTGCGGCATCTGTTTCAA]	p.[Val1113_Ser1114del;Val1112_Ala1115 insLeuArgHisLeuPheGln]	NA

Table S2. Immunophenotyping of Utx sh#1 mice

Utx sh#1	**CD8**	**CD4**	**CD3**
Utx sh#1_1	52.7	1.6	3.5
Utx sh#1_2	36.6	30.5	1.1
Utx sh#1_3	99.6	49.3	6.5
Utx sh#1_4	88.2	66.8	8.5
Utx sh#1_5	42.1	80.2	28.3
mean	**63.8**	**45.7**	**9.6**
sd	28.3	30.9	10.8

Table S3. Immunophenotyping of Utx sh#3 mice

Utx sh#3	**CD8**	**CD4**	**CD3**
Utx sh#3_1	18.2	17.5	27
Utx sh#3_2	67.3	55.6	17.5
Utx sh#3_3	67.1	58.1	6.8
Utx sh#3_4	99.9	87.7	38.7
mean	**63.1**	**54.7**	**22.5**
sd	33.7	28.8	13.6

Table S4. Immunophenotyping of Suz12 sh#3 mice

Suz12 sh#3	**CD8**	**CD4**	**CD3**
Suz12 sh#3_1	99.9	55.6	9.2
Suz12 sh#3_2	99.9	21.5	3.7
Suz12 sh#3_3	98.5	77	5.2
Suz12 sh#3_4	100	38.9	9.7
Suz12 sh#3_5	99.8	80.8	6
Suz12 sh#3_6	100	86.5	5.4
Suz12 sh#3_7	99.8	57.4	7.4
mean	**99.7**	**59.7**	**6.7**
sd	0.5	23.7	2.2

Table S5. Immunophenotyping of empty vector control mice

Control	**CD8**	**CD4**	**CD3**
Control_1	99.8	75.2	7.5
Control_2	74.9	15.9	41.6
Control_3	63	8.4	16.7
Control_4	99.7	99.7	5.4
Control_5	93.4	100	27.9
Control_6	99.4	93.2	44.4
Control_7	99.4	88.3	0.6

Control_8	99.6	57.2	3.3
Control_9	98.6	93.5	4.6
mean	**92.0**	**70.2**	**16.9**
sd	13.5	35.6	17.0

Table S6. Primers used for Sanger sequencing and SNP analysis

Primer name	Forward primer sequence	Reverse primer sequence
NOTCH1 exon 26	AGGAAGGCGGCCTGAGCGTGT	AGAGTTGCGGGGATTGACCGT
NOTCH1 exon 27	GTGGCGTCATGGGCCTCA	GCACAAACAGCCAGCGTGT
NOTCH1 exon 28	GATCGGTGTCATGTGAAGT	TCCCGGTGAGGATGCTCGG
NOTCH1 exon 34a	CTTCCTCTGGTGATGGAACCT	CATCCCAGGCAGGTGGTTGA
NOTCH1 exon 34b	GCCCTCCCCGTTCCAGCAGTCT	GCCTGGCTCGGCTCTCCACTCA
NOTCH1 exon 34c	AGCCGCACCTTGGCGTGAGC	TGGTCGGCCCTGGCATCCAC
FBXW7 exon 7	TTTATGCCTTCATTTTTCTCTT	GGGGAAAAAAGCTAAGTTATG
FBXW7 exon 8	TTTTCCAGTGTCTGAGAACAT	CCCAAATTCACCAATAATAGA
FBXW7 exon 9	TAAACGTGGGTTTTTTTGTT	TCAGCAATTTGACAGTGATT
FBXW7 exon 10	CCTGGCATTACCTGTTTC	AGGCTCCATATTTCTCTTGA
FBXW7 exon 11	GGACATGGGTTTCTAAATATGTA	CTGCACCACTGAGAACAAG
PTEN exon 1	AGCTTCTGCCATCTCTCTC	TTTCGCATCCGTCTACTC
PTEN exon 2	ACATTGACCACCTTTTATTACTC	GGTAAGCCAAAAAATGATTATAG
PTEN exon 3	ATGGTGGCTTTTTGTTTGT	GCTCTTGGACTTCTTGACTTA
PTEN exon 4	TCAGGCAATGTTTGTTAGTATT	ATCGGGTTTAAGTTATACAACATA
PTEN exon 5	TTGTATGCAACATTTCTAAAGTT	ATCTGTTTTCCAATAAATTCTCA
PTEN exon 6	ACGACCCAGTTACCATAGC	TAGCCCAATGAGTTGAACA
PTEN exon 7	AATCGTTTTTGACAGTTTGAC	TCACCAATGCCAGAGTAAG
PTEN exon 8	GATTGCCTTATAATAGTCTTTGTG	TTTTTGACGCTGTGTACATT
PTEN exon 9	GCCTCTTAAAGATCATGTTTG	GGTCCATTTTCAGTTTATTCA
PHF6 exon 2	TTTCTTGGGGCTTAGAGTG	AAATGGCATAGCATTAGTGA
PHF6 exon 3	GCTATGCCATTTTTACTAGAAA	GCTGGCTCAGAGAAAAAAAA
PHF6 exon 4	CCCCAGAAGAATTTTATTCC	CAAAAGCCCAAAGAAAGTAT
PHF6 exon 5	AAAGGGTGTTTTTGATAAGA	AAACGTGGCTAAATGATGTA
PHF6 exon 6	GGGTGGCTTTATTGAACAT	GCTATCGGTATTTCAAGCTTA
PHF6 exon 7	TTGGATTCTTACTTTTGTTGC	GGGGAAATTTTTTGGTTAC
PHF6 exon 8	TTTTCCTGCATTTTTCTTCT	GCAAATGCCTTGAAATGTAT
PHF6 exon 9	GAGGGCTTATCAAAGTATGG	AGGAAAATGCCAATTGTAGT
PHF6 exon 10	AGCCTCATCCACTAATGTTG	GAGTTGGGCAGTAAAAAGTT
UTX exon 1	ATGTGACCCTACAGCCGAAA	ATCTCACGAACCCAAAGAGG
UTX exon 2	CTCGGTTTGGCGCTCTTC	GAAAAGAGCGATTTCGCAAG
UTX exon 3	AATATTGACTTCTTAGGTGATCGAA	TCTATATCAAACTGGGTCACTTTCT
UTX exon 4	TATCTACTGGGAGGTGGGTGTG	CAGCCTTCTTTTACTCCCAGG
UTX exon 5	GTTGATTGGAATCTGTGCCA	CCAAAAAGCTTTCTAATCTAAGCC
UTX exon 6	CATATGCCCCTTTTCAATTTT	TGTTACCATGGAAGTCTTAGCA
UTX exon 7	GGCTAGTGTATTTTATTTGCATAGCAT	CCAGCAAAACCTGTTTTTAATCC
UTX exon 8	GACAGAAATTTCATTTGATAATGACC	GGAATTAATTTGTACACAGCAAGC
UTX exon 9	CAACTGTCTGATGTTAAAGAAACATTC	GGGTTAAATACTAGGGAGTAATTTTGA
UTX exon 10	ATGGCCAGAATTGGCAGT	GTCCTGCTAGACCAGATTATGCT
UTX exon 11	CAGCATGCTTTTTAGCACCT	GGCTGATTTTGCTGCTGATA
UTX exon 12	CAGATACATGGTGTTCAATAGGG	GGAAACAGATTATAGACATCAAAACA
UTX exon 13	GGTTTATATTCCGGTTACCCTGT	AGGTTCTAAGTTGGTACCCCAAA
UTX exon 14	AATGTTGGATCTAGTGGACAGTG	TTAATACTTGTTTGCTACCTCTACTCC
UTX exon 15	TGACCAGATAGTGGTTCTGAGTTT	AGCCCTAAAAACCTTGCCTC
UTX exon 16a	CACACATTCCCTAATTATACATCTTCA	AGTTGGTTTTTCCACGGCT
UTX exon 16b	GGCCAATGGACCCTTTTC	CCACTGTAAATTAATGGTGCATTTT
UTX exon 17a	AGGACTTGGGTCAAATTATCTTATACA	TCAACAAGGCAGAGAGCTGA
UTX exon 17b	TACCTCAGGTGGACAACAAGG	GCAGATCTGTTTTCATGGGG
UTX exon 17c	AACTCTGTTGCCTCTTCACCA	GGGCAGTAACAGCACAATCA

UTX exon 18	TGGACTTGTGCAAATGCCT	GCTGCTCAAAATTAGGGCAAT
UTX exon 19	TCACCCCATAAAATGCGTTA	CACAATTATGTAAACGGACCAAA
UTX exon 20	ATAGCTCAGGTTGTGCAGAGG	GAGACAACTGGAGAACACTTACAAA
UTX exon 21	TTTTTCAGTTGTATGGTGGAAAG	AATGACAATAAATGAAACAGAAGAGG
UTX exon 22	CCAGTTGTAGAACACTAAACTAGACTG	ATGACAATAAATGAAACAGAAGAGG
UTX exon 23	TTTTGTTGGGAAGTTTTCTTTGG	ATGAAAAGGGGAAAAATCTTAATCTG
UTX exon 24	TGAGCATTTGTAAGGTTTTGTTT	CTTTTCTATCTTCTTAATTCATGGGT
UTX exon 25	ATATACATACAGCAGATCTTTTTGCAC	TACTACGAATTACAATTCTATGCAAGG
UTX exon 26	GTTTTGAGGTTTTCAGAATTGATG	TGGGAAAGAAGCACAGGTCT
UTX exon 27	TCAGGCCTGCTGAGCATT	AATGGCTAAGCAACAAAATTGAA
UTX exon 28	AACCAGAGATCACTGTCCACAA	CTCACCCAGGAAAACTGAAAA
UTX exon 29	AGCAGGCTGTTGAACTTTTTG	AAGGGGGAAAAGACAGATGAA
3'UTR UTX SNP	TTCTGCACCACTGGTTTTTG	AGATGTTGCCAGTTTTGTCAGA
UTX exon 20 cDNA	GTGATGCTTTCTTTCCTCCA	CGATGTAGATTCACTATCTGAGTGG

Table S7. Primers used for qPCR

Primer name	**Forward primer sequence**	**Reverse primer sequence**
Utx mouse	ATCCCAGCTCAGCAGAAGTT	GGAGGAAAGAAAGCATCACG
Suz12 mouse	AGGCTGCCTCCATTTGAGA	TGGTTTCTCCTGTCCATCG
Gapdh mouse	CGGAGTCAACGGATTTGGTCGTAT	AGCCTTCTCCATGGTGGTGAAGAC
Tbp mouse	CCCCACAACTCTTCCATTCT	GCAGGAGTGATAGGGGTCAT
Ppia mouse	CAGACGCCACTGTCGCTTT	TGTCTTTGGAACTTTGTCTGCAA
Ubc mouse	GCAGATCTTTGTGAAGACCC	GAAGGTACGTCTGTCTTCCT

Table S8. shRNA sequences

Primer name	**Sequence**
Utx sh1 mouse	TTAAACTAGACTCATAGTCTG
Utx sh2 mouse	TAGGACTGCAAACAGCATCTG
Utx sh3 mouse	ATAACGTTCCACTGCTAACTT
Suz12 sh1 mouse	TTGATTGAAACATCTATCCTA
Suz12 sh2 mouse	TATTGGACAACTTACATCCTT
Suz12 sh3 mouse	TTGAACTTGTAACACAACTGA

2. MicroRNAs in T-cell acute lymphoblastic leukemia

PAPER 3
A cooperative microRNA – tumor suppressor gene network in acute T-cell lymphoblastic leukemia (T-ALL)

PAPER 4
MicroRNA-193b-3p acts as a tumor suppressor by targeting the *MYB* oncogene in T-cell acute lymphoblastic leukemia

PAPER 3

A cooperative microRNA – tumor suppressor gene network in acute T-cell lymphoblastic leukemia (T-ALL)

Van der Meulen J*, Mavrakis KJ*, Wolfe AL, Liu X, Mets E, Taghon T, Khan AA, Setty M, Rondou P, Vandenberghe P, Delabesse E, Benoit Y, Socci NB, Leslie CS, Van Vlierberghe P, Speleman F* & Wendel HG*. Nat Genet. 2011 Jun 5;43(7):673-8.

A cooperative microRNA-tumor suppressor gene network in acute T-cell lymphoblastic leukemia (T-ALL)

Konstantinos J Mavrakis[1,11], Joni Van Der Meulen[2,11], Andrew L Wolfe[1,3], Xiaoping Liu[1], Evelien Mets[2], Tom Taghon[4], Aly A Khan[3,5], Manu Setty[3,5], Pieter Rondou[2], Peter Vandenberghe[6], Eric Delabesse[7], Yves Benoit[8], Nicholas B Socci[9], Christina S Leslie[5], Pieter Van Vlierberghe[2,10], Frank Speleman[2,11] & Hans-Guido Wendel[1,11]

The importance of individual microRNAs (miRNAs) has been established in specific cancers. However, a comprehensive analysis of the contribution of miRNAs to the pathogenesis of any specific cancer is lacking. Here we show that in T-cell acute lymphoblastic leukemia (T-ALL), a small set of miRNAs is responsible for the cooperative suppression of several tumor suppressor genes. Cross-comparison of miRNA expression profiles in human T-ALL with the results of an unbiased miRNA library screen allowed us to identify five miRNAs (miR-19b, miR-20a, miR-26a, miR-92 and miR-223) that are capable of promoting T-ALL development in a mouse model and which account for the majority of miRNA expression in human T-ALL. Moreover, these miRNAs produce overlapping and cooperative effects on tumor suppressor genes implicated in the pathogenesis of T-ALL, including *IKAROS* (also known as *IKZF1*), *PTEN*, *BIM*, *PHF6*, *NF1* and *FBXW7*. Thus, a comprehensive and unbiased analysis of miRNA action in T-ALL reveals a striking pattern of miRNA-tumor suppressor gene interactions in this cancer.

T-ALL arises as a consequence of several cooperating genetic lesions[1]. For example, most affected individuals harbor activating lesions of *NOTCH1* (ref. 2), and tumor suppressor genes including *PTEN* (ref. 3), *NF1* (ref. 4), *PHF6* (ref. 5), *PTPN2* (ref. 6), *IKAROS* (refs. 7–11) and *FBXW7* (refs. 12,13) are targets of inactivating somatic mutations or deletions in T-ALL. Individual miRNAs have also been implicated in T-ALL. For example, miR-19b is a member of the oncogenic miR-17-92 cluster, which is targeted by the t(13;14)(q32;q11) translocation in T-ALL[14,15]. miRNA expression analyses in various cancers indicate that only a few miRNAs are highly expressed in cancer cells, and that a pattern reminiscent of the tissue of origin is maintained[16,17]. How a set of abundantly expressed miRNAs acts in leukemogenesis is currently unclear.

The regulation of gene expression by miRNAs is complex. Many mRNAs contain 3′ untranslated region (UTR) binding sites for multiple miRNAs, and likewise, most miRNAs can potentially target a large number of genes[18]. Clearly, not all predicted miRNA targets contribute to a phenotype, and in some instances, a coordinate effect on a cellular pathway has been shown. For example, miR-19b controls multiple regulators of phosphatidylinositol-3-OH kinase (PI3K) signaling[15], and miR-181a can adjust the sensitivity of T-cell receptor activation[19]. It is unclear whether a group of miRNAs can produce cooperative effects on genes, pathways and processes involved in tumor suppression.

To comprehensively assess miRNA action in T-ALL, we compared miRNA expression data with an unbiased miRNA library screen and computational analyses and tested candidates in a T-ALL model (**Fig. 1a**). First, we measured the expression of 430 miRNAs in 50 clinical T-ALL specimens representing distinct cytogenetic groups[1] (*MLL* ($n = 4$), *Calm-Af10* ($n = 3$), *Inv(7)* ($n = 5$), *LMO2* ($n = 7$), *SIL-TAL* ($n = 8$), *TLX3* ($n = 10$), *TLX1* ($n = 5$) and unknown ($n = 8$)) and 18 T-ALL cell lines by quantitative RT-PCR (qRT-PCR)[20]. Ten miRNAs were highly expressed, whereas others were less abundant. The 'top-ten' miRNAs were (in descending order) miR-223, miR-19b, miR-20a, miR-92, miR-142-3p, miR-150, miR-93, miR-26a, miR-16 and miR-342 (**Fig. 1b** and **Supplementary Table 1**). In our series, hierarchical clustering and principal component analysis did not distinguish between the major cytogenetic groups (HOXA, TAL or LMO and TLX1 or TLX3), which differed in a few miRNAs (**Fig. 1c**, **Supplementary Fig. 1** and **Supplementary Table 2**). Sequence analysis confirmed mutations in *NOTCH1* (21/37 clinical specimens) and *FBXW7* (9/37) (**Supplementary Fig. 2** and **Supplementary Table 3**). Hierarchical clustering of the miRNA expression data recovered *NOTCH1* mutational status but not *FBXW7*. In a pairwise comparison, miR-200b segregated with *NOTCH1*, whereas miR-100, miR-484 and miR-589 segregated with *FBXW7* status (**Supplementary Fig. 3** and **Supplementary Table 4**). The pattern of miRNA expression was preserved in human T-ALL cell lines (**Supplementary Fig. 4a** and **Supplementary Table 5**). Pairwise comparisons by *NOTCH1*, *FBXW7*, *PTEN* and *PHF6* mutation status or sensitivity to gamma secretase

[1]Cancer Biology & Genetics Program, Memorial Sloan-Kettering Cancer Center, New York, New York, USA. [2]Center for Medical Genetics, Ghent University Hospital, Ghent, Belgium. [3]Weill Cornell Graduate School of Medical Sciences, New York, New York, USA. [4]Department of Clinical Chemistry, Microbiology and Immunology, Ghent University Hospital, Ghent, Belgium. [5]Computational Biology, Memorial Sloan-Kettering Cancer Center, New York, New York, USA. [6]Centre for Human Genetics, University Hospital Leuven, Leuven, Belgium. [7]INSERM U563, Toulouse, France. [8]Department of Pediatric Hematology-Oncology, Ghent University Hospital, Ghent, Belgium. [9]Computational Biology Center, Memorial Sloan-Kettering Cancer Center, New York, New York, USA. [10]Institute for Cancer Genetics, Columbia University, New York, New York, USA . [11]These authors contributed equally to this work. Correspondence should be addressed to H.-G.W. (wendelh@mskcc.org).

Received 12 November 2010; accepted 16 May 2011; published online 5 June 2011; corrected after print 11 July 2011; doi:10.1038/ng.858

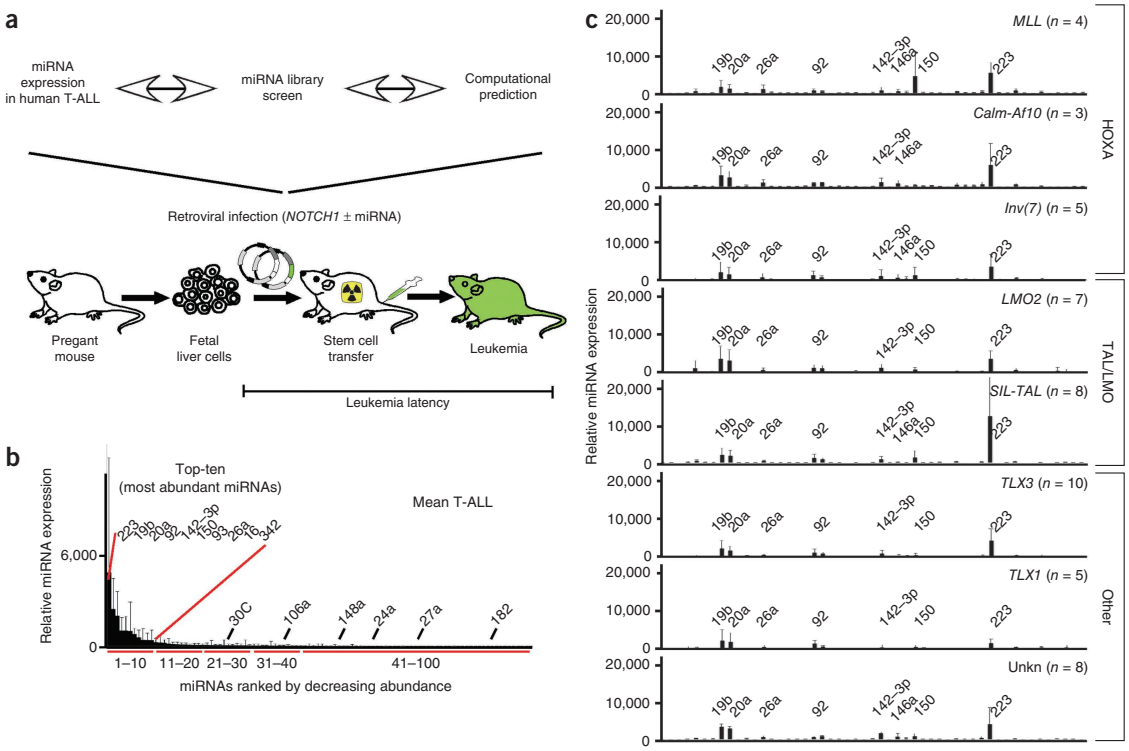

Figure 1 Comprehensive study of oncogenic miRNAs in T-ALL. (**a**) Schematic of the experimental strategy. (**b**) Average miRNA expression across 50 T-ALL samples by quantitative RT-PCR and normalized to the mean expression value of all expressed miRNAs in a given sample (mean and s.d.); miRNAs are ordered by expression levels, and the 'top-ten' most abundantly expressed miRNAs are indicated. (**c**) miRNA expression in different cytogenetic subgroups of T-ALL (mean and s.d.; ordered numerically, and the most abundant miRNAs are indicated).

inhibition revealed differentially expressed miRNAs[12] (**Supplementary Table 6**). Comparisons with purified progenitors ($CD34^+$ and $CD4^+CD8^+CD3^-$) and differentiated T-cells ($CD4^+CD8^+CD3^+$ and $CD4^+$ or $CD8^+$) revealed leukemia-specific increases in miR-223, but less of an increase in miR-376 and miR-662 (**Supplementary Fig. 4b,c** and **Supplementary Tables 7,8**). Hence, a small number of miRNAs are highly expressed in T-ALL, and among them, miR-223 is most strongly upregulated in leukemia.

Next, we analyzed the 3′ UTRs of twelve tumor suppressor genes (*FBXW7, PTEN, PHF6, PTPN2, IKAROS (IKZF1), NF1, BIM, CDK8, CYCLINC, NLK, RB* and *P53)* implicated in T-ALL for miRNA binding sites[21,22]. As expected, many miRNAs are predicted to bind these genes, and we generated a rank order by calculating a cumulative context score (**Table 1** and **Supplementary Table 9a**) or by adding the number of conserved 7- and 8-mer sites (**Supplementary Table 9b**), in both cases restricting the calculations to broadly conserved miRNA seed families. Notably, five of the ten most highly expressed miRNAs ranked highest in this analysis: miR-19b, miR-20a/93, miR-26a, miR-92 and miR-223. This enrichment was significant compared to random sets of 10,000 genes of the same size ($P < 0.043$, empirical P value). Hence, highly expressed miRNAs in T-ALL preferentially target tumor suppressor genes.

In parallel, we conducted an unbiased miRNA library screen for potentially oncogenic miRNAs (oncomirs). We used a two-step, sibling-selection protocol and first screened for bypass of *c-MYC*–induced apoptosis[23] and second for cytokine independence in lymphocytes[15] (**Fig. 2a**). *c-MYC* is a key effector of *NOTCH1* in T-ALL[24–26]. We collected the surviving cells from the primary screen and identified the miRNAs, which included the highly expressed miR-25/92, miR-19b and miR-223 (**Fig. 2b** and **Supplementary Table 10**). To generate a secondary library, we sub-cloned all miRNAs from the primary screen and partially transduced FL5-12 lymphocytes with the pooled vectors expressing individual miRNAs along with the GFP reporter. Upon enrichment of miRNA and GFP expressing cells, we identified the most abundant miRNAs by sequence analysis (**Fig. 2c** and **Supplementary Table 11**). Ultimately, retesting confirmed *in vitro* protection for miR-148a/152, miR-22, miR-19b, miR-101, miR-25/92 and miR-20a/106 (the pairs miR-148/152, miR-20/106 and miR-25/92 have identical seed sequences) (**Fig. 2d**).

To summarize the interim results, we found ten miRNAs that account for most detectable miRNAs in human T-ALL cells, five of which are predicted to target tumor suppressor genes implicated in T-ALL and readily emerge from an unbiased screen for oncogenic activities (**Fig. 2e**). Hence, using complementary approaches, we identified several candidate oncomirs in T-ALL.

Next, we directly tested candidate oncomirs in a mouse model of *NOTCH1*-induced T-ALL. Briefly, we transduced hematopoietic progenitors (HPCs) with *NOTCH1* and either empty vector or miRNA, transplanted the HPCs into lethally irradiated recipients and monitored the animals for leukemia[15] (**Fig. 3a**). As expected, miR-19b

Table 1 Computational analysis and ranking of miRNA binding sites in candidate tumor suppressor genes implicated in T-ALL

miRNA/context score[a,b]	*FBXW7*	*BIM*	*NF1*	*PTEN*	*IKZF1*	*PHF6*	*Sum*[c]
miR-25/92[d]	−0.9	−0.6	−0.2	−0.4	−0.2	0.0	−3.2
miR-27	−0.8	−0.2	−0.2	0.0	−0.4	0.0	−3.0
miR-203	0.0	−0.2	−0.2	0.0	−0.7	−0.6	−2.9
miR-148/152[d]	0.0	−0.8	0.0	−0.7	−0.3	0.0	−2.4
miR-101	−0.2	−0.3	−0.4	0.0	−0.1	−0.2	−2.3
miR-26	0.0	0.0	0.0	−0.9	0.0	−0.4	−2.3
miR-103	−0.3	0.0	−0.9	−0.6	0.0	0.0	−2.2
miR-200	−0.6	−0.2	−0.4	−0.2	0.0	−0.4	−2.2
miR-144	0.0	−0.2	−0.9	−0.3	0.0	−0.2	−2.0
miR-128	−0.3	0.0	−0.3	0.0	−0.4	−0.5	−1.9
miR-19	0.0	−0.3	−0.3	−0.6	−0.1	0.0	−1.8
miR-223	−1.4	0.0	0.0	0.0	0.0	0.0	−1.8
miR-137	−0.3	−0.1	−0.4	0.0	−0.2	0.0	−1.7
miR-217	0.0	−0.2	−0.6	−0.1	−0.2	−0.5	−1.6
miR-20/93/106[d]	0.0	−0.2	0.0	−0.3	0.0	−0.2	−1.5

[a]The context score was calculated by correlating contextual features at a predicted site (local AU content, predicted binding at the 3′ end of the miRNA and position in the 3′ UTR) with extent of downregulation in miRNA transfection experiments and indicates the strength of the miRNA-mRNA interaction; larger negative values correspond to more effective sites; only values less than −0.1 are shown; scores are rounded to one decimal place. [b]We tested the significance of this enrichment by randomly sampling 10,000 gene sets of the same size as the tumor suppressor gene set and computed how often the positive miRNAs showed the same enrichment. The enrichment of highly expressed miRNAs targeting tumor suppressor genes was significant ($P < 0.043$, empirical P value). [c]The sum is calculated for all 12 genes included in the analysis; see **Supplementary Table 9** for the full list of genes and miRNAs. [d]Indicates homologous miRNAs with identical seed sequences. See **Supplementary Table 9** for the full analysis.

accelerated leukemia development ($n = 7$, $P < 0.01$) compared to vector ($n = 13$)[15]. miR-20a ($n = 4$, $P < 0.001$), miR-26a ($n = 5$, $P < 0.001$), miR-92 ($n = 5$, $P = 0.02$) and miR-223 ($n = 7$, $P < 0.01$) similarly produced leukemia within 75 days; at this time >80% of vector or miR-30 controls ($n = 5$, $P = 0.15$) were disease free (**Fig. 3b**). Some less abundant miRNAs also enhanced leukemogenesis. Specifically, miR-148 ($n = 7$, $P < 0.01$) and miR-27 ($n = 5$, $P = 0.05$) were leukemogenic, whereas miR-23 ($n = 5$, $P > 0.05$) and miR-24 ($n = 5$, $P > 0.05$) showed no effect (**Supplementary Fig. 5a**). In all cases, pathology revealed CD4-CD8 double positive T-ALL (**Supplementary Fig. 5b** and **Supplementary Table 12**), high proliferation (Ki67 stain), absence of apoptosis by TUNEL and widespread organ infiltration that included the lungs and brain (**Fig. 3c**). miRNAs were twofold and sixfold increased in miRNA-expressing leukemia compared to controls, and twofold and 25-fold increased compared to normal thymocytes (**Supplementary Fig. 5c**,**d**). Thus, the abundantly expressed miR-19b, miR-20a, miR-26a, miR-92 and miR-223 act as oncomirs *in vivo*.

These experimentally validated oncomirs were significantly enriched among the highest-ranking miRNAs in our computational analysis of target genes (empirical $P < 1 \times 10^{-4}$ for number of seeds or context scores) (**Table 1** and **Supplementary Table 9**). We used an unbiased machine learning approach based on lasso regression to identify the targets that discriminate between oncomirs and random miRNAs. Accounting for the small number of positive training examples, we performed a stability analysis by repeating the learning procedure 50 times with different sets. Among the top 15 most frequently included target genes, we found *FBXW7* (identified in 46/50 runs), *BIM* (in 21/50 runs) and *PTEN* (in 11/50 runs) (**Supplementary Table 13**).

We experimentally tested these target predictions in mouse leukemic cells using reporter assays (**Fig. 4a** and **Supplementary Fig. 6**), qRT-PCR (**Fig. 4b**) and immunoblots (**Fig. 4c–g**). Briefly, miR-19b regulates Pten expression[15] (**Supplementary Fig. 7a**). miR-20a and miR-26a reduce levels of Pten and Phf6, and miR-20a has similar effects on Bim. Ikzf1, Nf1 and Fbxw7 are regulated by miR-27a, and miR-148a regulates Ikzf1, Pten and Bim. Similarly, miR-92 affects Ikzf1, Fbxw7 and, to a lesser extent, Bim and Pten, but not mouse Nf1. miR-223 is a strong regulator of Fbxw7. We confirmed these findings in FL5-12 cells (**Supplementary Fig. 7b–e**). Hence, oncomirs produce partially overlapping effects on key tumor suppressor genes implicated in T-ALL.

Next, we directly examined the tumor suppressor function of these target genes in our mouse T-ALL model. Briefly, we used short-hairpin RNAs (shRNAs) directed against *Pten*[15], *Bim*[15], *Nf1*, *Phf6* and *Fbxw7* (**Supplementary Fig. 8**) and a dominant negative *Ikzf1* allele (*Dn-Ikzf1*)[27] in the same adoptive transfer model described above. *NOTCH1*-triggered leukemia was accelerated by shRNAs against *Pten* ($n = 3$, $P < 0.05$), *Bim* ($n = 6$, $P < 0.01$)[15], *Nf1* ($n = 6$, $P < 0.01$), *Phf6* ($n = 3$, $P < 0.05$) and *Dn-Ikzf1* ($n = 10$, $P < 0.01$); *Fbxw7* showed a trend ($n = 4$, $P = 0.1$) (**Fig. 5a**). MCL1 is a target of the FBXW7 E3 ligase[28,29] and accordingly, we found that MCL1 levels are increased

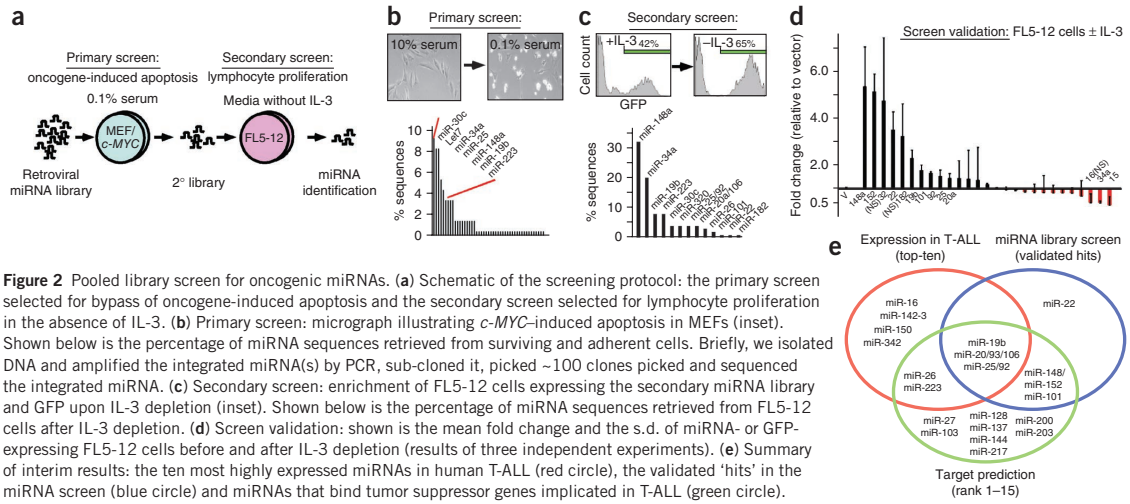

Figure 2 Pooled library screen for oncogenic miRNAs. (**a**) Schematic of the screening protocol: the primary screen selected for bypass of oncogene-induced apoptosis and the secondary screen selected for lymphocyte proliferation in the absence of IL-3. (**b**) Primary screen: micrograph illustrating *c-MYC*–induced apoptosis in MEFs (inset). Shown below is the percentage of miRNA sequences retrieved from surviving and adherent cells. Briefly, we isolated DNA and amplified the integrated miRNA(s) by PCR, sub-cloned it, picked ~100 clones picked and sequenced the integrated miRNA. (**c**) Secondary screen: enrichment of FL5-12 cells expressing the secondary miRNA library and GFP upon IL-3 depletion (inset). Shown below is the percentage of miRNA sequences retrieved from FL5-12 cells after IL-3 depletion. (**d**) Screen validation: shown is the mean fold change and the s.d. of miRNA- or GFP-expressing FL5-12 cells before and after IL-3 depletion (results of three independent experiments). (**e**) Summary of interim results: the ten most highly expressed miRNAs in human T-ALL (red circle), the validated 'hits' in the miRNA screen (blue circle) and miRNAs that bind tumor suppressor genes implicated in T-ALL (green circle).

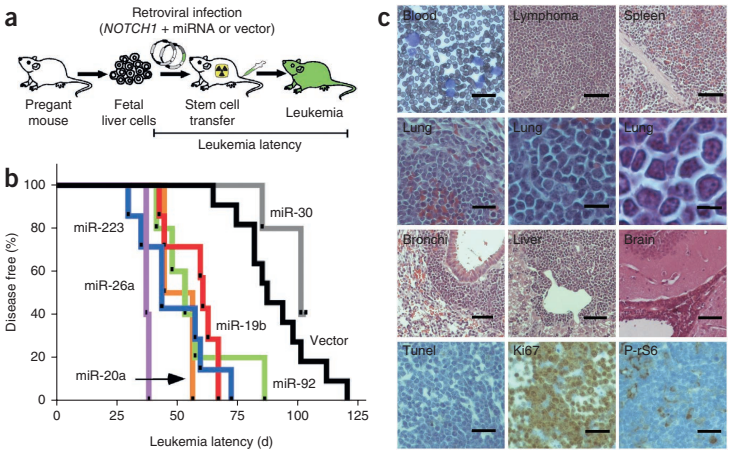

Figure 3 Candidate miRNAs act as oncogenes in a mouse T-ALL model. (**a**) Schematic of the adoptive transfer model of *NOTCH1*-driven T-ALL. (**b**) Kaplan-Meier analysis of leukemia-free survival after transplantation of HPCs expressing *NOTCH1-ICN* and either vector (black, $n = 13$) or miR-19b (red, $n = 7$), miR-20a (orange, $n = 4$), miR-26a (magenta, $n = 5$), miR-30 (gray, $n = 5$), miR-92 (green, $n = 5$) or miR-223 (blue, $n = 7$). (**c**) Representative microphotographs of *NOTCH1*-induced T-ALL (all 10×; for lung, 40× and 100× shown; scale bars indicated). The pathologic appearance of leukemias expressing different miRNAs is identical (not shown).

in mouse leukemias expressing miR-223 and miR-92, both of which target *Fbxw7* (**Supplementary Fig. 9a**). Moreover, the homologous *Bcl2* ($n = 4$; $P < 0.001$ for *Bcl2* versus vector) strongly accelerates leukemia development with *Notch1* (**Supplementary Fig. 9b**). Similarly, *Mcl1* and *Bcl2* promote tumor development triggered by *c-Myc*, a key effector of *Notch1* (refs. 25,30,31). This indicates that FBXW7 acts, at least in part, through regulation of the anti-apoptotic BCL2 family member MCL1. shRNAs and miRNAs may differ in their mechanism and efficiency of target knockdown, and our results indicate the tumor suppressive function of these genes in *NOTCH1*-triggered T-ALL.

Given the pleiotropic and overlapping pattern of tumor suppressor regulation by miRNAs, we wondered about the relevant contribution of each miRNA (**Fig. 5**). The human TALL-1 cell line expresses miR-19a, miR-19b, miR-26a and miR-92 but lacks miR-148a and miR-182 (**Fig. 5b** inset and **Supplementary Table 5**). Antagomirs against miR-19a/b, miR-26a and miR-92 reduce growth and viability ($P < 0.05$ for each antagomir versus vector) (**Fig. 5b**,**c**). These antagomirs cause derepression of *PTEN* and *BIM* (**Fig. 5d**,**f**). By contrast, antagomirs against miR-148a and miR-182 have no effect ($P > 0.05$). There are cell-line–specific differences, and in KOPTK1 cells, which express high levels of miR-148, an antagomir against miR-148 restores *BIM* and *PTEN* expression (**Supplementary Fig. 10**). This indicates that miR-148 maintains *BIM* and *PTEN* repression in KOPTK1 cells but not in TALL-1 cells. Hence, individual miRNAs make relevant contributions that affect the viability of T-ALL cells.

Do miRNAs that bind common target genes produce cooperative effects? Co-expression of antagomirs against miR-19a/b, miR-26a and miR-92 had a stronger effect on the growth of TALL-1 cells than the individual antagomirs ($P < 0.001$ combined antagomirs versus vector) (**Fig. 5b**). The effect on cell viability was even more pronounced, such that the three antagomirs together produced twice

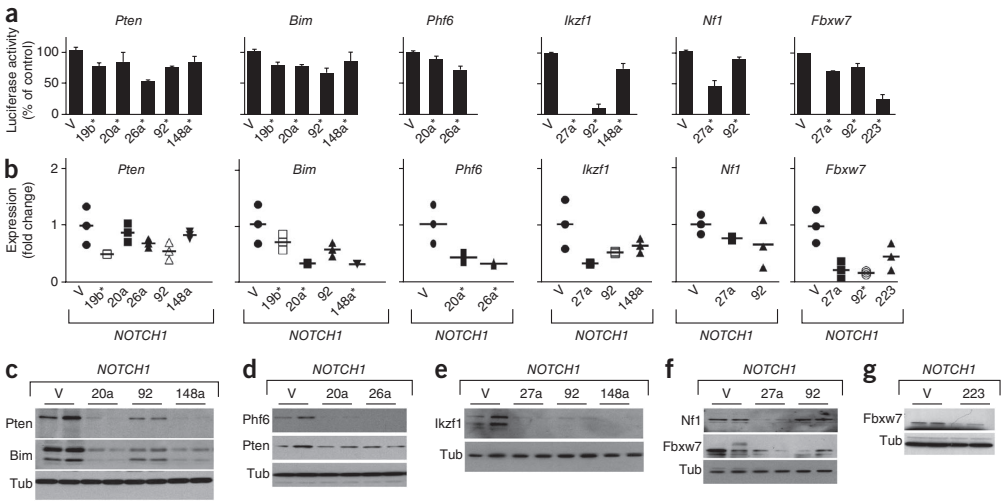

Figure 4 miRNAs regulate the expression of tumor suppressor genes in mouse T-ALL. (**a**) Luciferase reporter assays testing the effect of miRNAs on 3′ UTRs of the indicated genes (shown are mean and s.d. of triplicate experiments; V, vector; numbers indicate the miRNA name; $*P < 0.05$ compared to vector). (**b**) Quantitative RT-PCR (qRT-PCR) measurement of gene expression in mouse T-ALLs expressing *NOTCH1* and the indicated miRNA (shown is the range and mean of the measurement as a fold change compared to T-ALLs expressing the control vector; $*P < 0.05$). (**c**–**g**) Immunoblots on lysates from mouse T-ALLs expressing *NOTCH1* and vector or the indicated miRNAs and probed with the indicated antibodies.

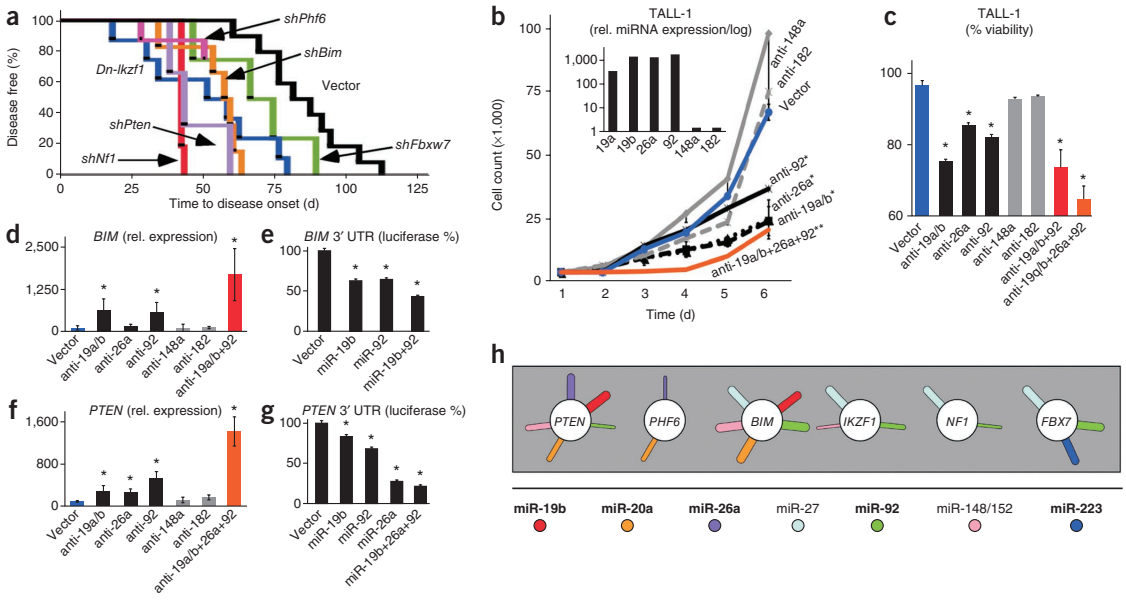

Figure 5 Individual and cooperative miRNA effects on T-ALL suppressor genes. (**a**) Kaplan-Meier analysis of leukemia-free survival after HPC transplantation. All HPCs express *NOTCH1-ICN* and vector (black, $n = 13$), or *shNf1* (red, $n = 6$), *shBim* (orange, $n = 6$), *shPten* (magenta, $n = 3$), *shFbxw7* (green, $n = 4$), *DN-Ikzf1* (blue, $n = 10$) or *shPhf6* (violet, $n = 3$). (**b**) Cell number during *in vitro* culture of TALL-1 cells expressing the indicated antagomirs (shown are mean and s.d. for each time point, significant differences ($P < 0.05$) at day 6 (*) and over the 6 day period (**)). The inset shows qRT-PCR measurement of miRNA expression in TALL-1 cells. (**c**) Viability of TALL-1 cells transduced with the indicated antagomirs (mean and s.d.; $*P < 0.05$). (**d**,**f**) qRT-PCR of *BIM* (**d**) and *PTEN* (**f**) mRNA levels in TALL-1 cells expressing the indicated antagomirs (mean and s.d.; $*P < 0.05$ compared to vector). (**e**,**g**) 3′ UTR luciferase reporter assays of *BIM* (**e**) and *PTEN* (**g**) in cells transduced with the indicated miRNAs (mean and s.d.; $*P < 0.05$ in triplicate measurements). (**h**) Diagrammatic summary of the overlapping regulation of six tumor suppressor genes (circles) by miRNAs (sticks) identified in this study; each miRNA is represented by a stick, and the width of each stick is proportional to the calculated strength and conservation of the miRNA-mRNA interaction (P_{ct} value); bold letters indicate highly expressed miRNAs in human T-ALL. Rel. relative.

as much apoptosis in a short-term assay than the individual antagomirs (**Fig. 5c**). Accordingly, the combined treatment produced larger increases in *BIM* and *PTEN* expression compared to the individual antagomirs (**Fig. 5d**,**f**). Similarly, co-expression of miR19b and miR-92 or miR-19b, miR-26a and miR-92 produced additive effects on the *BIM* and *PTEN* 3′ UTR reporter activity, respectively (**Fig. 5e**,**g**). Thus, highly expressed miRNAs cooperate in regulating key tumor suppressor genes in human T-ALL cells.

Our study provides new insights into miRNA action in leukemia. We obtained a comprehensive view of oncomirs in T-ALL by comparing miRNA expression data, computational analyses and an unbiased screen. A small number of abundantly expressed miRNAs target a set of key tumor suppressor genes and promote T-ALL *in vivo* (**Fig. 5h**). These oncomirs act in a miRNA-tumor suppressor gene network that is partially redundant and includes unique and cooperative miRNA effects. In this manner, miR-19b, miR-20a/93, miR-26a, miR-92 and miR-223 act as multi-targeted regulators of T-ALL tumor suppressors including *PTEN, BIM, NF1, FBXW7, IKZF1* and *PHF6*. mir-223 is notable for its differential upregulation in T-ALL; it promotes *NOTCH1*-driven leukemia at least in part by controlling the E3 ligase FBXW7 (ref. 32), which directs degradation of the anti-apoptotic MCL1 protein[28,29]. Other miRNAs are also found in normal progenitors and differentiated T-cells, and their oncogenic potential may only be realized in the context of additional mutations. Our study delineates the key oncomirs in T-ALL and informs therapeutic strategies using antagomirs. The description of genetic networks by experimental means is limited by technology, and our study exemplifies how computational approaches can complement such analyses. Additional studies need to address potential tumor suppressive miRNAs. In summary, we provide a conceptual framework for oncomir-tumor suppressor gene interactions that may also apply to other cancers.

METHODS

Methods and any associated references are available in the online version of the paper at http://www.nature.com/naturegenetics/.

Note: Supplementary information is available on the Nature Genetics website.

ACKNOWLEDGMENTS

We thank A.J. Capobianco, L. Beverly, A.A. Ferrando, J. Cools and W. Pear for reagents. The Memorial Sloan Kettering (MSK) animal facility and Research Animal Resource Center (RARC), A. Viale of the MSK Genomics Core, H. Zhao of Computational Biology (cBIO) program, K. Huberman of the Geoffrey Beene Translational Oncology Core Facility and J. Schatz for editorial advice. This work is supported by grants from the National Cancer Institute (NCI) (R01-CA142798-01) (H.-G.W.), and a P30 supplemental award (H.-G.W.), the Louis V. Gerstner Foundation (H.-G.W.), the William Lawrence and Blanche Hughes (WLBH) Foundation (H.-G.W.), the Society of MSKCC (H.-G.W.), the Geoffrey Beene Foundation (H.-G.W.), and May & Samuel Rudin Foundation Award (H.-G.W.); W.H. Goodwin and A. Goodwin and the Commonwealth Foundation for Cancer Research, The Experimental Therapeutics Center of Memorial Sloan-Kettering Cancer Center (H.-G.W.), the Fund for Scientific Research (FWO) Flanders (postdoctoral grants to T.T. and P.V.V., PhD grant to J.V.d.M., P.V.V. is a Senior Clinical Investigator of FWO-Vlaanderen, Odysseus program grant to T.T., and project grants G.0198.08 and G.0869.10N to F.S.); the GOA-UGent (grant no. 12051203); Stichting tegen Kanker, FOD ALL the Children Cancer Fund Ghent (F.S.); and the Belgian Program of Interuniversity Poles of Attraction and the Belgian Foundation Against Cancer.

AUTHOR CONTRIBUTIONS
K.J.M., A.L.W. and X.L. performed the screen, mouse model and data analysis. J.V.d.M. and P.V.V. performed miRNA profiling on T-ALL samples. E.M. and P.R. performed studies on miR-223 and FBXW7. T.T. performed cell sorting and miRNA profiling. P.V. and E.D. performed genetic analyses on T-ALL samples. Y.B. was the co-supervisor of the miRNA profiling project on childhood ALLs and integrated clinical data management. A.A.K., M.S., C.S.L. and N.D.S. performed computational analyses. F.S. supervised the miRNA expression analyses. H.G.W. designed the study and wrote the paper.

COMPETING FINANCIAL INTERESTS
The authors declare no competing financial interests.

Published online at http://www.nature.com/naturegenetics/.
Reprints and permissions information is available online at http://www.nature.com/reprints/index.html.

1. Aifantis, I., Raetz, E. & Buonamici, S. Molecular pathogenesis of T-cell leukaemia and lymphoma. *Nat. Rev. Immunol.* **8**, 380–390 (2008).
2. Weng, A.P. *et al.* Activating mutations of *NOTCH1* in human T cell acute lymphoblastic leukemia. *Science* **306**, 269–271 (2004).
3. Palomero, T. *et al.* Mutational loss of *PTEN* induces resistance to NOTCH1 inhibition in T-cell leukemia. *Nat. Med.* **13**, 1203–1210 (2007).
4. Balgobind, B.V. *et al.* Leukemia-associated NF1 inactivation in patients with pediatric T-ALL and AML lacking evidence for neurofibromatosis. *Blood* **111**, 4322–4328 (2008).
5. Van Vlierberghe, P. *et al. PHF6* mutations in T-cell acute lymphoblastic leukemia. *Nat. Genet.* **42**, 338–342 (2010).
6. Kleppe, M. *et al.* Deletion of the protein tyrosine phosphatase gene *PTPN2* in T-cell acute lymphoblastic leukemia. *Nat. Genet.* **42**, 530–535 (2010).
7. Dail, M. *et al.* Mutant Ikzf1, KrasG12D, and Notch1 cooperate in T lineage leukemogenesis and modulate responses to targeted agents. *Proc. Natl. Acad. Sci. USA* **107**, 5106–5111 (2010).
8. Winandy, S., Wu, P. & Georgopoulos, K. A dominant mutation in the *Ikaros* gene leads to rapid development of leukemia and lymphoma. *Cell* **83**, 289–299 (1995).
9. Marçais, A. *et al.* Genetic inactivation of Ikaros is a rare event in human T-ALL. *Leuk. Res.* **34**, 426–429 (2010).
10. Sun, L. *et al.* Expression of dominant-negative Ikaros isoforms in T-cell acute lymphoblastic leukemia. *Clin. Cancer Res.* **5**, 2112–2120 (1999).
11. Mullighan, C.G. *et al.* Genome-wide analysis of genetic alterations in acute lymphoblastic leukaemia. *Nature* **446**, 758–764 (2007).
12. O'Neil, J. *et al. FBW7* mutations in leukemic cells mediate NOTCH pathway activation and resistance to gamma-secretase inhibitors. *J. Exp. Med.* **204**, 1813–1824 (2007).
13. Thompson, B.J. *et al.* The SCFFBW7 ubiquitin ligase complex as a tumor suppressor in T cell leukemia. *J. Exp. Med.* **204**, 1825–1835 (2007).
14. Landais, S., Landry, S., Legault, P. & Rassart, E. Oncogenic potential of the miR-106–363 cluster and its implication in human T-cell leukemia. *Cancer Res.* **67**, 5699–5707 (2007).
15. Mavrakis, K.J. *et al.* Genome-wide RNA-mediated interference screen identifies miR-19 targets in Notch-induced T-cell acute lymphoblastic leukaemia. *Nat. Cell Biol.* **12**, 372–379 (2010).
16. Lu, J. *et al.* MicroRNA expression profiles classify human cancers. *Nature* **435**, 834–838 (2005).
17. Landgraf, P. *et al.* A mammalian microRNA expression atlas based on small RNA library sequencing. *Cell* **129**, 1401–1414 (2007).
18. Bartel, D.P. MicroRNAs: genomics, biogenesis, mechanism, and function. *Cell* **116**, 281–297 (2004).
19. Li, Q.J. *et al.* miR-181a is an intrinsic modulator of T cell sensitivity and selection. *Cell* **129**, 147–161 (2007).
20. Mestdagh, P. *et al.* A novel and universal method for microRNA RT-qPCR data normalization. *Genome Biol.* **10**, R64 (2009).
21. Lewis, B.P., Shih, I.H., Jones-Rhoades, M.W., Bartel, D.P. & Burge, C.B. Prediction of mammalian microRNA targets. *Cell* **115**, 787–798 (2003).
22. Friedman, R.C., Farh, K.K., Burge, C.B. & Bartel, D.P. Most mammalian mRNAs are conserved targets of microRNAs. *Genome Res.* **19**, 92–105 (2009).
23. Evan, G.I. *et al.* Induction of apoptosis in fibroblasts by c-myc protein. *Cell* **69**, 119–128 (1992).
24. Palomero, T. *et al.* NOTCH1 directly regulates c-MYC and activates a feed-forward-loop transcriptional network promoting leukemic cell growth. *Proc. Natl. Acad. Sci. USA* **103**, 18261–18266 (2006).
25. Weng, A.P. *et al.* c-Myc is an important direct target of Notch1 in T-cell acute lymphoblastic leukemia/lymphoma. *Genes Dev.* **20**, 2096–2109 (2006).
26. Klinakis, A. *et al.* Myc is a Notch1 transcriptional target and a requisite for Notch1-induced mammary tumorigenesis in mice. *Proc. Natl. Acad. Sci. USA* **103**, 9262–9267 (2006).
27. Beverly, L.J. & Capobianco, A.J. Perturbation of Ikaros isoform selection by MLV integration is a cooperative event in Notch(IC)-induced T cell leukemogenesis. *Cancer Cell* **3**, 551–564 (2003).
28. Inuzuka, H. *et al.* SCFFBW7 regulates cellular apoptosis by targeting MCL1 for ubiquitylation and destruction. *Nature* **471**, 104–109 (2011).
29. Wertz, I.E. *et al.* Sensitivity to antitubulin chemotherapeutics is regulated by MCL1 and FBW7. *Nature* **471**, 110–114 (2011).
30. Schmitt, C.A., Rosenthal, C.T. & Lowe, S.W. Genetic analysis of chemoresistance in primary murine lymphomas. *Nat. Med.* **6**, 1029–1035 (2000).
31. Wendel, H.G. *et al.* Dissecting eIF4E action in tumorigenesis. *Genes Dev.* **21**, 3232–3237 (2007).
32. Maser, R.S. *et al.* Chromosomally unstable mouse tumours have genomic alterations similar to diverse human cancers. *Nature* **447**, 966–971 (2007).

ONLINE METHODS

T-ALL samples. Diagnostic bone marrow samples of 50 individuals with T-ALL were obtained from different European centers (Universitair Ziekenhuis (UZ) Ghent, Ghent, Belgium; UZ Leuven, Leuven, Belgium; Hôpital Purpan, Toulouse, France; Centre Hospitalier Universitaire (CHU) de Nancy-Brabois, Vandoeuvre-Les-Nancy, France). The resulting T-ALL cohort consisted of 15 *TAL* or *LMO* (7 *LMO2* and 8 *SIL-TAL*), 12 *HOXA* (4 *MLL*, 6 inv(7)(p15q35) and 2 *CALM-AF10*), 10 *TLX3* and 5 *TLX1* cases, and 8 cases could not be categorized. Total RNA was isolated using the miRNeasy mini kit (QIAGEN).

This study (2008/531) was approved by the Medical Ethical Commission of Ghent University Hospital (Belgium, registration B67020084745).

T-ALL cell lines. Eighteen T-ALL cell lines cultured in RPMI-1640 (Invitrogen), 15% FCS, 1% penicillin and streptomycin and 1% kanamycin, 1% glutamine. RNA isolation was performed as described above.

Subsets of normal T-cell populations. Normal T-cell populations from pediatric thymuses ($CD34^+$, $CD4^+CD8^+CD3^-$, $CD4^+CD8^+CD3^+$, $CD3^+CD4^+CD8^-$ and $CD3^+CD4^-CD8^+$) were obtained by FACS and MACS[33] using CD34 microbeads (Miltenyi Biotec), double positive were isolated by staining with $CD3^-$FITC, $CD8^-$PE and $CD4^-$APC, and single positive were depleted $CD1^+$ thymocytes by Dynabeads (Dynal Biotech) and were subsequently labeled with $CD3^-$FITC, $CD8^-$PE and $CD4^-$APC. The purity of the different subsets of normal T-cell populations was always at least 98%. RNA isolation was performed as described above.

MicroRNA profiling. miRNA profiling was performed using stem-loop reverse transcriptase primers for miRNA complementary DNA (cDNA) synthesis followed by a pre-amplification step and TaqMan PCR analysis (Applied Biosystems)[34]. In brief, 20 ng of total RNA was reverse transcribed by use of the megaplex reverse transcriptase stem-loop primer pool for miRNA cDNA synthesis of 448 small RNAs, including 430 miRNAs and 18 small RNA controls. Pre-amplification of cDNA was performed in a 14-cycle PCR reaction by use of TaqMan PreAmp Master Mix (2×) and PreAmp Primer Mix (5×) (Applied Biosystems) consisting of a miRNA-specific forward primer and a universal reverse primer[35]. Finally, the 448 small RNAs were profiled for each sample using a 40-cycle PCR protocol. SDS software version 2.1 was used to calculate the raw Cq values, using automatic base line settings and a threshold of 0.05. For normalization of the qPCR data of the miRNA expression profiles, we used the mean expression value of all expressed miRNAs in a given sample as the normalization factor; miRNAs with a Cq value >32 were considered unexpressed[20].

Cell culture, viability, proliferation assays and vectors constructs. FL5-12 mouse lymphocytes, cell cycle, apoptosis studies and viral transductions were as previously described[36,37]. Vectors are based on murine stem cell virus (MSCV)[35,38,39]. The pooled library[35,38] has been expanded by PCR cloning to contain ~300 miRNAs. The antagomirs MZIP19a-PA-1, MZIP19b-PA-1, MZIP26a-PA-1, MZIP92a-PA-1, MZIP148a-PA-1 and MZIP182-PA1 and the scrambled control (MZIP000-PA-1) were from System Biosciences.

Library screens. The primary screen is based on *c-MYC*–induced apoptosis in mouse embryo fibroblasts (MEFs)[23]. MEFs were transduced with *c-MYC* and the miRNA library, puromycin was selected and apoptosis was triggered by reducing the serum to 0.1%. Surviving and adherent cells were collected for DNA isolation, and we performed PCR amplification of the integrated miRNA library constructs, sub-cloning into pGEM-T vector, bacterial transformation and sequence identification of ~100 colonies. A secondary library was constructed by sub-cloning all miRNAs from the primary screen into an MSCV construct. The secondary screen was for IL-3 independence[15,37]. FL5-12 cells were transduced with the library and were IL-3 depleted. miRNAs were identified as above and individually retested.

Generation of mice. The mouse T-ALL model has been previously reported[39,40]. Data were analyzed in Kaplan-Meier format using the log-rank (Mantel-Cox) test for statistical significance. The surface marker analysis was as described[40].

Protein blot analysis. Immunoblots were performed from whole cell lysates as described[40]. Antibodies were against Bim (AAP-330, 1:1,000, Assay Designs), Nf1 (sc67, 1:100, Santa Cruz), Cdc4/Fbw7 (ab7405, 1:500, Abcam), Ikzf1 (sc-13039, 1:500, Santa Cruz), Phf6 (NB100-79861, 1:1,000, Novus Biologicals), Pten (9559, 1:1,000, Cell Signaling), Tubulin (1:5,000, Sigma, B-5-1-2), Actin (1:5,000, Sigma, AC-15) and Mcl1 (1:1,000, Rockland 600-401-394).

Real time quantitative PCR for gene expression. Total RNA and miRNA-enriched RNA was extracted using the AllPrep DNA/RNA/Protein and miRNeasy Mini. cDNA synthesis and qRT-PCR and analysis by the ΔΔ Ct method was performed as described[36]. TaqMan Gene Expression Assays: Bim (Mm00437796_m1), BIM (Hs00197982_m1), Pten (Mm01212532_m1), PTEN (Hs02621230_s1), Nf1 (Mm00812430_m1), NF1 (Hs01035104_m1), Ikzf1 (Mm01187878_m1), IKZF1 (Hs00172991_m1), Fbxw7 (Mm00504452_m1), FBXW7 (Hs00217794_m1), Phf6 (Mm00804415_m1) and mouse GAPD (GAPDH) (4352932, Applied Biosystems), and expression was normalized to RNU6B (001093, Applied Biosystems). Primer sequences are available upon request.

Computational analyses of microRNA-target gene interaction. To generate training data, we carried out a supervised learning approach to identify, in an unbiased way, target genes that could discriminate between miRNAs that passed all screens (+1 class) and those that did not pass (−1 class). As positive training data (+1 class), we took the miRNAs that validated through the screen (miR-19, miR-20/93, miR-25/92, miR-148, miR-26a, miR-223 and miR-27ab). miR-20/93 and miR-25/92 were grouped together in the subsequent analysis because the respective seed sequence (pos 2:8) were identical. As negative training data (−1 class), we included three miRNAs that failed to validate at the final stage (miR-30a, miR-23a and miR-24), as well as five additional miRNAs that are highly expressed in T-ALL but which failed in the initial screen (miR-142-3p, miR-150, miR-342-3p, miR-146 and miR-16).

Target prediction. Using the seed sequence (position 2:8) for each miRNA, we identified conserved mRNA targets by requiring the complementary sequence to occur in both mouse and human 3′ UTRs of orthologous mRNAs. We used the minimum number of seed matches from both UTRs as the conserved 7-mer count for each miRNA-mRNA pair. We used Biopython to extract 3′ UTR sequences for mouse and human using RefSeq (Release 42). The longest 3′ UTR was used when multiple RefSeq transcripts were present for a single gene.

Lasso regression. We used lasso regression to identify 'discriminative' gene sets between positive miRNAs and negative miRNAs. In this approach, each miRNA (positive or negative) is represented by its vector $\mathbf{X}_{\text{miR}}$ of conserved 7-mer seed counts over all possible genes. The regression learns a weight vector $\mathbf{W}$ over genes such that the weighted sum of 7-mer seed counts for positive (or negative) miRNAs is close to +1 (or −1). The lasso constraint in the regression model encourages sparsity, meaning most of the genes will have a weight (regression coefficient) equal to 0. In this way, lasso regression identifies a smaller number of target genes that can discriminate between the two classes. Formally, we solve the optimization problem:

$$\min_w \sum_{\text{miR}} (y_{\text{miR}} - w \bullet x_{\text{miR}})^2 + \lambda \sum_g |w_g|$$

where y_{miR} is +1 for validated miRNAs and −1 for non-validated miRNAs, $\mathbf{X}_{\mathbf{miR}}$ is the vector of conserved 7-mer counts and λ is the regularization parameter, which we chose to give ten nonzero weights. Lasso regression was performed using the glmnet package from Bioconductor.

Enrichment of miRNAs. The empirical *P* value for enrichment of miRNAs in **Table 1** was determined by selecting 10,000 random samples of genes (of size equal to the set of tumor suppressor genes) from the full list of human genes for which we had 3′ UTRs and target predictions. We computed the sum of TargetScan context scores for each broadly conserved miRNA seed family relative to each of these random gene sets and ranked the miRNA families according to these scores. This procedure generates a randomized version of **Table 1** for each randomly selected gene set. We then calculated enrichment scores for these rankings using a Wilcoxon rank sum statistic comparing the 'positive' miRNAs (passed all screens) versus all other miRNAs. Finally, to compute the

empirical *P* value, we counted the number of times over the 10,000 randomly sampled gene sets we obtained a Wilcoxon rank sum score as good or better than the one we obtained with the tumor suppressor gene set. We found that 428 random samplings performed as well or better than the tumor suppressor gene set, corresponding to a significant empirical *P* value ($P < 0.043$).

Comparison of cytogenetic and mutational subgroups. Differential miRNA expression analysis was performed using *t*-tests for groups of subject samples by cytogenetic criteria or presence and absence of NOTCH1 or FBXW7 mutations. Cell lines were grouped by the indicated mutations and sensitivity to gamma secretase inhibitors as reported[12]. A Benjamini-Hochberg correction was used for multiple hypotheses correction.

Analyses of miRNA-3′ UTR interaction. By Targetscan 5.1 software[21,22], a rank-order was based on a cumulative measure of site efficacy, by summing the context scores of predicted binding sites for a given miRNA across the set of tumor suppressor genes.

Luciferase assays. The mouse Fbxw7 (2,793–4,139 bp; NM_001177773), human NF1 (10,033–10,666 bp; NM_000267), human PHF6 (3,271–4,299 bp; NM_001015877) and Bim (3,155–4,773 bp; NM_009754) 3′ UTR fragments were generated by PCR and cloned into the psi-CHECK-2 vector (Promega), with the exception of the IKZF1 UTR, which was purchased from Genecopoeia (HmiT000397b, 2,343–4,471 bp of the UTR). For the IKZF1 UTR luciferase assays, WT refers to the fragment containing the miR-92 binding site (from 2,343–4,470 bp), and MT refers to the fragment (containing positions 1–2,343 bp of the UTR) in which the miR-92 binding site is absent. The Pten UTR has been previously described[41]. The assays were performed as described[42]. Details of the 3′ UTR cloning and mutagenesis are shown in **Supplementary Tables 14,15**.

***NOTCH1* and *FBXW7* mutation analysis on 37 primary T-ALL samples.** Primers used for amplification of exon 26, 27, 28 and 34 of *NOTCH1* and exons 7, 8, 9, 10 and 11 of *FBXW7* are reported in **Supplementary Table 16** (refs. 43,44). For *NOTCH1* amplification, PCR was performed making use of the PCRx enhancer system (Invitrogen). A 50 µl PCR reaction contained 20 ng of DNA, 2.5U *KapaTaq* DNA Polymerase, 1× PCRx Amplification Buffer, 2× PCRx Enhancer Solution, 0.2 mM dNTP, 1.5 mM MgSO4 and 0.2 mM of each primer. *FBXW7* amplification used of 20 ng of DNA, 1× KapaTaq reaction buffer (KapaBiosystems), 1U KapaTaq DNA polymerase, 0.2 mM dNTP, 2.5 µM MgCl2, 0.2 mM forward and reverse primer in a 25 µl PCR reaction. PCR conditions were as follows: 10 min at 95 °C, 40 cycles (15 s at 96 °C, 1 min at 57 °C and 1 min at 72 °C) and 10 at min 72 °C. Subsequently, PCR products were enzymatically purified followed by primer extension sequencing using dye terminator sequencing chemistry and electrophoresis by ABI3730xl (Applied Biosystems).

33. Van de Walle, I. *et al.* An early decrease in Notch activation is required for human TCR-alphabeta lineage differentiation at the expense of TCR-gammadelta T cells. *Blood* **113**, 2988–2998 (2009).
34. Chen, C. *et al.* Real-time quantification of microRNAs by stem-loop RT-PCR. *Nucleic Acids Res.* **33**, e179 (2005).
35. Mestdagh, P. *et al.* High-throughput stem-loop RT-qPCR miRNA expression profiling using minute amounts of input RNA. *Nucleic Acids Res.* **36**, e143 (2008).
36. Mavrakis, K.J. *et al.* Tumorigenic activity and therapeutic inhibition of Rheb GTPase. *Genes Dev.* **22**, 2178–2188 (2008).
37. Plas, D.R., Talapatra, S., Edinger, A.L., Rathmell, J.C. & Thompson, C.B. Akt and Bcl-xL promote growth factor-independent survival through distinct effects on mitochondrial physiology. *J. Biol. Chem.* **276**, 12041–12048 (2001).
38. He, L. *et al.* A microRNA polycistron as a potential human oncogene. *Nature* **435**, 828–833 (2005).
39. Pear, W.S. *et al.* Exclusive development of T cell neoplasms in mice transplanted with bone marrow expressing activated Notch alleles. *J. Exp. Med.* **183**, 2283–2291 (1996).
40. Wendel, H.G. *et al.* Survival signaling by Akt and eIF4E in oncogenesis and cancer therapy. *Nature* **428**, 332–337 (2004).
41. Huse, J.T. *et al.* The PTEN-regulating microRNA miR-26a is amplified in high-grade glioma and facilitates gliomagenesis *in vivo*. *Genes Dev.* **23**, 1327–1337 (2009).
42. Xiao, C. *et al.* Lymphoproliferative disease and autoimmunity in mice with increased miR-17–92 expression in lymphocytes. *Nat. Immunol.* **9**, 405–414 (2008).
43. Zuurbier, L. *et al. NOTCH1* and/or *FBXW7* mutations predict for initial good prednisone response but not for improved outcome in pediatric T-cell acute lymphoblastic leukemia patients treated on DCOG or COALL protocols. *Leukemia* **24**, 2014–2022 (2010).
44. Asnafi, V. *et al. NOTCH1/FBXW7* mutation identifies a large subgroup with favorable outcome in adult T-cell acute lymphoblastic leukemia (T-ALL): a Group for Research on Adult Acute Lymphoblastic Leukemia (GRAALL) study. *Blood* **113**, 3918–3924 (2009).

Corrigendum: A cooperative microRNA-tumor suppressor gene network in acute T-cell lymphoblastic leukemia (T-ALL)

Konstantinos J Mavrakis, Joni Van Der Meulen, Andrew L Wolfe, Xiaoping Liu, Evelien Mets, Tom Taghon, Aly A Khan, Manu Setti, Pieter Rondou, Peter Vandenberghe, Eric Delabesse, Yves Benoit, Nicholas B Socci, Christina S Leslie, Pieter Van Vlierberghe, Frank Speleman & Hans-Guido Wendel

***Nat. Genet.* 43, 673–678 (2011); published online 5 June; corrected after print 11 July 2011**

In the version of this article initially published, the name of author Manu Setty was incorrectly spelled as Manu Setti. The error has been corrected in the HTML and PDF versions of the article.

a

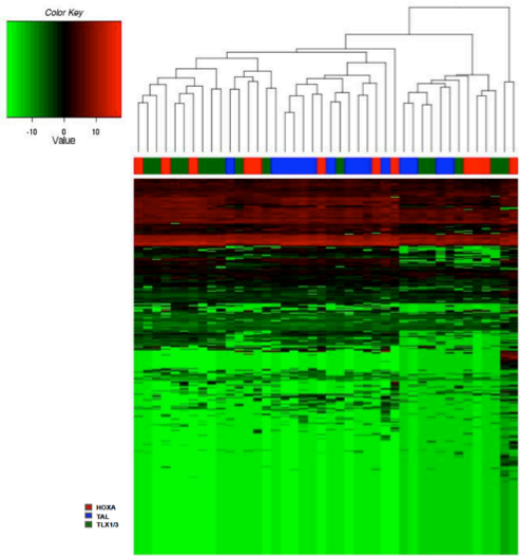

b

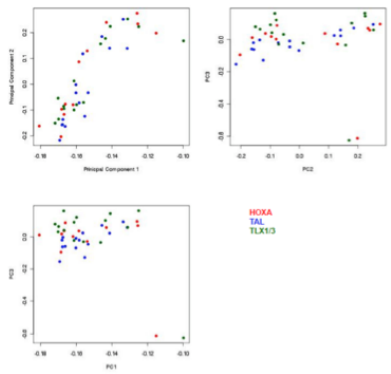

c

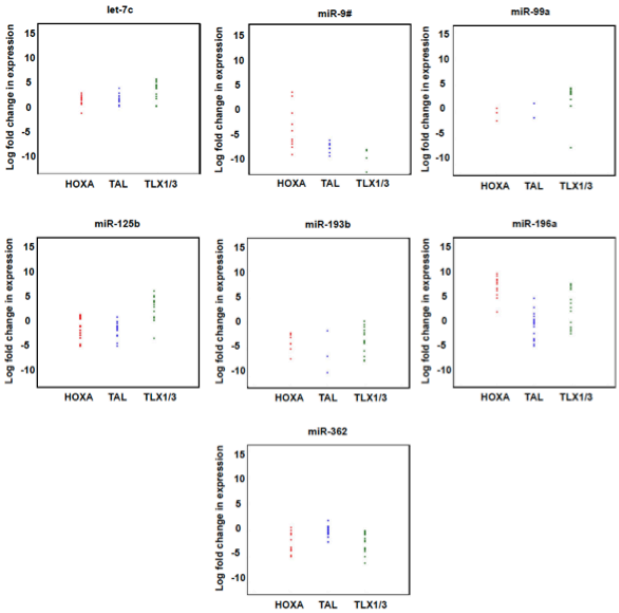

Suppl. Figure 1 Analysis of miRNA expression and its association with cytogenetic subgroups. a, Hierarchical clustering of miRNA expression analysis of HOXA, TAL and TNX1/3 subgroups. Unsupervised clustering does not recover the cytogenetic subgroups (Red-HOXA, Blue-TAL, Green-TLX1/3); **b,** Principle component analysis (PCA) of miRNA expression in cytogenetic subgroups. PCA by the three main components separates normal from leukemia samples (not shown), but does not separate the cytogenetic subgroups (Red-HOXA, Blue-TAL, Green-TLX1/3); **c,** Differentially expressed miRNA between cytogenetic subgroups. In a pair wise comparison miR-125b, miR-153, miR-196a and miR-196b show significantly different expression between subgroups ($p < 0.05$). (Red-HOXA, Blue-TAL, Green-TLX1/3).

Nature Genetics: doi.10.1038/ng.858

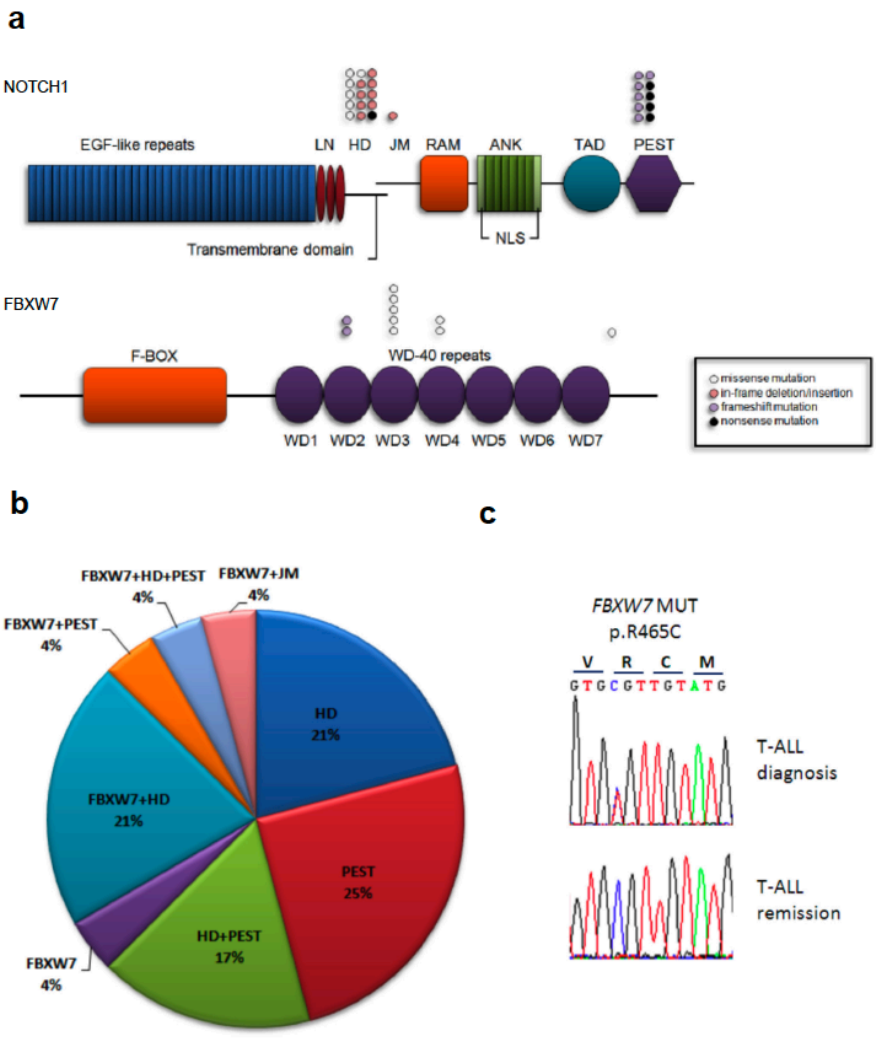

Suppl. Figure 2 **Sequence analysis of *NOTCH1* and *FBXW7* in 37 human T-ALL samples.** **a,** Diagram of *NOTCH1* and *FBXW7* indicating domain structure and sites of mutations; **b,** Relative frequency of *NOTCH1* and *FBXW7* mutations. Note that in our series *NOTCH1* PEST domain and *FBXW7* mutations are not mutually exclusive; **c,** Example of a new *FBXW7* mutation in diagnosis and not a remission sample.

Nature Genetics: doi.10.1038/ng.858

a

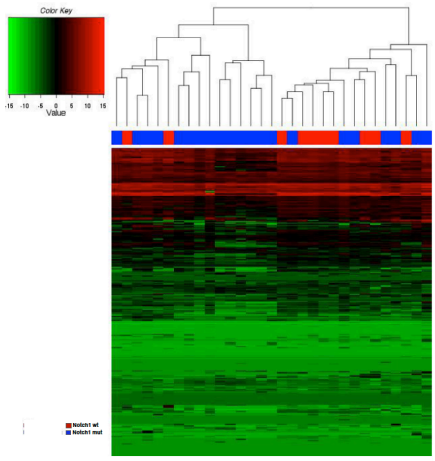

d

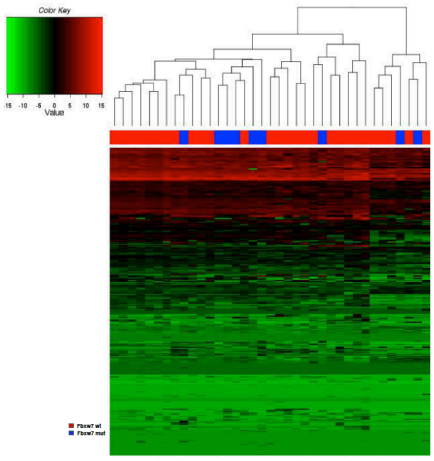

b

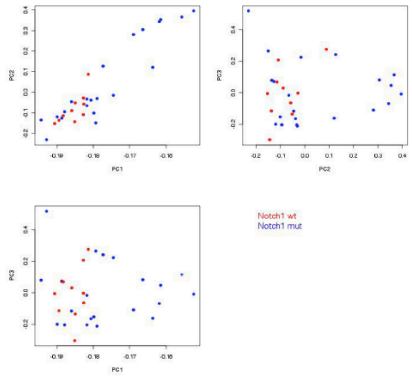

e

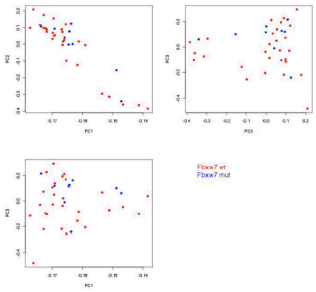

c

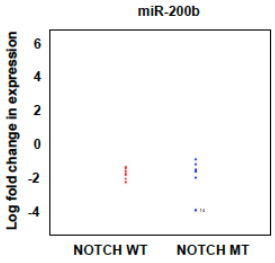

f

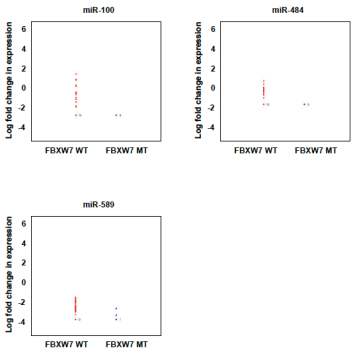

Nature Genetics: doi.10.1038/ng.858

Suppl. Figure 3 Association of miRNA expression and Notch or Fbxw7 mutations. a, Hierarchical clustering of miRNA expression analysis of *NOTCH1* wild type and mutant cases. Unsupervised clustering produces a grouping of cases by *NOTCH1* status, although 7 wild type cases cluster with the mutant group. (Red-NOTCH MT, Blue-NOTCH WT). **b**, Principle component analysis (PCA) of miRNA expression by *NOTCH1* mutation status. The three plots show the pair wise comparisons of the first three principal components. (Red-NOTCH MT, Blue-NOTCH WT); **c,** Differential expression of miR-200b between *NOTCH1* wild type and mutant cases. Only miR-200b is significantly different ($p < 0.05$). (Red-NOTCH MT, Blue-NOTCH WT); **d,** Hierarchical clustering of miRNA expression analysis by *FBXW7* status. Unsupervised clustering does not recover the groups based on *FBXW7* status. (Red-FBXW7 MT, Blue-FBXW7 WT); **e,** Principle component analysis (PCA) of miRNA expression by *FBXW7* status. PCA does not separate the subgroups. (Red-FBXW7 MT, Blue-FBXW7 WT); **f,** Differentially expressed miRNA by *FBXW7* status. In a pair wise comparison miR-100, miR-484, and miR-589 show significantly different expression between wild type and mutant cases ($p < 0.05$). (Red-FBXW7 MT, Blue-FBXW7 WT).

Nature Genetics: doi.10.1038/ng.858

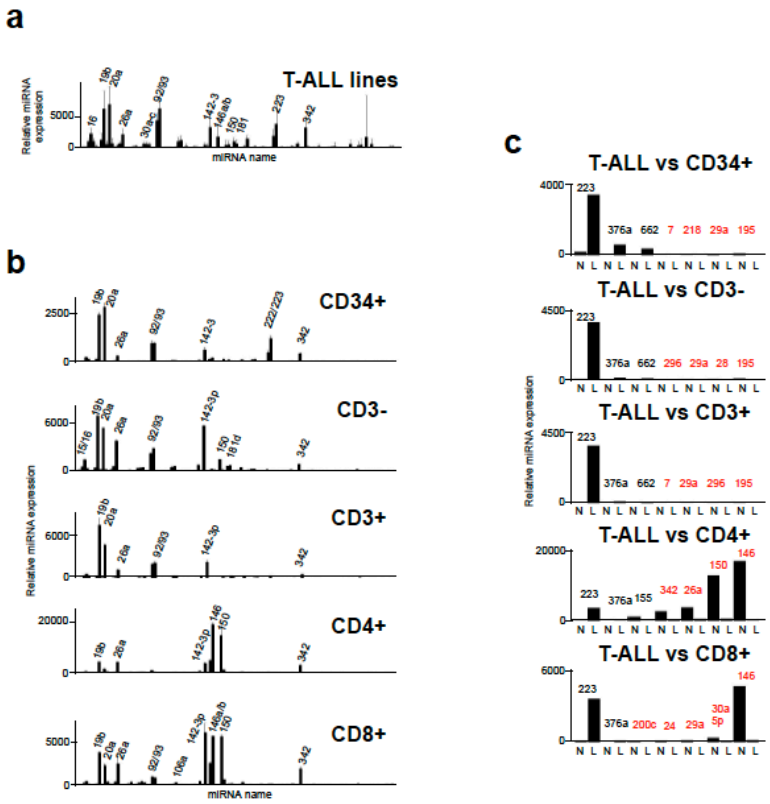

Suppl. Figure 4 **MiRNA expression analyses. a,** qRT-PCR measurement of miRNA expression in 18 human T-ALL cell lines (shown are mean and SD); **b,** qRT-PCR measurement of miRNA expression in FACS sorted normal cell populations (shown are mean and SD of two replicate profilings on one sample); **c,** Differential miRNA expression comparing the average value across all human T-ALL samples (L) to the indicated normal cell populations (N). Shown are only miRNAs with a fold change difference > 5 and detectable expression (relative value > 50) in either normal or leukemic sample; black numbers indicate higher expression in leukemic cells, red numbers indicate higher expression in normal cells.

Nature Genetics: doi.10.1038/ng.858

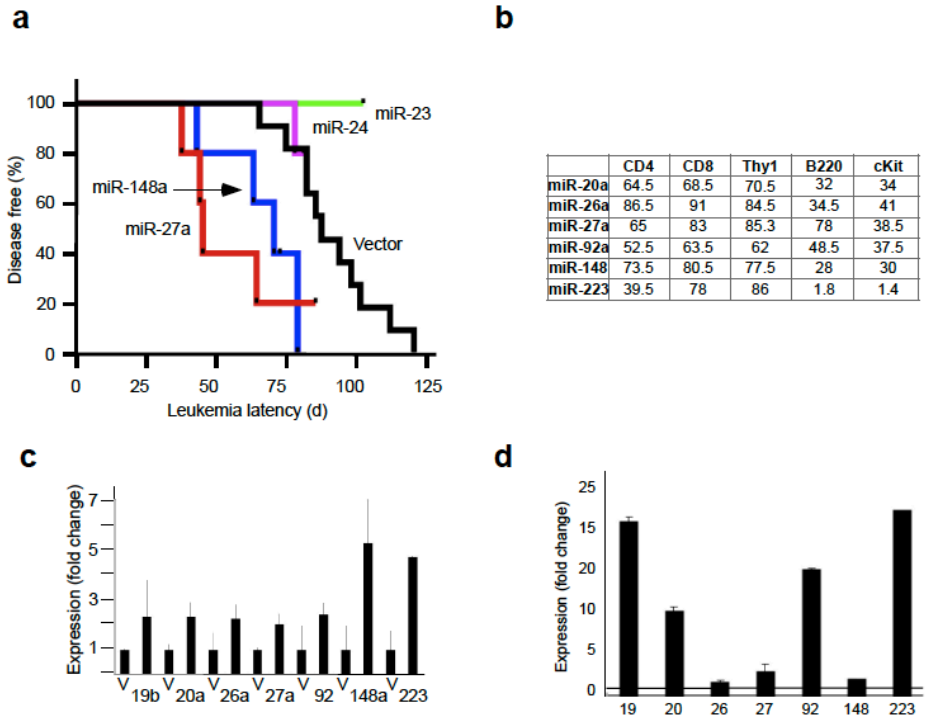

	CD4	CD8	Thy1	B220	cKit
miR-20a	64.5	68.5	70.5	32	34
miR-26a	86.5	91	84.5	34.5	41
miR-27a	65	83	85.3	78	38.5
miR-92a	52.5	63.5	62	48.5	37.5
miR-148	73.5	80.5	77.5	28	30
miR-223	39.5	78	86	1.8	1.4

Suppl. Figure 5 **Candidate miRNAs act as oncogenes in a murine T-ALL model. a,** Kaplan-Meier analysis of leukemia free survival after transplantation of HPCs expressing *NOTCH1-ICN* and vector (black, n=13), or miR-27a (red, n=5; $p < 0.05$ compared to vector), miR-24 (magenta, n=5; $p = 0.5$), miR-23a (green, n=5; $p < 0.05$), miR-148a (blue, n=7; $p < 0.05$); **b,** Analysis of surface marker expression on murine T-ALLs, indicated is the percentage of cells staining positive for the indicated marker; **c**, qRT-PCR measurement of miRNA expression in murine leukemic cells expressing the indicated miRNA compared to leukemias arising in vector controls; **d,** qRT-PCR measurement of miRNA expression in murine leukemic cells expressing the indicated miRNA compared to murine thymocytes.

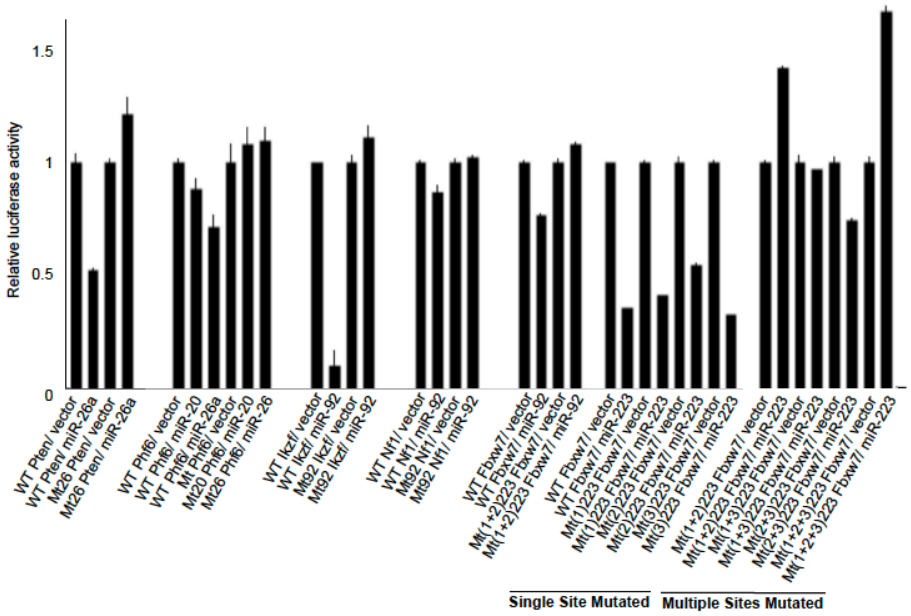

Suppl. Figure 6 **Reporter assay for 3'UTR repression**. Inhibition of the 3'UTR by the indicated miRNA compared to vector as mean +/- SD ratio of Renilla to Firefly luciferase activity (RLuc/Luc). Shown are effects of the indicated miRNAs on wild type (WT) and mutated (Mt) miRNA 3'UTR binding sites of *Pten, Phf6, Ikzf, Nf1, Fbxw7*. The *Ikzf* Mt 3'UTR is truncated and missing the miR-92 site, and in the case of *Fbxw7* we mutated single and combinations of all three binding sites for miR-223 (labelled Mt1-3).

Nature Genetics: doi.10.1038/ng.858

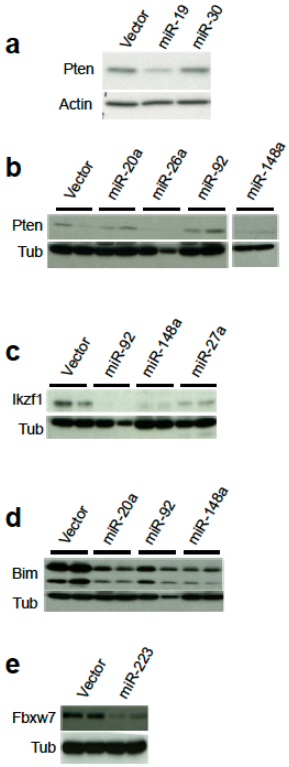

Suppl. Fig. 7 **MiRNAs affect the expression of several tumor suppressor genes in murine FL5-12 cells. a-e,** Lysates of GFP-sorted FL5-12 cells expressing either empty vector or the indicated miRNA were probed for the indicated proteins.

Nature Genetics: doi.10.1038/ng.858

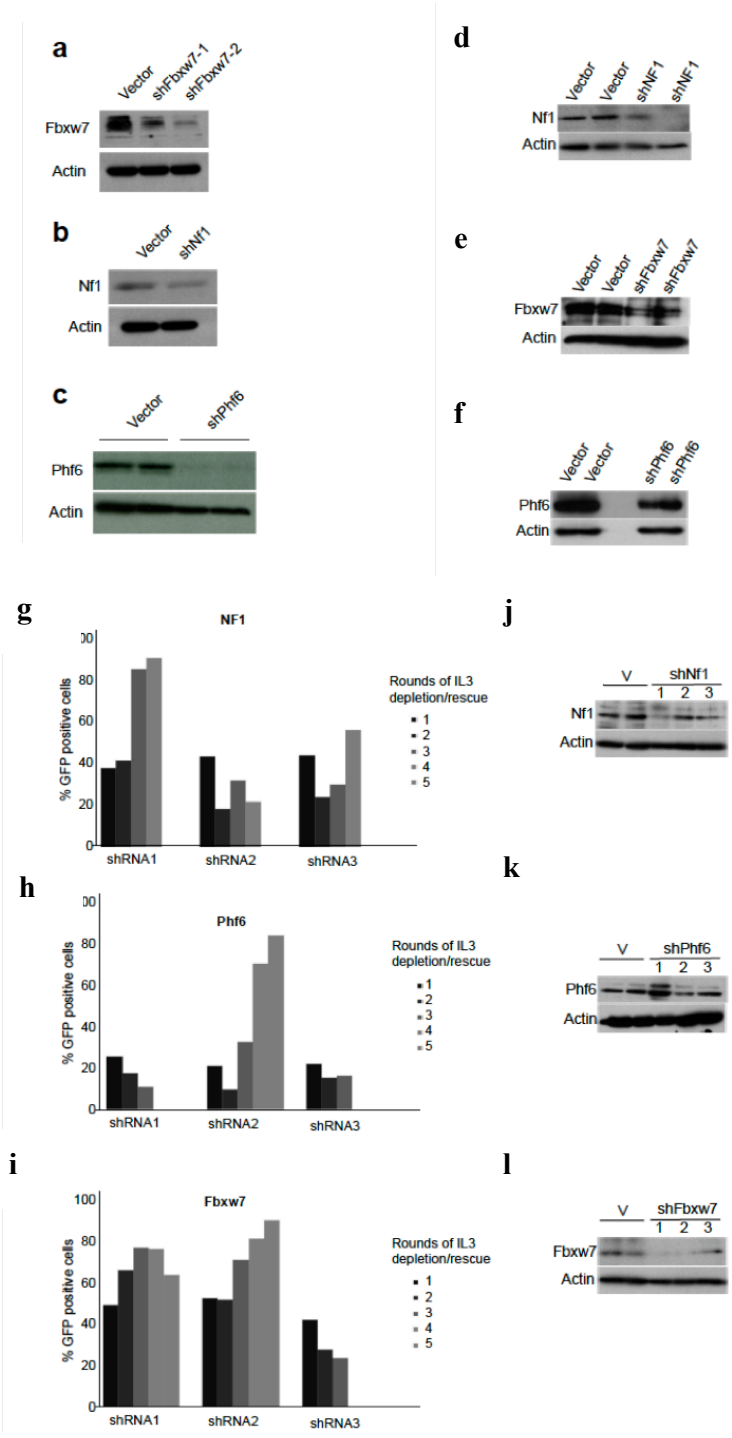

Nature Genetics: doi.10.1038/ng.858

m

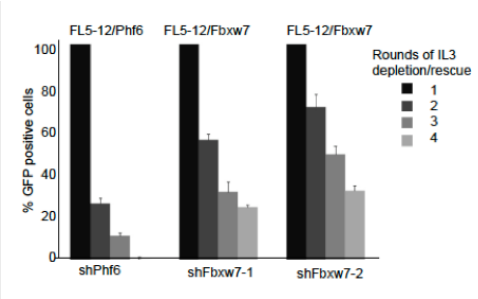

Suppl. Figure 8 **shRNA validation and control experiments; a-c,** Protein knockdown by shRNAs in FL5-12 cells. Lysates of GFP-sorted FL5-12 cells expressing either empty vector or the indicated shRNAs were probed for the indicated proteins; **d-f**, Protein knockdown by shRNAs in murine leukemias expressing the shRNAs or vector. Lysates of murine leukemic cells expressing either empty vector or the indicated shRNAs were probed for the indicated proteins; **g, I, k,** Evaluation of mutiple shRNAs against Nf1, Phf6 and Fbxw7. Enrichment of shRNA and GFP expressing FL5-12 cells in subsequent rounds of IL3 depletion and rescue by addition of IL3; **h, j l,** corresponding immunoblots on lysates of shRNA expressing FL5-12 cells probed as indicated; **m,** Reversion of shRNA effect by cDNA expression. Expression of indicated cDNAs reverses the protective effect of shRNAs and causes a negative selection (loss of cDNA expressing cells) upon IL-3 depletion.

Nature Genetics: doi.10.1038/ng.858

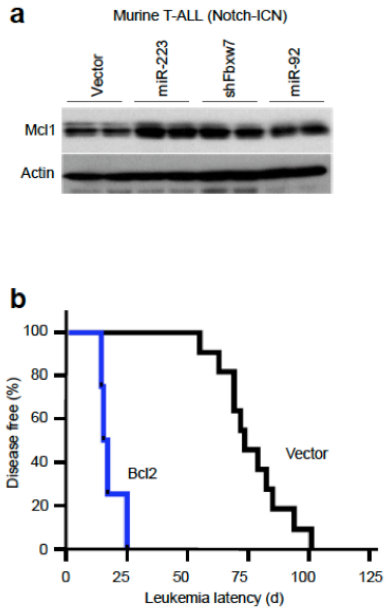

Suppl. Fig. 9 **Deregulation of Mcl1 in miR-223 and miR-92 expressing murine leukemias. a)** Immunoblot on lysates from *Notch1*-driven leukemias that express the indicated miRNAs or shRNA; **b)** *Bcl2* (blue; n = 4) cooperates with *Notch1-ICN* in murine leukemogenesis compared to *Notch1-ICN/* vector (black, n = 13; $p < 0.001$).

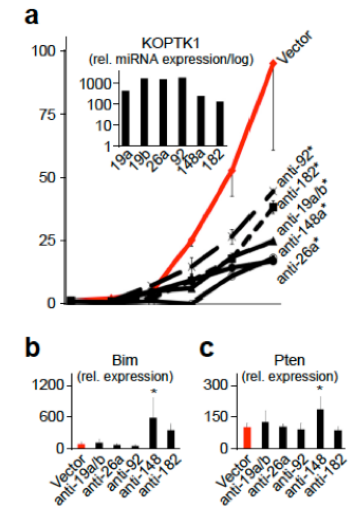

Suppl. Figure 10 **Antagomir studies in the human KOPTK1 T-ALL cell line. a,** Cell number during in vitro culture of KOPTK1 cells expressing the indicated antagomirs (shown are mean and SD for each time point, *indicates significant ($p < 0.05$) growth delay; **b**, and **c**, qRT-PCR of *Bim* (b) and *Pten* (c) mRNA levels in KOPTK1 cells expressing the indicated antagomirs (mean and SD, * is $p < 0.05$ compared to vector).

Nature Genetics: doi.10.1038/ng.858

Suppl. Table 2) Comparison of miRNA expression between cytogentic subgroups (only significant differences are shown)

	p-value	HOXA mean	Other mean	TAL mean
hsa-mir-125b	0.0124	-2.2938	2.1695	-1.819
hsa-mir-153	0.0076	-5.4164	-5.5594	-9.1937
hsa-mir-196a	0.0045	7.1794	3.3939	-0.7036
hsa-mir-196b	0.0045	7.2014	3.3183	-0.7178

Nature Genetics: doi.10.1038/ng.858

Suppl. Table 3) Mutation analysis for NOTCH1 and FBXW7 in human T-ALL samples

ID	Age	Gender	Genetic subtype	*NOTCH1* mutation			*FBXW7* mutation		
				Nucleotide change	*Predicted protein lesion*	*Domain*	*Nucleotide change*	*Predicted protein lesion*	*Domain*
1	16	M	Unknown	c.4737G_4738CinsGTG	p.V1579_L1580insV	HD	c.1393C>T c.2065C>T	p.R465C p.R689W	WD3
2	29	M	HOXA (inv(7))	c.4802T>C	p.L1601P	HD	c.1393C>T	p.R465C	WD3
3	11	M	TLX3	c.7510C>T	p.Q2504*	PEST	c.[1318delGATCGGACAC; 1317_1318insCACCT]	p.D440fs*30	WD2
4	8	M	Unknown	c.5229C_5230GinsAGATTCCCTTATGGGACC	p.A1743_A1744insRFPYGT	JM	c.1513C>T	p.R505C	WD4
5	16	M	TAL/LMO (LMO2)	c.4858_4864TACTACG>CCCGTCC	p.1620_1622YYG>PDR	HD	c.1513C>T	p.R505C	WD4
6	13	F	Unknown	c.7504C>T	p.Q2502*	PEST	c.1270_1271insGGAG	p.V424fs*14	WD2
				c.5036T>C	p.L1679P	HD	-		
7	3	F	Unknown	c.4748_4749insCCCCCCTTATAC	p.P1583_E1584insPPYT	HD	c.1436G>A	p.R479Q	WD3
8	2	F	Unknown	c.[4749_4752delGGAG; 4748_4749insC]	p.E1584del	HD	c.1436G>A	p.R479Q	WD3
9	11	M	HOXA (inv(7))	-			c.1436G>A	p.R479Q	WD3
10	14	F	TAL/LMO (LMO2)	c.4732_4737delGTGGTG	p.V1578_V1579del	HD	-		
				c.7462C>T	p.Q2488*	PEST			
11	5	F	HOXA (CALM-AF10)	c. [7545_7548delTGAG; 7545_7546insCTTT;7552_7553insGAGC]	p.[E2516F;P2518fs*3]	PEST	-		
12	4	M	TAL/LMO (SIL-TAL)	c.7331_7332insCG	p.V2444fs*35	PEST	-		
13	16	M	TLX3	c.7318delG	p.P2439fs*39	PEST	-		
				c.4728_4729insTTTCTCTTG	p.V1576_V1577insFLL	HD	-		
14	7	M	TLX3	c.7563G>A	p.W2521*	PEST			
15	18	F	TAL/LMO (LMO2)	c.[7372delC; 7372_7374insGGT]	p.L2458fs*21	PEST	-		
				c.4802T>C	p.L1601P	HD	-		
16	3	M	TAL/LMO (SIL-TAL)	c.7393delC	p.L2465fs*13	PEST			
17	17	M	TAL/LMO (LMO2)	c.7462C>T	p.Q2488*	HD	-		
18	12	M	TAL/LMO (LMO2)	c.4821_4822insGGATTC	p.F1607>LDS	HD	-		
19	8	M	TLX3	c.4802T>C	p.L1601P	HD	-		
20	4	M	TLX1	c.4781T>C	p.L1594P	HD	-		
21	7	M	TAL/LMO (SIL-TAL)	c.4782_4783insCCC	p.L1594_R1595insP	HD	-		
22	6	M	TLX1	c.4802T>A	p.L1601Q	HD	-		
23	1	F	HOXA (MLL)	-			-		
24	16	M	HOXA (MLL)	-			-		
25	3	M	TAL/LMO (LMO2)	-			-		
26	5	M	TAL/LMO (LMO2)	-			-		
27	16	M	TAL/LMO (SIL-TAL)	-			-		
28	14	M	TAL/LMO (SIL-TAL)	-			-		
29	9	F	TAL/LMO (SIL-TAL)	-			-		
30	13	M	TAL/LMO (SIL-TAL)	-			-		
31	4	M	TLX3	-			-		
32	6	M	TLX3	-			-		
33	9	M	TLX1	-			-		
34	22	F	TLX1	-			-		
35	13	M	Unknown	-			-		
36	14	F	Unknown	-			-		
37	6	M	Unknown	-			-		

Nature Genetics: doi.10.1038/ng.858

Suppl. Table 4) Differential microRNA expression by FBXW7 and NOTCH mutation status in T-ALL patient samples

1. Fbxw7 wild type versus Fbxw7 mutant.

microRNA	p-value	mutant mean exp	wt mean exp
miR-100	0.0143	-5.718	-2.6865
miR-484	7.00E-04	-3.369	-1.307
miR-589	0.0363	-7.3454	-5.467

2. Notch1 wild type versus Notch1 mutant

microRNA	p-value	mutant mean exp	wt mean exp
miR-200b	0.0143	-6.4442	-3.3669

Nature Genetics: doi.10.1038/ng.858

Suppl. Table 6) Differential microRNA expression by mutation status in T-ALL cell lines

1. Fbxw7 wild type versus Fbxw7 mutant: No significant differences.
2. Notch1 wild type versus Notch1 mutant H: No significant differences.
3. Notch1 wild type versus Notch1 mutant (any).

microRNA	p-value	mutant mean exp	wt mean exp
miR-449b	0.0339	-8.1629	-4.7352

4. NCID Status: No significant differences
5. Pten wild type versus Pten mutant: No significant differences.
6. GSI S/R: No significant differences.
7. Phf6 wild type versus Phf6 mutant.

microRNA	p-value	mutant mean exp	wt mean exp
miR-125b	0.0339	3.6653	-5.5518

Nature Genetics: doi.10.1038/ng.858

Suppl. Table 10) Results of primary screen: Myc-induced apoptosis in MEFs

MicroRNA	# sequences	% of sequences
miR-30	10	9.803921569
let7	9	8.823529412
miR-34	9	8.823529412
miR-25	6	5.882352941
miR-148	5	4.901960784
miR-19b	4	3.921568627
miR-223	4	3.921568627
miR-125/351	4	3.921568627
miR-23	4	3.921568627
miR-21	2	1.960784314
miR-22	2	1.960784314
miR-106	2	1.960784314
miR-138	2	1.960784314
miR-146	2	1.960784314
miR-154	2	1.960784314
miR-217	2	1.960784314
miR-101	2	1.960784314
miR-221	2	1.960784314
miR-7	1	0.980392157
miR-9	1	0.980392157
miR-16	1	0.980392157
miR-99	1	0.980392157
miR-100	1	0.980392157
miR-103	1	0.980392157
miR-122	1	0.980392157
miR-124	1	0.980392157
miR-128	1	0.980392157
miR-135	1	0.980392157
miR-136	1	0.980392157
miR-140	1	0.980392157
miR-150	1	0.980392157
miR-181	1	0.980392157
miR-189	1	0.980392157
miR-196	1	0.980392157
miR-200	1	0.980392157
miR-201	1	0.980392157
miR-206	1	0.980392157
miR-211	1	0.980392157
miR-295	1	0.980392157
miR-302	1	0.980392157
miR-322	1	0.980392157
miR-325	1	0.980392157
miR-328	1	0.980392157
miR-339	1	0.980392157
miR-337	1	0.980392157
miR371	1	0.980392157
miR-27	1	0.980392157

Nature Genetics: doi.10.1038/ng.858

Suppl. Table 11) Result of secondary screen

	Sequences
miR-148/152	32
miR-34a	20
miR-19b	8
miR-223	8
mi-30	4
miR-320	4
miR-9	4
miR-96	4
miR-25/32/92	3
miR-20/106	2
miR-26	1
miR-23	1
miR-24	1
miR-27	1
miR-101	1
miR-128	1
miR-15	1
miR-16	1
miR-181c	1
miR-200	1
miR-221	1
miR-137	1
miR-217	1
miR-22	1
miR-182	1

Nature Genetics: doi.10.1038/ng.858

Suppl. Table 12) Surface marker analysis on murine leukemias

			Marker		
Tumor	CD4	CD8	Thy-1	C-Kit	B220
27a-1	64	83	83.6	77	34
27a-2	66	83	87	79	43
mean	65	83	85.3	78	38.5
sdev	1.414213562	0	2.404163056	1.414213562	6.363961031
92a-1	69	83.3	86	78	52
92a-2	36	44	38	19.2	23
mean	52.5	63.65	62	48.6	37.5
sdev	23.33452378	27.7892965	33.9411255	41.57787873	20.50609665
20a	57	53	66	10	15
20a-2	72	84	75	54	53
	64.5	68.5	70.5	32	34
sdev	10.60660172	21.92031022	6.363961031	31.11269837	26.87005769
26a	81	86	87	7	30
26a-2	92	96	82	62.1	52
mean	86.5	91	84.5	34.55	41
sdev	7.778174593	7.071067812	3.535533906	38.96158364	15.55634919
148a	68	76	72	21	40
148a-2	79	85	83	35	20
mean	73.5	80.5	77.5	28	30
sdev	7.778174593	6.363961031	7.778174593	9.899494937	14.14213562
223-1	50.24	70.48	78.46	1.71	2.02
223-2	28.85	85.77	93.43	1.97	0.72
mean	39.545	78.125	85.945	1.84	1.37
sdev	15.12501405	10.81166268	10.58538851	0.183847763	0.919238816
19b-1	81.98	65	99.97	1.1	11.38
19b-2	97.46	80.7	99.32	1.83	13.16
mean	89.72	72.85	99.645	1.465	12.27
sdev	10.94601297	11.10157646	0.459619408	0.51618795	1.258650071
Vector-1	49.98	82.62	85.08	1.98	76.66
Vector-2	86.83	94.72	76.92	1.2	12.44
mean	68.405	88.67	81	1.59	44.55
sdev	26.05688489	8.555992052	5.769991334	0.551543289	45.41039749

Nature Genetics: doi.10.1038/ng.858

Suppl. Table 13) Results of an unbiased machine learning approach to identify target genes that discriminate oncogenic and non-oncogenic miRNAs.

Lasso regression was run 50 times comparing experimentally confirmed oncomirs to randomly selected groups of 30 miRNAs that did not pass the screen.
The number of non-zero coefficients indicates how often (out of 50 runs) the gene was identified in this analysis.
The Mean coefficient is the actual coefficient for each gene; a coeeficient >0 implies positive association with the oncomir group.

Gene	No. of non zero coefficients	Mean coefficient
FBXW7	46	0.2919
CHIC1	36	0.1114
MAP3K2	31	0.0566
ABL2	30	0.0725
SNN	29	0.0815
BIM	21	0.0707
MED12L	20	0.0728
BBX	19	0.0733
ANKIB1	18	0.0422
PPARA	12	0.0274
PTEN	11	0.0587
SLC8A1	11	0.031
DMXL1	11	0.0271
PTPRD	10	0.0306
DCP2	8	0.0067
LPP	7	0.0152
CREB1	6	0.006
MKL2	5	0.0054
MFHAS1	5	0.0122
EIF2C1	5	0.0138
TNRC6B	5	0.006
FBXL17	4	-0.006
NFIC	3	-0.0022
STRBP	3	-0.004
TULP3	3	-4.00E-04
NUFIP2	3	0.0103
RAP2C	2	0.0041
ADCY1	2	3.00E-04
PPP1R9A	2	9.00E-04
CELF2	2	-0.0164
SLC24A2	2	2.00E-04
FAM53C	2	-9.00E-04
SCAI	2	-0.0012
PRX	2	-0.0014
FUT9	2	1.00E-04
STEAP2	2	-2.00E-04
TARDBP	2	-3.00E-04
MYLK4	2	-5.00E-04
PLXNA4	2	-0.0037
WASL	2	8.00E-04
DOCK5	1	0
HIF3A	1	-0.0012
ANKRD45	1	0
AAK1	1	9.00E-04
WNK3	1	0
TMEM170B	1	-9.00E-04
RFNG	1	-0.0032
TBL1XR1	1	0
ATXN1L	1	0.0021
MDGA2	1	-4.00E-04
YWHAZ	1	-4.00E-04
SP1	1	-0.0011
CBX5	1	-3.00E-04
CLMN	1	-0.0021
SPAG9	1	-0.0018
DENND5B	1	1.00E-04
GNAO1	1	-4.00E-04
CLOCK	1	0.0053
SYNJ2BP	1	-3.00E-04
ONECUT2	1	-4.00E-04
KRAS	1	-0.0038
TET3	1	-0.0012
MAN2A1	1	5.00E-04
SH3PXD2B	1	-2.00E-04
UNC5C	1	0
CYYR1	1	-2.00E-04
LAPTM5	1	-1.00E-04
OTUD7B	1	-0.0015
CDC14B	1	0
TBX22	1	-1.00E-04
QSER1	1	1.00E-04
FRS2	1	5.00E-04

Nature Genetics: doi.10.1038/ng.858

FZD5	1	-0.0017
PRTG	1	-0.0012
NEURL1B	1	0.006
TLN2	1	-1.00E-04
HOOK3	1	-4.00E-04
GPM6B	1	-6.00E-04
CACNB4	1	0
AKAP13	1	-2.00E-04
SYNPO	1	-3.00E-04
RUFY2	1	0
STXBP5L	1	-0.0011
XPO7	1	0
RASAL2	1	-9.00E-04
RGS17	1	0
SRF	1	-7.00E-04
PTPN2	1	0
TMF1	1	0
SHISA7	1	-6.00E-04
PGR	1	0
PHIP	1	6.00E-04
DENND1B	1	0.0074
ZYG11B	1	-2.00E-04
BTBD3	1	-6.00E-04
ZBTB41	1	0
SLC1A2	1	0.0012
ARIH1	1	-1.00E-04
INO80D	1	0.0036
SHISA6	1	0
PAPPA	1	-7.00E-04
RAP1GAP2	1	-5.00E-04
CDS1	1	1.00E-04
PACS1	1	0
DNM3	1	-6.00E-04
ARRB1	1	-4.00E-04
NUCKS1	1	-3.00E-04
NAV1	1	-0.0022
AMOTL1	1	-6.00E-04
PRKCA	1	-0.002

Suppl. Table 14) Primers used to generate 3'UTR fragments

UTR	Primer Sequence Forward	Primer Sequence Reverse
Bim	5'-GATCTCGAGTAAAGTGACTTCACCTC-3'	5'-ATGCGGCCGCTTTTAGTCGCAAGTTT-3'
fbxw7	5'-GATCTCGAGGTGATGAGGGGCAGCTT-3'	5'-ATGCGGCCGCCACCTTAAGTTATAAG-3'
PHF6	5'-CCGCTCGAGCCTTTTTCTGCCACTAGCAAC-3'	5'-CGACTGCGGCCGCATGAGAGGAATGTTTGATTTTTGAC-3'
NF1	5'-CCGCTCGAGGGTTATATATGCTAGAATTGCATTTAA-3'	5'-CGACTGCGGCCGCAAGTTTAGTAAATTGCACCTGTCTTC-3'

Primers Used for Site-Directed Mutagenesis of 3'UTR miRNA binding sites

PHF6-miR-20a site	5'-CTGCCACTAGCAACCAGAATAGCACTTTACCTTTTGGTTGGCTAGATAAG-3'
PHF6-miR-26a site	5'-CTATTGAATCAGAATCTGTGGATGGGAACAAATGTGTGAATCTC-3'
NF1-miR-92a site	5'-GTTGGAAATACTGAAGACAGTTTAGATTTACTAAACTTTTG-3'
FBXW7-miR-92a site 1	5'-TGAGACTTTCTAAATCAAACCAGTTTAGATTATTTCTTTATTTTCTTCTCCAGTG-3'
FBXW7-miR-92a site 2	5'-ATTTTCTTATAACTTAATTTTGATAAAATGTGTTTTTTC-3'

Hairpin	stem-loop Sequence
Nf1	5'-CACCTTTGTTTGGAATATA-3'
Fbxw7	5'-CACGTTAGAATCTGTGACATA-3'
PHF6	5'-TTTCTTACTAACATTTCTGGT-3'

Nature Genetics: doi.10.1038/ng.858

Suppl. Table 15) Mutagenesis of 3'UTR miRNA binding sites

PHF6 mir-20a binding site
Position 2330-2336 of PHF6 3' UTR

```
                          T  GTG
                          X  XXX
5'  ...CUAGCAACCAGAAUAGCACUUUA...-Phf6 3'UTR
                          |||||||
3'     GAUGGACGUGAUAUUCGUGAAAU  -miR-20a
```

PHF6 mir-26a binding site
Position 3152-3158 of PHF6 3' UTR

```
                          G  TGG
                          X  XXX
5'  ...GAAUCAGAAUCUGUGUACUUGAA...-Phf6 3'UTR
                          |||||||
3'      UCGGAUAGGACCUAAUGAACUU   -miR-26a
```

NF1 miR-92a binding site
Position 1810-1816 of NF1 3' TTR

```
                          T  TAG
                          X  XXX
5' ...AAATACTGAAGACAGGTGCAATT...  -NF1 3'UTR
                          |||||||
3'     TGTCCGGCCCTGTTCACGTTAT     -miR-92a
```

FBXW7 miR-92a binding site
Position 285-291 of FBXW7 3' UTR

```
                          T  TTG
                          X  XXX
5' ...TCTAAATCAAACCAGGTGCAATT...  -FBXW7 3'UTR
                          |||||||
3'     TGTCCGGCCCTGTTCACGTTAT     -miR-92a
```

Nature Genetics: doi.10.1038/ng.858

FBXW7 miR-92a binding site
Position 1595-1601 of FBXW7 3' UTR

```
                          T  TTG
                          X  XXX
5' ...TTTCTTATAACTTAAGTGCAATA...   -FBXW7 3'UTR
                          |||||||
3'    TGTCCGGCCCTGTTCACGTTAT      -miR-92a
```

FBXW7 miR-223 binding site 1
Position 189-195 of FBXW7 3' UTR

```
                          C  GT
                          X  XX
5' ...GAGAUGACAAACCAUAACUGACA... -FBXW7 3'UTR
                          |||||||
3'   ACCCCAUAAACUGUUUGACUGU      -miR-223
```

FBXW7 miR-223 binding site 2
Position 1144-1150 of FBXW7 3' UTR

```
                          C  GT
                          X  XX
5' ...GAACGUACAUCGUAAAACUGACA... -FBXW7 3'UTR
                          |||||||
3'   ACCCCAUAAACUGUUUGACUGU      -miR-223
```

FBXW7 miR-223 binding site 3
Position 1260-1266 of FBXW7 3' UTR

```
                          C  GT
                          X  XX
5'   ...UUUAUUGCUCUGAGUAACUGACA...-FBXW7 3'UTR
                          |||||||
3'     ACCCCAUAAACUGUUUGACUGU     -miR-223
```

Nature Genetics: doi.10.1038/ng.858

Suppl. Table 16

Primer name	Primer sequence	Protein domain
NOTCH1 exon26 F	AGGAAGGCGGCCTGAGCGTGT	Heterodimerization domain (HD) N-terminal
NOTCH1 exon26 R	AGAGTTGCGGGGATTGACCGT	
NOTCH1 exon27 F	GTGGCGTCATGGGCCTCA	HD C-terminal
NOTCH1 exon27 R	GCACAAACAGCCAGCGTGT	
NOTCH1 exon28 F	GATCGGTGTCATGTGAAGT	Juxtamembrane (JM) domain
NOTCH1 exon28 R	TCCCGGTGAGGATGCTCGG	
NOTCH1 exon34a F	CTTCCTCTGGTGATGGAACCT	Transactivation (TAD) domain and proline glutamate serine threonine (PEST) domain
NOTCH1 exon34a R	CATCCCAGGCAGGTGGTTGA	
NOTCH1 exon34b F	GCCCTCCCCGTTCCAGCAGTCT	
NOTCH1 exon34b R	GCCTGGCTCGGCTCTCCACTCA	
NOTCH1 exon34c F	AGCCGCACCTTGGCGTGAGC	
NOTCH1 exon34c R	TGGTCGGCCCTGGCATCCAC	
FBXW7 exon7 F	TTTATGCCTTCATTTTTCTCTT	WD40-repeats
FBXW7 exon7 R	GGGGAAAAAAGCTAAGTTATG	
FBXW7 exon8 F	TTTTCCAGTGTCTGAGAACAT	
FBXW7 exon8 R	CCCAAATTCACCAATAATAGA	
FBXW7 exon9 F	TAAACGTGGGTTTTTTTGTT	
FBXW7 exon9 R	TCAGCAATTTGACAGTGATT	
FBXW7 exon10 F	CCTGGCATTACCTGTTTC	
FBXW7 exon10 R	AGGCTCCATATTTCTCTTGA	
FBXW7 exon11 F	GGACATGGGTTTCTAAATATGTA	
FBXW7 exon11 R	CTGCACCACTGAGAACAAG	

Nature Genetics: doi.10.1038/ng.858

PAPER 4

MicroRNA-193b-3p acts as a tumor suppressor by targeting the *MYB* oncogene in T-cell acute lymphoblastic leukemia

Mets E, Van der Meulen J, Van Peer G, Boice M, Mestdagh P, Van de Walle I, Lammens T, De Moerloose B, Benoit Y, Van Roy N, Clappier E, Poppe B, Vandesompele J, Wendel HG, Taghon T, Rondou P, Soulier J, Van Vlierberghe P & Speleman F. Submitted to Leukemia (April 2014).

MicroRNA-193b-3p acts as a tumor suppressor by targeting the *MYB* oncogene in T-cell acute lymphoblastic leukemia

Evelien Mets[1], Joni Van der Meulen[1], Gert Van Peer[1], Michael Boice[2], Pieter Mestdagh[1], Inge Van de Walle[3], Tim Lammens[4], Barbara De Moerloose[4], Yves Benoit[4], Nadine Van Roy[1], Emmanuelle Clappier[5], Bruce Poppe[1], Jo Vandesompele[1], Hans-Guido Wendel[2], Tom Taghon[3], Pieter Rondou[1], Jean Soulier[5], Pieter Van Vlierberghe[1] and Frank Speleman[1]

[1]Center for Medical Genetics, Ghent University, Ghent, Belgium. [2]Cancer Biology and Genetics, Memorial Sloan-Kettering Cancer Center, New York, USA. [3]Department of Clinical Chemistry, Microbiology and Immunology, Ghent University Hospital, Ghent, Belgium. [4]Department of Pediatric Hematology-Oncology and Stem Cell Transplantation, Ghent University Hospital, Ghent, Belgium. [5]Genome Rearrangements and Cancer Laboratory, U462 INSERM, Laboratoire Central d'Hématologie and Institut Universitaire d'Hématologie, Hôpital Saint-Louis, Paris, France.

Correspondence
Frank Speleman
Center for Medical Genetics Ghent
Ghent University Hospital
Medical Research Building, room 120.032
De Pintelaan 185
9000 Ghent
Belgium
Tel: +32-9-3322451
Fax: +32-9-3326549
franki.speleman@ugent.be

Condensed Title
miR-193b-3p targets MYB in T-cell leukemia

Total number of words
4100 words

Conflict of Interest Statement
No conflicts of interest to declare

Abstract

The *MYB* oncogene is a leucine zipper transcription factor essential for normal and malignant hematopoiesis. In T-cell acute lymphoblastic leukemia (T-ALL), elevated MYB levels can arise directly through T-cell receptor mediated *MYB* translocations, genomic *MYB* duplications or enhanced TAL1 complex binding at the *MYB* locus, or indirectly through the TAL1/miR-223/FBXW7 regulatory axis. In this study, we used an unbiased *MYB* 3'UTR – microRNA library screen and identified 33 putative MYB targeting microRNAs. Subsequently, transcriptome data from two independent T-ALL cohorts and different subsets of normal T-cells were used to select microRNAs with relevance in the context of normal and malignant T-cell transformation. Hereby, miR-193b-3p was identified as a novel *bona fide* tumor suppressor microRNA that targets MYB during malignant T-cell transformation thereby offering an entry point for efficient MYB targeting oriented therapies for human T-ALL.

3-6 keywords

T-ALL, MYB, miR-193b-3p, T-cells

Introduction

T-cell acute lymphoblastic leukemia (T-ALL) is an aggressive hematological malignancy affecting children, adolescents and adults. In T-ALL development, immature thymocytes undergo oncogenic transformation caused by cooperative genetic lesions that affect proliferation, survival and differentiation[1]. Constitutive activation of NOTCH1 signaling, provoked by activating *NOTCH1* mutations[2] or inactivating *FBXW7* aberrations[3], is the most prominent oncogenic pathway in T-ALL pathogenesis. In addition, T-ALL patients often display recurrent translocations, duplications and interstitial deletions resulting in aberrant expression of several transcription factor oncogenes including *MYB*. Illegitimate expression of these transcriptional regulators drives specific gene expression programs that catalogue T-ALL patients in different molecular genetic subgroups[4-6].

The *MYB* proto-oncogene is a leucine zipper transcription factor that is aberrantly activated in a subset of T-ALL patients through a recurrent T-cell receptor mediated translocation t(6;7)(q23;q34) leading to *TCR*β mediated *MYB* overexpression in of cases 7% or somatic duplications in 10-15% of cases[7, 8]. Furthermore, additional mechanisms of MYB activation include direct MYB up regulation by the oncogenic TAL1/GATA3/RUNX1 complex[9] or indirect through the TAL1/miR-223/FBXW7 regulatory axis[10, 11]. In line with this notion, T-ALL patients that show aberrant expression of the *TAL1* oncogene (60%)[4] are characterized by high levels of *MYB* expression[9]. During normal hematopoiesis, MYB plays a major role in directing proliferation, lineage commitment and differentiation[12, 13]. Interestingly, T-cell specific ectopic expression of v-Myb, a truncated and rearranged form of MYB, in transgenic mice gives rise to high grade T-cell lymphomas underscoring the driver role of MYB in normal and malignant T-cell development[14]. Finally, *MYB* is an essential downstream target of homeobox (*HOX*) genes, which serve as critical regulators of normal and malignant hematopoiesis[15].

In the past decades, microRNAs (miRNAs) were identified as a group of small non-coding RNA molecules that negatively regulate gene expression. Sequence complementarity of the seed of the miRNA and the 3'UTR of the target mRNA initiates the formation of the RISC complex leading to mRNA degradation or inhibition of translation[16]. Deregulated miRNA expression is a common feature of human cancers and can be caused by specific chromosomal abnormalities including somatic deletions (for example, miR-15a/miR-16-1 deletions in chronic lymphoblastic leukemia[17] or translocations (for example, *TCR*β-miR-17-92 translocation in T-ALL[18]). Importantly, some of these small RNA molecules have emerged as important players in the control of driver genes implicated in T-ALL[10, 11, 18-20] and might serve as excellent candidates for miRNA-based therapies in the treatment of T-ALL[21].

Thus far, the miRNA regulatory network controlling T-ALL oncogenes has not been extensively studied. Here, we selected the *MYB* proto-oncogene as the first candidate for an in-depth exploration of this miRNA network through an unbiased, high throughput 3'UTR - miRNA library screen and subsequent analyses of miRNA-mRNA correlation data during normal T-cell differentiation and in primary T-ALL patient samples. Using this unique integrative approach and subsequent *in vitro* and *in vivo* validation, we identified miR-193b-3p as a *bona fide* T-ALL tumor suppressor miRNA, targeting MYB.

Materials and methods

MicroRNA profiling of T-ALL patient samples and normal T-cell subsets

MicroRNA profiling (430 miRNAs) was performed on a T-ALL patient cohort of 50 primary patient samples (15 *TAL/LMO,* 15 *TLX1/TLX3, 12 HOXA* and 8 cases could not be categorized) and on 5 normal thymocyte subsets ($CD34^+$, $CD4^+CD8^+CD3^-$, $CD4^+CD8^+CD3^+$, $CD4^+$, $CD8^+$). This miRNA dataset was reported before, for a detailed description of the miRNA profiling protocol, we refer to Mavrakis et al[19]. This study (2008/531) was approved by the Medical Ethical Commission of Ghent University Hospital (Belgium, registration B67020084745)[19].

In addition, we performed microRNA profiling (755 miRNAs) of a second T-ALL patient cohort of 64 primary patient samples (15 immature, 25 *TAL/LMO*, 17 *TLX1/TLX3* and 7 *HOXA*). These patient samples were previously investigated in a study of Clappier et al.[22]. The samples were collected with informed consent according to the declaration of Helsinki from Saint-Louis Hospital (Paris, France) and the study was approved by the Institut Universitaire d'Hematologie Institutional Review Board.

Transcriptome profiling of T-ALL patient samples

On the cohort of 64 primary T-ALL patient samples, gene expression analysis was performed. Briefly, RNA quality was evaluated on the Agilent 2100 bioanalyzer (Agilent Technologies, Santa Clara, CA, USA). Next, transcriptome profiling was performed on GeneChip Human Genome U133 2.0 Plus arrays (Affymetrix, Santa Clara, CA, USA) according to standardized procedures at the IGBMC (www.igbmc.fr, Strasbourg, France). Normalization of the gene expression profiles was done using the variance stabilization and calibration (VSN) R package[23]. Correlation analysis was performed using the Spearman rank correlation analysis in R statistical programming environment (version 3.0.1). Microarray data files are available from ArrayExpress under accession no. E-MTAB-604[22].

MYB 3'UTR-miRNA library screen

Twenty-four hours after seeding, HEK-293T cells (10 000 cells/well in 96-well plates) were transfected with a pRL-TK control vector (20 ng) containing *Renilla* luciferase (Promega, Madison, WI, USA) and a reporter vector (100 ng) containing wild-type 3'UTR of *MYB* downstream of *Firefly* luciferase (SwitchGear Genomics, Menlo Park, CA, USA) together with a library of 470 miRNA mimics (2.5 pmol) (Ambion's Pre-miR miRNA Precursor Library - Human V3, design based on miRBase release 9.2 with exclusion of hsa-miR-122a, Life Technologies, Carlsbad, CA, USA) by use of Dharmafect (Dharmacon, Thermo Fisher Scientific, Waltham, MA, USA). After 48h, luciferase activities were measured using the Dual-Luciferase Reporter assay (Promega) on a Fluostar Optima (BMG Labtech, Ortenberg, Germany). For each miRNA a robust Z-score was calculated, which represents the ratio between *Firefly/Renilla* luciferase activities of a specific miRNA subtracted with the median *Firefly/Renilla* value of the 96-well plate. An interaction score was then calculated which represents the robust Z-score of a miRNA subtracted with the median robust Z-score of this miRNA over all the screens that were performed. This screen is part of a large screening effort of 17 known cancer genes (Van Peer et al., manuscript in preparation). Notably, the lower the interaction score, the more likely a miRNA will interact with the 3'UTR of interest. Two criteria were used to determine the cut-off with the highest accuracy using a ROC–curve analysis (cut-off < -1.93, specificity = 99%, sensitivity = 51%) to separate interactions from non-interactions. To perform this ROC-curve analysis, interaction scores were taken

into account of a set of selected miRNA interactions that were validated in literature as well as interaction scores of miRNAs derived from an empty 3'UTR vector miRNA library screen. Our *MYB* 3'UTR-miRNA library screen was performed in duplicate to determine the reproducibility of our screening method.

Single 3'UTR-miRNA reporter gene assays and rescue experiments

To produce a *MYB* 3'UTR mutant vector in which the two 6-mer target sites for miR-193b-3p were mutated, the Site-Directed Mutagenesis Kit (Stratagene, Agilent Technologies) was used according to manufacturer's guidelines.
Primer sequences for mutagenesis:

6mer1 F	GGTAATGAATTGTATCACTTTGTTAATATCTTAATGCAG
6mer1 R	CTGCATTAAGATATTAACAAAGTGATACAATTCATTACC
6mer2 F	CTGTGGTTGATAGTCACTTCACTGCCTTAAG
6mer2 R	CTTAAGGCAGTGAAGTGACTATCAACCACAG

The wild-type or mutant 3'UTR vector of *MYB* (SwitchGear Genomics) and a pRL-TK control vector (Promega) were co-transfected in HEK-293T cells with either a miRNA mimic for miR-193b-3p (PM12383, Ambion) or a scrambled, non-targeting control (NTC) miRNA mimic (AM17111, Ambion), followed by luciferase measurements as described above.

Electroporation of miRNA mimics in T-ALL cell lines

First, 64 x10^6 cells from T-ALL cell lines were suspended in 2 ml RPMI-1640 medium together with the miRNA mimic or NTC (final concentration: 400 nM). Next, 500 µl of each cell suspension was transferred to electroporation tubes followed by electroporation (0.300 kV and 1 mF) with the Gene Pulser II (Bio-Rad Laboratories, Hercules, CA, USA). The cells from 1 electroporation were divided over 4 wells of a 12-well plate and diluted to a final cell suspension of 1.6 x 10^6/ml. Finally, cells were collected for RNA and protein isolation after 24, 48 and 72 hours.

NOTCH1-induced T-ALL mouse model

The institutional and national guide for the care and use of laboratory animals was followed. At embryonic day 13-14, we isolated fetal liver cells with hematopoietic progenitor cells (HPCs) from pregnant mice. Next, we transduced the HPCs with ICN1 (active NOTCH1, co-expression of mCherry) and a vector encoding antagomiR (sequence = AGCGGGACTTTGAGGGCCAGTT) against miR-193b-3p or an empty vector control (co-expressing GFP). After irradiation of mouse recipients, the transduced HPCs were injected using tail vein injection followed by monitoring of leukemia onset. Various tissues were collected at time of leukemia formation and fixed in formaldehyde for immunohistochemistry. Spleen and thymus cells were mashed to single-cell suspensions and frozen in 10% DMSO. RNA and protein lysates were generated from the mouse samples and used for qPCR and western blot analysis. Leukemia onset data was analyzed using the Kaplan-Meier method and the log-rank test for statistical significance.

Immunohistochemistry of mouse leukemias

Tissue-specific samples (kidney, liver, lung and lymph node) of mouse leukemias were washed, paraffin-embedded and sectioned at 5 mm according to standard procedures. Next, sections were stained with hematoxylin and eosin (H&E) or a rabbit polyclonal anti-Ki67 primary antibody (dilution 1/1000, Cell Signaling). Visualization was done using DAB kit

(Dako), analyzed with a BX51 Discussion microscope (Olympus, Shinjuku, Tokyo, Japan) and pictures were taken with a cooled interline CCD camera.

T-test

We identified all differential expressed miRNAs between T-ALL patient samples and normal thymocyte subsets by use of the standard t-test combined with Benjamini-Hochberg multiple testing correction ($p<0.05$). We applied the same t-test to identify all miRNAs that are differential expressed between the TAL subgroup and other T-ALL subgroups ($p<0.05$).

miR-193b-3p nomenclature

Official nomenclature and sequence annotation for miR-193b-3p by the miRBase database (http://www.mirbase.org/) changed a few times during the course of this study. During the time of the 3'UTR high throughput screening effort and the miRNA profiling of cohort 1, miR-193b was annotated in miRbase with the following mature sequence: AACUGGCCCUCAAAGUCCCGCUUU. Before profiling of cohort 2, the sequence of this miRNA changed to AACUGGCCCUCAAAGUCCCGCU but the nomenclature remained unchanged. As the sequence change occurred at the 3' end of the miRNA's sequence, the seed sequence remained unchanged, which likely does not affect the function of miR-193b. At the start of our validation studies, a new miRbase release was published and the nomenclature for miR-193b changed to miR-193b-3p. In this manuscript, we therefore refer to this miRNA by miR-193b-3p according to the latest miRBase release.

Results

Identification of miRNAs targeting MYB using an unbiased MYB 3'UTR – miRNA library screen

Given the oncogenic role of MYB in T-ALL and the relevance of perturbed miRNA signaling in T-cell transformation, we conducted a miRNAome-wide screen to identify novel miRNAs that target the *MYB* proto-oncogene. More specifically, we performed a high-throughput dual luciferase-based *MYB* 3'UTR – miRNA library screen to explore possible interactions between 470 miRNA mimics and the 3'UTR of *MYB* in HEK-293T cells. After co-transfection of the miRNA mimics together with the *MYB* 3'UTR and control vector, we measured the luciferase activities and calculated a miRNA interaction score for each miRNA mimic (see Materials and methods) (Figure 1a). We conducted 2 independent *MYB* 3'UTR library screens to evaluate the reproducibility of our screening method and ensure the reliable identification of positive miRNA hits (Figure 1b, Pearson correlation coefficient r = 0.85). Next, we determined positive hits based upon interaction scores < -1.93, a cut-off that was established based on 3'UTR library screens for 17 known cancer genes (see Materials and methods; Van Peer et al., manuscript in preparation). As such, this *MYB* 3'UTR screening analysis yielded a total of 33 miRNAs that could potentially target *MYB* (Figure 1c and Supplemental Table 1). Eleven out of these 33 hits were not predicted by various target prediction programs (TargetScan, PicTar, miRanda, MirTarget2, DianamicroT) emphasizing the strength of our screening method as an unbiased tool for the identification of novel non-predicted miRNA-target gene interactions. The fact that the number of experimentally identified 33 hits through the 3'UTR library screen is significantly lower as those generated by online target prediction databases (e.g. 74 predicted miRNAs by TargetScan or 159 predicted miRNAs using, DianamicroT) underscores the significant level of false negatives generated by computational prediction programs. In addition, our analysis identified 5 out of 8 (63%) known miRNA-MYB interactions described in literature including miR-150[24], miR-200b[25], miR-424[26], miR-429[27] and miR-126[28]. The 3 remaining miRNAs (miR-155[26], miR-15a[29] and miR-200c[30]) could represent false negatives in our screen.

MicroRNA-193b-3p potentially targets MYB in normal and malignant T-cell development and shows low expression in the *TAL* rearranged T-ALLs

Following the unbiased identification of 33 positive miRNA hits in our *MYB* 3'UTR-miRNA library screen, we explored the miRNA expression profiles of normal T-cell subsets representing major stages of thymocyte maturation[31] and two genetically well–characterized T-ALL patient cohorts to identify relevant miRNAs in the context of normal and malignant T-cell development. First, we evaluated the expression of 430 miRNAs in a primary T-ALL cohort consisting of 50 T-ALL patient cases as well as 5 normal T-cell subsets ($CD34^+$, $CD4^+CD8^+CD3^-$ ($DP3^-$), $CD4^+CD8^+CD3^+$ ($DP3^+$), $CD4^+$ ($SP4^+$) and $CD8^+$ ($SP8^+$))[19]. Next, we explored both the miRNAome (755 miRNAs) (Supplemental Table 2) and transcriptome[22] of a second independent T-ALL patient cohort of 64 primary T-ALL cases to identify putative miRNA-mRNA interactions based on integrative miRNA-mRNA correlation analysis.

By performing differential miRNA expression analysis, we first identified 36 putative tumor suppressor miRNAs with significant reduced levels of expression in T-ALL patients as compared to normal T-cell subsets ($p<0.05$; Supplemental Table 3). Cross-comparison of the 36 putative tumor suppressor miRNAs with the 33 hits identified in the *MYB* 3'UTR screen retained 5 miRNAs shared in both analyses (Figure 2a). Interestingly, two miRNAs out of these 5 common miRNAs, namely miR-195 and miR-193b-3p, showed strong opposite

expression patterns with *MYB* expression during normal T-cell differentiation (Pearson correlation coefficient r = -0.75 for miR-193b-3p and r = -0.66 for miR-195, Figure 2b-c, Supplemental Figure 1a-d). However, only miR-193b-3p was negatively correlated with *MYB* expression in primary T-ALLs (Spearman rank correlation with correlation factor < -0.5; Supplemental Table 4), suggesting that MYB regulation by miR-193b-3p might be functional in both normal and malignant T-cell context (Figure 2b-f, Supplemental Figure 1e). Finally, we evaluated the miR-193b-3p expression in molecular genetic subtypes of human T-ALL. Significantly lower expression levels of miR-193b-3p were identified in *TAL* rearranged T-ALLs in both patient cohorts (Supplemental Table 5-6, Figure 2d-f), which corresponds to the previously reported higher expression levels of *MYB* in TAL rearranged leukemias[9].

***In vitro* validation of the interaction between MYB and miR-193b-3p in T-ALL cells**

Following the selection of miR-193b-3p as putatively functionally relevant miRNA in the context of normal T-cell maturation and T-ALL oncogenesis, we decided to validate the direct interaction between miR-193b-3p and the 3'UTR of *MYB* using single luciferase-based reporter assays to confirm the 3'UTR-miRNA library screen results. This assay showed a substantial down-regulatory effect of miR-193b-3p on luciferase activity as compared to a non-targeting miRNA control (NTC) (Figure 3a). We identified two potential 6mer binding sites for miR-193b-3p (Figure 3b) and mutation of both target sites abolished the down-regulatory effect of miR-193b-3p on luciferase activity, demonstrating the seed-specific interaction between miR-193b-3p and the 3'UTR of *MYB* (Figure 3c).

Next, we investigated whether miR-193b-3p regulates MYB expression levels in the T-ALL cell line RPMI-8402, which contains a genomic *MYB* duplication, and in the T-ALL cell line LOUCY, which harbors high MYB protein expression levels as compared to other T-ALL cell lines (Supplemental Figure 2)[8]. In both T-ALL cell lines, overexpression of miR-193b-3p induced down regulation of MYB protein levels compared to a non-targeting miRNA control at different time points (Figure 3d-e). Previous studies identified MCL1 as a miR-193b-3p target in other cancer types[32, 33]. Importantly, MCL1 was also shown to contribute to T-ALL formation[19]. Therefore we tested the effect of overexpression of miR-193b-3p on MCL1 levels and observed miR-193b-3p induced down regulation of MCL1 protein levels in both T-ALL cell lines (Figure 3d-e). Hence, the putative tumor suppressor miR-193b-3p interacts with both MYB and MCL1 by site-specific complementarity and affects MYB and MCL1 protein levels in T-ALL thus further broadening the miR-193b-3p network in T-ALL.

***In vivo* down regulation of miR-193b-3p accelerates T-ALL onset**

Next, we evaluated the oncogenic effect of loss of the putative T-ALL tumor suppressor miR-193b-3p in a NOTCH1-induced T-ALL mouse model[34]. In brief, fetal liver cells were retrovirally transduced with an ICN1 (NOTCH1) construct (co-expressing mCherry) as well as a construct encoding antagomiR against miR-193b-3p (co-expressing GFP) or an empty vector construct. Next, the transduced hematopoietic precursor cells (HPCs) were tail vein injected into lethally irradiated recipient mice and T-ALL onset monitored (Figure 4a). We observed accelerated leukemia onset in mice injected with HPCs containing the antagomiR against miR-193b-3p (n=4, mean latency = 43 days, log-rank test p=0.02) compared to NOTCH1-only controls (n=7, mean latency = 56 days) (Figure 4b). Notably, the T-cell lymphoblasts derived from the murine leukemias displayed a clear GFP enrichment at time of disease onset (data not shown). Furthermore, an increase in MYB protein levels was observed in the leukemias with reduced miR-193b-3p compared to controls (Figure 4c). Finally, immunohistochemistry analysis of the murine leukemias showed an aggressive

leukemia phenotype with infiltration of highly proliferative T-cell lymphoblasts in liver, kidney, spleen and lungs in both miR-193b-3p loss and NOTCH1-only control samples (Figure 4d). No difference in H&E or Ki67 levels between the miR-193b-3p loss and NOTCH1-only control samples was observed (Figure 4d).

Discussion

The *MYB* oncogene was discovered more than 30 years ago as a viral-transforming gene in hematopoietic cells[35]. More recently, two independent research groups described *MYB* duplications (10-15%) and translocations (7%) in primary T-ALL patient samples[7, 8], linking oncogenic MYB activity to T-ALL pathogenesis. Furthermore, T-ALL patient samples marked with aberrant TAL1 expression display high *MYB* expression levels directly provoked by TAL1 complex binding[9]. Therapeutic approaches targeting MYB include direct strategies like the antisense MYB oligodeoxynucleotides currently tested in clinical trials[36] as well as indirect strategies like histone deacetylase inhibitors (HDACi)[37, 38]. Therapeutic miRNA delivery might represent an alternative approach for targeting MYB[39].

Hence, we designed and performed a miRNAome-wide MYB 3'UTR-miRNA library screen in HEK-293T cells in which 33 miRNAs (positive hits) were identified that putatively target MYB. In our screen, one third of the positive miRNA hits were not predicted by five different miRNA target prediction programs underlining the power of this unbiased strategy in the identification of non-predicted miRNA-target gene interactions. Alternatively, comparison of the 33 hits from the screen to the extensive list of miRNAs predicted by computational prediction programs suggests that online tools predict many false negatives. Literature data on other genes that where tested in our library screens also show that many bona fide targets remain undetected using prediction tools and likewise only a small fraction of the predicted miRNAs were identified as hits in these library screens[40, 41]. To our knowledge, this is the first unbiased 3'UTR library screen that was conducted for the identification of MYB targeting miRNAs.

Integration of these results with miRNA and mRNA expression profiles of primary T-ALL patient samples as well as normal thymocytes allowed us to identify miR-193b-3p as the top candidate putative tumor suppressive miRNA targeting MYB in normal and malignant T-cell development. In our sorted normal T-cell subsets, we observed and validated that *MYB* expression levels drastically decrease during T-cell differentiation[42]. *MYB* expression levels are tightly regulated in this developmental process, whereby MYB essentially contributes to three specific T-cell developmental stages[43, 44]. Next to MYB, microRNAs are also essential contributors to correct T-cell development as deletion of Dicer, an essential component in the miRNA biogenesis pathway, in mice impedes the survival of αβ T-cells in early T-cell stages [45]. In our data, miR-193b-3p was shown to be strongly anti-correlated with *MYB* expression during normal T-cell differentiation and miR-193b-3p controlled regulation of MYB levels through a seed-specific interaction. Taken together, we can propose miR-193b-3p as an important regulator of *MYB* expression during normal T-cell development.

Based on T-ALL patient data and miR-193b-3p perturbation studies in T-ALL cell lines and the NOTCH1 T-ALL mouse model, we could demonstrate that miR-193b-3p acts as *bona fide* tumor suppressor gene targeting MYB in T-ALL. The oncogene MCL1 has previously been described as a miR-193b-3p target in liver cancer and melanoma[32, 33], which we could confirm in our *in vitro* model system. Of interest, TAL1 knockdown in T-ALL cell lines[10] or enforced expression of miR-92a and miR-223 in NOTCH1-driven T-ALL mouse leukemias also influences MCL1 protein levels in T-ALL. Mechanistically, MCL1 is a downstream target of the TAL1/miR-223/FBXW7[10] or miR-92a/FBXW7 regulatory axes[19, 46]. Hence, in our study we identified the novel tumor suppressor miR-193b-3p that can directly regulate MYB and MCL1 levels in T-ALL. Importantly, this indicates that the *in vivo* tumor suppressor activity of miR-193b-3p will be mediated by the cooperative and simultaneous activation of multiple oncogenes, a notion that has been postulated for multiple other miRNAs[19].

In line with previous studies[9], *MYB* expression levels were elevated in TAL positive T-ALLs in both leukemic patient cohorts that we analyzed. Furthermore, miR-193b-3p is low expressed in *TAL* rearranged T-ALLs, which corresponds with the unraveled miR-193b-3p – MYB interaction shown in our study. In the paper of Correia et al., miR-193b-3p is down regulated after TAL1 overexpression in the P12-ICHI T-ALL cell line[11] indicating that the TAL1 complex can putatively indirectly repress miR-193b-3p expression.

Finally, using the NOTCH1 T-ALL induced mouse model, we could show for the first time that elevated MYB levels, caused by introduction of an antagomiR against miR-193b-3p, cooperate *in vivo* with ectopic expression of NOTCH1. Accordingly, a strong synergistic inhibitory effect on proliferation and viability was already demonstrated *in vitro* after combined knockdown of MYB and NOTCH1 in GSI-sensitive T-ALL cell lines[8]. Hence, we conclude that the novel tumor suppressor miR-193b-3p can cooperate with NOTCH1 in T-ALL pathogenesis.

Acknowledgments

The authors would like to thank the members of the Wendel lab and the members of the Speleman lab for experimental support and discussions during this research project and Aline Eggermont for excellent technical assistance. Furthermore, we would like to thank The Memorial Sloan Kettering (MSK) animal facility and Research Animal Resource Center (RARC) for assistance with mouse experiments.

This work is supported by: the Fund for Scientific Research Flanders (FWO) (research projects G.0202.09, G.0869.10N to F.S., 3GA00113N to P.V.V. and G0B2913N and G037514N to T.T., research grant 1.5.210.11N to P.R.; PhD grant to J.V.d.M.; postdoctoral grants to T.T., P.M., P.V.V., S.G., I.V.d.W. and P.R.; B.P. is a senior clinical investigator), the Belgian Foundation against Cancer (F.S., J.Vds. (SCIE 2010-177) and S.G.), the Flemish Liga against Cancer (VLK) (PhD grant to J.V.d.M. and G.V.P.); Ghent University (GOA grant 12051203 to F.S.; BOF10/PDO/140 to P.R.; BOF01D35609 to G.V.P.), the Cancer Plan from the Federal Public Service of Health (F.S.), the Children Cancer Fund Ghent (F.S) and the Belgian Program of Interuniversity Poles of Attraction (365O9110 to F.S., project grant 2010-187 to T.L.). Additional funding was provided by the NCI (R01-CA142798-01 and U01CA105492-08 to H.G.W.), the Leukemia Research Foundation (H.G.W.), the Experimental Therapeutics Center at MSKCC (H.G.W.), the American Cancer Society (H.G.W.) and the Geoffrey Beene Cancer Center (H.G.W.). This work was further supported by the Cancéropôle d'Ile de France (IDF)(J.S.), the program Carte d'Identité des Tumeurs (CIT) from the Ligue Nationale contre le Cancer (J.S.), ERC St Grant Consolidator 311660 (J.S.) and the ANR-10-IBHU-0002 Saint-Louis Institute program (J.S.).

Author contributions

E.M. and J.V.d.M. performed the laboratory experiments and data analysis; G.V.P., P.M., P.R. and M.B. assisted with experiments and data-mining. G.V.P., P.M. and J.VdS. designed the high-throughput 3'UTR-miRNA library screens. J.V.d.M., M.B. and H-G.W. performed and coordinated the mouse experiments. T.T., I.V.d.W., Y.B., B.D.M., N.V.R., B.P., J.S. and E.C. collected and analyzed diagnostic T-ALL and normal thymocyte samples. E.M., J.V.d.M., P.V.V., F.S. and P.R. designed the experiments, coordinated the research and wrote the paper.

References

1. Van Vlierberghe P, Ferrando A. The molecular basis of T cell acute lymphoblastic leukemia. *The Journal of clinical investigation* 2012 Oct 1; **122**(10)**:** 3398-3406.

2. Weng AP, Ferrando AA, Lee W, Morris JPt, Silverman LB, Sanchez-Irizarry C*, et al.* Activating mutations of NOTCH1 in human T cell acute lymphoblastic leukemia. *Science* 2004 Oct 8; **306**(5694)**:** 269-271.

3. O'Neil J, Grim J, Strack P, Rao S, Tibbitts D, Winter C*, et al.* FBW7 mutations in leukemic cells mediate NOTCH pathway activation and resistance to gamma-secretase inhibitors. *The Journal of experimental medicine* 2007 Aug 6; **204**(8)**:** 1813-1824.

4. Ferrando AA, Neuberg DS, Staunton J, Loh ML, Huard C, Raimondi SC*, et al.* Gene expression signatures define novel oncogenic pathways in T cell acute lymphoblastic leukemia. *Cancer cell* 2002 Feb; **1**(1)**:** 75-87.

5. Soulier J, Clappier E, Cayuela JM, Regnault A, Garcia-Peydro M, Dombret H*, et al.* HOXA genes are included in genetic and biologic networks defining human acute T-cell leukemia (T-ALL). *Blood* 2005 Jul 1; **106**(1)**:** 274-286.

6. Homminga I, Pieters R, Langerak AW, de Rooi JJ, Stubbs A, Verstegen M*, et al.* Integrated transcript and genome analyses reveal NKX2-1 and MEF2C as potential oncogenes in T cell acute lymphoblastic leukemia. *Cancer cell* 2011 Apr 12; **19**(4)**:** 484-497.

7. Clappier E, Cuccuini W, Kalota A, Crinquette A, Cayuela JM, Dik WA*, et al.* The C-MYB locus is involved in chromosomal translocation and genomic duplications in human T-cell acute leukemia (T-ALL), the translocation defining a new T-ALL subtype in very young children. *Blood* 2007 Aug 15; **110**(4)**:** 1251-1261.

8. Lahortiga I, De Keersmaecker K, Van Vlierberghe P, Graux C, Cauwelier B, Lambert F*, et al.* Duplication of the MYB oncogene in T cell acute lymphoblastic leukemia. *Nature genetics* 2007 May; **39**(5)**:** 593-595.

9. Sanda T, Lawton LN, Barrasa MI, Fan ZP, Kohlhammer H, Gutierrez A*, et al.* Core transcriptional regulatory circuit controlled by the TAL1 complex in human T cell acute lymphoblastic leukemia. *Cancer cell* 2012 Aug 14; **22**(2)**:** 209-221.

10. Mansour MR, Sanda T, Lawton LN, Li X, Kreslavsky T, Novina CD*, et al.* The TAL1 complex targets the FBXW7 tumor suppressor by activating miR-223 in human T cell acute lymphoblastic leukemia. *The Journal of experimental medicine* 2013 Jul 29; **210**(8)**:** 1545-1557.

11. Correia NC, Durinck K, Leite AP, Ongenaert M, Rondou P, Speleman F*, et al.* Novel TAL1 targets beyond protein-coding genes: identification of TAL1-regulated microRNAs in T-cell acute lymphoblastic leukemia. *Leukemia* 2013 Jul; **27**(7)**:** 1603-1606.

12. Emambokus N, Vegiopoulos A, Harman B, Jenkinson E, Anderson G, Frampton J. Progression through key stages of haemopoiesis is dependent on distinct threshold levels of c-Myb. *The EMBO journal* 2003 Sep 1; **22**(17)**:** 4478-4488.

13. Sakamoto H, Dai G, Tsujino K, Hashimoto K, Huang X, Fujimoto T*, et al.* Proper levels of c-Myb are discretely defined at distinct steps of hematopoietic cell development. *Blood* 2006 Aug 1; **108**(3)**:** 896-903.

14. Badiani PA, Kioussis D, Swirsky DM, Lampert IA, Weston K. T-cell lymphomas in v-Myb transgenic mice. *Oncogene* 1996 Nov 21; **13**(10)**:** 2205-2212.

15. Hess JL, Bittner CB, Zeisig DT, Bach C, Fuchs U, Borkhardt A*, et al.* c-Myb is an essential downstream target for homeobox-mediated transformation of hematopoietic cells. *Blood* 2006 Jul 1; **108**(1)**:** 297-304.

16. Bartel DP. MicroRNAs: target recognition and regulatory functions. *Cell* 2009 Jan 23; **136**(2)**:** 215-233.

17. Calin GA, Dumitru CD, Shimizu M, Bichi R, Zupo S, Noch E*, et al.* Frequent deletions and down-regulation of micro- RNA genes miR15 and miR16 at 13q14 in chronic lymphocytic leukemia. *Proceedings of the National Academy of Sciences of the United States of America* 2002 Nov 26; **99**(24)**:** 15524-15529.

18. Mavrakis KJ, Wolfe AL, Oricchio E, Palomero T, de Keersmaecker K, McJunkin K*, et al.* Genome-wide RNA-mediated interference screen identifies miR-19 targets in Notch-induced T-cell acute lymphoblastic leukaemia. *Nature cell biology* 2010 Apr; **12**(4)**:** 372-379.

19. Mavrakis KJ, Van Der Meulen J, Wolfe AL, Liu X, Mets E, Taghon T*, et al.* A cooperative microRNA-tumor suppressor gene network in acute T-cell lymphoblastic leukemia (T-ALL). *Nature genetics* 2011 Jul; **43**(7)**:** 673-678.

20. Li X, Sanda T, Look AT, Novina CD, von Boehmer H. Repression of tumor suppressor miR-451 is essential for NOTCH1-induced oncogenesis in T-ALL. *The Journal of experimental medicine* 2011 Apr 11; **208**(4)**:** 663-675.

21. Jackson AL, Levin AA. Developing microRNA therapeutics: approaching the unique complexities. *Nucleic acid therapeutics* 2012 Aug; **22**(4)**:** 213-225.

22. Clappier E, Gerby B, Sigaux F, Delord M, Touzri F, Hernandez L*, et al.* Clonal selection in xenografted human T cell acute lymphoblastic leukemia recapitulates gain of malignancy at relapse. *The Journal of experimental medicine* 2011 Apr 11; **208**(4)**:** 653-661.

23. Huber W, von Heydebreck A, Sultmann H, Poustka A, Vingron M. Variance stabilization applied to microarray data calibration and to the quantification of differential expression. *Bioinformatics* 2002; **18 Suppl 1:** S96-104.

24. Xiao C, Calado DP, Galler G, Thai TH, Patterson HC, Wang J*, et al.* MiR-150 controls B cell differentiation by targeting the transcription factor c-Myb. *Cell* 2007 Oct 5; **131**(1)**:** 146-159.

25. Cesi V, Casciati A, Sesti F, Tanno B, Calabretta B, Raschella G. TGFbeta-induced c-Myb affects the expression of EMT-associated genes and promotes invasion of ER+ breast cancer cells. *Cell cycle* 2011 Dec 1; **10**(23)**:** 4149-4161.

26. Imig J, Motsch N, Zhu JY, Barth S, Okoniewski M, Reineke T*, et al.* microRNA profiling in Epstein-Barr virus-associated B-cell lymphoma. *Nucleic acids research* 2011 Mar; **39**(5)**:** 1880-1893.

27. Luo Z, Zhang L, Li Z, Li X, Li G, Yu H*, et al.* An in silico analysis of dynamic changes in microRNA expression profiles in stepwise development of nasopharyngeal carcinoma. *BMC medical genomics* 2012; **5:** 3.

28. Grabher C, Payne EM, Johnston AB, Bolli N, Lechman E, Dick JE*, et al.* Zebrafish microRNA-126 determines hematopoietic cell fate through c-Myb. *Leukemia* 2011 Mar; **25**(3)**:** 506-514.

29. Chung EY, Dews M, Cozma D, Yu D, Wentzel EA, Chang TC*, et al.* c-Myb oncoprotein is an essential target of the dleu2 tumor suppressor microRNA cluster. *Cancer biology & therapy* 2008 Nov; **7**(11)**:** 1758-1764.

30. Siebzehnrubl FA, Silver DJ, Tugertimur B, Deleyrolle LP, Siebzehnrubl D, Sarkisian MR*, et al.* The ZEB1 pathway links glioblastoma initiation, invasion and chemoresistance. *EMBO molecular medicine* 2013 Aug; **5**(8)**:** 1196-1212.

31. Taghon T, Waegemans E, Van de Walle I. Notch Signaling During Human T cell Development. In: Radtke F (ed). *Notch Regulation of the Immune System*. Springer Berlin, Heidelberg, 2012, pp 75-97.

32. Braconi C, Valeri N, Gasparini P, Huang N, Taccioli C, Nuovo G*, et al.* Hepatitis C virus proteins modulate microRNA expression and chemosensitivity in malignant hepatocytes. *Clinical cancer research : an official journal of the American Association for Cancer Research* 2010 Feb 1; **16**(3)**:** 957-966.

33. Chen J, Zhang X, Lentz C, Abi-Daoud M, Pare GC, Yang X*, et al.* miR-193b Regulates Mcl-1 in Melanoma. *The American journal of pathology* 2011 Nov; **179**(5)**:** 2162-2168.

34. Pear WS, Aster JC, Scott ML, Hasserjian RP, Soffer B, Sklar J*, et al.* Exclusive development of T cell neoplasms in mice transplanted with bone marrow expressing activated Notch alleles. *The Journal of experimental medicine* 1996 May 1; **183**(5)**:** 2283-2291.

35. Beug H, von Kirchbach A, Doderlein G, Conscience JF, Graf T. Chicken hematopoietic cells transformed by seven strains of defective avian leukemia viruses display three distinct phenotypes of differentiation. *Cell* 1979 Oct; **18**(2)**:** 375-390.

36. Gewirtz AM. Myb targeted therapeutics for the treatment of human malignancies. *Oncogene* 1999 May 13; **18**(19)**:** 3056-3062.

37. Amaru Calzada A, Todoerti K, Donadoni L, Pellicioli A, Tuana G, Gatta R*, et al.* The HDAC inhibitor Givinostat modulates the hematopoietic transcription factors NFE2 and C-MYB in JAK2(V617F) myeloproliferative neoplasm cells. *Experimental hematology* 2012 Aug; **40**(8)**:** 634-645 e610.

38. Chambers AE, Banerjee S, Chaplin T, Dunne J, Debernardi S, Joel SP*, et al.* Histone acetylation-mediated regulation of genes in leukaemic cells. *European journal of cancer* 2003 May; **39**(8)**:** 1165-1175.

39. Kota J, Chivukula RR, O'Donnell KA, Wentzel EA, Montgomery CL, Hwang HW*, et al.* Therapeutic microRNA delivery suppresses tumorigenesis in a murine liver cancer model. *Cell* 2009 Jun 12; **137**(6)**:** 1005-1017.

40. Cheng J, Guo S, Chen S, Mastriano SJ, Liu C, D'Alessio AC*, et al.* An Extensive Network of TET2-Targeting MicroRNAs Regulates Malignant Hematopoiesis. *Cell reports* 2013 Oct 31; **5**(2)**:** 471-481.

41. Zhou P, Xu W, Peng X, Luo Z, Xing Q, Chen X*, et al.* Large-scale screens of miRNA-mRNA interactions unveiled that the 3'UTR of a gene is targeted by multiple miRNAs. *PloS one* 2013; **8**(7)**:** e68204.

42. Ramsay RG, Gonda TJ. MYB function in normal and cancer cells. *Nature reviews Cancer* 2008 Jul; **8**(7)**:** 523-534.

43. Bender TP, Kremer CS, Kraus M, Buch T, Rajewsky K. Critical functions for c-Myb at three checkpoints during thymocyte development. *Nature immunology* 2004 Jul; **5**(7)**:** 721-729.

44. Allen RD, 3rd, Bender TP, Siu G. c-Myb is essential for early T cell development. *Genes & development* 1999 May 1; **13**(9)**:** 1073-1078.

45. Cobb BS, Nesterova TB, Thompson E, Hertweck A, O'Connor E, Godwin J*, et al.* T cell lineage choice and differentiation in the absence of the RNase III enzyme Dicer. *The Journal of experimental medicine* 2005 May 2; **201**(9)**:** 1367-1373.

46. Inuzuka H, Shaik S, Onoyama I, Gao D, Tseng A, Maser RS*, et al.* SCF(FBW7) regulates cellular apoptosis by targeting MCL1 for ubiquitylation and destruction. *Nature* 2011 Mar 3; **471**(7336)**:** 104-109.

Figure Legends

Figure 1. An unbiased high-throughput *MYB* 3'UTR-miRNA library screen identifies 33 candidate miRNAs targeting MYB

(**a**) HEK-293T cells were transfected with a reporter vector containing the wild-type 3'UTR of *MYB* downstream of a *Firefly* luciferase gene and a control vector containing a *Renilla* luciferase gene together with a library of 470 miRNA mimics. Forty-eight hours later, *Firefly* and *Renilla* luciferase activities were measured. After normalization, inter-plate calibration and correction for systemic error, a miRNA interaction score was calculated for each miRNA in the screen. The lower the interaction score, the more likely a miRNA will interact with the 3'UTR of *MYB*. (**b**) The plot of the interaction scores for each miRNA from two independent *MYB* 3'UTR library screens demonstrates the high reproducibility of our assay (Pearson correlation coefficient r = 0.85). (**c**) Our screens reveals 33 candidate miRNAs (Supplemental Table 1) targeting the 3'UTR of *MYB* (interaction score < -1.93). The average interaction score of the 2 screens is plotted on the y-axis for each miRNA that was included in the screen (x-axis).

Figure 2. Selection of miR-193b-3p as a top candidate *MYB* targeting miRNA in T-ALL

(a) Selection criteria to identify top candidate miRNAs targeting MYB in T-ALL: (1) positive hits from the MYB 3'UTR-miRNA library screen, (2) miRNAs that are significantly lower expressed in T-ALL versus normal T-cell subsets (t-test, $p<0.05$), (3) miRNAs that display anti-correlation with *MYB* expression in primary human T-ALL patient samples (Spearman rank correlation factor < -0.5). (**b**) *MYB* is highly expressed in the immature CD34+ stage and thereafter decreases during T-cell development. **(c)** MicroRNA-193b-3p exhibit lower expression in the immature CD34+ stage followed by a strong up regulation in the more mature stages. (**d**) *MYB* is highly expressed in the TAL positive T-ALL subgroup. **(e-f**) miR-193b-3p is significantly lower expressed in the TAL rearranged patients samples compared to other T-ALL subgroups (t-test, $p<0.05$) in both T-ALL patient cohorts.

Figure 3. MicroRNA-193b-3p directly targets the 3'UTR of *MYB* and down regulates MYB expression in T-ALL cell lines

(**a**) Transfection of miR-193b-3p reduces the luciferase activity of the wild-type *MYB* 3'UTR reporter construct in HEK-293T cells. Bar graphs represent the mean (+/- SD) of 4 independent experiments relative to the non-targeting miRNA transfection control (NTC). (**b**) The human MYB 3'UTR contains two 6mer sites for miR-193b-3p. The sequences for the wild-type (WT) vector, the mutated (MUT) vector and miR-193b-3p are depicted. (**c**) Mutation of the two 6mer target sites of miR-193b-3p in the 3'UTR *MYB* vector completely abolishes the down regulatory effect of miR-193b-3p on luciferase activity. Bar graphs represent the mean (+/- SD) of 2 independent experiments relative to NTC. (**d**-**e**) MicroRNA-193b-3p overexpression down regulates MYB and MCL1 levels in LOUCY (**d**) and RPMI-8402 (**e**) T-ALL cell lines. The results shown from one experiment are representative for two independent biological replicates. MYB and Tubulin protein levels were quantified by use of Image J software. Subsequently MYB levels were normalized to Tubulin levels and compared to the relative MYB levels of the NTC samples.

Figure 4. Down regulation of miR-193b-3p accelerates T-ALL onset *in vivo*

(**a**) Schematic representation of the NOTCH1-induced T-ALL mouse model. Fetal liver cells derived from pregnant mice were partially transduced with a vector encoding antagomiR against miR-193b-3p or an empty vector control (labeled in GFP),together with the NOTCH1 (ICN1) construct (co-expressing mCherry). Next, the transduced cells were tail vein injected in irradiated mouse recipients followed by monitoring of leukemia formation. (**b**) Survival

plot (Kaplan-Meier) depicting accelerated leukemia onset in the mouse recipients with reduced miR-193b-3p levels (n=4, p=0.02 log-rank test, red) compared to NOTCH1-only controls (n=7, black). (**c**) Western blot analysis of Myb protein levels in mouse tumor samples from both groups. Myb protein levels are quantified by Image J, normalized to Tubulin levels and compared to NOTCH1-only vector controls. (**d**) H&E and Ki67 staining of lymphoblasts in kidney, liver, lung and spleen tissue of a representative antagomiR miR-193b-3p and control mouse leukemia sample (10x magnification).

Supplemental Figure Legends

Supplemental Figure 1. MiRNA-429, miR-503, miR-200, miR-195 and miR-193b-3p expression during normal T-cell differentiation. MiRNA-193b-3p expression in T-ALL patient samples

(**a**-**c**) The expression patterns of (a) miR-429 (**a**), miR-503 (**b**) miR-200b (**c**) and miR-195 (**d**) in 5 sorted T-cell subsets during normal T-cell development are depicted (all miRNAs: Pearson correlation coefficient with MYB > -0.5). (**d**) miR-195 exhibit lower expression in the immature CD34+ stage followed by a strong up regulation in the more mature stages. (**e**) Expression levels of miR-193b-3p in T-ALL patient samples and normal T-cell subsets.

Supplemental Figure 2. MYB expression levels in T-ALL cell lines

MYB protein levels in a set of T-ALL cell lines

Supplemental Materials and methods

Cell lines

All cell lines used were obtained from DSMZ (Braunschweig, Germany) and cultured in RPMI-1640 (Gibco, Life Technologies, Carlsbad, CA, USA) supplemented with 10% FCS, L-glutamine (10 ml/L), penicillin (100 µg/ml) and streptomycin (100 µg/ml).

Protein isolation and Western blot

Cell pellets were lysed in RIPA buffer (32 mM Sodium Deoxycholate, 150 mM NaCl, 50mM TrisHCl (pH 7.5), 0.1% SDS en 1% NP-40) with protease inhibitors (cOmplete Protease Inhibitor Cocktail Tablets; Roche, Basel, Switzerland). For denaturation of the samples, 20 µl cell lysate was mixed with 5 µl of denaturation buffer (5x laemli buffer (25 ml 10% SDS-solution, 20 ml 100% glycerol, 7.75 ml 1M TrisHCl pH 6.8 en 1.25 ml 1% BromoPhenol Blue solution), 1:7 40x β-mercaptoethanol), and incubated at 95°C for 10min. Next, 20 µl of the denatured fractions were loaded on precast gels (10% SDS; Bio-Rad) and subjected to SDS-PAGE (100V and 0.25A, 1-2 hours). Additionally, a biotinylated protein ladder was used (7727S; Cell Signaling, Danvers, MA, USA). Next, proteins were transferred onto a nitrocellulose membrane (nitrocellulose/Filter Paper Sandwiches 0.2µm; Bio-Rad) (100V, 0.25A, 1-2 hours). Primary antibodies used: anti-MYB (mouse, 05-175, dilution 1/1000; Upstate, Millipore, Billerica, MA, USA), anti-MCL1 (rabbit, 5453S, dilution 1/1000; Cell Signaling) and anti-Tubulin (mouse, T5168, dilution 1/5000; Sigma-Aldrich, St. Louis, MI, USA). Secondary antibodies used: HRP-linked anti-mouse or anti-rabbit (7076S - 7074S, dilution 1/5000; Cell Signaling) and HRP-linked anti-biotin (7075S, dilution 1/1000; Cell Signaling). For chemiluminescent detection, membranes were incubated with luminal/enhancer buffer (Super Signal West Dura Extended Duration Substrate; Thermo Fisher Scientific) and developed using the UCP chemiDoc-it®500 Imaging System (UVP, Upland, CA, USA). To remove antibodies, stripping buffer (Restore PLUS Western Blot Stripping Buffer; Thermo Fisher Scientific) was used.

RNA isolation, cDNA synthesis and qPCR

RNA isolation and DNase-treatment on column was performed using the miRNeasy Mini Kit and the RNase-Free DNase Set (Qiagen, Hilden, Germany). RNA concentration was measured on Nanodrop (Thermo Fisher Scientific). For cDNA synthesis, 500 ng input RNA, 4 µl iScript reaction mix and 1 µl of iScript reverse transcriptase (iScript; Bio-Rad) was used in a final volume of 20 µl and samples were incubated for 5’ at 25°C, 30’ at 42°C and 5’ at 85°C using the iCycler (Bio-Rad). qPCR experiments were performed according to the MIQE guidelines. The qPCR reactions were executed using 5 ng cDNA, 250 nM primers and 2.5 µl SsoAdvanced master mix (Bio-Rad) in a final volume of 5 µl and run on the LightCycler 480 instrument (Roche). Normalization of expression values was done against a set of reference genes and analyzed using the qBasePlus software (http://www.biogazelle.com). The qPCR primers were developed using RTPrimerDB (http://www.rtprimerdb.org) and are listed in Supplemental Table 7.

Figure 1

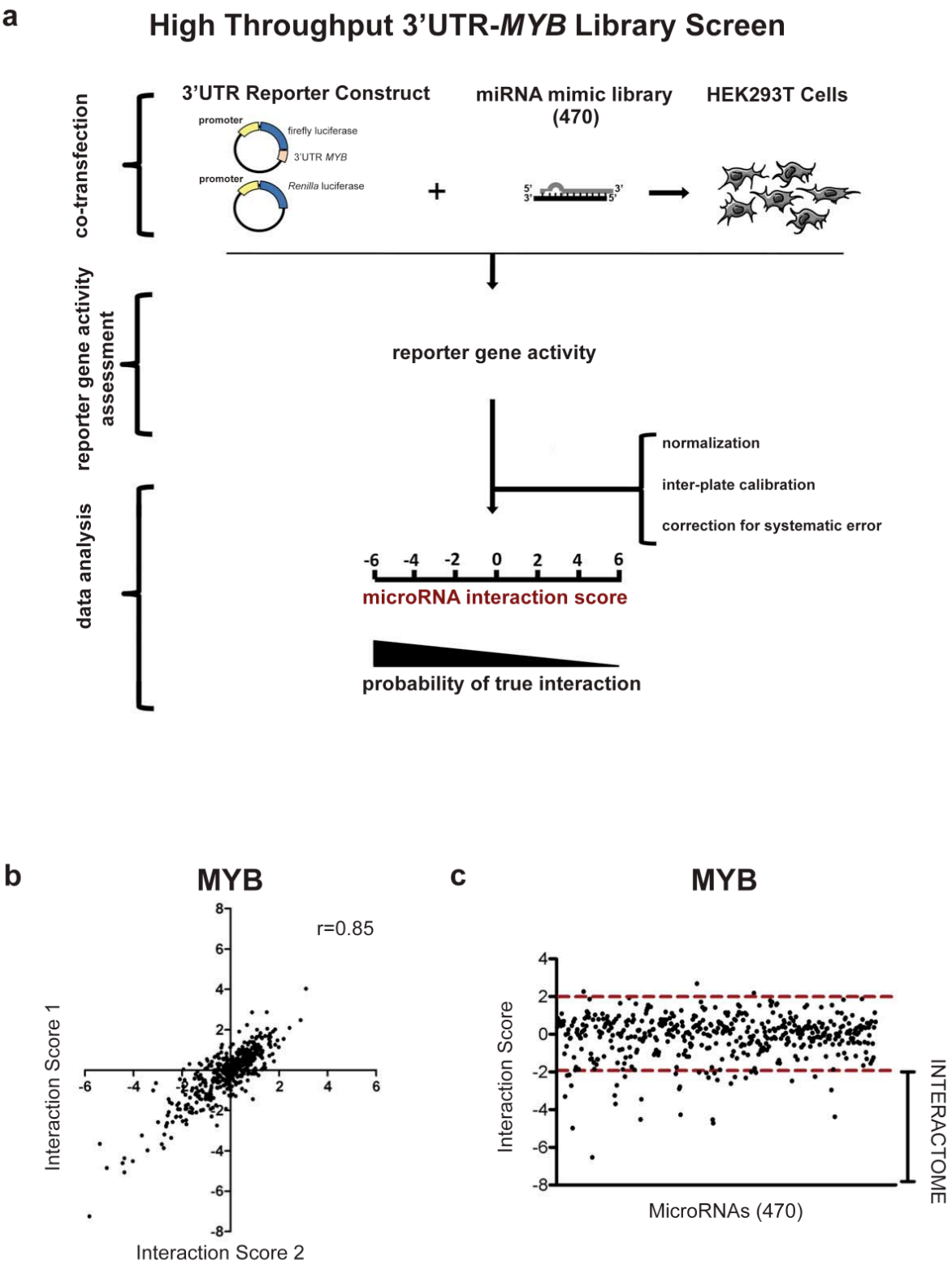
a
High Throughput 3'UTR-MYB Library Screen
3'UTR Reporter Construct
miRNA mimic library (470)
HEK293T Cells
promoter
firefly luciferase
3'UTR MYB
promoter
Renilla luciferase
co-transfection
reporter gene activity assessment
reporter gene activity
data analysis
normalization
inter-plate calibration
correction for systematic error
-6 -4 -2 0 2 4 6
microRNA interaction score
probability of true interaction
b
MYB
r=0.85
Interaction Score 1
Interaction Score 2
c
MYB
Interaction Score
MicroRNAs (470)
INTERACTOME

Figure 2

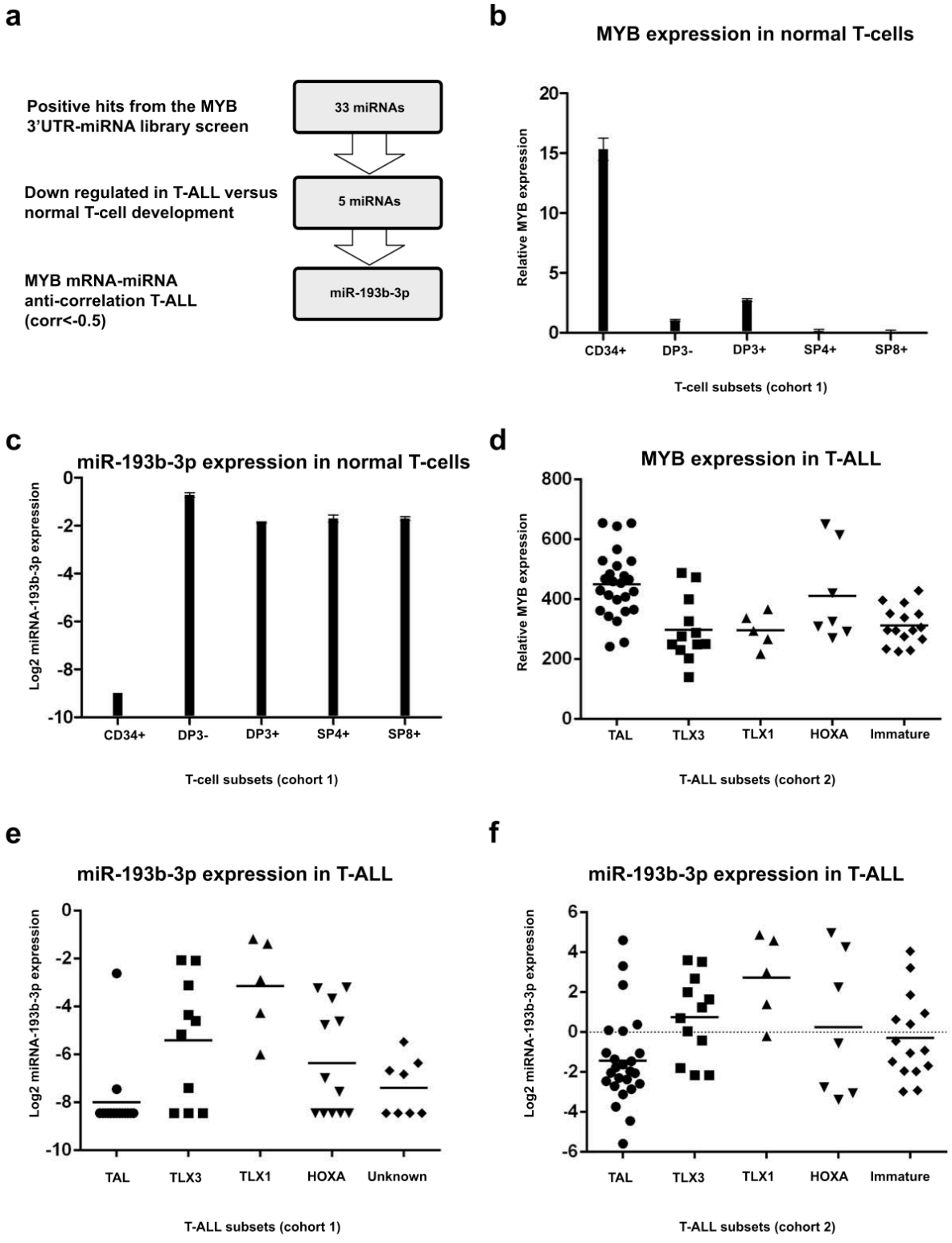
a
Positive hits from the MYB 3'UTR-miRNA library screen
33 miRNAs
Down regulated in T-ALL versus normal T-cell development
5 miRNAs
MYB mRNA-miRNA anti-correlation T-ALL (corr<-0.5)
miR-193b-3p
b
MYB expression in normal T-cells
Relative MYB expression
20
15
10
5
0
CD34+
DP3-
DP3+
SP4+
SP8+
T-cell subsets (cohort 1)
c
miR-193b-3p expression in normal T-cells
Log2 miRNA-193b-3p expression
0
-2
-4
-6
-8
-10
CD34+
DP3-
DP3+
SP4+
SP8+
T-cell subsets (cohort 1)
d
MYB expression in T-ALL
Relative MYB expression
800
600
400
200
0
TAL
TLX3
TLX1
HOXA
Immature
T-ALL subsets (cohort 2)
e
miR-193b-3p expression in T-ALL
Log2 miRNA-193b-3p expression
0
-2
-4
-6
-8
-10
TAL
TLX3
TLX1
HOXA
Unknown
T-ALL subsets (cohort 1)
f
miR-193b-3p expression in T-ALL
Log2 miRNA-193b-3p expression
6
4
2
0
-2
-4
-6
TAL
TLX3
TLX1
HOXA
Immature
T-ALL subsets (cohort 2)

Figure 3

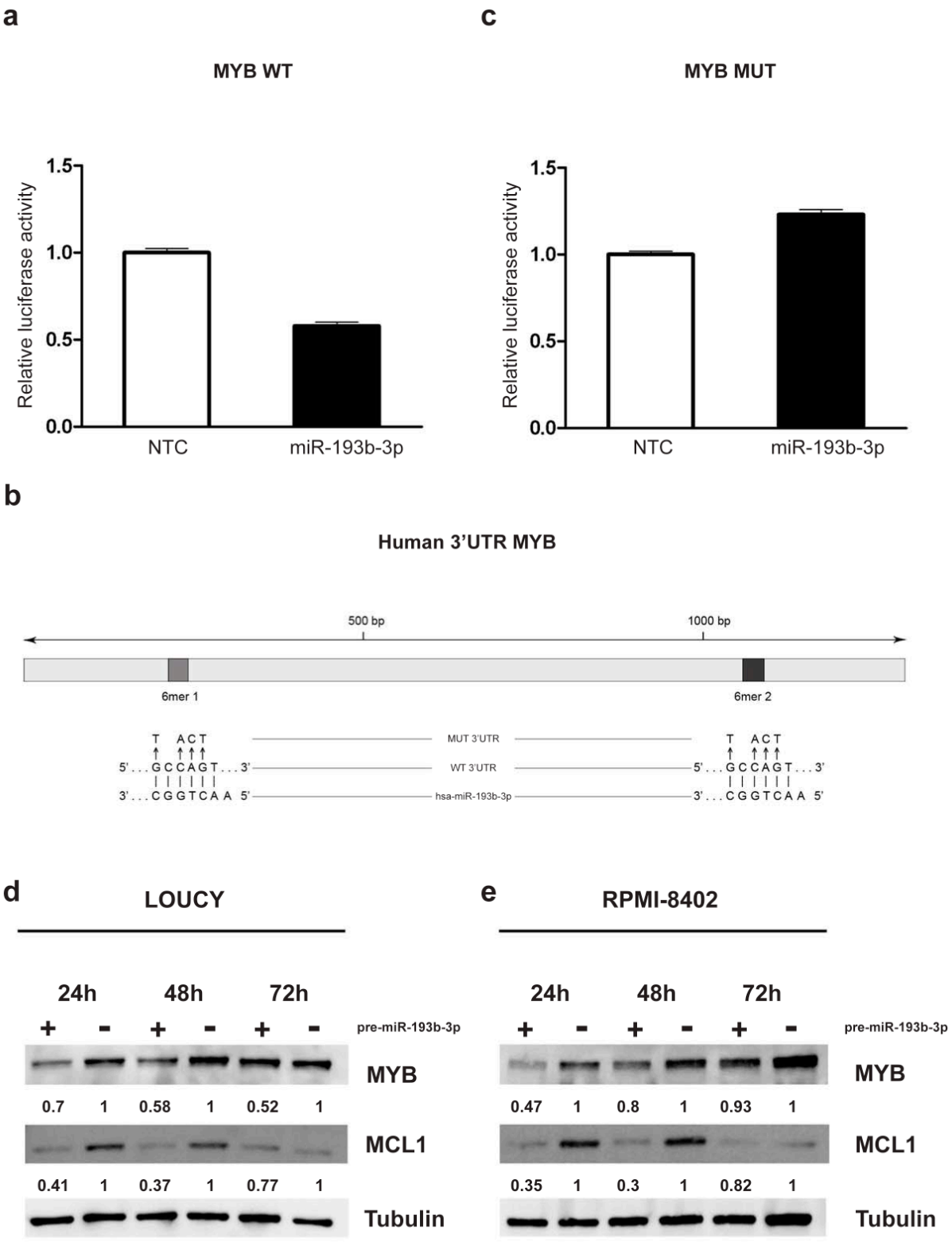
a
MYB WT
Relative luciferase activity
1.5
1.0
0.5
0.0
NTC
miR-193b-3p
c
MYB MUT
Relative luciferase activity
1.5
1.0
0.5
0.0
NTC
miR-193b-3p
b
Human 3'UTR MYB
500 bp
1000 bp
6mer 1
6mer 2
T ACT
5'...GCCAGT...3'
3'...CGGTCAA 5'
MUT 3'UTR
WT 3'UTR
hsa-miR-193b-3p
T ACT
5'...GCCAGT...3'
3'...CGGTCAA 5'
d
LOUCY
24h
48h
72h
+ - + - + -
pre-miR-193b-3p
MYB
0.7 1 0.58 1 0.52 1
MCL1
0.41 1 0.37 1 0.77 1
Tubulin
e
RPMI-8402
24h
48h
72h
+ - + - + -
pre-miR-193b-3p
MYB
0.47 1 0.8 1 0.93 1
MCL1
0.35 1 0.3 1 0.82 1
Tubulin

Figure 4

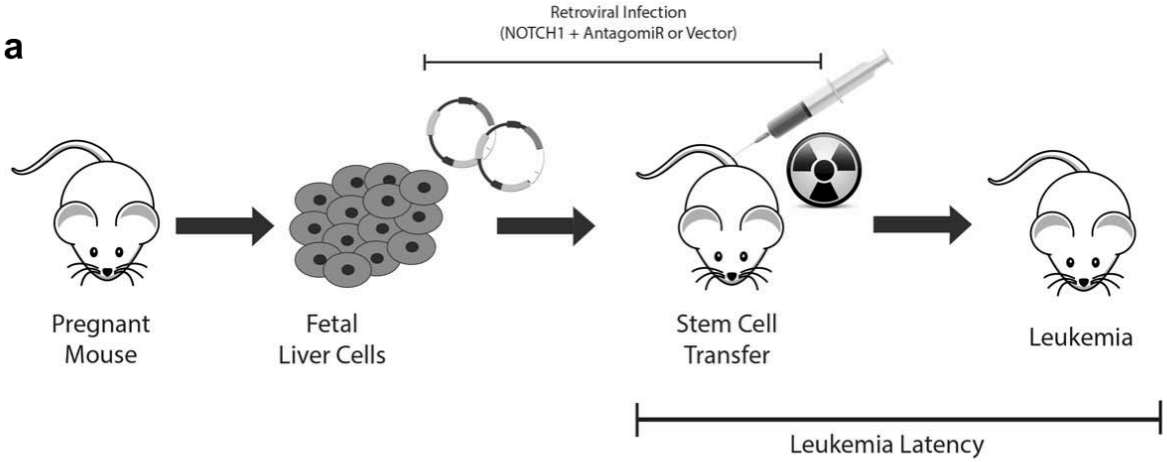
a
Retroviral Infection
(NOTCH1 + AntagomiR or Vector)
Pregnant Mouse
Fetal Liver Cells
Stem Cell Transfer
Leukemia
Leukemia Latency

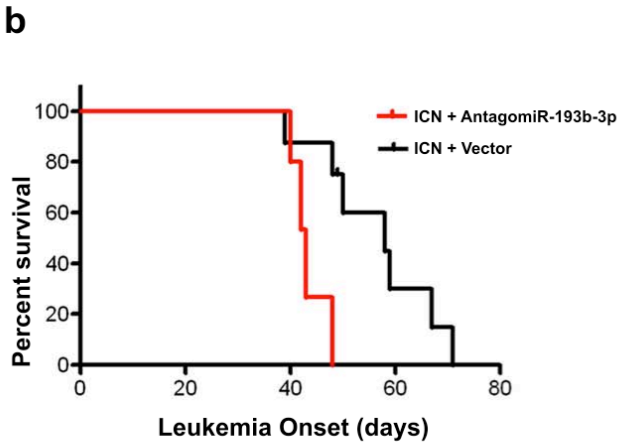
b
Percent survival
100
80
60
40
20
0
0
20
40
60
80
Leukemia Onset (days)
ICN + AntagomiR-193b-3p
ICN + Vector

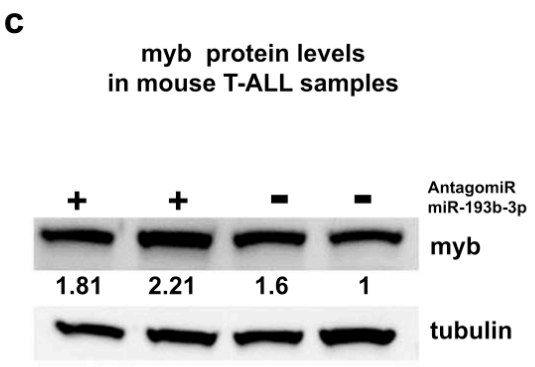
c
myb protein levels
in mouse T-ALL samples
AntagomiR
miR-193b-3p
+
+
-
-
myb
1.81
2.21
1.6
1
tubulin

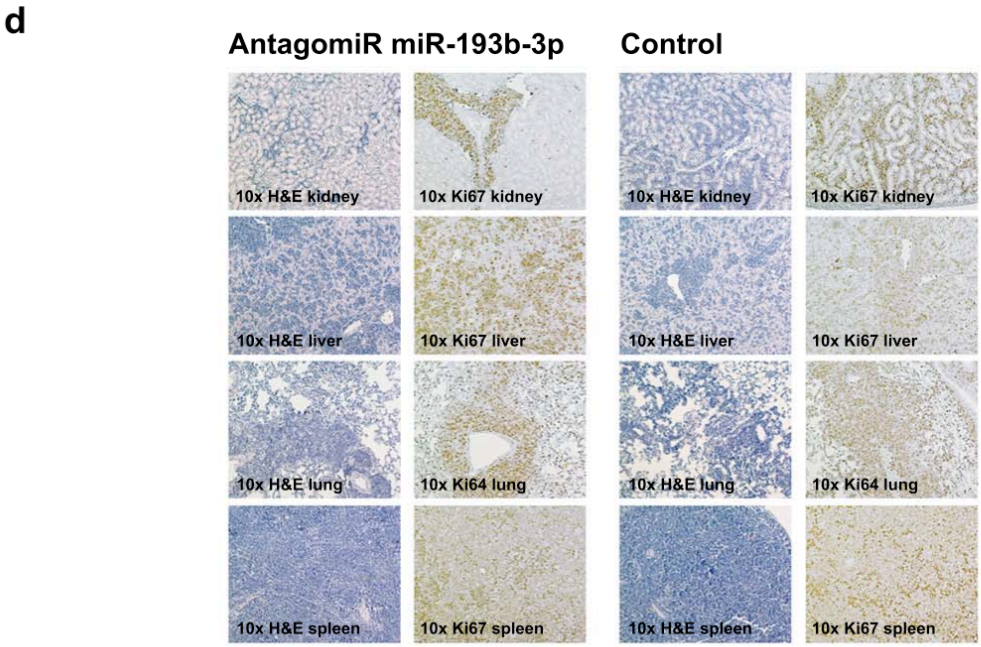
d
AntagomiR miR-193b-3p
Control
10x H&E kidney
10x Ki67 kidney
10x H&E kidney
10x Ki67 kidney
10x H&E liver
10x Ki67 liver
10x H&E liver
10x Ki67 liver
10x H&E lung
10x Ki64 lung
10x H&E lung
10x Ki64 lung
10x H&E spleen
10x Ki67 spleen
10x H&E spleen
10x Ki67 spleen

Supplemental Figure 1

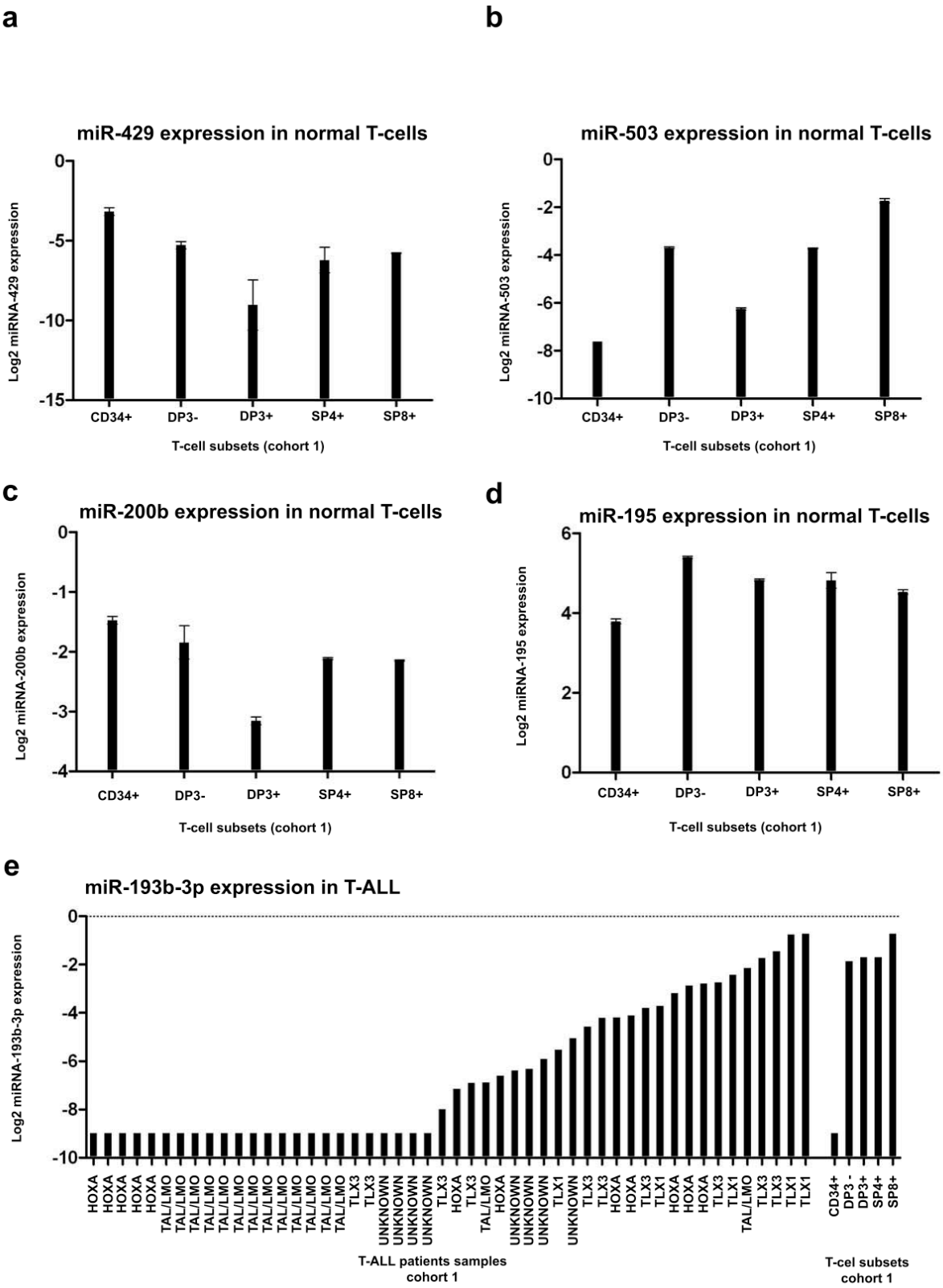

Supplemental Figure 2

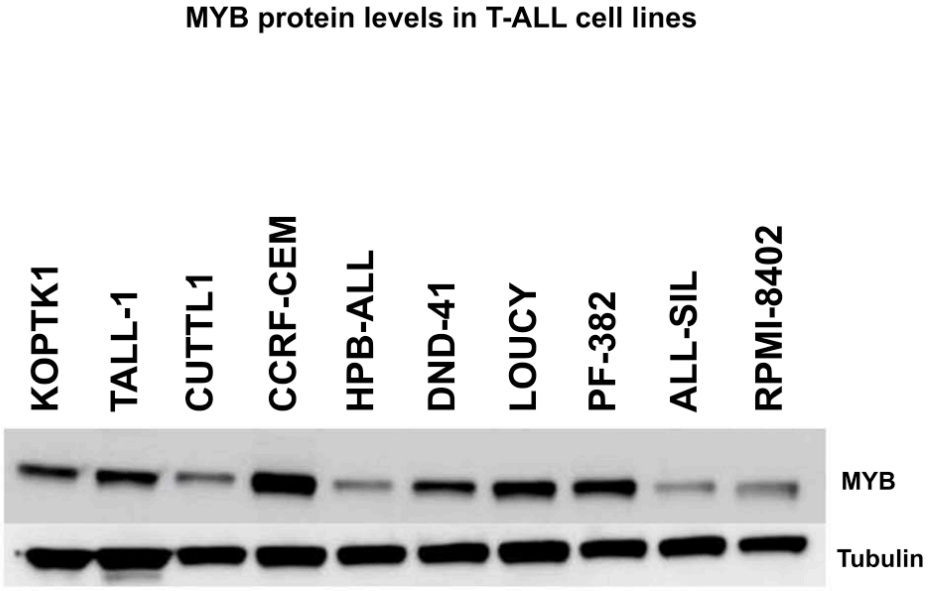

Supplemental Tables

Supplemental Table 1. 3'UTR *MYB* library screen (only shown 33 hits)
Average interaction scores of the 2 3'UTR *MYB*-microRNA library screens, 33 positive microRNA hits (interaction score < -1,93) are indicated in bold
* Accession number in miRBase
** Mature microRNA sequence of the microRNAs used in the library
*** MicroRNAs that are predicted by at least one of the following *in silico* prediction algorithms: TargetScan, PicTar, miRanda, MirTarget2, Diana, microT --> indicated by "x" (only indicated for the 33 positive hits)

MicroRNA ID	Accession number*	Mature miRNA sequence**	Interaction score	Predicted ***
hsa-miR-150	**MIMAT0000451**	**UCUCCCAACCCUUGUACCAGUG**	**-6.529**	**x**
hsa-miR-127	**MIMAT0000446**	**UCGGAUCCGUCUGAGCUUGGCU**	**-4.973**	
hsa-miR-449b	**MIMAT0003327**	**AGGCAGUGUAUUGUUAGCUGGC**	**-4.719**	**x**
hsa-miR-449	**MIMAT0001541**	**UGGCAGUGUAUUGUUAGCUGGU**	**-4.527**	**x**
hsa-miR-221	**MIMAT0000278**	**AGCUACAUUGUCUGCUGGGUUUC**	**-4.517**	
hsa-miR-629	**MIMAT0003298**	**GUUCUCCCAACGUAAGCCCAGC**	**-4.371**	
hsa-miR-34c	**MIMAT0000686**	**AGGCAGUGUAGUUAGCUGAUUGC**	**-4.267**	**x**
hsa-miR-193b	**MIMAT0002819**	**AACUGGCCCUCAAAGUCCCGCUUU**	**-3.698**	**x**
hsa-miR-222	**MIMAT0000279**	**AGCUACAUCUGGCUACUGGGUCUC**	**-3.445**	
hsa-miR-105	**MIMAT0000102**	**UCAAAUGCUCAGACUCCUGU**	**-3.307**	**x**
hsa-miR-193a	**MIMAT0000459**	**AACUGGCCUACAAAGUCCCAG**	**-3.248**	**x**
hsa-miR-624	**MIMAT0003293**	**UAGUACCAGUACCUUGUGUUCA**	**-2.956**	
hsa-miR-34a	**MIMAT0000255**	**UGGCAGUGUCUUAGCUGGUUGUU**	**-2.900**	**x**
hsa-miR-34b	**MIMAT0000685**	**UAGGCAGUGUCAUUAGCUGAUUG**	**-2.785**	**x**
hsa-miR-126	**MIMAT0000445**	**UCGUACCGUGAGUAAUAAUGC**	**-2.721**	
hsa-miR-195	**MIMAT0000461**	**UAGCAGCACAGAAAUAUUGGC**	**-2.702**	**x**
hsa-miR-497	**MIMAT0002820**	**CAGCAGCACACUGUGGUUUGU**	**-2.619**	**x**
hsa-miR-565	**MIMAT0003229**	**GGCUGGCUCGCGAUGUCUGUUU**	**-2.479**	
hsa-miR-454-3p	**MIMAT0003885**	**UAGUGCAAUAUUGCUUAUAGGGUUU**	**-2.420**	**x**
hsa-miR-516-5p	**MIMAT0002859**	**CAUCUGGAGGUAAGAAGCACUUU**	**-2.313**	
hsa-miR-429	**MIMAT0001536**	**UAAUACUGUCUGGUAAAACCGU**	**-2.291**	**x**
hsa-miR-503	**MIMAT0002874**	**UAGCAGCGGGAACAGUUCUGCAG**	**-2.266**	**x**
hsa-miR-600	**MIMAT0003268**	**ACUUACAGACAAGAGCCUUGCUC**	**-2.250**	**x**
hsa-miR-200b	**MIMAT0000318**	**UAAUACUGCCUGGUAAUGAUGAC**	**-2.249**	**x**
hsa-miR-107	**MIMAT0000104**	**AGCAGCAUUGUACAGGGCUAUCA**	**-2.183**	**x**
hsa-miR-124a	**MIMAT0000422**	**UUAAGGCACGCGGUGAAUGCCA**	**-2.157**	**x**
hsa-miR-33b	**MIMAT0003301**	**GUGCAUUGCUGUUGCAUUGCA**	**-2.094**	**x**
hsa-miR-451	**MIMAT0001631**	**AAACCGUUACCAUUACUGAGUUU**	**-2.054**	
hsa-miR-424	**MIMAT0001341**	**CAGCAGCAAUUCAUGUUUUGAA**	**-2.049**	**x**
hsa-miR-519c	**MIMAT0002832**	**AAAGUGCAUCUUUUUAGAGGAU**	**-2.040**	**x**
hsa-miR-383	**MIMAT0000738**	**AGAUCAGAAGGUGAUUGUGGCU**	**-2.016**	
hsa-miR-518c*	**MIMAT0002847**	**UCUCUGGAGGGAAGCACUUUCUG**	**-1.994**	
hsa-miR-519b	**MIMAT0002837**	**AAAGUGCAUCCUUUUAGAGGUUU**	**-1.967**	**x**

Supplemental Table 2. Normalized logarithmic microRNA expression values in 64 primary T-ALL patient samples (cohort 2)

Not shown in thesis

Supplemental Table 3. MicroRNAs significantly (p-value <0.05) higher expressed in normal thymocyte subsets compared to T-ALL samples (t-test with Benjamini-Hochberg correction)

MicroRNA ID	t-test (p-value)	Benjamini-Hochberg	Fold Change
hsa-mir-195	6.713E-71	0.0001618	-9.7496195
hsa-mir-662	1.924E-35	0.0003236	11.1918201
hsa-mir-29a	6.862E-32	0.0004854	-5.3857330
hsa-mir-376a	2.317E-22	0.0006472	13.5329875
hsa-mir-7	2.460E-21	0.0008091	-2.6219184
hsa-mir-223	5.219E-13	0.0009709	5.6164570
hsa-mir-503	1.287E-11	0.0011327	-2.1598713
hsa-mir-95	1.671E-10	0.0012945	-4.5268055
hsa-mir-23b	2.093E-10	0.0014563	-0.8762993
hsa-mir-205	2.823E-09	0.0016181	-3.2165296
hsa-mir-296	2.931E-09	0.0017799	-3.6639771
hsa-mir-520d	1.357E-08	0.0019417	3.3680172
hsa-mir-141	2.710E-08	0.0021036	-4.1685127
hsa-mir-651	3.849E-08	0.0022654	-2.6730653
hsa-mir-100	0.0000001	0.0024272	-5.6657351
hsa-mir-373	0.0000001	0.0025890	-3.0880892
hsa-mir-520c	0.0000001	0.0027508	6.7330880
hsa-mir-200c	0.0000004	0.0029126	-2.4689724
hsa-mir-99a	0.0000005	0.0030744	-5.2848169
hsa-mir-210	0.0000006	0.0032362	-3.2328291
hsa-miR-645	0.0000010	0.0033981	2.7928400
hsa-mir-365	0.0000022	0.0035599	-2.7198946
hsa-mir-200a*	0.0000038	0.0037217	-0.9497195
hsa-miR-589	0.0000063	0.0038835	-2.4041596
hsa-miR-606	0.0000063	0.0040453	1.9699663
hsa-mir-627	0.0000064	0.0042071	-2.0415349
hsa-miR-363*	0.0000073	0.0043689	-2.2591361
hsa-mir-574	0.0000108	0.0045307	2.8307624
hsa-mir-580	0.0000163	0.0046926	-1.3622854
hsa-mir-219	0.0000200	0.0048544	-1.4469472
hsa-mir-34b	0.0000202	0.0050162	-0.3656468
hsa-mir-145	0.0000297	0.0051780	2.6493413
hsa-mir-526b*	0.0000298	0.0053398	-1.0748624
hsa-miR-599	0.0000414	0.0055016	-0.6880783
hsa-mir-132	0.0000420	0.0056634	-3.0212290

hsa-mir-449	0.0000527	0.0058252	-1.2066026
hsa-mir-30e-5p	0.0000609	0.0059871	2.3165613
hsa-mir-338	0.0000760	0.0061489	-2.6201088
hsa-mir-192	0.0000928	0.0063107	-2.7723308
hsa-mir-363	0.0001200	0.0064725	1.2885197
hsa-mir-218	0.0001405	0.0066343	-2.2704391
hsa-mir-137	0.0001646	0.0067961	3.6809823
hsa-mir-200b	0.0002030	0.0069579	-2.8418783
hsa-mir-520b	0.0002388	0.0071197	-1.1285756
hsa-mir-193b	0.0003037	0.0072816	-3.2876925
hsa-mir-425	0.0003123	0.0074434	-2.0688926
hsa-mir-501	0.0003996	0.0076052	-1.0622761
hsa-mir-491	0.0007698	0.0077670	-3.6667433
hsa-mir-324-5p	0.0009583	0.0079288	-1.5877612
hsa-mir-451	0.0011086	0.0080906	4.3005311
hsa-mir-422a	0.0011654	0.0082524	-1.2449892
hsa-mir-542-5p	0.0012136	0.0084142	-0.2999885
hsa-mir-650	0.0012499	0.0085761	-1.9485388
hsa-mir-28	0.0013181	0.0087379	-1.3525218
hsa-mir-496	0.0013440	0.0088997	1.8356225
hsa-mir-586	0.0014230	0.0090615	-0.2110830
hsa-mir-148a	0.0016438	0.0092233	-2.3600147
hsa-mir-200a	0.0017042	0.0093851	-1.3636241
hsa-mir-186	0.0018389	0.0095469	-1.3769981
hsa-mir-26a	0.0020069	0.0097087	-1.4617675
hsa-miR-532	0.0023106	0.0098706	-2.3333986
hsa-mir-181b	0.0025073	0.0100324	-1.3934098
hsa-mir-429	0.0025617	0.0101942	-2.0352242
hsa-mir-584	0.0029069	0.0103560	0.0000000
hsa-miR-567	0.0029069	0.0105178	0.0000000
hsa-mir-331	0.0029672	0.0106796	-0.9358149
hsa-mir-140	0.0030062	0.0108414	-2.3069168
hsa-miR-126	0.0032826	0.0110032	2.5332965
hsa-mir-616	0.0038812	0.0111650	-1.5885154
hsa-mir-381	0.0042010	0.0113269	1.3888124
hsa-mir-342	0.0048092	0.0114887	-1.1844081
hsa-mir-135b	0.0049608	0.0116505	-2.7111468
hsa-mir-502	0.0053141	0.0118123	-1.0241894
hsa-mir-610	0.0054653	0.0119741	-1.4935623
hsa-mir-193a	0.0058309	0.0121359	-1.4646607
hsa-mir-383	0.0062825	0.0122977	-1.2746388
hsa-mir-375	0.0064374	0.0124595	-1.6612633
hsa-miR-596	0.0064878	0.0126214	0.0000000
hsa-mir-30a-5p	0.0066291	0.0127832	-1.0154704
hsa-mir-187	0.0070678	0.0129450	-0.9742990

hsa-mir-30b	0.0073376	0.0131068	-1.0131250
hsa-mir-106a	0.0075057	0.0132686	-1.2576614
hsa-mir-18a	0.0075492	0.0134304	-1.6392437
hsa-mir-155	0.0075906	0.0135922	-1.6153726
hsa-mir-660	0.0077540	0.0137540	-2.1595295
hsa-mir-10a	0.0084745	0.0139159	1.8086133
hsa-miR-579	0.0085684	0.0140777	-1.8828573
hsa-mir-24	0.0090554	0.0142395	-1.3748805
hsa-mir-106b	0.0099932	0.0144013	-1.6189324
hsa-mir-559	0.0104168	0.0145631	-0.5886012
hsa-mir-632	0.0111769	0.0147249	-1.4962236
hsa-mir-142-3p	0.0115358	0.0148867	-3.1319298
hsa-mir-34c	0.0116842	0.0150485	-0.7266410
hsa-mir-30c	0.0121314	0.0152104	-0.8788309
hsa-mir-98	0.0135380	0.0153722	-2.2402383
hsa-mir-31	0.0135954	0.0155340	-2.4044068
hsa-mir-486	0.0136460	0.0156958	3.5125262
hsa-mir-410	0.0141069	0.0158576	1.7235875
hsa-miR-450	0.0141620	0.0160194	-0.6475819
hsa-mir-224	0.0146627	0.0161812	1.7923700
hsa-mir-324-3p	0.0156962	0.0163430	-1.3357590

Supplemental Table 4. miRNAs - MYB correlations in primary T-ALL patient samples (only shown miRNAs with a correlation score of < -0,5)

MicroRNAs	Correlation score
hsa-miR-876-3p	**-0.797802198**
hsa-miR-1285	**-0.754545455**
hsa-miR-100	**-0.581203008**
hsa-miR-155	**-0.575412088**
hsa-miR-1303	**-0.560714286**
hsa-miR-326	**-0.554179567**
hsa-miR-21*	**-0.524904215**
hsa-miR-125a-3p	**-0.517857143**
hsa-miR-193b	**-0.503479853**
hsa-miR-548a-5p	**-0.5**

Supplemental Table 5. MicroRNAs significantly (p <0.05) differentially expressed between the TAL subtype and other T-ALL subtypes in cohort 1 (t-test with Benjamini-Hochberg correction)

microRNA ID	t-test (p-value)	Benjamini-Hochberg	Fold Change
hsa-miR-200c	0.000007	0.000167	1.561932
hsa-miR-592	0.000032	0.005255	2.054280
hsa-miR-196b	0.000041	0.005405	-4.659506
hsa-miR-196a	0.000048	0.005556	-4.684535
hsa-miR-646	0.000079	0.005706	0.000000
hsa-miR-589	0.000128	0.005856	1.441916
hsa-miR-567	0.000414	0.006006	0.000000
hsa-miR-135a	0.000528	0.006156	-4.352846
hsa-miR-484	0.000722	0.006306	1.152414
hsa-miR-362	0.000764	0.006456	1.877522
hsa-miR-153	0.001060	0.006607	-2.057982
hsa-miR-502	0.002047	0.006757	0.914466
hsa-miR-422a	0.002268	0.006907	0.981960
hsa-miR-193b	0.003167	0.007057	-2.126321
hsa-miR-532	0.003345	0.007207	1.994637
hsa-miR-148a	0.006293	0.007357	1.811322
hsa-miR-125b	0.006434	0.007508	-2.172430
hsa-miR-130b	0.007325	0.007658	1.041703

Supplemental Table 6. MicroRNAs significantly (p<0.05) differentially expressed between the TAL subtype and other T-ALL subtypes of cohort 2 (t-test with Benjamini-Hochberg correction)

microRNA ID	t-test (p-value)	Benjamini-Hochberg	Fold Change
hsa-miR-15b*	0.0000001	0.0001190	2.1082243
hsa-miR-148a	0.0000005	0.0002381	3.2249217
hsa-miR-140-3p	0.0000009	0.0003571	-4.4621059
hsa-miR-200c	0.0000012	0.0004762	1.5013635
hsa-miR-1275	0.0000013	0.0005952	1.4690232
hsa-miR-450a	0.0000035	0.0007143	2.3650028
hsa-miR-141	0.0000036	0.0008333	1.7252399
hsa-miR-155*	0.0000045	0.0009524	-1.5357130
hsa-miR-135b	0.0000052	0.0010714	-2.8707393
hsa-miR-155	0.0000059	0.0011905	-1.1840741
hsa-miR-542-3p	0.0000095	0.0013095	2.0830691
hsa-miR-199a-3p	0.0000137	0.0014286	-2.2132103
rno-miR-29c*	0.0000233	0.0015476	1.3388016
hsa-miR-29c	0.0000284	0.0016667	1.4381646
hsa-miR-130b	0.0000743	0.0017857	1.2494804
hsa-miR-146b-5p	0.0000763	0.0019048	-1.2458543
hsa-miR-424	0.0000829	0.0020238	1.8914370
hsa-miR-625*	0.0001027	0.0021429	0.9115379

hsa-miR-454*	0.0001038	0.0022619	1.1192530
hsa-miR-454	0.0001228	0.0023810	0.8860373
hsa-miR-301b	0.0001611	0.0025000	1.0638763
hsa-miR-133a	0.0001796	0.0026190	-2.4124848
hsa-miR-942	0.0002136	0.0027381	0.8041648
hsa-miR-146b-3p	0.0002477	0.0028571	-1.4372405
hsa-miR-222	0.0003794	0.0029762	-1.1558824
hsa-miR-221*	0.0006076	0.0030952	-1.3214459
hsa-miR-31	0.0006614	0.0032143	1.8566747
hsa-miR-502-3p	0.0008211	0.0033333	1.3276797
hsa-miR-126*	0.0010863	0.0034524	-1.5275477
hsa-miR-301a	0.0011211	0.0035714	0.7397356
hsa-miR-31*	0.0011790	0.0036905	1.5421801
hsa-miR-15b	0.0012758	0.0038095	0.6859589
hsa-miR-18a*	0.0013089	0.0039286	0.7357702
hsa-miR-376a	0.0014459	0.0040476	1.4921312
hsa-miR-15a*	0.0019645	0.0041667	0.5371654
hsa-miR-1244	0.0020943	0.0042857	1.9340694
hsa-miR-455-5p	0.0021894	0.0044048	-1.8964802
hsa-miR-125a-5p	0.0023960	0.0045238	-2.0778450
hsa-miR-126	0.0025778	0.0046429	-1.5131013
hsa-miR-193b	0.0027420	0.0047619	-1.9393058
hsa-miR-411	0.0027428	0.0048810	1.2588644
hsa-miR-503	0.0032276	0.0050000	1.1878642
hsa-miR-125a-3p	0.0034847	0.0051190	-0.7306363
hsa-miR-96	0.0048807	0.0052381	1.0792698
hsa-miR-450b-5p	0.0051980	0.0053571	0.8109941
hsa-miR-362-5p	0.0054464	0.0054762	1.2215247

Supplemental Table 7. Primers for qPCR

Gene	Forward	Reverse
MYB	GCTGCTTCCCAAGTCTGGAA	CCACCAGCTTCTTCAGTTTTTCA
B2M	TGCTGTCTCCATGTTTGATGTATCT	TCTCTGCTCCCCACCTCTAAGT
SDHA	TGGGAACAAGAGGGCATCTG	CCACCACTGCATCAAATTCATG
TBP	CACGAACCACGGCACTGATT	TTTTCTTGCTGCCAGTCTGGAC
HPRT1	TGACACTGGCAAAACAATGCA	GGTCCTTTTCACCAGCAAGCT
UBC	ATTTGGGTCGCGGTTCTTG	TGCCTTGACATTCTCGATGGT

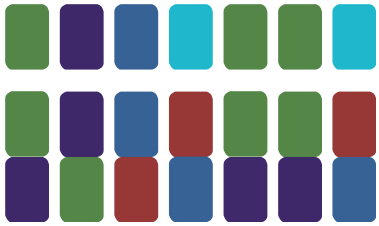

Chapter 4

Discussion & Future perspectives

Discussion & Future perspectives

The genetic landscape of T-ALL has been a very active area of research during the past decades. This delivered an overwhelming body of exciting novel findings providing insight into (1) the genetic heterogeneity of the disease with marked genetic subsets, (2) the mechanisms of disruption of normal T-cell development during leukemogenesis and (3) emerging opportunities for novel therapeutic interventions[1-4]. Of further interest, recent genome wide sequencing studies identified involvement of a novel class of proteins as emerging oncogenes and tumor suppressor genes in T-ALL[5-9] that actively participate in the regulation of the T-cell epigenome[5-9]. In my own work, I contributed to the unraveling of the epigenomic landscape of T-ALL by the identification of recurrent inactivating defects in the putative chromatin reader *PHF6* (**paper 1**[6]) and the histone H3K27me2/3 demethylase *UTX* in pediatric and adult T-ALL cases (**paper 2**, reviewed chapter 2[10]). Next to the broadening of the epigenetic landscape in T-ALL, I contributed to the exploration of the role of miRNAs in T-ALL pathogenesis. Using primary T-ALL patient data and *in vivo* modeling in the NOTCH1 T-ALL mouse model, we could identify a set of oncomiRs that are capable of co-regulating several T-ALL tumor suppressor genes (**paper 3**[11]). Furthermore, implementation of a 3'UTR *MYB* library screen followed by validation of candidate miRNAs in T-ALL model systems enabled us to identify a miR-193b-3p mediated deregulation of MYB in T-cell leukemia (**paper 4**).

PART 1. Identification of X-linked epigenetic drivers in T-ALL and their role in sensitivity to epigenetic therapy

Given the higher incidence of T-ALL in males (~3:1), we hypothesized that the presence of tumor suppressor genes on the X-chromosome could be a possible explanation for this skewed gender distribution. In the early days of exome sequencing, it was therefore decided to perform sequencing of the entire X-chromosome exome in an attempt to identify one or more X-linked tumor suppressor genes (**paper 1**)[6]. This pioneering study, performed as collaborative effort with the Ferrando lab (Columbia, NY, USA), revealed *PHF6* mutations in a set of pediatric (16%) and adult (38%) T-ALL patient samples[6].

Several genetic defects present in T-ALL are marked by a discrepancy in occurrence between childhood and adult T-ALL. *TLX3* translocations are present in 22.4% of childhood and 13.1% of adult T-ALL[12]. In contrast, *TLX1* rearrangements are more frequently present in adult (30%) compared to childhood T-ALL (5-10%)[4]. Furthermore, *JAK1* mutations are present in only 2% of pediatric T-ALL whereas 26.3% of adults with T-ALL bear *JAK1* mutations[13]. As *PHF6* mutations are significantly associated with *JAK1*, *TLX1* and *TLX3* aberrations, the higher frequency of *PHF6* mutations in adults can be in line with the age-dependent occurrence of defects in these other 3 genes[6,14].

Somatic *PHF6* mutations were also identified, although less frequent, in other cancer types including AML[15-17], CML in blast crisis[18], bladder cancer[19] and hepatocellular carcinoma[16]. As the *PHF6* gene is most commonly targeted in T-cell leukemia by mutations[6], deletions[6] or hypermethylation[20] and hereby quite restricted to malignant T-cell pathogenesis, we hypothesize a particular vulnerability for PHF6 loss in normal thymocytes towards malignant transformation. The molecular basis for this is currently under investigation in our lab in close collaboration with the Taghon lab (UGent, Ghent, Belgium) and yielding some novel and exciting preliminary insights.

As cancer is a multi step process driven by typically at least 5 or more (epi)genetic events, it is interesting to investigate to what extent such mutations contribute to early steps of transformation rather than late or cooperative events. In this context, much can be learned from familial cancer syndromes. Many of the now known tumor suppressor genes following the classical Knudson two-hit hypothesis were identified as familial cancer predisposing genes, thus implicating these tumor suppressors can act as early events in tumor formation in certain tissues. In this context, it is of interest that *PHF6* mutations are also found to be the causal event in the development of the mental retardation syndrome BFLS[21]. Being extremely rare, a thorough study of series of patients for risk in cancer development is precluded. But it is remarkably that of the few patients reported thus far, the only one developing cancer was described to have T-ALL[22]. In agreement, loss of PHF6 resulted in a strong acceleration of leukemia onset in the well-established NOTCH1 T-ALL mouse model (**paper 3**[11]). These findings further underscore the crucial role of PHF6 in T-ALL and its possible function in the early process of tumor development.

The PHF6 protein contains two PHD-like zinc finger domains. As similar domains are commonly present in nuclear proteins and chromatin-associated factors and given the nuclear localization of PHF6, it has been postulated that PHF6 acts as a modifier of the chromatin structure and thus implicated in gene regulation[23]. PHF6 was shown to cooperate with the chromatin remodeler complex NuRD[24]. Many members of the NuRD complex are linked to negative regulation of gene transcription[25]. The HDAC members of NuRD erase acetyl groups on lysines, a histone modification mark linked to active transcription; whereas the MBD proteins can recognize DNA methylation present in closed chromatin conformations[25]. The NuRD complex also associates with LSD1, a histone demethylase that can erase methyl groups on H3K4 leading again to compaction of the chromatin[26]. Notably, the NuRD complex plays an important role in hematopoietic differentiation and more specifically in transcriptional regulation of crucial genes during T-cell development[25]. Herewith it is intriguing to explore if PHF6 has a role in negative transcriptional regulation in accordance with the NuRD complex in normal and malignant T-cell development. For this, our lab has generated functional *in vitro* and *in vivo* model systems to explore the transcriptional network regulated by PHF6. Of further notice, *PHF6* mutations are most frequently detected in the TLX1 and TLX3 T-ALL subgroups. Exploration of the link between the TLX1, TLX3 and PHF6 proteins is ongoing in our lab through *in vitro* modeling of TLX1- or TLX3-rearranged human T-ALL cell lines and *in vivo* crossing of zebrafish strains in collaboration with the Langenau Lab (Massachusetts General Hospital, Boston, USA).

Intriguingly, PHF6 has also been linked to yet another protein complex broadly implicated in epigenetic remodeling, i.e. the SWI/SNF complex. Indeed, PHF6 was recently found to be mutated in patients with the Coffin-Siris developmental disorder[27]. The discovery of *PHF6* aberrations in the Coffin-Siris syndrome was quite surprising since this syndrome is mainly provoked by mutations in known components of the SWI/SNF remodeling complex[27]. Hence it might be of interest to further investigate if PHF6 plays a role in cooperating or antagonizing this ATPase-dependent remodeling complex. This hypothesis is currently investigated in-depth in our lab.

Finally, functional studies have unraveled that the PHD-containing protein PHF6 has a role in DNA damage response[6,28] and PHF6 loss induces an increase in the global levels of γH2A.X present in the chromatin (**paper 1**)[6,28]. The NuRD complex becomes likewise PHF6 phosphorylated after DNA damage by the ATM and ATR DNA damage checkpoint kinases[28] and actively aids in the repair after DNA damage[24,25]. Hereby the NURD-PHF6 complex might

be involved in active DNA repair, a research question that is currently addressed in our lab as well.

The recent discovery of inactivating mutations in the four members *EZH2*, *EED*, *SUZ12* and *JARID2* of the PRC2 complex in primary T-ALL patient samples[5,7,29] further stresses, like in most other cancer types, the broad implication of epigenetic perturbations, in particular for T-ALL an imbalance in H3K27 methylation. Another regulator of H3K27 methylation levels is the histone H3K27me2/3 demethylase *UTX*, already described as tumor suppressor gene in many cancer types and like the *PHF6* gene also located on the X-chromosome[30-34]. Accordingly, we hypothesized that the X-linked epigenetic regulator UTX might also be implicated in T-ALL possibly further contributing to the increased T-ALL incidence in males. Inactivating mutations in the *UTX* gene were detected in 5 of 35 primary T-ALL patient samples (**paper 2**). Intriguingly, these loss-of-function mutations were all present in the functional JmjC domain of UTX presumably affecting the H3K27me2/3 demethylase function.

As we detected *UTX* mutations in T-ALL patient samples solely in the functional Jmjc domain and *UTX* mutant samples are more sensitive to DZNep treatment, the oncogenic effect of loss of UTX in T-ALL might be mainly provoked by disruption of its H3K27me2/3 demethylase activity. But we can't rule out that this oncogenicity in T-ALL is caused through other mechanisms since a demethylase-independent role for UTX was demonstrated in the interaction with the BRG1-containing SWI/SNF remodeling complex promoting general chromatin remodeling[35,36]. To address this question, one experimental set-up would be to test if a catalytic inactive Utx protein could rescue the oncogenic effect of Utx loss in the MOHITO cell line.

Of particular interest, the identified *UTX* mutations were only detected in male T-ALL patient samples. Since previous studies have shown that *UTX* can escape chromosome X-inactivation in certain tissues[37], we explored if *UTX* is expressed also from both X-chromosomes in lymphoblasts of female T-ALL patients. By sequencing of two silent SNPs on genomic DNA (gDNA) and on complementary DNA (cDNA), we could confirm that *UTX* is bi-allelically expressed in female T-ALL lymphoblasts (**paper 2**). This important observation is in contrast to the other identified X-linked tumor suppressor genes *PHF6* (**paper 1**[6]) and *RPL10*[8] in T-ALL, which are not able to escape X-inactivation in female T-ALL lymphoblasts. Hence the identification of mutations in the *UTX* gene in males provides a further possible explanation for the skewed gender distribution observed in T-ALL.

UTX is a frequent mutational target in many solid tumors and leukemias[30], whereas the second family member and also bona fide H3K27me2/3 demethylase JMJD3 is rarely mutated (COSMIC database: *JMJD3* mutations detected in about 1% of tumors). This discrepancy underscores the partially non-overlapping roles of UTX and JMJD3. Namely, the H3K27me2/3 demethylases UTX and JMJD3 share common functionalities but also possess non-redundant roles. For example, the RAS-RAF signaling pathway induces JMJD3, but not UTX, leading to transcriptional activation of *CDKN2A*[38]. Vice versa JMJD3, unlike UTX, is not required for efficient induction and re-establishment of pluripotency during iPSC formation[39]. So the strong oncogenic effect of *UTX* loss observed in our T-ALL mouse model is presumably not compensated by the other H3K27me2/3 demethylase JMJD3.

Likewise *UTX*, the epigenetic players *DNMT3A* and *EZH2* are more frequently affected by somatic mutations compared to their close family members *DNMT1*/*DNMT3B* and *EZH1*, respectively[40]. A higher prevalence of *DNMT3A* mutations in myeloid malignancies and T-ALL

can relate to the presumed unique role for DNMT3A in hematopoiesis[40]. The H3K27 methyltransferases EZH1 and EZH2 are incorporated in the PRC2 complex depending on the cellular context. EZH2 is expressed in actively dividing cells, whereas EZH1 is present in resting cells[41,42]. In conditional EZH2 knockout mice that spontaneously develop T-ALL, the EZH1 protein was detectable but could not rescue the decrease in global H3K27me2/3 levels caused by EZH2 loss[29]. Furthermore, EZH1 is unable to rescue embryonic lethality caused by EZH2 loss in germline EZH2 knockouts[41,42]. So epigenetic players with redundant enzymatic activities can contain unique roles in the regulation of specific biological processes depending on the cell-type and the cellular context.

Our finding that both UTX and the PRC2 complex act as tumor suppressors in T-ALL is quite surprising and intriguing given their opposing enzymatic activities (**Table 1**). Similar loss-of-function mutations in *UTX* and the four members *EZH2*, *SUZ12*, *EED* and *JARID2* of the PRC2 are detected in myeloid malignancies including AML and MDS[30,43-46]. One possible explanation for this apparent contradiction is that UTX and PRC2 regulate a different set of target genes[35]. Alternatively, the other H3K27me2/3 demethylase JMJD3 can act at some PRC2 target genes instead of UTX as both H3K27me2/3 demethylases were shown to exert a distinct biology[34,35,47,48]. Moreover, both UTX and JMJD3 have a demethylase-independent role interacting with the BRG1-containing SWI/SNF remodeling complex promoting general chromatin remodeling[35,36], hence UTX-JMJD3 and PRC2 might regulate different biological processes even independent of H3K27me3 regulation.

Table1. Comparison of UTX and PRC2 characteristics

Functions	UTX	PRC2
T-ALL	tumor suppressor	tumor suppressor
Cancer	tumor suppressor	dual: oncogene or tumor suppressor
Developmental disease	Kabuki syndrome	Weaver syndrome (EZH2)
H3K27	H3K27me2/3 eraser	H3K27 methyltransferase
Target genes	HOX, RB	HOX, developmental regulators, 10% of all genes in ESCs, …
Interaction	MLL2, CBP, BRG1 - SWI/SNF	JARID2, AEBP2, PCL, HDAC1, DNMTs, XIST, HOTAIR, …
Family members	JMJD3, UTY	PRC1, PRC2
Knockout mice	embryonic lethality at E10.5-12.5 for $Utx^{-/-}$	embryonic lethality before E10.5 for $Ezh2^{-/-}$
Loss in ESCs	differentiation defect	differentiation defect, loss of pluripotency delayed
Inhibitors	GSKJ4	GSK126, EPZ-6438, …

In our *in vitro* and *in vivo* murine T-ALL models with UTX or SUZ12 loss, we could provide some clues that UTX and SUZ12 exert different roles in T-cell transformation as gene expression profiling showed that non-overlapping genetic pathways were affected between the two loss-of-function models (**paper 2**). Next to the gene expression profiles, RNA-sequencing and chromatin immunoprecipitation (ChIP) followed by high-throughput sequencing (seq) of UTX, SUZ12 as well as H3K27me3 in our *in vitro* and *in vivo* model systems would enable a more detailed characterization of the direct UTX and SUZ12 target genes and non-coding genes. Given that UTX can physically associate with MLL2, it would be

interesting to investigate if this is also true in a T-ALL context using mass-spectrometry & co-immunoprecipitation studies. Also ChIP-seq of H3K4me3 levels after UTX loss might indicate if UTX is essential in T-ALL for the functional activity of MLL2 in H3K4me3 regulation. Similar approaches using gene expression profiling and ChIP-seq have been undertaken in cancer models, for example to identify the *HOXA* cluster as target of the epigenetic regulator ASXL1 in myeloid malignancies[49].

Knockdown of UTX and SUZ12 provided a clear acceleration in leukemia onset in the commonly used NOTCH1 T-ALL mouse model[50] (**paper 2**). Furthermore, mutations targeting *UTX* or the *PRC2* complex both frequently co-occur with *NOTCH1* mutations (**paper 2**)[5]. This implicates that both loss of UTX or PRC2 can cooperate with NOTCH1 in T-ALL pathogenesis. A previous study of the Aifantis lab (NYU, NY, USA) has demonstrated that NOTCH1 signaling in T-ALL promotes the reduction in PRC2 activity at NOTCH1 target genes marked by loss of H3K27me3, these NOTCH1 target genes being enriched for known PRC2 target genes[5]. Moreover, several NOTCH1 ligands and HES1 family members have been shown to be direct targets of the PRC2 complex in human ESCs and embryonic fibroblasts[51,52]. This indicates that the NOTCH1 pathway might be under influence of PRC2 activity in mammals (**Figure 1**)[53].

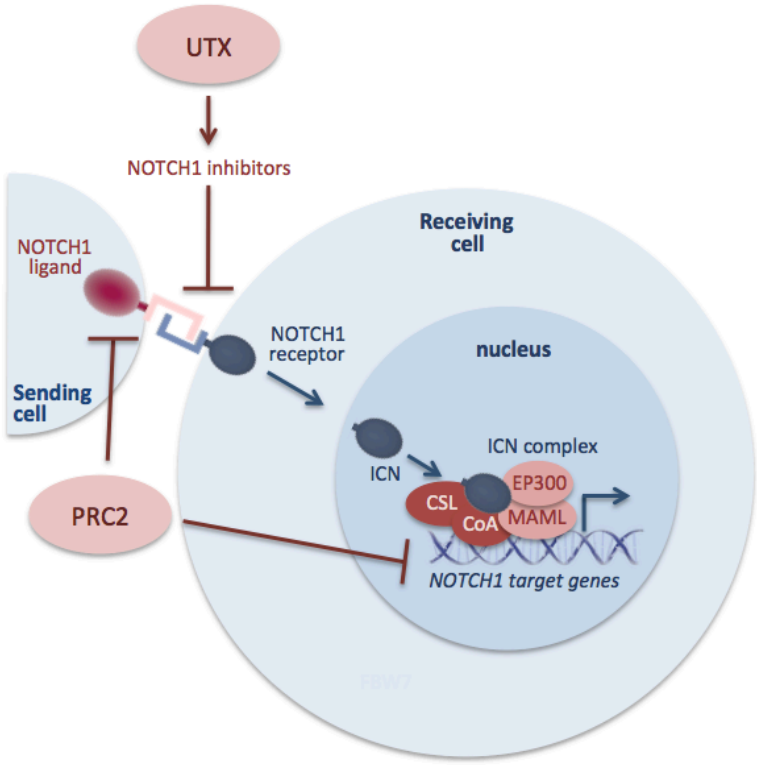

Figure 1. The histone methyltransferase PRC2 and the histone demethylase UTX control the NOTCH1 signaling pathway at different levels[53] (graphics from www.somersault1824.com)

In addition, in flies dUTX loss-of-function mutants give rise to decreased mRNA levels of negative regulators of Notch and elevated protein levels of Notch[53,54] (**Figure 1**). So both H3K27me3 regulators seem to influence the NOTCH1 signaling pathway through regulation of negative NOTCH1 regulators by UTX and regulation of NOTCH1 ligands and NOTCH1 target genes by PRC2[53,55] (**Figure 1**). Thus this distinct regulation of the NOTCH1 signaling might be a possible explanation for why these epigenetic players with opposing enzymatic

activities are both inactivated in T-ALL, but more research is needed to validate this hypothesis.

Both H3K27me2/3 regulators UTX and PRC2 are essential during normal embryonic development since loss of *Utx* (together with *Uty* in males), *Ezh2*, *Suz12* or *Eed* leads to embryonic lethality[56-61]. Furthermore, these chromatin regulators seem to play crucial roles during hematopoiesis[58,60,62-64]. Loss of Ezh2 provokes an early arrest in B-cell and T-cell development[64], whereas loss of Utx gives rise to an enlarged spleen, reduced hemoglobin levels, anemia, thrombocytopenia and mild leukocytopenia[60]. Moreover, loss of Ezh2 in mouse HSCs induced murine T-ALL formation[29], in accordance with the observation that adult mice bearing a hypomorphic *Eed* allele develop severe lymphoid and myeloid disorders[65]. In our study, we provide first evidence that the PRC2 member Suz12 also contributes *in vivo* to lymphoid tumor formation (**paper 2**).

The identification of these epigenetic drivers in T-ALL can provide novel therapeutic angles in this aggressive disease, since epigenetic therapies are promising agents in cancer therapy. Moreover, the first epigenetic therapies have already been approved by the FDA as effective cancer treatments, which are the DNMTi vidaza and decitabine approved for treatment of MDS[66,67] and the HDACi vorinostat and romidepsin approved for treatment of T-cell cutaneous lymphoma[66,68]. In our UTX study, we were able to show that *UTX* mutant T-ALL cells are more sensitive to the H3K27me3 inhibitor DZNep suggesting that this drug might serve as a new therapeutic strategy for *UTX* mutant T-ALL patients (**paper 2**). DZNep is a competitive inhibitor of the S-adenosylhomocysteine hydrolase leading to an accumulation of S-adenosylhomocysteine and blocking the production of the essential HMT co-factor SAM[69]. Subsequently, H3K27 methylation levels decline leading to apoptosis of cancer cell lines[69] and *UTX* mutant T-ALL samples (**paper 2**). In addition, specific EZH2 inhibitors were developed including GSK-126 that enable direct EZH2 blockage followed by H3K27me3 loss and provoking reactivation of PRC2 target genes[70]. Since PRC2 and UTX presumably exert differential roles in malignant T-cells, the use of these specific EZH2 inhibitors like GSK-126 in *UTX* mutant T-ALL samples seems dual as direct EZH2 inhibition might cause unwanted effects. To conclude, we could demonstrate that restoring the precise balance of H3K27 methylation by use of DZNep can restrain *UTX* mutant T-cell leukemia (**paper 2**). In addition, precaution is warranted in selecting T-ALL patients for specific epigenetic therapies, since both UTX and PRC2 are acting as tumor suppressors in this disease.

To conclude, we identified the X-linked *PHF6* and *UTX* genes as mutational targets and *bona fide* tumor suppressor genes in T-ALL (**paper 1[6] & 2**). Until now, we and others were unable to show any prognostic relevance to the occurrence of *PHF6* or *UTX* loss-of-function defects in T-ALL (**paper 1[6] & 2**). For this, detailed mutational and clinical characterization of large T-ALL cohorts is needed to connect these genetic defects to specific prognostic or treatment-response values. Also, these large T-ALL cohorts can be used to further explore which lesions co-occur together with *UTX* and *PHF6* mutations in primary T-ALL patient samples.

Furthermore, we could show an oncogenic role for loss of UTX (**paper 2**) and PHF6[11] in our T-ALL mouse model. Further exploration of PHF6 and UTX loss to T-ALL pathogenesis by gene expression and ChIP-seq profiling is essential to grasp how these epigenetic players mechanistically contribute to this aggressive cancer type. Establishment of hematopoietic-specific conditional knockout mice for UTX, SUZ12 or PHF6, likewise the conditional EZH2 knockout mice[29], can further unravel how these different epigenetic players contribute to T-ALL formation.

In paper 2, we observed a co-occurrence of *UTX* mutations and *SUZ12* deletions in primary T-ALL patient samples, a quite remarkable finding given their opposite roles on H3K27 regulation. Generation of double knockouts with concurrent loss of two epigenetic regulators has been already explored *in vivo*, for example the TET2 – EZH2 double knockout in myeloid malignancies[71]. Hereby the generation and genomic exploration of UTX – SUZ12 double knockouts can shed light on the cooperativity of these two epigenetic evens in T-ALL.

PART 2. Search for deregulated microRNA networks in T-ALL

Twenty years ago, the first miRNA lin-4 was discovered which was shown to have a negative impact on the development of *Caenorhabditis elegans*[72]. A small decade later, the first chromosomal defects leading to miRNA deregulation were found through the discovery of recurrent translocations and deletions targeting the miR-15a/miR-16-1 locus in chronic lymphocytic leukemia (CLL) leading to a decreased expression of both miRNAs[73]. One of the first key observations for involvement of miRNAs in T-ALL was the finding of a chromosomal translocation juxtaposing the miR-17-92 cluster under the control of the T-cell specific enhancer of the *TCR*β leading to strong induction of miR-17-92[74]. This polycistronic miRNA cluster was described as one of the first oncomiRs in cancer[75]. The miR-17-92 cluster encodes 6 miRNAs (miR-17, miR-18a, miR-19a, miR-20a, miR-19b-1 and miR-92a-1) and is located in the non-protein-coding gene *C13orf25* at chromosome 13. Importantly, these polycistronic miRNA members are co-transcribed but are individually processed, so different expression levels of the individual members can be present in a specific cell-type. Furthermore, the mature and seed sequences differ between the miR-17-92 members thereby a specific set of target genes can be regulated by each member[76].

Of interest, the miR-17-92 cluster plays a role in animal development, since lack of miR-17-92 in mice leads to postnatal lethality[77]. More specifically, the miR-17-92 cluster was shown to play a role in B-cell differentiation as miR-17-92 ablation leads to enhanced pro-B-cell apoptosis during the pro- to pre-B-cell stage[77]. Also in T-cell development the miR-17-92 cluster contributes by promoting CD4+ T-cell helper cell responses[78] and effector CD8+ T-cell expansion[79]. This data supports the oncogenic effects observed after deregulation of the miR-17-92 cluster in normal T-cells.

The miR-19 member was shown by Mavrakis et al. and other groups to be the key oncogenic determinant of the miR-17-92 cluster contributing to lymphoma and T-ALL formation[59,66,67]. In contrast, the miR-17/20a miRNA members were shown to be the main oncogenic components in retinoblastoma working in concert with Rb loss[80]. So depending on the cell-type and context, a different miRNA cluster member can play a key role in cancer formation. In our study, we could demonstrate that miR-20a and miR-92 are also oncogenic in T-ALL in addition to miR-19, both *in vitro* in human T-ALL cell lines and *in vivo* in the NOTCH1 T-ALL mouse model (**paper 3**)[11,74]. Furthermore, our study showed that the different members miR-19b, miR-20a and miR-92 are capable of targeting the common T-ALL tumor suppressor genes *PTEN* and *BIM*. These findings are in agreement with a study in which a miR-17-92 transgenic mouse model with specific enhanced miR-17-92 expression in lymphocytes was shown to develop a lymphoproliferative disease and suppress Bim and Pten expression[81]. Moreover, miR-20a is also capable of targeting the tumor suppressor PHF6 and miR-92 can additionally regulate IKZF1, NF1 and FBXW7 in T-ALL (**paper 3**)[11]. Thus the miR-17-92 members can cooperate in promoting T-ALL formation presumably through silencing of a larger group of T-ALL tumor suppressor genes than is plausible by only one miR-17-92 cluster member[11,76].

Besides cooperation with NOTCH1 as we have shown in our oncomiR story (**paper 3**)[10,60], the miR-17-92 cluster can also work in concert with the *MYC* oncogene[11,74,82]. Overexpression of the miR-17-19b-1 cluster (vertebrate portion of the miR-17-92 cluster) together with the *MYC* oncogene showed an accelerated MYC-induced B-cell lymphomagenesis in mice[82]. Furthermore, MYC was shown to directly control the expression of miR-17-92 and the cell cycle regulator *E2F1* promoting cell cycle progression. Surprisingly, both miR-17 and miR-20a can negatively regulate E2F1 protein expression leading to a tightly controlled proliferative signal through MYC and its regulated miRNA cluster[83]. In addition, several MLL-fusions were shown to directly drive miR-17-92 expression leading to aberrant H3 acetylation and H3K4 trimethylation[84].

In addition to the miR-17-92 cluster, we also identified miR-223, miR-26a, miR-27a and miR-148a/152 as *bona fide* oncomiRs in T-ALL. MiR-26a targets the T-ALL tumor suppressors PHF6 and PTEN[11], miR-223 targets the negative NOTCH1 regulator FBXW7[11,85,86], miR-27a regulates BIM, IKZF1, NF1 and FBXW7[11] whereas miR-148a/152 targets PTEN, BIM and IKZF1[11]. To conclude, we could show that miR-19b, miR-20a, miR-92, miR-223, miR-26a, miR-27a and miR-148a/152 regulate a defined set of tumor suppressors in T-ALL including BIM, PTEN, PHF6, IKZF1, NF1 and FBXW7 (**paper 3**)[11]. This is one of the first miRNA networks that was described in cancer and illustrates how coordinated regulation of multiple tumor suppressor genes in T-ALL is controlled by different miRNAs[87]. Other miRNA – protein-coding networks encompass the miR-17-92 cluster/MYC/E2F1 described in lymphoma[83] and the miR-15a/miR-16-1/miR-34abc/TP53/ZAP70/BCL2/MCL1 network in CLL[88].

Subsequent to oncomiRs, we have explored the presence of tumor suppressor miRNAs in T-ALL. Therefore we selected the oncogene *MYB* as a first candidate for exploration of a possible miRNA-MYB network in T-ALL by use of an in-house designed 3'UTR library screen. This miRNAome-wide 3'UTR *MYB* library screen unraveled 33 miRNA candidates directly regulating the *MYB* oncogene. Filtering of these candidates using normal and malignant T-cell data enabled the identification of miR-193b-3p as a top candidate tumor suppressor miRNA targeting MYB in T-ALL, which we validated using *in vitro* and *in vivo* functional studies (**paper 4**). This is the first time that a miR-193b-3p – MYB connection is described both in normal or malignant development. Other MYB targeting miRNAs have already been identified in other specific cellular contexts like miR-150 in normal B-cell differentiation[89] and in MLL-fusion driven leukemia[90]. Of the 8 known miRNA-MYB interactions, we could confirm 5 in our MYB library screen (**paper 4**). Vice versa miR-193b-3p is already described to target other oncogenes like MCL1 and stathmin 1 in melanoma[91,92]. Since MCL1 was already shown to play an oncogenic role in T-ALL[11,86], we investigated and confirmed a miR-193b-3p interaction with MCL1 in T-ALL samples. In addition to the identification of the tumor suppressor miR-193b-3p in T-ALL, we are collaborating on a broader T-ALL tumor suppressor network study with the Wendel lab (MSKCC, NY, USA) (Sanghvi et al., Genes & Development, under review).

As we have shown that miRNAs can work together with NOTCH1 in T-ALL, we were also wondering if NOTCH1 could regulate miRNAs that mediate human T-cell development under normal physiological circumstances in the thymus. Therefore, we investigated which miRNAs are under the control of NOTCH1 in normal T-cell development using detailed miRNA expression profiles of in-depth sorted normal T-cell subsets, the OP9-DL1 normal T-cell model system and publically available NOTCH1 ChIP-sequencing data[93]. We first selected those miRNAs that are positively correlated to *NOTCH1* expression during normal T-cell development. These miRNAs were further evaluated for their sensitivity to NOTCH1

stimulation in an *in vitro* model mimicking normal T-cell development. Out of these candidates, the miR-17-92 cluster and miR-484 are directly regulated by NOTCH1[93]. Interestingly, miR-484 is strongly anti-correlated and predicted to interact with the T-cell regulator RORC. The candidate NOTCH1 driven miRNAs and their target genes are presently functionally modeled in the OP9-DL1 system to clearly define their contribution in normal T-cell development (Van der Meulen et al. in preparation). We have demonstrated that for miR-17-92 contributes to T-ALL pathogenesis[11,74], but until now miR-484 was not described yet in normal or malignant T-cell development. As we have now identified miR-484 as a NOTCH1-driven miRNA in normal T-cell differentiation, an oncogenic role for miR-484 in malignant T-cell transformation seems plausible and would be interesting to further investigate.

MiRNA therapeutics have the advantage that many target genes are hit simultaneously through targeting of only one miRNA or miRNA cluster[87]. As miR-17-92, miR-26a, miR-223, miR-27a and miR-148a/152 seem to be the key oncomiRs in T-ALL regulating many T-ALL tumor suppressor genes[11,74,85,86], the use of antisense oligonucleotide (ASO) approaches or miRNA sponges against these miRNAs are possible options. In our oncomiR story, we have shown that antagomiRs against miR-19a/b, miR-26a and miR-92 are able to reduce cell viability of T-ALL cell lines[11]. Moreover, an even stronger effect was seen, both on cell viability as on target gene expression, when these antagomiRs were introduced together[11]. Furthermore, the combination of miRNA directed therapies together with chemotherapeutics or molecular therapies, could be a powerful approach to tackle resistance against the latter[87]. For example, PI3K/AKT/mTOR inhibitors were shown to work in concert with GSIs or glucocorticoids hereby abrogating GSI/glucocorticoid acquired resistance[94,95]. Targeting of miR-17-92, miR-26a and/or miR-148a/152 might also be beneficial to treatment with GSIs or glucocorticoids, since these miRNAs were shown to decrease PTEN activity.

Next to miRNAs, a novel class of non-coding RNAs was identified coined long non-coding RNAs (lncRNAs). These lncRNAs have been shown to be implicated in many different cellular processes acting as guides, scaffolds or decoys, and can be implicated in cancer[96]. These non-coding RNAs represent interesting therapeutic targets since they are to a large extent expressed in specific tissue-types[97]. Targeting or restoring of lncRNAs has been already described by the use of siRNAs, ASOs, ribozymes and synthetic lncRNA mimics[87]. In our lab, a new research pipeline regarding the role of lncRNAs in normal and malignant T-cell development has been successfully initiated and will be explored in detail with the goal of identifying novel therapeutic targets in T-ALL.

References

1. Ferrando, A.A. *et al.* Gene expression signatures define novel oncogenic pathways in T cell acute lymphoblastic leukemia. *Cancer Cell* **1**, 75-87 (2002).
2. Homminga, I. *et al.* Integrated transcript and genome analyses reveal NKX2-1 and MEF2C as potential oncogenes in T cell acute lymphoblastic leukemia. *Cancer Cell* **19**, 484-97 (2011).
3. Soulier, J. *et al.* HOXA genes are included in genetic and biologic networks defining human acute T-cell leukemia (T-ALL). *Blood* **106**, 274-86 (2005).
4. Van Vlierberghe, P. & Ferrando, A. The molecular basis of T cell acute lymphoblastic leukemia. *J Clin Invest* **122**, 3398-406 (2012).
5. Ntziachristos, P. *et al.* Genetic inactivation of the polycomb repressive complex 2 in T cell acute lymphoblastic leukemia. *Nat Med* **18**, 298-301 (2012).
6. Van Vlierberghe, P. *et al.* PHF6 mutations in T-cell acute lymphoblastic leukemia. *Nat Genet* **42**, 338-42 (2010).
7. Zhang, J. *et al.* The genetic basis of early T-cell precursor acute lymphoblastic leukaemia. *Nature* **481**, 157-63 (2012).
8. De Keersmaecker, K. *et al.* Exome sequencing identifies mutation in CNOT3 and ribosomal genes RPL5 and RPL10 in T-cell acute lymphoblastic leukemia. *Nat Genet* **45**, 186-90 (2013).
9. Neumann, M. *et al.* Whole-exome sequencing in adult ETP-ALL reveals a high rate of DNMT3A mutations. *Blood* **121**, 4749-52 (2013).
10. Van der Meulen, J., Speleman, F. & Van Vlierberghe, P. The H3K27me3 demethylase UTX in normal development and disease. *Epigenetics* **9**(2014).
11. Mavrakis, K.J. *et al.* A cooperative microRNA-tumor suppressor gene network in acute T-cell lymphoblastic leukemia (T-ALL). *Nat Genet* **43**, 673-8 (2011).
12. Berger, R. *et al.* t(5;14)/HOX11L2-positive T-cell acute lymphoblastic leukemia. A collaborative study of the Groupe Francais de Cytogenetique Hematologique (GFCH). *Leukemia* **17**, 1851-7 (2003).
13. Flex, E. *et al.* Somatically acquired JAK1 mutations in adult acute lymphoblastic leukemia. *J Exp Med* **205**, 751-8 (2008).
14. Wang, Q. *et al.* Mutations of PHF6 are associated with mutations of NOTCH1, JAK1 and rearrangement of SET-NUP214 in T-cell acute lymphoblastic leukemia. *Haematologica* **96**, 1808-14 (2011).
15. Van Vlierberghe, P. *et al.* PHF6 mutations in adult acute myeloid leukemia. *Leukemia* **25**, 130-4 (2011).
16. Yoo, N.J., Kim, Y.R. & Lee, S.H. Somatic mutation of PHF6 gene in T-cell acute lymphoblatic leukemia, acute myelogenous leukemia and hepatocellular carcinoma. *Acta Oncol* **51**, 107-11 (2012).
17. Patel, J.P. *et al.* Prognostic relevance of integrated genetic profiling in acute myeloid leukemia. *N Engl J Med* **366**, 1079-89 (2012).
18. Li, X. *et al.* Somatic mutations of PHF6 in patients with chronic myeloid leukemia in blast crisis. *Leuk Lymphoma* **54**, 671-2 (2013).
19. Kandoth, C. *et al.* Mutational landscape and significance across 12 major cancer types. *Nature* **502**, 333-9 (2013).
20. Kraszewska, M.D. *et al.* DNA methylation pattern is altered in childhood T-cell acute lymphoblastic leukemia patients as compared with normal thymic subsets: insights into CpG island methylator phenotype in T-ALL. *Leukemia* **26**, 367-71 (2012).
21. Lower, K.M. *et al.* Mutations in PHF6 are associated with Borjeson-Forssman-Lehmann syndrome. *Nat Genet* **32**, 661-5 (2002).

22. Chao, M.M. *et al.* T-cell acute lymphoblastic leukemia in association with Borjeson-Forssman-Lehmann syndrome due to a mutation in PHF6. *Pediatr Blood Cancer* **55**, 722-4 (2010).
23. Chi, P., Allis, C.D. & Wang, G.G. Covalent histone modifications--miswritten, misinterpreted and mis-erased in human cancers. *Nat Rev Cancer* **10**, 457-69 (2010).
24. Todd, M.A. & Picketts, D.J. PHF6 interacts with the nucleosome remodeling and deacetylation (NuRD) complex. *J Proteome Res* **11**, 4326-37 (2012).
25. Lai, A.Y. & Wade, P.A. Cancer biology and NuRD: a multifaceted chromatin remodelling complex. *Nat Rev Cancer* **11**, 588-96 (2011).
26. Wang, Y. *et al.* LSD1 is a subunit of the NuRD complex and targets the metastasis programs in breast cancer. *Cell* **138**, 660-72 (2009).
27. Wieczorek, D. *et al.* A comprehensive molecular study on Coffin-Siris and Nicolaides-Baraitser syndromes identifies a broad molecular and clinical spectrum converging on altered chromatin remodeling. *Hum Mol Genet* **22**, 5121-35 (2013).
28. Matsuoka, S. *et al.* ATM and ATR substrate analysis reveals extensive protein networks responsive to DNA damage. *Science* **316**, 1160-6 (2007).
29. Simon, C. *et al.* A key role for EZH2 and associated genes in mouse and human adult T-cell acute leukemia. *Genes Dev* **26**, 651-6 (2012).
30. van Haaften, G. *et al.* Somatic mutations of the histone H3K27 demethylase gene UTX in human cancer. *Nat Genet* **41**, 521-3 (2009).
31. Lan, F. *et al.* A histone H3 lysine 27 demethylase regulates animal posterior development. *Nature* **449**, 689-94 (2007).
32. Lee, M.G. *et al.* Demethylation of H3K27 regulates polycomb recruitment and H2A ubiquitination. *Science* **318**, 447-50 (2007).
33. De Santa, F. *et al.* The histone H3 lysine-27 demethylase Jmjd3 links inflammation to inhibition of polycomb-mediated gene silencing. *Cell* **130**, 1083-94 (2007).
34. Agger, K. *et al.* UTX and JMJD3 are histone H3K27 demethylases involved in HOX gene regulation and development. *Nature* **449**, 731-4 (2007).
35. Hock, H. A complex Polycomb issue: the two faces of EZH2 in cancer. *Genes Dev* **26**, 751-5 (2012).
36. Miller, S.A., Mohn, S.E. & Weinmann, A.S. Jmjd3 and UTX play a demethylase-independent role in chromatin remodeling to regulate T-box family member-dependent gene expression. *Mol Cell* **40**, 594-605 (2010).
37. Greenfield, A. *et al.* The UTX gene escapes X inactivation in mice and humans. *Hum Mol Genet* **7**, 737-42 (1998).
38. Agger, K. *et al.* The H3K27me3 demethylase JMJD3 contributes to the activation of the INK4A-ARF locus in response to oncogene- and stress-induced senescence. *Genes Dev* **23**, 1171-6 (2009).
39. Mansour, A.A. *et al.* The H3K27 demethylase Utx regulates somatic and germ cell epigenetic reprogramming. *Nature* **488**, 409-13 (2012).
40. Shih, A.H., Abdel-Wahab, O., Patel, J.P. & Levine, R.L. The role of mutations in epigenetic regulators in myeloid malignancies. *Nat Rev Cancer* **12**, 599-612 (2012).
41. Shen, X. *et al.* EZH1 mediates methylation on histone H3 lysine 27 and complements EZH2 in maintaining stem cell identity and executing pluripotency. *Mol Cell* **32**, 491-502 (2008).
42. Margueron, R. *et al.* Ezh1 and Ezh2 maintain repressive chromatin through different mechanisms. *Mol Cell* **32**, 503-18 (2008).
43. Jankowska, A.M. *et al.* Mutational spectrum analysis of chronic myelomonocytic leukemia includes genes associated with epigenetic regulation: UTX, EZH2, and DNMT3A. *Blood* **118**, 3932-41 (2011).

44. Score, J. *et al.* Inactivation of polycomb repressive complex 2 components in myeloproliferative and myelodysplastic/myeloproliferative neoplasms. *Blood* **119**, 1208-13 (2012).
45. Nikoloski, G. *et al.* Somatic mutations of the histone methyltransferase gene EZH2 in myelodysplastic syndromes. *Nat Genet* **42**, 665-7 (2010).
46. Ernst, T. *et al.* Inactivating mutations of the histone methyltransferase gene EZH2 in myeloid disorders. *Nat Genet* **42**, 722-6 (2010).
47. Barradas, M. *et al.* Histone demethylase JMJD3 contributes to epigenetic control of INK4a/ARF by oncogenic RAS. *Genes Dev* **23**, 1177-82 (2009).
48. Wang, J.K. *et al.* The histone demethylase UTX enables RB-dependent cell fate control. *Genes Dev* **24**, 327-32 (2010).
49. Abdel-Wahab, O. *et al.* ASXL1 mutations promote myeloid transformation through loss of PRC2-mediated gene repression. *Cancer Cell* **22**, 180-93 (2012).
50. Pear, W.S. *et al.* Exclusive development of T cell neoplasms in mice transplanted with bone marrow expressing activated Notch alleles. *J Exp Med* **183**, 2283-91 (1996).
51. Bracken, A.P., Dietrich, N., Pasini, D., Hansen, K.H. & Helin, K. Genome-wide mapping of Polycomb target genes unravels their roles in cell fate transitions. *Genes Dev* **20**, 1123-36 (2006).
52. Lee, T.I. *et al.* Control of developmental regulators by Polycomb in human embryonic stem cells. *Cell* **125**, 301-13 (2006).
53. Mills, A.A. Throwing the cancer switch: reciprocal roles of polycomb and trithorax proteins. *Nat Rev Cancer* **10**, 669-82 (2010).
54. Herz, H.M. *et al.* The H3K27me3 demethylase dUTX is a suppressor of Notch- and Rb-dependent tumors in Drosophila. *Mol Cell Biol* **30**, 2485-97 (2010).
55. Schuettengruber, B., Martinez, A.M., Iovino, N. & Cavalli, G. Trithorax group proteins: switching genes on and keeping them active. *Nat Rev Mol Cell Biol* **12**, 799-814 (2011).
56. Lee, S., Lee, J.W. & Lee, S.K. UTX, a histone H3-lysine 27 demethylase, acts as a critical switch to activate the cardiac developmental program. *Dev Cell* **22**, 25-37 (2012).
57. Welstead, G.G. *et al.* X-linked H3K27me3 demethylase Utx is required for embryonic development in a sex-specific manner. *Proc Natl Acad Sci U S A* **109**, 13004-9 (2012).
58. Wang, C. *et al.* UTX regulates mesoderm differentiation of embryonic stem cells independent of H3K27 demethylase activity. *Proc Natl Acad Sci U S A* **109**, 15324-9 (2012).
59. Shpargel, K.B., Sengoku, T., Yokoyama, S. & Magnuson, T. UTX and UTY demonstrate histone demethylase-independent function in mouse embryonic development. *PLoS Genet* **8**, e1002964 (2012).
60. Thieme, S. *et al.* The histone demethylase UTX regulates stem cell migration and hematopoiesis. *Blood* **121**, 2462-73 (2013).
61. Margueron, R. & Reinberg, D. The Polycomb complex PRC2 and its mark in life. *Nature* **469**, 343-9 (2011).
62. Liu, J. *et al.* A functional role for the histone demethylase UTX in normal and malignant hematopoietic cells. *Exp Hematol* **40**, 487-98 e3 (2012).
63. Kamminga, L.M. *et al.* The Polycomb group gene Ezh2 prevents hematopoietic stem cell exhaustion. *Blood* **107**, 2170-9 (2006).
64. Su, I.H. *et al.* Polycomb group protein ezh2 controls actin polymerization and cell signaling. *Cell* **121**, 425-36 (2005).
65. Lessard, J. *et al.* Functional antagonism of the Polycomb-Group genes eed and Bmi1 in hemopoietic cell proliferation. *Genes Dev* **13**, 2691-703 (1999).

66. Jones, P.A. & Baylin, S.B. The epigenomics of cancer. *Cell* **128**, 683-92 (2007).
67. Plass, C. *et al.* Mutations in regulators of the epigenome and their connections to global chromatin patterns in cancer. *Nat Rev Genet* **14**, 765-80 (2013).
68. Baylin, S.B. & Jones, P.A. A decade of exploring the cancer epigenome - biological and translational implications. *Nat Rev Cancer* **11**, 726-34 (2011).
69. Tan, J. *et al.* Pharmacologic disruption of Polycomb-repressive complex 2-mediated gene repression selectively induces apoptosis in cancer cells. *Genes Dev* **21**, 1050-63 (2007).
70. McCabe, M.T. *et al.* EZH2 inhibition as a therapeutic strategy for lymphoma with EZH2-activating mutations. *Nature* **492**, 108-12 (2012).
71. Muto, T. *et al.* Concurrent loss of Ezh2 and Tet2 cooperates in the pathogenesis of myelodysplastic disorders. *J Exp Med* **210**, 2627-39 (2013).
72. Lee, R.C., Feinbaum, R.L. & Ambros, V. The C. elegans heterochronic gene lin-4 encodes small RNAs with antisense complementarity to lin-14. *Cell* **75**, 843-54 (1993).
73. Calin, G.A. *et al.* Frequent deletions and down-regulation of micro- RNA genes miR15 and miR16 at 13q14 in chronic lymphocytic leukemia. *Proc Natl Acad Sci U S A* **99**, 15524-9 (2002).
74. Mavrakis, K.J. *et al.* Genome-wide RNA-mediated interference screen identifies miR-19 targets in Notch-induced T-cell acute lymphoblastic leukaemia. *Nat Cell Biol* **12**, 372-9 (2010).
75. Ota, A. *et al.* Identification and characterization of a novel gene, C13orf25, as a target for 13q31-q32 amplification in malignant lymphoma. *Cancer Res* **64**, 3087-95 (2004).
76. Olive, V., Li, Q. & He, L. mir-17-92: a polycistronic oncomir with pleiotropic functions. *Immunol Rev* **253**, 158-66 (2013).
77. Ventura, A. *et al.* Targeted deletion reveals essential and overlapping functions of the miR-17 through 92 family of miRNA clusters. *Cell* **132**, 875-86 (2008).
78. Jiang, S. *et al.* Molecular dissection of the miR-17-92 cluster's critical dual roles in promoting Th1 responses and preventing inducible Treg differentiation. *Blood* **118**, 5487-97 (2011).
79. Wu, T. *et al.* Temporal expression of microRNA cluster miR-17-92 regulates effector and memory CD8+ T-cell differentiation. *Proc Natl Acad Sci U S A* **109**, 9965-70 (2012).
80. Conkrite, K. *et al.* miR-17~92 cooperates with RB pathway mutations to promote retinoblastoma. *Genes Dev* **25**, 1734-45 (2011).
81. Xiao, C. *et al.* Lymphoproliferative disease and autoimmunity in mice with increased miR-17-92 expression in lymphocytes. *Nat Immunol* **9**, 405-14 (2008).
82. He, L. *et al.* A microRNA polycistron as a potential human oncogene. *Nature* **435**, 828-33 (2005).
83. O'Donnell, K.A., Wentzel, E.A., Zeller, K.I., Dang, C.V. & Mendell, J.T. c-Myc-regulated microRNAs modulate E2F1 expression. *Nature* **435**, 839-43 (2005).
84. Mi, S. *et al.* Aberrant overexpression and function of the miR-17-92 cluster in MLL-rearranged acute leukemia. *Proc Natl Acad Sci U S A* **107**, 3710-5 (2010).
85. Correia, N.C. *et al.* Novel TAL1 targets beyond protein-coding genes: identification of TAL1-regulated microRNAs in T-cell acute lymphoblastic leukemia. *Leukemia* **27**, 1603-6 (2013).
86. Mansour, M.R. *et al.* The TAL1 complex targets the FBXW7 tumor suppressor by activating miR-223 in human T cell acute lymphoblastic leukemia. *J Exp Med* **210**, 1545-57 (2013).

87. Ling, H., Fabbri, M. & Calin, G.A. MicroRNAs and other non-coding RNAs as targets for anticancer drug development. *Nat Rev Drug Discov* **12**, 847-65 (2013).
88. Fabbri, M. *et al.* Association of a microRNA/TP53 feedback circuitry with pathogenesis and outcome of B-cell chronic lymphocytic leukemia. *JAMA* **305**, 59-67 (2011).
89. Xiao, C. *et al.* MiR-150 controls B cell differentiation by targeting the transcription factor c-Myb. *Cell* **131**, 146-59 (2007).
90. Jiang, X. *et al.* Blockade of miR-150 maturation by MLL-fusion/MYC/LIN-28 is required for MLL-associated leukemia. *Cancer Cell* **22**, 524-35 (2012).
91. Chen, J. *et al.* Stathmin 1 is a potential novel oncogene in melanoma. *Oncogene* **32**, 1330-7 (2013).
92. Chen, J. *et al.* miR-193b Regulates Mcl-1 in Melanoma. *Am J Pathol* **179**, 2162-8 (2011).
93. Wang, H. *et al.* Genome-wide analysis reveals conserved and divergent features of Notch1/RBPJ binding in human and murine T-lymphoblastic leukemia cells. *Proc Natl Acad Sci U S A* **108**, 14908-13 (2011).
94. Piovan, E. *et al.* Direct Reversal of Glucocorticoid Resistance by AKT Inhibition in Acute Lymphoblastic Leukemia. *Cancer Cell* **24**, 766-76 (2013).
95. Shepherd, C. *et al.* PI3K/mTOR inhibition upregulates NOTCH-MYC signalling leading to an impaired cytotoxic response. *Leukemia* **27**, 650-60 (2013).
96. Spizzo, R., Almeida, M.I., Colombatti, A. & Calin, G.A. Long non-coding RNAs and cancer: a new frontier of translational research? *Oncogene* **31**, 4577-87 (2012).
97. Djebali, S. *et al.* Landscape of transcription in human cells. *Nature* **489**, 101-8 (2012).

Summary

T-ALL is an aggressive hematological malignancy, in which undifferentiated normal T-cells acquire a set of (epi)genetic defects giving rise to a strong accumulation of malignant T-cell lymphoblasts. Cure rates in T-ALL range from 50-75% depending on the age, but unfortunately still a significant number of T-ALL patients relapse early during therapy with little chances for survival. Current treatment regimes encompass risk-adapted chemotherapy, hematopoietic stem cell transplantation and supportive care. I anticipate that a detailed characterization of the (epi)genetic landscape in T-ALL patient samples will provide a basis for novel molecular therapies with higher efficiencies and less toxicity. In this doctoral thesis, I have investigated the epigenetic landscape and the miRNAome of T-ALL patient samples and identified different novel players in T-ALL. Subsequently, I have explored the feasibility of targeted therapies against these players in different T-ALL model systems.

One of the remarkable aspects of T-ALL is the presence of a skewed gender distribution, with a threefold higher T-ALL occurrence in males. We hypothesized that the possible existence of X-linked tumor suppressors might be able to explain this gender bias. Therefore we explored the X-linked exome of primary T-ALL patient samples for possible genetic defects. The first novel epigenetic regulator found to be implicated in a large proportion of T-ALL cases in this study was the putative chromatin reader *PHF6*. We observed recurrent *PHF6* loss-of-function mutations and deletions in primary T-ALL patient samples, and these inactivating defects are most frequently detected in the TLX1 and TLX3 T-ALL subgroups. In recent literature, PHF6 was shown to interact with the ATPase chromatin remodeling complex NuRD and to be involved in DNA damage repair. The contribution of PHF6 to DNA damage repair was illustrated in T-ALL, as PHF6 loss in T-ALL cell lines induced an increase in the global levels of γH2A.X. The further unraveling of the role of PHF6 in normal and malignant T-cells is currently under investigation in our lab and yielding exiting new insights into the role of PHF6 during normal T-cell differentiation and T-ALL oncogenesis.

In view of the success of identifying *PHF6* as a *bona fide* tumor suppressor gene in T-ALL and assuming that possible additional X-linked epigenetic suppressors could also be involved, I investigated the histone H3K27me2/3 demethylase *UTX* and indeed observed recurrent genetic inactivation in male T-ALL patient samples. Furthermore, we could show that *UTX* is able to escape X-inactivation in female T-ALL patient samples, in contrast to *PHF6*, and provide hereby further explanation for the skewed gender distribution in T-ALL. UTX loss provided a strong oncogenic advantage in accelerating T-ALL onset in a NOTCH1 driven T-ALL mouse model, underscoring a *bona fide* tumor suppressor role for UTX in T-ALL. Finally, as an important translational component of this investigation, I could show that *UTX* mutant T-cell leukemias have a stronger sensitivity towards treatment with the H3K27me3 inhibitor DZNep, thus opening a possibility for therapeutic restoration of the precise balance of H3K27 methylation.

Exploration of the T-ALL miRNAome in primary T-ALL patient samples and *in vivo* modeling enabled the identification of a set of oncogenic miRNAs (miR-17-92, miR-223, miR-26a, miR-27a and miR-148a/152) that can co-regulate several T-ALL tumor suppressors (FBXW7, PHF6, NF1, PTEN, IKZF1 and BIM). Next, we have undertaken a miRNA-based therapeutic approach through introducing antagomiRs against the identified oncomiRs in T-ALL cell lines, resulting in a clear reduction in cell viability. Importantly, an additive effect was observed when antagomiRs directed against several oncomiRs were introduced simultaneously. Hence, the blockage of multiple miRNAs in T-ALL might collectively contribute to effective reactivation

of a larger set of tumor suppressors and underscores the importance of this miRNA-tumor suppressor network identified in T-ALL.

In the last part of my thesis, I identified one of the first tumor suppressor miRNAs in T-ALL, miR-193b-3p, through the exploration of miRNAs capable of regulating the MYB oncoprotein in T-ALL. To this end, an in-house designed 3'UTR *MYB* library screen was performed, identifying 33 miRNAs putatively targeting MYB. Next, we filtered these miRNA candidates for their involvement in T-ALL pathogenesis by using miRNA profiles of normal T-cell subsets and primary T-ALL patient samples. Finally, functional modeling enabled and confirmed the identification of miR-193b-3p as a novel tumor suppressor miRNA targeting MYB and MCL1 in T-ALL.

To conclude, the exploration of the epigenetic make-up and miRNAome in T-ALL enabled us to identify novel epigenetic drivers and miRNAs in T-ALL. The identification of these perturbed molecular events in T-ALL pathogenesis can contribute to the further exploration of novel therapies in this cancer type. As the first epigenetic therapies are already approved by the FDA and the first clinical trials with miRNA-based therapeutics are currently ongoing, we can be assured that targeted therapies against novel epigenetic and miRNA players offer good prospects for T-ALL treatment.

Samenvatting

T-ALL is een agressieve hematologische maligniteit. In deze ziekte verwerven ongedifferentieerde normale T-cellen een reeks (epi)genetische defecten wat leidt tot een sterke accumulatie van maligne T-cel lymfoblasten. Afhankelijk van de leeftijd van de patiënt schommelen de genezingskansen bij T-ALL tussen 50-75%. Helaas hervallen een significant aantal T-ALL patiënten in een vroeg stadium van de behandeling. De behandelings-protocollen die vandaag toegepast worden, omvatten risico-aangepaste chemotherapie, hematopoëtische stamceltransplantatie en ondersteunende zorg. Ik anticipeer dat de gedetailleerde ontrafeling van het (epi)genetisch landschap in T-ALL een aangrijpingspunt kan vormen voor nieuwe moleculaire therapieën met betere efficiëntie en lagere toxiciteit. In deze doctorale thesis onderzocht ik het epigenetische landschap en het miRNAoom van T-ALL patiënten en identificeerde ik verschillende nieuwe spelers in T-ALL. Vervolgens testte ik mogelijke doelgerichte behandelingen uit tegen deze nieuwe spelers in verschillende T-ALL modelsystemen.

Eén van de opmerkelijke aspecten/vaststellingen bij T-ALL is de aanwezigheid van een verstoorde gender distributie: T-ALL komt namelijk 3 keer meer voor bij mannen dan bij vrouwen. We hypothiseerden dat dit mogelijks zou kunnen wijzen op het bestaan van X-gebonden tumor suppressor genen in deze ziekte. In dit doctoraatsonderzoek hebben we daarom onderzocht of genetische defecten aanwezig zijn in het X-chromosoom exoom van primaire T-ALL patiëntenstalen. De eerste X-gebonden epigenetische regulator geïdentificeerd in deze studie is de veronderstelde chromatine lezer *PHF6*, mutationeel geïnactiveerd in een hoog percentage van T-ALL patiënten. Dit gen is frequent het doelwit van inactiverende mutaties en deleties in primaire T-ALL patiënten stalen, welke het vaakst vastgesteld worden bij patiënten van de TLX1 en TLX3 T-ALL subgroepen. In de recente literatuur werd reeds beschreven dat PHF6 kan samenwerken met het ATPase chromatine remodeling complex NuRD en dat PHF6 betrokken is bij herstel van DNA-schade. Dit laatste werd in onze studie ook geïllustreerd in T-ALL, daar verlies van PHF6 in T-ALL cellijnen een toename in globale niveaus van γH2A.X kan induceren. De verdere ontrafeling van de rol van PHF6 in normale en maligne T-cellen wordt momenteel onderzocht in ons labo en leverde reeds nieuwe interessante inzichten op naar de rol van PHF6 in normale T-cel differentiatie en T-ALL oncogenese.

Gezien het succes van de identificatie van *PHF6* als *bona fide* tumor suppressor gen in T-ALL en veronderstellende dat additionele X-gebonden epigenetische suppressors betrokken zouden kunnen zijn in T-ALL, onderzocht ik de X-gebonden histon H3K27me2/3 demethylase *UTX*. We vonden in deze tweede epigenetische regulator eveneens recurrente inactiverende genetische defecten, en dit in bijzonder enkel bij mannelijke T-ALL patiënten. Verder konden we aantonen dat *UTX* in vrouwelijke T-ALL patiënten stalen aan chromosoom X-inactivatie kan ontsnappen, wat niet het geval was voor het X-gebonden *PHF6* gen. Deze bevindingen kunnen verder bijdragen tot een mogelijke verklaring voor de verstoorde gender distributie in T-ALL. Verder demonstreerden we dat verlies van UTX een sterk oncogeen voordeel oplevert in T-ALL. Met name, UTX verlies leidde tot een versnelde ontwikkeling van leukemie in het NOTCH1 T-ALL muismodel, wat aantoont dat UTX een *bona fide* tumor suppressor is in T-ALL. Finaal konden we aantonen dat *UTX* mutante T-cel leukemieën gevoeliger zijn voor behandeling met de H3K27me3 inhibitor DZNep, waarbij we een mogelijke therapeutische restoratie van de balans in H3K27 methylatie konden aantonen.

Onderzoek van het miRNAoom in primaire T-ALL patiëntenstalen en *in vivo* modelering liet ons toe een reeks oncogene miRNAs te identificeren (miR-17-92, miR-223, miR-26a, miR-27a

en miR-148a/152) die gezamenlijk verschillende T-ALL tumor suppressors (FBXW7, PHF6, NF1, PTEN, IKZF1 en BIM) kunnen reguleren. Daarna onderzochten we een miRNA-gebaseerde behandelingsstrategie in T-ALL, waarbij we antagomiRs introduceerden tegen de geïdentificeerde oncomiRs in T-ALL cellijnen. Deze behandeling resulteerde in een duidelijke afname van celviabiliteit. Daarenboven konden we een additief effect waarnemen wanneer antagomiRs tegen verschillende oncomiRs gezamenlijk werden toegediend. We kunnen dus besluiten dat het tegelijkertijd blokkeren van verschillende miRNAs in T-ALL kan bijdragen tot een effectieve reactivatie van een grotere groep tumor suppressors en onderstreept het belang van het door ons geïdentificeerde miRNA-tumorsuppressor netwerk in T-ALL.

In het laatste deel van de thesis identificeerden we één van de eerste tumor suppressor miRNAs in T-ALL, met name miR-193b-3p. Dit miRNA werd ontdekt bij onderzoek naar mogelijke miRNAs die in staat zouden zijn MYB negatief te reguleren in T-ALL. Hiervoor hebben we een uitgebreide screening uitgevoerd met een specifieke in-huis ontworpen 3'UTR *MYB* library screen, waarbij we 33 miRNAs identificeerden die mogelijks MYB kunnen reguleren. Vervolgens onderzochten we in hoeverre deze 33 miRNA kandidaten betrokken zijn in T-ALL pathogenese. Hiervoor maakten we gebruik van miRNA profielen van normale T-cel subsets en primaire T-ALL patiënten stalen. Via functionele modelering konden we finaal het miRNA miR-193b-3p identificeren als een nieuwe tumor suppressor miRNA dat MYB en MCL1 reguleert in T-ALL.

Als besluit kunnen we stellen dat ons onderzoek van het epigenetische landschap en het miRNAoom in T-ALL leidde tot de identificatie van verschillende nieuwe epigenetische drijvers en miRNAs in T-ALL. Via het achterhalen van deze moleculaire defecten in T-ALL pathogenese hebben we bijgedragen tot de verdere exploratie van nieuwe mogelijke therapieën in dit kankertype. De eerste epigenetische therapieën zijn reeds aanvaard door het FDA en de eerste klinische trials met miRNA-gebaseerde therapieën zijn momenteel reeds lopende. Hierdoor kunnen we er zeker van zijn dat gerichte therapieën tegen nieuw geïdentificeerde epigenetische en miRNA spelers mooie vooruitzichten bieden voor de behandeling van T-ALL.

Dankwoord

Na bloed, zweet, tranen en vooral vele zjatjes kaffe zijn we toegekomen aan het finale stukje tekst in mijn thesis! Terugkijkend naar de voorbij gevlogen jaren, heb ik vooral genoten van de leuke tijd op het lab, het uitdagende en interessante onderzoek, de buitenlandse ervaring in de zalige stad New York, de stimulerende binnen- en buitenlandse meetings en de leuke afterworks. Ik ben heel veel mensen dankbaar die me geholpen hebben met het behalen van deze doctoraatsthesis en ben vooral heel trots dat ik heb kunnen genieten van een zeer goede werkomgeving, leuke collega's in binnen- en buitenland en de vele uitdagingen die een doctoraatsthesis je kan bieden. Daarenboven zou ik zonder een bende van vrienden en familie die je steun geven in je interesses in- en buiten je werk mijn doctoraatsperiode nooit op deze manier hebben kunnen ervaren.

Ik ben blij en trots op de directe en diverse samenwerkingen waarvan ik heb mogen genieten. Mijn promotor prof. dr. Frank Speleman gaf me direct de juiste spirit mee voor het kankeronderzoek, de drive voor het uitspitten van nieuwigheden in je onderzoeksdomein, het eureka gevoel bij positieve onderzoeksresultaten, de eerste 10/10 voor mijn eerste mondelinge presentatie op een congres, alsook mooie uitspraken zoals catch 22 (volgens Wikipedia: een term waarin een algemene situatie wordt beschreven waarin een individu twee acties dient te verwezenlijken die wederzijds afhankelijk zijn van de andere actie, die als eerste dient te zijn voltooid), 'having said that..', … . Bedankt Frank voor de vele kansen die je me gaf, om mezelf te ontplooien en beter te leren kennen; ik heb van deze periode veel geleerd en genoten! Mijn co-promotor prof. dr. Yves Benoit gaf me de waarden mee van kankeronderzoek en het enthousiasme voor nieuwe resultaten die mogelijks kunnen bijdragen naar nieuwe aangrijpingspunten voor betere behandeling van leukemiepatiënten. Bedankt Yves voor de kansen die je me gaf om deel te nemen aan dit interessant leukemieonderzoek in Gent!

Een belangrijk plaatsje in deze thesis wil ik daarnaast heel graag geven aan dr. Pieter Van Vlierberghe. Onze samenwerking, ondanks of juist mede door de tussenliggende Atlantische Oceaan, was zeer tof, leerrijk en daarenboven succesvol. Ik heb veel geleerd van je vastberadenheid, doorzetting, inzicht en enthousiasme voor het T-ALL onderzoek. De goesting om 'GO WEST' te gaan heb ik ook zeker mede te danken aan jou en zal tot nu toe 1 van de 'beste' beslissingen van mijn doctoraatsperiode zijn (aka FNII). Bedankt Pieter voor de mooie opportuniteiten die je me gaf waaronder mee deel te kunnen nemen aan verschillende toponderzoeksprojecten, en ik wens je ook nog heel veel succes met je

verdere carrière! Daarnaast wil ik ook graag ons diensthoofd prof. dr. Anne De Paepe bedanken dat ik deel mocht uitmaken van deze mooie onderzoeksgroep en onderzoek heb kunnen verrichten in deze bijzondere onderzoeksomgeving. I would also like to thank the members of the examination committee to spend valuable time in the critical reading of my thesis and making suggestions and comments on this work.

Ik kijk ook zeer blij en tevreden terug naar de leuke tijd die ik beleefd heb met mijn vele bureaugenootjes en het (steeds groter wordende) leukemieteam: Nadine, Bruce, Evelien, Aline, Pieter, Kaat, Suzanne, Annelynn, Filip, Sofie, Els, Hetty, Fary, Gloria, An, Tim, Barbara, Bea en Evelien. Allen een dikke merci voor de leuke momenten op het werk, op congres en naast het werk, de leute, ontspanning, gelach, af en toe eens een sappige roddel, het gezamenlijk DJ moment (Nadine blijft menig man, inclusief mezelf, altijd verrassen!), en het leren kennen van enkele Gentse uitspraken zoals 'Ja santé mijn ratse!' (aka Bruce). Daarnaast wil ik ook graag het GKC team en alle collega's van het CMGG bedanken, jullie zijn een heel leuke enthousiaste bende, nogmaals gemerkt op FNII, en dat zal hoogstwaarschijnlijk opnieuw in de verf gezet worden met ons nakend fietsavontuur naar Keulen. Ben zeer trots hiervan deel uit te (mogen) maken en hoop dat ik velen van jullie nog vaak zal terugzien in de nabije toekomst!! Heel erg bedankt allemaal voor de leuke doctoraatsperiode en toffe samenwerking!

In 2012, I have got the nice opportunity to go to New York City, and be part of the Wendel lab. This experience was, like a true American would say, AMAZING in all aspects! I learned new techniques, new skills, broadened my view of the (scientific) world and learned to work in a very international environment. I was spoiled with a great research team and PI, made many new friends including the special NY 'James' group, viewed the fireworks of the 4th of July in a 50th floor apartment, went skiing in the first weekend in the USA, played golf for the first time and enjoyed Halloween and Thanksgiving. Especially, I would like to thank Dino, Viraj, Nanna and Silvi for the time we had together in NY. Thanks all for this great experience!!

Last but not least, mijn familie en vrienden wil ik heel graag bedanken voor er steeds te zijn voor mij, hun eindeloze belangstelling in mijn doen en laten in- en buiten het werk, de ontelbare genietmomenten, de feestjes en vertier, de dozijnen 'clubs', de leutige avonturen, en de steun bij het komende fietsavontuur. New York, inclusief mezelf, heeft bijna elk familielid alsook menig vriend(in) mogen verwelkomen en verrassen met zijn culturele en culinaire specialiteiten. Heel tof dat jullie er waren! In het bijzonder wil ik ook graag mijn ouders en zus bedanken, zij betekenen heel veel voor me en samen staan we super sterk, dat hebben we meermaals mogen ondervinden de laatste jaren. Daarenboven wil ik mijn moeder ook graag extra bedanken voor de heel mooie design van mijn cover en uitnodiging! Ik ben een heel trotse dochter en zus! Tenslotte, terugkijkend naar het hele traject van enthousiast thesisstudentje tot contente 'senior' doctoraatstudent, ben ik heel blij de uitdaging te zijn aangegaan en kijk ik uit naar nieuwe avonturen in het verschiet!

Curriculum Vitae

Joni Van der Meulen

Personalia

Address:	Sint-Pietersnieuwstraat 66
Postcode/city:	9000 Gent, Belgium
Mobile:	+32484127133
Date of birth:	17/07/1985
E-mail address:	joni.vandermeulen@ugent.be
Nationality:	Belgian

Experience

Doctoral Research Assistant, 4 years PhD grant of FWO and 1 year PhD grant of VLK Emmanuel van der Schueren scholarship

Period:	2008 - present
Institute:	Ghent University, Center for Medical Genetics, Ghent, Belgium
Thesis:	Molecular-genetic defects in T-cell acute lymphoblastic leukemia Promotors: prof. dr. Frank Speleman & prof. dr. Yves Benoit Guiding committee: dr. ir. Pieter Van Vlierberghe & prof. dr. Bruno Verhasselt
Stay abroad:	February 2012 – December 2012 Lab of dr. Hans-Guido Wendel, Memorial Sloan-Kettering Cancer Center, NY, USA

Education

Master of Science in Bioengineering: cell- and gene biotechnology

Period:	2003-2008
Institute:	Ghent University
Thesis:	The role of *EVI1* in myeloid leukemia Promotors: prof. dr. Frank Speleman and prof. dr. Godelieve Gheysen
Erasmus:	September 2006 - January 2007 Swedish University of Agricultural Sciences

Scientific Achievements

Publications, awards, oral presentations, posters, conferences and supervision of students

Publications:

- ***PHF6* mutations in T-cell acute lymphoblastic leukemia.** Van Vlierberghe P*, Palomero T*, Khiabanian H, Van der Meulen J, Castillo M, Van Roy N, De Moerloose B, Philippé J, González-García S, Toribio ML, Taghon T, Zuurbier L, Cauwelier B, Harrison CJ, Schwab C, Pisecker M, Strehl S, Langerak AW, Gecz J, Sonneveld E, Pieters R, Paietta E, Rowe JM, Wiernik PH, Benoit Y, Soulier J, Poppe B, Yao X, Cordon-Cardo C, Meijerink J, Rabadan R, Speleman F* & Ferrando AA*. Nat Genet. 2010 Apr;42(4):338-42. Impact factor 35.5; Citations 56.

- **The TLX1 oncogene drives aneuploidy in T cell transformation.** De Keersmaecker K*, Real PJ*, Gatta GD*, Palomero T, Sulis ML, Tosello V, Van Vlierberghe P, Barnes K, Castillo M, Sole X, Hadler M, Lenz J, Aplan PD, Kelliher M, Kee BL, Pandolfi PP, Kappes D, Gounari F, Petrie H, Van der Meulen J, Speleman F, Paietta E, Racevskis J, Wiernik PH, Rowe JM, Soulier J, Avran D, Cavé H, Dastugue N, Raimondi S, Meijerink JP, Cordon-Cardo C, Califano A & Ferrando AA. Nat Med. 2010 Nov;16(11):1321-7. Impact factor 22.4; Citations 30.

- **A cooperative microRNA – tumor suppressor gene network in acute T-cell lymphoblastic leukemia (T-ALL).** Mavrakis KJ*, Van der Meulen J*, Wolfe AL, Liu X, Mets E, Taghon T, Khan AA, Setty M, Rondou P, Vandenberghe P, Delabesse E, Benoit Y, Socci NB, Leslie CS, Van Vlierberghe P, Speleman F* & Wendel HG*. Nat Genet. 2011 Jun 5;43(7):673-8. Impact factor 35.5; Citations 47.

- **EVI1 mediated down regulation of miR-449a is essential for the survival of EVI1 positive leukemic cells.** De Weer A, Van der Meulen J, Rondou P, Taghon T, Konrad TA, De Preter K, Mestdagh P, Van Maerken T, Van Roy N, Jeison M, Yaniv I, Cauwelier B, Noens L, Poirel HA, Vandenberghe P, Lambert F, De Paepe A, Sánchez MG, Odero M, Verhasselt B, Philippé J, Vandesompele J, Wieser R, Dastugue N, Van Vlierberghe P, Poppe B & Speleman F. Br J Haematol. 2011 Aug;154(3):337-48. Impact factor 4.941; Citations 5.

- **Effective Alu Repeat Based RT-Qpcr Normalization in Cancer Cell Perturbation Experiments.**
  Rihani A, Van Maerken T, Pattyn F, Van Peer G, Beckers A, De Brouwer S, Kumps C, Mets E, Van der Meulen J, Rondou P, Leonelli C, Mestdagh P, Speleman F & Vandesompele J. PLoS One. 2013 Aug 14;8(8):e71776. Impact factor 3.7; Citations 0.

- **The need for transparency and good practices in the qPCR literature.** Bustin SA, Benes V, Garson J, Hellemans J, Huggett J, Kubista M, Mueller R, Nolan T, Pfaffl MW, Shipley G, Wittwer CT, Schjerling P, Day PJ, Abreu M, Aguado B, Beaulieu JF, Beckers A, Bogaert S, Browne J, Carrasco-Ramiro F, Ceelen L, Ciborowski K, Cornillie P, Coulon S, Cuypers A, De Brouwer S, De Ceuninck L, De Craene J, De Naeyer H, De Spiegelaere W, Deckers K, Dheedene A, Durinck K, Ferreira-Teixeira M, Fieuw A, Gallup J, Gonzalo-Flores S, Goossens K, Heindryckx F, Herring E, Hoenicka H, Icardi L, Jaggi R, Javad F, Karampelias M, Kibenge F, Kibenge M, Kumps C, Lambertz I, Lammens T, Markey A, Messiaen P, Mets E, Morais S, Mudarra-Rubio A, Nakiwala J,

Nelis H, Olsvik PA, Pérez-Novo C, Plusquin M, Remans T, Rihani A, Rodrigues-Santos P, Rondou P, Sanders R, Schmidt-Bleek K, Skovgaard K, Smeets K, Tabera L, Tögel S, Van Acker T, Van den Broeck W, Van der Meulen J, Van Gele M, Van Peer G, Van Poucke M, Van Roy N, Vergult S, Wauman J, Wiklander M, Willems E, Zaccara S, Zeka F & Vandesompele J. Nat Methods. 2013 Nov;10(11):1063-7. Impact factor 23.56; Citations 0.

- **The H3K27me3 demethylase UTX in normal development and disease.** Van der Meulen J, Speleman F & Van Vlierberghe P. Epigenetics. 2014 Feb 21;9(5). Review.

- **The 5'UTRs of many oncogenes and transcription factors encode a targetable requirement for the eIF4A RNA helicase.** Wolfe AL*, Singh K*, Zhong Y, Drewe P, Rajasekhar VK, Sanghvi VR, Mavrakis KJ, Roderick JE, Van der Meulen J, Schatz JH, Rodrigo CM, Jiang M, Zhao C, Rondou P, de Stanchina E, Teruya-Feldstein J, Kelliher MA, Speleman F, Porco Jr. JA, Pelletier J, Rätsch G** & Wendel HG**. Accepted in Nature.

- **The epigenetic landscape of T-cell acute lymphoblastic leukemia.** Van der Meulen J, Van Roy N, Van Vlierberghe P* & Speleman F*. Review. Accepted in IJBCB.

- **ZEB2 drives immature T-cell lymphoblastic leukemia development via altered IL-7 receptor signalling and enhanced tumor-initiating potential.** Goossens S, Taghon T, Blanchet O, Durinck K, Van der Meulen J, Radaelli E, Peirs S, Ghahremani MF, De Medts J, Bartunkova S, Haigh K, Pieters T, Best JA, Deswarte K, Bogaert P, Canté-Barrett K, Haenebalcke L, Clappier E, Rondou P, Slowicka K, Berx G, Huylebroeck D, Goldrath AW, Janzen V, Speleman F, Meijerink JPP, Soulier J, Van Vlierberghe P & Haigh JJ. Under review in Nature Medicine.

- **MiR-128-3p is a novel oncomiR targeting PHF6 in T-ALL.** Mets E, Van Peer G, Van der Meulen J, Boice M, Taghon T, Goossens S, Mestdagh P, Benoit Y, De Moerloose B, Van Roy N, Poppe B, Vandesompele J, Wendel HG, Van Vlierberghe P, SpelemanF* & Rondou P*. Accepted in Haematologica.

- **A MYC-regulated network of tumor suppressor microRNAs restrains MYB activity and T-Cell Leukemogenesis.** Sanghvi VR*, Mavrakis KJ*, Van der Meulen J, Boice M, Wolfe AL, Carty M, Rondou P, Socci ND, Mayr C, Benoit Y, Taghon T, Van Vlierberghe P, Leslie CS, Speleman F & Wendel HG. Under review in Genes & Development.

- **The H3K27me3 demethylase UTX is a gender-specific tumor suppressor in T-cell acute lymphoblastic leukemia.** Van der Meulen J, Sanghvi V, Mavrakis K, Durinck K, Fang F, Matthijssens F, Rondou P, Vandenberghe P, Delabesse E, De Moerloose B, Menten B, Van Roy N, Verhasselt B, Poppe B, Benoit Y, Taghon T, Melnick A, Speleman F, Wendel HG* & Van Vlierberghe P*. Submitted to Cancer Discovery (April 2014).

- **MicroRNA-193b-3p acts as a tumor suppressor by targeting the MYB oncogene in T-cell acute lymphoblastic leukemia.** Mets E, Van der Meulen J, Van Peer G, Boice M, Mestdagh P, Van de Walle I, Lammens T, De Moerloose B, Benoit Y, Van Roy N, Clappier E, Poppe B, Vandesompele J, Wendel HG, Taghon T, Rondou P, Soulier J, Van Vlierberghe P & Speleman F. Submitted to Leukemia (April 2014).

Awards:

- **Best Oral presentation award** on the 24th BHS meeting, January 30, 2009, Ostend, Belgium
- **Best Poster award** on the 28th BHS meeting, January 25, 2013, Ghent, Belgium

Oral presentations:

- **MicroRNA signatures in Genetic Subtypes of T-Cell Acute Lymphoblastic Leukemia**. Van Vlierberghe P, Van der Meulen J, Mestdagh P, Vandesompele J, Poppe B, Van Roy N, Taghon T, Plum J, Cauwelier B, Selleslag DLD, Heimann P, Vandenberghe P, Dastugue N, Delabesse E, Gervais C, Gregoire MJ, Mozzicconacci MJ, Lefebvre C, Meijerink JPP, Buijs-Gladdines J, De Moerloose B, Benoit Y, De Paepe A & Speleman F. 24th BHS meeting, January 30-31, 2009, Ostend, Belgium

- **MicroRNA signatures in Genetic Subtypes of T-Cell Acute Lymphoblastic Leukemia**. Van Vlierberghe P, Van der Meulen J, Mestdagh P, Vandesompele J, Poppe B, Van Roy N, Taghon T, Plum J, Cauwelier B, Selleslag DLD, Heimann P, Vandenberghe P, Dastugue N, Delabesse E, Gervais C, Gregoire MJ, Mozzicconacci MJ, Lefebvre C, Meijerink JPP, Buijs-Gladdines J, De Moerloose B, Benoit Y, De Paepe A & Speleman F. 9th BeSHG meeting, February 13, 2009, Brussels, Belgium

- **MicroRNA signatures in Genetic Subtypes of T-Cell Acute Lymphoblastic Leukemia**. Van Vlierberghe P, Van der Meulen J, Mestdagh P, Vandesompele J, Poppe B, Van Roy N, Taghon T, Plum J, Cauwelier B, Selleslag DLD, Heimann P, Vandenberghe P, Dastugue N, Delabesse E, Gervais C, Gregoire MJ, Mozzicconacci MJ, Lefebvre C, Meijerink JPP, Buijs-Gladdines J, De Moerloose B, Benoit Y, De Paepe A & Speleman F. 14th EHA meeting, June 4-7, 2009, Berlin, Germany

- **MicroRNA signatures in Genetic Subtypes of T-Cell Acute Lymphoblastic Leukemia**. Van Vlierberghe P, Van der Meulen J, Mestdagh P, Vandesompele J, Poppe B, Van Roy N, Taghon T, Plum J, Cauwelier B, Selleslag DLD, Heimann P, Vandenberghe P, Dastugue N, Delabesse E, Gervais C, Gregoire MJ, Mozzicconacci MJ, Lefebvre C, Meijerink JPP, Buijs-Gladdines J, De Moerloose B, Benoit Y, De Paepe A & Speleman F. EORTC CLG meeting, November 20-21, 2009, Strasbourg, France

- **Downregulation of *miR-449a* is essential for the survival of *EVI1* positive leukemic cells through modulation of *NOTCH1* and *BCL2***. De Weer A, Mestdagh P, De Preter K, Van der Meulen J, Van Vlierberghe P, Van Maerken T, Van Roy N, Jeison M, Yaniv I, Cauwelier B, Noens L, Poirel HA, Vandenberghe P, Lambert F, De Paepe A, Konrad T, Wieser R, García Sánchez M, Odero M, Verhasselt B, Philippé J, Vandesompele J, Dastugue N, Poppe B* & Speleman F*. 10th BeSHG meeting, February 26, 2010, Ghent, Belgium

- ***PHF6* mutations in T-cell acute lymphoblastic leukemia**. Van Vlierberghe P*, Palomero T*, Khiabanian H, Van der Meulen J, Castillo M, Piovan E, Hadler M, Van Roy N, De Moerloose B, Phillipé J, Verhasselt B, Taghon T, Cauwelier B, Harrison C, Strehl S, Soulier J, Langerak T, Gecz J, Pieters R, Paietta E, Rowe J, Wiernik P, Meijerink J, Benoit Y, Poppe B, Cordon-Cardo C, Rabadan R, Speleman F* & Ferrando AA*. EORTC CLG meeting, March 1, 2011, Brussels, Belgium

- **MicroRNA signatures in normal and malignant T-cell development**. Van der Meulen J*, Mavrakis KJ, Wolfe AL, Mets E, Taghon T, Khan AA, Setty M, Liu X, Rondou R, Vandenberghe P, Delabesse E, Benoit Y, Socci ND, Leslie CS, Poppe B, Van Vlierberghe P, Wendel HG* & Speleman F*. 16th congress of EHA, June 9-12, 2011, London, UK

- **H3K27me3 erasers, novel targets in T-cell acute lymphoblastic leukemia.** Van der Meulen J, Mavrakis KJ, Sanghvi VR, Van Roy N, Poppe B, Vandenberghe P, Delabesse E, De Moerloose B, Benoit Y, Rondou P, Van Vlierberghe P, Ferrando AA, Wendel HG* & Speleman F*. 2nd ESH-EHA Scientific Workshop on T-cell acute lymphoblastic leukemia, March 22-24, 2013, Lisbon, Portugal

Posters:

- **Cryptic 9p24 microdeletions covering *hsa-mir-101-2* are recurrent in hematological malignancies**. Van Roosbroeck K, Lahortiga I, Finalet Ferreiro J, Van der Meulen J, Vandenberghe P, Cools J, Speleman F, Marynen P & Wlodarska I. 14th EHA meeting, June 4-7, 2009, Berlin, Germany

- **MicroRNA signatures in Genetic Subtypes of T-Cell Acute Lymphoblastic Leukemia**. Van Vlierberghe P, Van der Meulen J, Mestdagh P, Vandesompele J, Poppe B, Van Roy N, Taghon T, Plum J, Cauwelier B, Selleslag DLD, Heimann P, Vandenberghe P, Dastugue N, Delabesse E, Gervais C, Gregoire MJ, Mozziconacci MJ, Lefebvre C, Meijerink JPP, Buijs-Gladdines J, De Moerloose B, Benoit Y, De Paepe A & Speleman F. Summer conferences FASEB, August 2-7, 2009, Vermont, USA

- **MicroRNA Signatures in Genetic Subtypes of T-Cell Acute Lymphoblastic Leukemia**. Van der Meulen J*, Van Vlierberghe P*, Mestdagh P, Fieuw A, Van Roy N, De Preter K, Taghon T, Plum J, Cauwelier B, Selleslag DLD, Heimann P, Vandenberghe P, Dastugue N, Delabesse E, Gervais C, Gregoire MJ, Mozziconacci MJ, Lefebvre C, Meijerink J, Buijs-Gladdines J, Lammens T, De Paepe A, De Moerloose B, Vandesompele J, Benoit Y, Poppe B & Speleman F. 7th Bi-annual Childhood Leukemia Symposium, April 25-27, 2010, Antalya, Turkey

- **MicroRNA Signatures in Genetic Subtypes of T-Cell Acute Lymphoblastic Leukemia.** Van der Meulen J*, Van Vlierberghe P*, Mestdagh P, Fieuw A, Van Roy N, De Preter K, Taghon T, Plum J, Cauwelier B, Selleslag DLD, Heimann P, Vandenberghe P, Dastugue N, Delabesse E, Gervais C, Gregoire MJ, Mozziconacci MJ, Lefebvre C, Meijerink J, Buijs-Gladdines J, Lammens T, De Paepe A, De Moerloose B, Vandesompele J, Benoit Y, Poppe B & Speleman F. ESH-EHA Scientific Workshop on T-cell acute lymphoblastic leukemia meets normal T-cell development, May 7-9, 2010, Mandelieu, France

- **Cooperative miRNA mediated FBXW7 suppression contributes to T-cell lymphoblastic leukemogenesis**. Mets E, Van der Meulen J, Mavrakis KJ, Wolfe AL, Taghon T, Khan AA, Setty M, Liu X, Vandenberghe P, Delabesse E, Benoit Y, Socci ND, Leslie CS, Van Vlierberghe P, Wendel HG, Rondou P & Speleman F. Keystone Symposia: MicroRNAs and Human Disease, February 11-16, 2011, Banff, Alberta, Canada

- **Regulatory networks governed by microRNAs in T-ALL oncogenesis and normal T-cell development.** Van der Meulen J, Mets E, Mestdagh P, Pipelers P, Taghon T, Camacho-Trujillo D, Avran D, Van Peer G, Van Roy N, Thas O, Benoit Y, Vandesompele J, Poppe B, Van Vlierberghe P, Rondou P, Soulier J & Speleman F. 53rd ASH meeting, December 10-13, 2011, San Diego, California, USA

- **Improved risk-stratification and outcome prediction in children with average risk precursor-B acute lymphoblastic leukemia using a nineteen-microRNA signature.** Ghazavi F, Lammens T, Suciu S, Laureys G, Bakkus M, Ferster A, Uyttebroeck A, Lutz P, Cavé H, Plat G, Dastugue N, Dresse MF, Van der Meulen J, Mestdagh P, Vandesompele J, Speleman F, De Moerloose B & Benoit Y. 27th BHS meeting, January 27-28, 2012, Liege, Belgium

- **Regulatory networks governed by microRNAs in T-ALL oncogenesis and normal T-cell development.** Van der Meulen J, Mets E, Mestdagh P, Pipelers P, Van Peer G, Taghon T, Camacho-Trujillo D, Avran D, Van Roy N, Thas O, Benoit Y, Vandesompele J, Poppe B, Van Vlierberghe P, Rondou P, Soulier J & Speleman F. 12th BeSHG meeting, March 2, 2012, Liege, Belgium

- **Unraveling a *NOTCH1*-lncRNA-miRNA regulatory network in acute T-cell lymphoblastic leukemia and normal T-cell development.** Durinck K, Mestdagh P, Taghon T, Van der Meulen J, Van de Walle I, Volders PJ, Pattyn F, Van Roy N, Benoit Y, Poppe B, Van Vlierberghe P, Menten B, Vandesompele J, Rondou P & Speleman F. Keystone meeting Non-Coding RNAs, March 31 - April 5, 2012, Snowbird, Utah, Belgium

- **Improved risk-stratification and outcome prediction in children with average risk precursor-B acute lymphoblastic leukemia using a nineteen-microRNA signature.** Ghazavi F, Lammens T, Suciu S, Laureys G, Bakkus M, Ferster A, Uyttebroeck A, Lutz P, Cavé H, Plat G, Dastugue N, Dresse MF, Van der Meulen J, Mestdagh P, Vandesompele J, Speleman F, De Moerloose B & Benoit Y. 17th EHA meeting, June 14-17, 2012, Amsterdam, The Netherlands.

- **NOTCH1 signaling induces global transcriptional changes in long non-coding RNA expression in T-cell acute lymphoblastic leukemia and normal T-cell development.** Durinck K, Mestdagh P, Volders PJ, Taghon T, Van de Walle I, Ongenaert M, Van der Meulen J, Vanhauwaert S, Wallaert A, Soulier J, Van Roy N, Benoit Y, Poppe B, Menten B, Vandesompele J, Van Vlierberghe P, Rondou P & Speleman F. Keystone Symposia, Noncoding RNAs in development and cancer, January 20-25, 2013, Vancouver, Canada.

- **H3K27me3 erasers, novel targets in T-cell acute lymphoblastic leukemia.** Van der Meulen J, Mavrakis KJ, Sanghvi VR, Poppe B, Van Roy N, Rondou P, Benoit Y, Van Vlierberghe P, Wendel HG & Speleman F. 28th BHS meeting, January 25-26, 2013, Ghent, Belgium

- **Extending the functional redundant cooperative miRNA tumor suppressor and oncogene network in T-ALL.** Mets E, Van Peer G, Van der Meulen J, Mestdagh P, Taghon T, Avran D, Benoit Y, Poppe B, Soulier J, Van Vlierberghe P, Rondou P, Vandesompele J* & Speleman F*. 28th BHS meeting, January 25-26, 2013, Ghent, Belgium

- **H3K27me3 erasers, novel targets in T-cell acute lymphoblastic leukemia.** Van der Meulen J, Mavrakis KJ, Sanghvi VR, Poppe B, Van Roy N, Rondou P, Benoit Y, Van Vlierberghe P, Wendel HG & Speleman F. 13th BeSHG meeting, March 15, 2013, Ghent, Belgium

- **NOTCH1 signaling induces global transcriptional changes in long non-coding RNA expression in T-cell acute lymphoblastic leukemia and normal T-cell development.** Durinck K, Mestdagh P, Volders PJ, Taghon T, Van de Walle I, Ongenaert M, Van der Meulen J, Vanhauwaert S, Wallaert A, Soulier J, Van Roy N, Benoit Y, Poppe B, Menten B, Vandesompele J, Van Vlierberghe P, Rondou P & Speleman F. 13th BeSHG meeting, March 15, 2013, Ghent, Belgium

- **Extending the functional redundant cooperative miRNA tumor suppressor and oncogene network in T-ALL.** Mets E, Van Peer G, Van der Meulen J, Mestdagh P, Taghon T, Avran D, Benoit Y, Poppe B, Soulier J, Van Vlierberghe P, Rondou P, Vandesompele J* & Speleman F*. 13th BeSHG meeting, March 15, 2013, Ghent, Belgium

- **NOTCH1 signaling induces global transcriptional changes in long non-coding RNA expression in T-cell acute lymphoblastic leukemia and normal T-cell development.** Durinck K, Mestdagh P, Volders PJ, Taghon T, Van de Walle I, Ongenaert M, Van der Meulen J, Vanhauwaert S, Wallaert A, Soulier J, Van Roy N, Benoit Y, Poppe B, Menten B, Vandesompele J, Van Vlierberghe P, Rondou P & Speleman F. 2nd ESH-EHA Scientific Workshop on T-cell acute lymphoblastic leukemia, March 22-24, 2013, Lisbon, Portugal

- **Notch driven miRNAs implicated in normal and malignant T-cell development.** Durinck K, Van der Meulen J, Van de Walle I, Pipelers P, Mestdagh P, Ongenaert M, Van Roy N, Benoit Y, Poppe B, Vandesompele J, De Preter K, Thas O, Van Vlierberghe P, Rondou P, Soulier J, Speleman F* & Taghon T*. 2nd ESH-EHA Scientific Workshop on T-cell acute lymphoblastic leukemia, March 22-24, 2013, Lisbon, Portugal

- **A miRNAome wide 3'UTR screen based mapping of convergent multi-miRNA targeting of tumor suppressor-oncogene networks in T-ALL.** Mets E, Van Peer G, Van der Meulen J, Mestdagh P, Taghon T, Avran D, Benoit Y, Poppe B, Soulier J, Van Vlierberghe P, Rondou P, Vandesompele J* & Speleman F*. 2nd ESH-EHA Scientific Workshop on T-cell acute lymphoblastic leukemia, March 22-24, 2013, Lisbon, Portugal

- **MiR-128 is a novel PHF6 targeting regulatory non-coding RNA acting as a T-ALL oncogene.** Mets E, Van der Meulen J, Van Peer G, Boice M, Mestdagh P, Taghon T, Avran D, De Moerloose B, Benoit Y, Poppe B, Soulier J, Vandesompele J, Van Vlierberghe P, Rondou P, Wendel G & Speleman F. 2nd ESH-EHA Scientific Workshop on T-cell acute lymphoblastic leukemia, March 22-24, 2013, Lisbon, Portugal

- **H3K27me3 erasers are novel targets in T-cell acute lymphoblastic leukemia.** Van der Meulen J, Mavrakis KJ, Sanghvi VR, Van Roy N, Poppe B, Vandenberghe P, Delabesse E, De Moerloose B, Benoit Y, Rondou P, Van Vlierberghe P, Ferrando AA, Wendel HG* & Speleman F*. EMBO Conference Series - Chromatin and Epigenetics, May 8-12, 2013, Heidelberg, Germany

- **The H3K27me3 demethylase UTX is a tumor suppressor in T-cell acute lymphoblastic leukemia.** Van der Meulen J, Mavrakis KJ, Sanghvi VR, Eggermont A, Van Roy N, Poppe B, Baeyens A, Vandenberghe P, Delabesse E, Verhasselt B, Taghon T, De Moerloose B, Benoit Y, Rondou P, Ferrando AA, Melnick A, Speleman F, Van Vlierberghe P* & Wendel HG*. Cell Symposia – Cancer Epigenomics, October 6-8, 2013, Sitges, Spain

- **The plant homeodomain (PHD)-like finger protein PHF6 chromatin binding pattern and transcriptional regulation indicates a functional link with NOTCH1 in T cell acute lymphoblastic leukemia.** Durinck K, Van der Meulen J, Ongenaert M, Verhasselt B, Taghon T, Van de Walle I, Van Roy N, Poppe B, Benoit Y, Gevaert K, Van Vlierberghe P, Rondou P & Speleman F. Cell Symposia – Cancer Epigenomics, October 6-8, 2013, Sitges, Spain

- **Expanding The TLX1-Regulome in T Cell Acute Lymphoblastic Leukemia Towards Long Non-Coding RNAs.** Durinck K, Van der Meulen J, Ongenaert M, Volders PJ, Wallaert A, Van Roy N, Benoit Y, Poppe B, Mestdagh P, Vandesompele J, Rondou P, Soulier J, Van Vlierberghe P, Speleman F. EMBO Conference Series – The non-coding genome, October 9-12, 2013, Heidelberg, Germany

- **Characterization of the NOTCH1-driven miRNA network that controls normal human T-cell development.** Van der Meulen J, Durinck K, Van de Walle I, Mestdagh P, Pipelers P, De Preter K, Van Peer G, Van Roy N, Poppe B, Ongenaert M, Vandesompele J, Thas O, Rondou P, Van Vlierberghe P, Speleman F & Taghon T. 14th BeSHG meeting, February 7, 2014, Antwerp, Belgium

- **The H3K27me3 demethylase UTX is a gender-specific tumor suppressor in T-cell acute lymphoblastic leukemia**. Van der Meulen J, Sanghvi VR, Mavrakis KJ, Durinck K, Rondou P, Vandenberghe P, Delabesse E, Lammens T, De Moerloose B, Menten B, Van Roy N, Verhasselt B, Poppe B, Benoit Y, Taghon T, Speleman F, Wendel HG & Van Vlierberghe P. 14th BeSHG meeting, February 7, 2014, Antwerp, Belgium

- **Expanding The TLX1-Regulome in T Cell Acute Lymphoblastic Leukemia Towards Long Non-Coding RNAs.** Durinck K, Van der Meulen J, Ongenaert M, Volders PJ, Wallaert A, Van Roy N, Benoit Y, Poppe B, Mestdagh P, Vandesompele J, Rondou P, Soulier J, Van Vlierberghe P, Speleman F. 14th BeSHG meeting, February 7, 2014, Antwerp, Belgium

- **MicroRNA-128-3p is a novel oncomiR targeting PHF6 in T-cell acute lymphoblastic leukemia.** Mets E, Van Peer G, Van der Meulen J, Boice M, Taghon T, Goossens S, Mestdagh P, Benoit Y, De Moerloose B, Van Roy N, Poppe B, Vandesompele J, Wendel HG, Van Vlierberghe P, Speleman F* & Rondou P*. 14th BeSHG meeting, February 7, 2014, Antwerp, Belgium

Conferences:

- 8th BeSHG meeting, April 25, 2008, Leuven, Belgium
- Benelux qPCR symposium, October 6, 2008, Ghent, Belgium
- 11th Post-ASH meeting, January 9, 2009, Brussels, Belgium
- 24th BHS meeting, January 30, 2009, Ostend, Belgium
- BACR meeting, January 31, 2009, ULB Brussels, Belgium
- 9th BeSHG meeting, February 13, 2009, ULB Brussels, Belgium
- 5de wintersymposium, March 7, 2009, Ghent, Belgium
- Journee d'honneur de Roland Berger, April 2, 2009, Paris, France
- 14th EHA meeting, June 4-7, 2009, Berlin, Germany
- Summer conferences FASEB, August 2-7, 2009, Vermont, USA
- EORTC CLG meeting, November 20-21, 2009, Strasbourg, France
- 51st ASH Annual Meeting and Exposition, December 5-8, 2009, New Orleans, Louisiana, USA
- Keystone Symposia, Molecular Basis for Chromatin Structure and Regulation, January 17-21, 2010, Taos, New Mexico, USA
- Advances in Genomics, January 28-29, 2010, Ghent, Belgium
- 10th BeSHG meeting, February 26, 2010, Ghent, Belgium
- 1st ESH-EHA Scientific Workshop on T-cell acute lymphoblastic leukemia meets normal T-cell development, May 7-9, 2010, Mandelieu, France
- 52nd ASH Annual Meeting and Exposition, December 4-7, 2010, Orlando, Florida, USA
- EORTC CLG meeting, March 1, 2011, Brussels, Belgium
- 11th BeSHG meeting, March 4, 2011, Louvain-la-Neuve, Belgium
- 16th EHA meeting, June 9-12, 2011, London, UK
- EMBO-EMBL Symposium: Cancer Genomics, September 17-19, 2011, Heidelberg, Germany
- 28th BHS meeting, January 25, 2013, Ghent, Belgium
- 13th BeSHG meeting, March 15, 2013, Brussels, Belgium
- 2nd ESH-EHA Scientific Workshop on T-cell acute lymphoblastic leukemia, March 22-24, 2013, Lisbon, Portugal
- EMBO Conference Series - Chromatin and Epigenetics, May 8-12, 2013, Heidelberg, Germany
- Cell Symposia – Cancer Epigenomics, October 6-8, 2013, Sitges, Spain
- Oncopoint II, February 6, 2014, Ghent, Belgium
- 14th BeSHG meeting, February 7, 2014, Antwerp, Belgium

Supervision of students:

- **Z-lijn paper, 2nd Bachelor of Medicine 2008-2009**: Sara David, Gamma secretase inhibitor behandeling in T-cel acute lymfoblastische leukemie. Supervision: Joni Van der Meulen, promotor: Frank Speleman.
- **Z-lijn paper, 2nd bachelor Geneeskunde 2009-2010**: Johannes Libeer, Prognostische relevantie van genetische defecten in TALL. Supervision: Joni Van der Meulen, promotor: Frank Speleman.
- **Master Thesis, 2nd Master of Biochemistry and Biotechnology 2009-2010**: Kaat Durinck, Evaluation of *PHF6* as a tumor suppressor in hematological malignancies. Supervision: Joni Van der Meulen and Pieter Rondou, promotors: Bruce Poppe and Geert Berx.

- **Master Thesis, 2nd Master of Biomedical Sciences 2010-2011**: Lies Bosman, Evaluation of *PHF6* as a tumor suppressor in hematological malignancies. Supervision: Joni Van der Meulen and Pieter Rondou, promotor: Frank Speleman.
- **Z-lijn paper, 2nd Bachelor of Medicine 2012-2013**: Stijn Bogaert, De dubbele rol van EZH2 in leukemie en lymphoma. Supervision: Joni Van der Meulen, promotor: Frank Speleman.
- **Z-lijn paper, 2nd Bachelor of Medicine 2012-2013**: Brecht Devriendt, De dubbele rol van EZH2 in leukemie en lymphoma. Supervision: Joni Van der Meulen, promotor: Frank Speleman.
- **Z-lijn Master Thesis, 1st -2nd Master of Medicine 2011-2013**: Laura Anrijs, De rol van genetische defecten in pediatrische B-cel acute lymfatische leukemie in relatie tot prognose en behandeling. Supervision: Joni Van der Meulen, promotor: Frank Speleman.